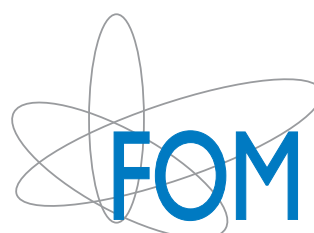


Polarization effects in proton-proton collisions within the Standard Model and beyond

Wilco J. den Dunnen



Dit werk maakt deel uit van het onderzoekprogramma van de Stichting voor Fundamenteel Onderzoek der Materie (FOM), die deel uit maakt van de Nederlandse Organisatie voor Wetenschappelijk Onderzoek (NWO).

VRIJE UNIVERSITEIT

Polarization effects in proton-proton collisions within the Standard Model and beyond

ACADEMISCH PROEFSCHRIFT

ter verkrijging van de graad Doctor aan
de Vrije Universiteit Amsterdam,
op gezag van de rector magnificus
prof.dr. L.M. Bouter,
in het openbaar te verdedigen
ten overstaan van de promotiecommissie
van de Faculteit der Exacte Wetenschappen
op vrijdag 15 februari 2013 om 11.45 uur
in de aula van de universiteit,
De Boelelaan 1105

door

Wilco Johannes den Dunnen

geboren te Dordrecht

promotoren: prof.dr. D. Boer
prof.dr. P.J.G. Mulders

Contents

List of publications	ix
1 Introduction	1
2 Factorized description of $pp \rightarrow VX$	7
2.1 Quark–antiquark annihilation	7
2.1.1 Inclusion of the gauge link	12
2.2 Parameterization of the quark correlator	19
2.2.1 TMD correlator	21
2.2.2 Collinear correlator	25
2.2.3 Evolution	26
2.3 Gluon-gluon fusion	27
2.3.1 Inclusion of the gauge link	28
2.4 Parameterization of the gluon correlator	30
2.4.1 TMD correlator	31
2.4.2 Collinear correlator	35
2.5 Summary	35
3 Standard Model TMD effects in $p^\uparrow p^\uparrow \rightarrow VX$	37
3.1 Introduction	37
3.2 Drell-Yan and W boson production in TMD factorization	40
3.3 Parameterization of the Sivers and worm-gear function	40
3.4 Spin asymmetries in the Drell-Yan process	43
3.5 Spin asymmetries in W boson production	48
3.6 Summary and conclusions	53
4 BSM effects in $p^\uparrow p^\uparrow \rightarrow WX \rightarrow \ell\nu X$	55
4.1 Introduction Left-Right models	56
4.1.1 General framework	57
4.1.2 Gauge boson masses, mixing and couplings	58
4.1.3 Quark masses, CKM matrices	61
4.1.4 Manifest/Pseudo manifest	62
4.1.5 Non-universal coupling	63
4.1.6 Discussion	63
4.2 Bounds on left-right models	64
4.2.1 Bounds on the W_2 mass	64

4.2.2	Bounds on the W -boson coupling to right-handed leptons	66
4.2.3	Bounds on the W -boson coupling to right-handed quarks	66
4.2.4	Summary	74
4.3	Cross section and asymmetries in $p^\uparrow p^\uparrow \rightarrow (W_1 + W_2)X \rightarrow \ell\nu X$	74
4.3.1	Cross section	75
4.3.2	Spin asymmetries	77
4.4	Transversity distribution	78
4.5	Numerical estimates for RHIC	79
4.6	Numerical estimates for a higher energy collider	81
4.7	Discussion	84
4.8	Summary	84
5	TMD effects in Higgs production	87
5.1	The Higgs transverse momentum distribution	88
5.1.1	Parameterization of the linearly polarized gluon distribution	92
5.1.2	Numerical predictions	93
5.1.3	Discussion	95
5.2	The diphoton transverse momentum distribution	95
5.2.1	Numerical predictions	98
5.2.2	Discussion	102
5.3	The $pp \rightarrow ZZ^*X \rightarrow 4\ell X$ transverse momentum distribution	102
5.3.1	Numerical predictions	107
5.3.2	Discussion	110
5.4	Summary and conclusions	110
6	Summary	113
A	Polarization vectors	117
A.1	Covariant form	117
A.1.1	Massless final state	118
A.1.2	Massive final state (with equal masses)	118
A.1.3	Massive final state (with unequal masses)	119
A.2	Useful contractions of polarization vectors	119
B	Frames	121
B.1	Equal mass final state	121
B.2	Unequal mass final state	124
B.3	Phase space	125
C	Helicity correlator	127
D	Weights & Convolutions	129
E	Partonic amplitudes	131
E.1	On-shell Higgs production	131
E.1.1	The process $gg \rightarrow H$	131
E.1.2	The process $gg \rightarrow A$	132

E.2	Diphoton production $gg \rightarrow \gamma\gamma$	133
E.2.1	The sub-process $gg \rightarrow H \rightarrow \gamma\gamma$	134
E.2.2	The sub-process $gg \rightarrow A \rightarrow \gamma\gamma$	135
E.2.3	The sub-process $gg \rightarrow \text{box} \rightarrow \gamma\gamma$	135
E.3	Z boson pair production $gg \rightarrow ZZ^*$	136
E.3.1	The sub-process $gg \rightarrow H \rightarrow ij$	137
E.3.2	The sub-process $gg \rightarrow A \rightarrow ij$	138
E.3.3	The sub-process $gg \rightarrow \text{box} \rightarrow ij$	140
F	Scalar integrals	143
	Nederlandse samenvatting	145
	Dankwoord	149
	Bibliography	151

List of publications

1. **“Linearly polarized Gluons and the Higgs Transverse Momentum Distribution”**
W. J. den Dunnen, D. Boer, C. Pisano, M. Schlegel and W. Vogelsang.
To appear in the proceedings of the 20th International Workshop on Deep-Inelastic Scattering and Related Subjects (DIS 2012).
arXiv:1205.6931 [hep-ph]
2. **“Linearly Polarized Gluons and the Higgs Transverse Momentum Distribution”**
D. Boer, W. J. den Dunnen, C. Pisano, M. Schlegel and W. Vogelsang.
arXiv:1109.1444 [hep-ph]
Phys. Rev. Lett. **108**, 032002 (2012)
3. **“Impact of Double TMD Effects on Transversity Measurements at RHIC”**
W. J. den Dunnen, D. Boer and A. Kotzinian.
To appear in the proceedings of the 19th International Workshop on Deep-Inelastic Scattering and Related Subjects (DIS 2011).
arXiv:1106.6164 [hep-ph]
4. **“Double Sivers effect asymmetries and their impact on transversity measurements at RHIC”**
D. Boer, W. J. den Dunnen and A. Kotzinian.
arXiv:1103.0908 [hep-ph]
Phys. Rev. D **83**, 114032 (2011)
5. **“Bounding W-W’ Mixing with Spin Asymmetries at RHIC”**
D. Boer and W. J. den Dunnen.
arXiv:1005.2956 [hep-ph]
Phys. Rev. Lett. **105**, 071801 (2010)

Chapter 1

Introduction

All of the more than 60 million [1] known chemical substances are built from no more than 118 smaller building blocks called chemical elements or *atoms*. By combining different atoms into different structures, matter with a vast variety of distinctive properties can be made. Just like Lego bricks, relatively few building blocks are sufficient to provide an astronomical versatility of products.

Zooming in on atoms, we see that all of the 118 known chemical elements are made of just *three* different fundamental particles: the electron, the up-quark and the down-quark. The quarks arrange themselves into protons and neutrons, which make up the nucleus of an atom, and the electrons form a cloud that surrounds the nucleus. By looking at smaller and smaller distances, the 60 million different forms of matter are reduced to just three fundamental building blocks.

In particle physics, the scientific discipline that investigates the smallest, most fundamental building blocks of matter, the guiding principle therefore is: when going to *smaller and smaller distance scales*, which corresponds to *higher and higher energy scales*, nature becomes *simpler and simpler*. The smaller the distance scale and the higher the energy, the less different forms of matter and the more *symmetry* nature has. It is therefore believed that nature is most easily described by a simple high energy theory that describes nature on very small distance scales, out of which all the low energy and large scale phenomena can be derived.

In their quest to study nature at higher and higher energy and thus smaller and smaller distance scales, particle physicists have built particle *accelerators*, that speed up particles to very high energies, to let them collide head on. Progress in particle physics has been relying on the ever-increasing collision energy (and size) of these accelerators. Figure 1.1 provides an overview of recent *electron-positron* and *hadron colliders* (the latter collide either protons with protons or protons with *anti-protons*).

Hadron colliders have traditionally been the machines that deliver the highest energetic collisions. Electron-positron colliders are limited in their center of mass energy in a circular accelerator by the loss of energy per turn through synchrotron radiation and in a linear accelerator by the limited length. Hadron colliders do not suffer as severely from this synchrotron radiation, as the energy loss per unit time is inversely proportional to the mass of the accelerated particle to the fourth power and the proton is approximately 2000 times as heavy as an electron. The energy frontier has, therefore, mostly been set by hadron colliders and *is* set at this moment by CERN's Large Hadron Collider (LHC).

On the other hand, electron-positron colliders provide the cleanest data. Electrons and

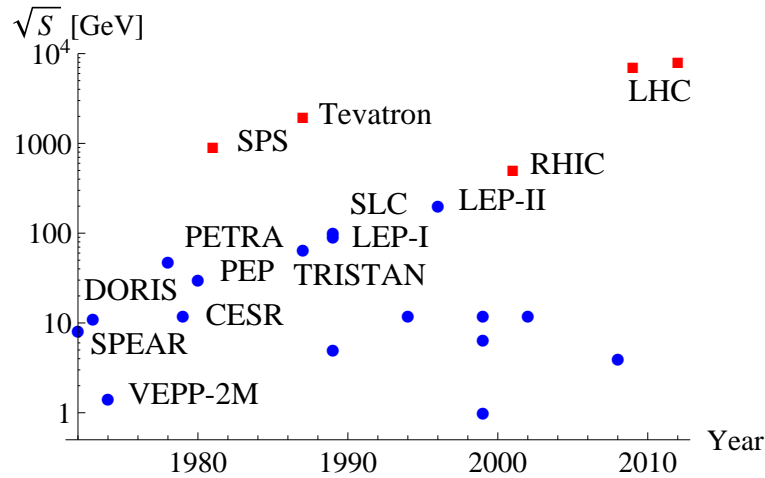


Figure 1.1: The center of mass energy of electron-positron (blue circles) and hadron (red squares) colliders as a function of the year of first operation.

positrons are fundamental particles and well understood within the Standard Model (SM) of particle physics. The proton, on the contrary, is a bound state of quarks held together by the strong interaction, which is described by *Quantum Chromo Dynamics* (QCD). This theory is too complicated to solve analytically and can only be handled within a certain approximation scheme that is called perturbation theory. Unfortunately, perturbation theory breaks down at the energy scales where quarks form bound states and thus the exact structure of a proton cannot be calculated. As a result, it is impossible, at this time at least, to calculate from first principles the chance that a proton-proton collision will end in a given final state, e.g., in 4 protons, 2 anti-protons, 8 neutral pions and a muon pair. This chance is related to what is called an *exclusive* cross section. In fact, it is not even possible to calculate from first principles an *inclusive* cross section (for example the chance that *at least* a muon pair is created in the collision). These problems make it much harder to interpret data from a proton-proton collider than from an electron-positron collider and the latter has therefore been the preferred choice for *precision* experiments, whereas the first is preferred for the *discovery* of new particles, where maximal collision energy is desired.

At this moment, the only high-energy colliders that are running are CERN's LHC (Figure 1.2) and Brookhaven National Laboratory's Relativistic Heavy Ion Collider (RHIC) (Figure 1.3), which are both proton-proton colliders. The LHC holds the world record for highest collision energy ($\sqrt{s} = 8$ TeV), whereas RHIC ($\sqrt{s} = 0.5$ TeV) is the only machine that has the ability to collide *polarized* protons. To interpret the results of these proton-proton colliders, it is necessary to compare the experimental data to theoretical predictions, which will be the subject of this thesis. To be able to make predictions, the proton is usually treated as a collection of *partons* (quarks, anti-quarks and gluons) each moving collinearly with the proton and carrying a fraction x of its momentum. The number of partons carrying a specific fraction of the proton's momentum is described by so called *parton distribution functions*, which, as they cannot be calculated, have to be measured. This is the way most theoretical predictions are made today.

There are, however, many observables that are sensitive to the transverse motion of the



Figure 1.2: Large Hadron Collider at CERN: the world’s most powerful particle collider, viewed from inside the tunnel (left) and an aerial view (right).



Figure 1.3: Relativistic Heavy Ion Collider at Brookhaven National Laboratory: the only place in the world where *polarized* protons can be collided, viewed from inside the tunnel (left) and an aerial view (right).

partons inside the proton. An example is the *transverse momentum distribution* of the produced particles. To describe such an observable well at all scales, we need to go beyond the collinear approximation, which is more specifically the subject of this thesis. The theory needed for this, *Transverse Momentum Dependent (TMD) factorization*, has been developed (and improved) over the years and will be discussed in Chapter 2.

The inclusion of the transverse motion of the partons in a proton gives rise to interesting ‘new’ QCD effects such as, for example, the Sivers, worm-gear and Boer-Mulders effect. These are all effects due to spin-momentum correlations and described by their own distribution functions. For example, the Sivers function describes an asymmetry in the transverse momentum distribution of quarks with respect to the proton’s transverse spin (see Figure 1.4). The worm-gear distribution expresses a correlation between the quark’s helicity and the angle between its transverse momentum and the proton’s transverse spin (see Figure 1.5). Also for gluons there are new correlation functions, such as the *linearly polarized gluon distribution*, that describes the linear polarization of the gluon field as a function of the gluon’s transverse momentum in an unpolarized proton (see Figure 1.6). To put it briefly, there are many new effects that are absent in the collinear treatment, of which we will investigate a couple we think might be experimentally relevant.



Figure 1.4: The Sivers effect describes a transverse momentum distribution that is anti-symmetric with respect to the proton's spin direction.



Figure 1.5: The worm-gear effect describes a correlation between the quark chirality and the angle between its transverse momentum and the proton's transverse spin direction.

What might be relevant, for example, is the linear polarization of gluons inside an unpolarized hadron as the Standard Model Higgs boson is mainly produced from gluons at the LHC. We will investigate the consequences of this polarization in Chapter 5. It is found that the transverse momentum distribution of scalar and pseudoscalar bosons produced through gluon-gluon fusion is modified in distinctive ways. This is an interesting result as the transverse momentum distribution of the newly found boson at the LHC might thus tell us whether it can be the Standard Model Higgs boson or it has to be some pseudoscalar boson predicted by physics beyond the SM.

TMD effects could therefore help in the search for physics beyond the SM, but they can also be mistaken for it. For example, double transverse spin asymmetries in W boson production, which can be investigated at RHIC, are zero within the SM using the collinear treatment, but nonzero once transverse momentum dependent effects are taken into account. Another source of these spin asymmetries could be the mixing of a hypothetical W_R boson, with the ordinary W boson, that happens, for example, in so called Left-Right models. TMD and beyond the SM effects thus give rise to the same signatures in the data and can be mistaken for each other. We will therefore estimate the double transverse spin asymmetries that arise in W boson



Figure 1.6: The linearly polarized gluon distribution describes the difference in gluon field polarization in the direction of the gluons' transverse momentum and the direction perpendicular to it.

production as a result of TMD effects in Chapter 3. The same TMD effects form a background for transversity measurements using the Drell-Yan process, for which we will also give numerical predictions.

The fact that double transverse spin asymmetries in W boson production are sensitive to a possible mixing of the ordinary W boson with a hypothetical W_R boson led us to investigate the possibility of measuring or bounding this mixing using spin asymmetries at RHIC. Given the best model independent bounds from the particle data group on the right-handed coupling of the W boson to the light quarks, at that time, it was concluded that RHIC could set competitive bounds if design goals would be met. In the meantime better bounds can be extracted from the literature, which will be explained in Chapter 4. Updated numerical predictions for the asymmetries at RHIC and possible future higher energy polarized colliders will be given.

The work and results of this thesis will be summarized in Chapter 6.

Chapter 2

Factorized description of $pp \rightarrow VX$

With factorization in hadronic collisions we mean the process of separating a high-energy scattering cross section into a *calculable* part and a part that needs to be *measured*. This latter part describes the structure of the hadron, which inevitably is a low-energy observable that falls outside the paradigm of perturbative QCD. The calculable part can be calculated using standard perturbative methods and used to test the high-energy model of your choice. In this thesis we will focus on inclusive W , Z and Higgs boson production from proton-proton collisions (usually followed by a decay) which we will refer to as $pp \rightarrow VX$.

In obtaining a factorized description, we have to treat (anti-) quark gluon scattering, quark-antiquark annihilation and gluon-gluon fusion separately. Of these, only the latter two will be relevant in this thesis and are discussed separately in the remaining two sections of this chapter.

2.1 Quark-antiquark annihilation

Within the context of quantum field theory, the leading order α_s contribution from quark-antiquark annihilation to the $pp \rightarrow VX$ hadronic scattering matrix element can be written as

$$\mathcal{M}\delta^4(P_1 + P_2 - P_X - q) = \int \frac{d^4k}{(2\pi)^4} \frac{d^4p}{(2\pi)^4} \int d^4\xi_2 d^4\xi_1 \delta^4(p + k - q) e^{ik \cdot \xi_2} e^{ip \cdot \xi_1} \times \\ H_{ij}(p, k, q) \langle X | \bar{\Psi}_i(\xi_2) \Psi_j(\xi_1) | P_1, S_1, P_2, S_2 \rangle, \quad (2.1)$$

where H is the leading order $q\bar{q} \rightarrow V$ scattering amplitude. We assume that the matrix element

$$\langle X | \bar{\Psi}_i(\xi_2) \Psi_j(\xi_1) | P_1, S_1, P_2, S_2 \rangle$$

factorizes into two separate matrix elements $\langle X_2 | \bar{\Psi}_i(\xi_2) | P_2, S_2 \rangle$ and $\langle X_1 | \bar{\Psi}_j(\xi_1) | P_1, S_1 \rangle$, that describe a transition between an initial state with an incoming proton with momentum P_i and spin S_i and a final state containing the hadronic remnant X_i . The $pp \rightarrow VX$ scattering matrix element can within that approximation be written as

$$\mathcal{M}\delta^4(P_1 + P_2 - P_{X_1} - P_{X_2} - q) = \int \frac{d^4k}{(2\pi)^4} \int d^4\xi_2 e^{ik \cdot \xi_2} \langle X_2 | \bar{\Psi}_i(\xi_2) | P_2, S_2 \rangle \times \\ \int \frac{d^4p}{(2\pi)^4} \int d^4\xi_1 e^{ip \cdot \xi_1} \langle X_1 | \Psi_j(\xi_1) | P_1, S_1 \rangle \delta^4(p + k - q) H_{ij}(p, k, q), \quad (2.2)$$

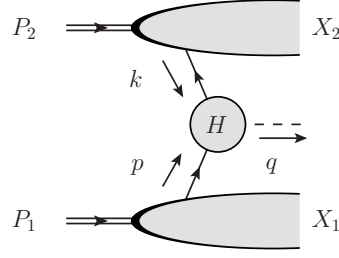


Figure 2.1: Diagrammatic representation of factorization of the quark–antiquark annihilation contribution to the $pp \rightarrow VX$ scattering matrix element.

which is depicted diagrammatically in Figure 2.1. In principle, the quark operator Ψ should also have a label indicating the quark flavor, u , d or s , but we will suppress this index for the sake of clarity. In the hypothetical situation that there would be no strong interaction and the initial state would consist of just a quark and an antiquark, the transition matrix elements would reduce simply to the spinors u and v , i.e.,

$$\begin{aligned} \int d^4\xi_2 e^{ik \cdot \xi_2} \langle X_2 | \bar{\Psi}_i(\xi_2) | P_2, S_2 \rangle &\rightarrow \bar{v}_i(k) \delta^4(P_2 - k), \\ \int d^4\xi_1 e^{ip \cdot \xi_1} \langle X_1 | \Psi_j(\xi_1) | P_1, S_1 \rangle &\rightarrow u_j(p) \delta^4(P_1 - p) \end{aligned} \quad (2.3)$$

and the matrix element would have the form familiar from Quantum Electro-Dynamics (QED),

$$\mathcal{M} \delta^4(P_1 + P_2 - q) = \bar{v}_i(k) H_{ij}(p, k, q) u_j(p) \delta^4(P_1 + P_2 - q). \quad (2.4)$$

Using the expression for the $pp \rightarrow VX$ matrix element, we can write the cross section for inclusive V production as

$$\begin{aligned} \frac{d\sigma}{d\mathcal{R}} &= \frac{(2\pi)^4}{2S} \sum_{X_1, X_2} \int \frac{d^3P_{X_1}}{(2\pi)^3 2E_{P_{X_1}}} \frac{d^3P_{X_2}}{(2\pi)^3 2E_{P_{X_2}}} |\mathcal{M}|^2 \delta^4(P_1 + P_2 - P_{X_1} - P_{X_2} - q) \\ &= \frac{(2\pi)^4}{2S} \int \frac{d^4k}{(2\pi)^4} \frac{d^4k'}{(2\pi)^4} \sum_{X_2} \int \frac{d^3P_{X_2}}{(2\pi)^3 2E_{P_{X_2}}} \int d^4\xi_2 d^4\eta_2 e^{ik \cdot \xi_2 - ik' \cdot \eta_2} \times \\ &\quad \langle P_2, S_2 | \Psi_k(\eta_2) | X_2 \rangle \langle X_2 | \bar{\Psi}_i(\xi_2) | P_2, S_2 \rangle \times \\ &\quad \int \frac{d^4p}{(2\pi)^4} \frac{d^4p'}{(2\pi)^4} \sum_{X_1} \int \frac{d^3P_{X_1}}{(2\pi)^3 2E_{P_{X_1}}} \int d^4\xi_1 d^4\eta_1 e^{ip \cdot \xi_1 - ip' \cdot \eta_1} \times \\ &\quad \langle P_1, S_1 | \bar{\Psi}_l(\eta_1) | X_1 \rangle \langle X_1 | \Psi_j(\xi_1) | P_1, S_1 \rangle \delta^4(p + k - q) H_{ij}(p, k, q) H_{kl}^*(p, k, q), \end{aligned} \quad (2.5)$$

where the n -particle phase space element is defined as

$$d\mathcal{R} \equiv \prod_{i=1}^n \frac{d^3\mathbf{q}_i}{(2\pi)^3 2E_{q_i}}. \quad (2.6)$$

The expression for the cross section is depicted diagrammatically in Figure 2.2. The next step

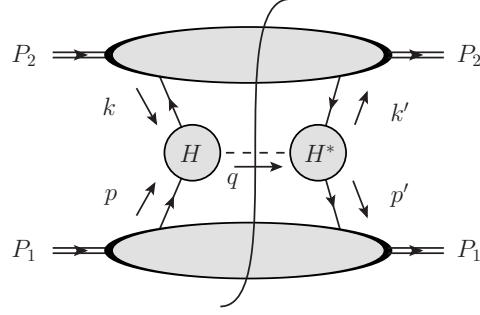


Figure 2.2: Diagrammatic representation of the quark–antiquark annihilation contribution to the $pp \rightarrow VX$ cross section.

is to use the fact that the projection on all possible remnant states X , is nothing but the unit operator, i.e.,

$$\sum_X \int \frac{d^3 P_X}{(2\pi)^3 2E_{P_X}} |X\rangle \langle X| = 1. \quad (2.7)$$

Replacing the sum over remnant states in the expression for the cross section, we get

$$\begin{aligned} \frac{d\sigma}{d\mathcal{R}} &= \frac{(2\pi)^4}{2S} \int \frac{d^4 k}{(2\pi)^4} \frac{d^4 k'}{(2\pi)^4} \int d^4 \xi_2 d^4 \eta_2 e^{ik \cdot \xi_2 - ik' \cdot \eta_2} \langle P_2, S_2 | \bar{\Psi}_k(\eta_2) \bar{\Psi}_i(\xi_2) | P_2, S_2 \rangle \times \\ &\int \frac{d^4 p}{(2\pi)^4} \frac{d^4 p'}{(2\pi)^4} \int d^4 \xi_1 d^4 \eta_1 e^{ip \cdot \xi_1 - ip' \cdot \eta_1} \langle P_1, S_1 | \bar{\Psi}_l(\eta_1) \Psi_j(\xi_1) | P_1, S_1 \rangle \times \\ &\delta^4(p + k - q) H_{ij}(p, k, q) H_{kl}^*(p, k, q). \end{aligned} \quad (2.8)$$

We now got rid of the transition matrix elements between an incoming proton and an unknown final state X in favor of an ‘ordinary’ matrix element of two quark fields between a well-defined proton state, which we will refer to as a *quark correlator*.

The following simplifying step will be based on the fact that the matrix element should be translation invariant. In other words, the matrix element should only depend on the *difference* of the positions of the quark fields, so

$$\begin{aligned} &\int d^4 \xi d^4 \eta e^{ip \cdot \xi - ip' \cdot \eta} \langle P, S | \bar{\Psi}_l(\eta) \Psi_j(\xi) | P, S \rangle \\ &= \int d^4(\xi + \eta) d^4(\xi - \eta) e^{\frac{i}{2}(p+p') \cdot (\xi - \eta) + \frac{i}{2}(p-p') \cdot (\xi + \eta)} \langle P, S | \bar{\Psi}_l(\eta) \Psi_j(\xi) | P, S \rangle \\ &= \int d^4(\xi - \eta) e^{\frac{i}{2}(p+p') \cdot (\xi - \eta)} \delta^4(p - p') (2\pi)^4 \langle P, S | \bar{\Psi}_l(\eta) \Psi_j(\xi) | P, S \rangle \\ &= \delta^4(p - p') (2\pi)^4 \int d^4 \xi e^{ip \cdot \xi} \langle P, S | \bar{\Psi}_l(0) \Psi_j(\xi) | P, S \rangle. \end{aligned} \quad (2.9)$$

Inserting this simplified form of the quark correlator into the expression for the cross section,

we get

$$\begin{aligned}
\frac{d\sigma}{d\mathcal{R}} &= \frac{(2\pi)^4}{2S} \int \frac{d^4k}{(2\pi)^4} \int d^4\xi_2 e^{ik \cdot \xi_2} \langle P_2, S_2 | \Psi_k(0) \bar{\Psi}_i(\xi_2) | P_2, S_2 \rangle H_{ij}(p, k, q) H_{kl}^*(p, k, q) \times \\
&\quad \int \frac{d^4p}{(2\pi)^4} \int d^4\xi_1 e^{ip \cdot \xi_1} \langle P_1, S_1 | \bar{\Psi}_l(0) \Psi_j(\xi_1) | P_1, S_1 \rangle \delta^4(p + k - q) \\
&= \frac{(2\pi)^4}{2S} \int d^4k d^4p \delta^4(p + k - q) \text{Tr} [H(p, k, q) \Phi(p, P_1, S_1) H^*(p, k, q) \bar{\Phi}(k, P_2, S_2)],
\end{aligned} \tag{2.10}$$

where, in the last step, we have defined the quark and antiquark correlators, Φ and $\bar{\Phi}$, as

$$\begin{aligned}
\Phi_{ij}(k, P, S) &\equiv \frac{1}{(2\pi)^4} \int d^4\xi e^{ik \cdot \xi} \langle P, S | \Psi_i(\xi) \bar{\Psi}_j(0) | P, S \rangle, \\
\bar{\Phi}_{ij}(k, P, S) &\equiv \frac{1}{(2\pi)^4} \int d^4\xi e^{ik \cdot \xi} \langle P, S | \Psi_i(0) \bar{\Psi}_j(\xi) | P, S \rangle.
\end{aligned} \tag{2.11}$$

The function $\Phi_{ij}(k, P, S)$ is called a *fully unintegrated quark correlator*. In most applications one can work with partially integrated correlators, because the incoming partons are almost collinear to the incoming hadrons and therefore

$$\begin{aligned}
k \cdot P_1 &\gg p \cdot P_1, \\
p \cdot P_2 &\gg k \cdot P_2.
\end{aligned} \tag{2.12}$$

This hierarchy allows us to approximate the delta function as

$$\begin{aligned}
\delta^4(p + k - q) &= P_1 \cdot P_2 \delta((p + k - q) \cdot P_1) \delta((p + k - q) \cdot P_2) \delta^2(\mathbf{p}_T + \mathbf{k}_T - \mathbf{q}_T) \\
&\simeq P_1 \cdot P_2 \delta(k \cdot P_1 - q \cdot P_1) \delta(p \cdot P_2 - q \cdot P_2) \delta^2(\mathbf{p}_T + \mathbf{k}_T - \mathbf{q}_T).
\end{aligned} \tag{2.13}$$

After insertion of the approximated delta function and rewriting the phase space element as

$$\int d^4p = \frac{1}{\sqrt{(P_1 \cdot P_2)^2 - M_1^2 M_2^2}} \int d(p \cdot P_1) d(p \cdot P_2) d^2\mathbf{p}_T \simeq \frac{2}{S} \int d(p \cdot P_1) d(p \cdot P_2) d^2\mathbf{p}_T \tag{2.14}$$

one can write the cross section in terms of partially integrated correlation functions $\Phi(x, \mathbf{p}_T, P, S)$ and $\bar{\Phi}(x, \mathbf{p}_T, P, S)$,

$$\begin{aligned}
\frac{d\sigma}{d\mathcal{R}} &= \frac{(2\pi)^4}{S^2} \int d(k \cdot P_1) d(p \cdot P_2) d^2\mathbf{p}_T d^2\mathbf{k}_T \delta(k \cdot P_1 - q \cdot P_1) \delta(p \cdot P_2 - q \cdot P_2) \times \\
&\quad \delta^2(\mathbf{p}_T + \mathbf{k}_T - \mathbf{q}_T) \text{Tr} [H(p, k, q) \Phi(x_1, \mathbf{p}_T, P_1, S_1) H^*(p, k, q) \bar{\Phi}(x_2, \mathbf{k}_T, P_2, S_2)], \\
&= \frac{(2\pi)^4}{S^2} \int dx_1 dx_2 d^2\mathbf{p}_T d^2\mathbf{k}_T \delta\left(x_1 - \frac{q \cdot P_2}{P_1 \cdot P_2}\right) \delta\left(x_2 - \frac{q \cdot P_1}{P_1 \cdot P_2}\right) \delta^2(\mathbf{p}_T + \mathbf{k}_T - \mathbf{q}_T) \\
&\quad \text{Tr} [H(p, k, q) \Phi(x_1, \mathbf{p}_T, P_1, S_1) H^*(p, k, q) \bar{\Phi}(x_2, \mathbf{k}_T, P_2, S_2)],
\end{aligned} \tag{2.15}$$

in which we have defined

$$\begin{aligned}
x_1 &\equiv \frac{p \cdot P_2}{P_1 \cdot P_2}, \\
x_2 &\equiv \frac{k \cdot P_1}{P_1 \cdot P_2}.
\end{aligned} \tag{2.16}$$

The x_1 and x_2 integrations can also be performed to remove the delta functions, i.e.,

$$\frac{d\sigma}{d\mathcal{R}} = \frac{(2\pi)^4}{S^2} \int d^2\mathbf{p}_T d^2\mathbf{k}_T \delta^2(\mathbf{p}_T + \mathbf{k}_T - \mathbf{q}_T) \times \text{Tr} [H(p, k, q) \Phi(x_1, \mathbf{p}_T, P_1, S_1) H^*(p, k, q) \bar{\Phi}(x_2, \mathbf{k}_T, P_2, S_2)], \quad (2.17)$$

with the correlators now evaluated at $x_1 = \frac{q \cdot P_2}{P_1 \cdot P_2}$ and $x_2 = \frac{q \cdot P_1}{P_1 \cdot P_2}$. The partially integrated correlation function is defined as

$$\begin{aligned} \Phi_{ij}(x, \mathbf{p}_T, P, S) &\equiv \int d(p \cdot P) \Phi_{ij}(p, P, S) \\ &= \int \frac{d(\xi \cdot P) d^2\xi_T}{(2\pi)^3} e^{ip \cdot \xi} \langle P, S | \Psi_i(\xi) \bar{\Psi}_j(0) | P, S \rangle \Big|_{\text{LF}}, \end{aligned} \quad (2.18)$$

where, in the right-hand side, the momentum p is parameterized as

$$p = \frac{x(P \cdot P')^2 - M^2(p \cdot P)}{(P \cdot P')^2 - M^4} P + p_T + \frac{[(p \cdot P) - xM^2]P \cdot P'}{(P \cdot P')^2 - M^4} P', \quad (2.19)$$

in which P' is an arbitrary vector not collinear to P that sets the transverse direction and can be taken as the momentum of the opposite proton or as $P' = (P^0, -\mathbf{P})$. In the second line of Eq. (2.18) the fields should be evaluated at the light-front, which is specified by

$$\xi \cdot P' = \xi \cdot P \frac{M^2}{P \cdot P'}. \quad (2.20)$$

Although the appearance of P' in the parameterization of the momentum, the correlator does not explicitly depend on it as

$$p \cdot \xi = xP \cdot \xi + p_T \cdot \xi_T, \quad (2.21)$$

it only sets the direction of the transverse plane. In the limit of vanishing proton mass the momentum parameterization simply reduces to

$$p = xP + p_T + \frac{p \cdot P}{P \cdot P'} P' \quad (2.22)$$

and the light-front condition becomes $\xi \cdot P' = 0$.

The correlator in Eq. (2.18) is also referred to as a *Transverse Momentum Dependent (TMD) correlation function*, because it depends on the parton's transverse momentum \mathbf{p}_T , in contrast to the so called collinear correlation function, which will be introduced in the next section.

Collinear case

If one is only interested in the *total* cross section for the process $PP \rightarrow VX$ and not in the differential cross section $d\sigma/d^2\mathbf{q}_T$, then one can write the cross section in terms of *collinear correlation functions*. Suppose we consider the production of some final state with four momentum q not necessarily on-shell. The phase space for such a process is given by

$$d\mathcal{R} = \frac{d^4q}{(2\pi)^4} = \frac{1}{2(2\pi)^4} dQ^2 dY d^2\mathbf{q}_T, \quad (2.23)$$

where $Q \equiv \sqrt{q^2}$, Y is the forward rapidity and \mathbf{q}_T the transverse momentum of the final state. The \mathbf{q}_T integrated cross section, differential in only Q and Y , can be given as

$$\begin{aligned} \frac{d\sigma}{dQ^2 dY} &= \frac{1}{2(2\pi)^4} \int d^2\mathbf{q}_T \frac{d\sigma}{d\mathcal{R}} \\ &= \frac{1}{2S^2} \text{Tr} \left[H_0 \left[\int d^2\mathbf{p}_T \Phi(x_1, \mathbf{p}_T, P_1, S_1) \right] H_0^* \left[\int d^2\mathbf{k}_T \bar{\Phi}(x_2, \mathbf{k}_T, P_2, S_2) \right] \right] \\ &= \frac{1}{2S^2} \text{Tr} [H_0 \Phi(x_1, P_1, S_1) H_0^* \bar{\Phi}(x_2, P_2, S_2)], \end{aligned} \quad (2.24)$$

where H_0 is the first order term in the collinear expansion of the hard matrix element,

$$H = H_0 + \mathbf{H}_1 \cdot \mathbf{q}_T + \mathbf{q}_T \cdot H_2 \mathbf{q}_T + \dots, \quad (2.25)$$

and $\Phi(x, P, S)$ is called a *collinear correlation function* and is defined by

$$\begin{aligned} \Phi_{ij}(x, P, S) &\equiv \int d^2\mathbf{p}_T \Phi_{ij}(x, \mathbf{p}_T, P, S) \\ &= \int \frac{d(\xi \cdot P)}{2\pi} e^{ix\xi \cdot P} \langle P, S | \Psi_i(\xi) \bar{\Psi}_j(0) | P, S \rangle \Big|_{\xi \cdot P' = \xi_T = 0}. \end{aligned} \quad (2.26)$$

The collinear correlator only depends on the longitudinal momentum fraction x and not on the transverse momentum of the parton.

The convergences of the series in Eq. (2.25) is determined by the available energy scales in the hard part. For Drell-Yan ($pp \rightarrow \gamma X \rightarrow \ell\bar{\ell}X$) the only compensating scale is Q and higher order terms are therefore suppressed by factors q_T/Q . In other processes the convergence might be worse, e.g., in W boson production in specific kinematical ranges, the suppression might be as small as q_T/Γ_W , where Γ_W is the width of the W boson. We will encounter this effect in Chapter 3. Higher order terms in the collinear expansion can also be included, which will lead to an expression involving \mathbf{p}_T weighted correlation functions.

Another regime of validity of the collinear approximation is high- q_T vector boson production. The large transverse momentum of the vector boson is generated by hard gluon radiation from an incoming parton, which is a higher order correction to the hard scattering amplitude. In that case the *total* transverse momentum of the final state is not observed (one integrates over the gluon transverse momentum), which can be used to remove the delta function. Furthermore, all the scales in the hard part are large ($q_T \sim Q \gg M$), which makes it possible to expand the hard part in $1/Q$ and $1/q_T$, of which the leading terms will not contain any \mathbf{p}_T or \mathbf{k}_T dependence and so those integrations can be performed, leading to an expression in terms of collinear correlators.

2.1.1 Inclusion of the gauge link

In the last section we derived an expression for the quark–antiquark annihilation contribution to the $pp \rightarrow VX$ cross section, factorized into a calculable hard part and two correlation functions, which parameterize the unknown low energy (soft) physics which we cannot calculate. In the derivation, we only took the leading order diagram, without any additional gluons coming from the soft part. One should, however, sum all diagrams with additional gluons, a couple of which are shown in figure 2.3. Note that the momentum transfer in the additional gluons is not necessarily large and one can thus not discard those diagrams on the basis of being higher

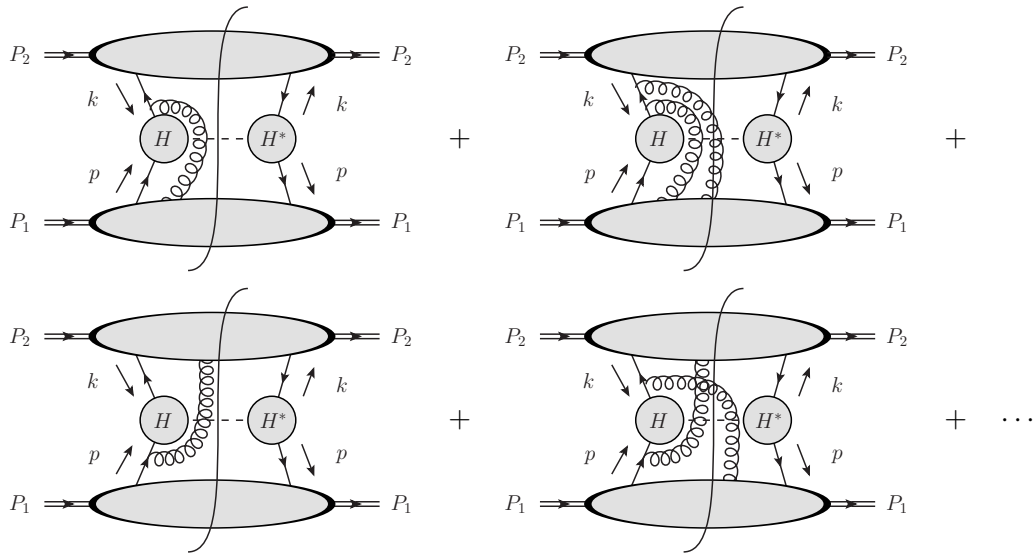


Figure 2.3: Diagrams with additional gluons that need to be included in the quark–antiquark annihilation channel in $pp \rightarrow VX$.

order in α_s . On the contrary, a diagram as in Figure 2.4 *would* be considered a higher order α_s correction to the hard scattering matrix element. In principle, every diagram in Figure 2.3 enters with its own matrix element, involving two quark fields and one or more gluon fields between the proton states. It is shown [2, 3, 4, 5], that the sum of all diagrams exponentiates

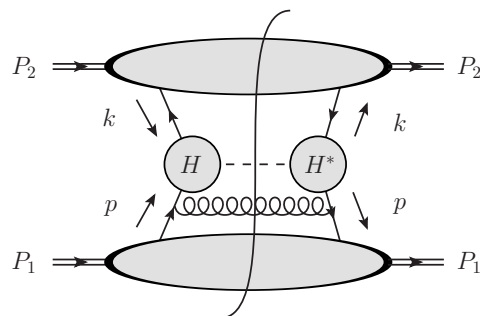


Figure 2.4: Example of a higher order α_s correction to the hard scattering matrix element in the quark–antiquark annihilation channel in $pp \rightarrow VX$.

and can be written as¹

$$\begin{aligned}
d\sigma_{DY} &\sim \text{Tr} \left[\Phi(x_1, \mathbf{p}_T, P_1, S_1) U_-^{[n]}[p_2] H^* U_-^{[n]\dagger}[p_1] \bar{\Phi}(x_2, \mathbf{k}_T, P_2, S_2) U_-^{[n]}[p_2] H U_-^{[n]\dagger}[p_2] \right] \\
&= \int d(p_1 \cdot P_1) d(p_2 \cdot P_2) d^4\xi_1 d^4\xi_2 e^{ip_1 \cdot \xi_1} e^{ip_2 \cdot \xi_2} \times \\
&\quad \text{Tr} \left[\langle P_1, S_1 | \Psi(\xi_1) \bar{\Psi}(0) | P_1, S_1 \rangle U_{2[\infty_T, 0_T]}^{[T]} U_{2[-\infty, 0]}^{[n]} H^* U_{1[0, -\infty]}^{[n]} U_{1[0_T, \infty_T]}^{[T]} \times \right. \\
&\quad \left. \langle P_2, S_2 | \Psi(0) \bar{\Psi}(\xi_2) | P_2, S_2 \rangle U_{1[\infty_T, \xi_{1T}]}^{[T]} U_{1[-\infty, \xi_1]}^{[n]} H U_{2[\xi_2, -\infty]}^{[n]} U_{2[\xi_{2T}, \infty_T]}^{[T]} \right], \quad (2.27)
\end{aligned}$$

where $U_{i[a,b]}^{[n]}$ is a *gauge connection*, defined by

$$U_{i[a,b]}^{[n]} \equiv \mathcal{P} \exp \left(-ig \int_{a \cdot P_i}^{b \cdot P_i} d(\eta \cdot P_i) A_i^n(\eta) \right). \quad (2.28)$$

The gauge connection $U_{i[a,b]}^{[n]}$ has the path of the integral along the n -direction, which is an (approximately) light-like vector conjugate to P_i . The transverse part of the gauge connection, $U_{i[a,b]}^{[T]}$, has its path along the transverse direction from a to b . The gauge connections contain gluon field operators A_i^μ , which should be placed within one of the two correlators to be meaningful. Here it is the i index on A_i^μ , that indicates that the field operator should be placed within correlator $\langle P_i, S_i | \dots | P_i, S_i \rangle$. Note that $A_i^\mu = A_{ia}^\mu T^a$ and can, therefore, not simply be moved through the color trace into the right correlator. The symbol \mathcal{P} in the connection means path ordered product, just like the ordinary time ordering symbol, but now with ordering along the path. The trace in Eq. (2.27) has to be taken over both Dirac and color indices. Eq. (2.27) takes into account the effect of all the additional gluons shown diagrammatically in figure 2.5 that contribute to leading order in $1/Q$, where Q is the hard scale of the process. The expression

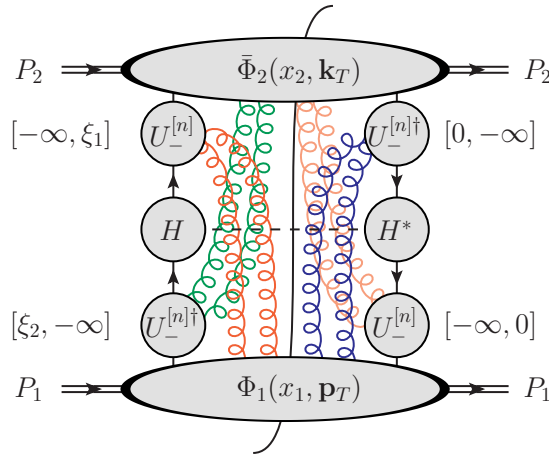


Figure 2.5: Diagram representing the sum of all additional gluon contributions in terms of the gauge connections U .

in Eq. (2.27) still consists of infinitely many different correlation functions, which are all gauge

¹We use the notation of Ref. [5].

dependent. However, Eq. (2.27) can be cast into a much simpler form by applying the gauge transformation $V(\xi) \equiv \mathcal{U}_{[0,\xi]}^{[-]}$, where $\mathcal{U}_{[0,\xi]}^{[-]}$ is a *gauge link*, defined by

$$\mathcal{U}_{[0,\xi]}^{[\pm]} \equiv \mathcal{P} \exp \left(-ig \int_0^\xi dz_\mu A^\mu(z) \right), \quad (2.29)$$

in which the path should be taken as is indicated in figure 2.6. The hard part H commutes with



Figure 2.6: The gauge link path for $\mathcal{U}_{[0,\xi]}^{[-]}$ (left) and $\mathcal{U}_{[0,\xi]}^{[+]}$ (right).

both the gauge links and connections, because it is proportional to a unit matrix in color space whereas the gauge links and connections are proportional to the unit matrix in Dirac space. After performing the gauge transformation and using the commutation relation, we can write the cross section as

$$\begin{aligned} d\sigma_{DY} \sim & \int d(p_1 \cdot P_1) d(p_2 \cdot P_2) d^4 \xi_1 d^4 \xi_2 e^{ip_1 \cdot \xi_1} e^{ip_2 \cdot \xi_2} \times \\ & \text{Tr} \left[\langle P_1 | \mathcal{U}_{[0,\xi_1]}^{[-]} \Psi(\xi_1) \bar{\Psi}(0) | P_1 \rangle H^* \underbrace{\mathcal{U}_{[0,\infty_T]}^{[-]} U_{2[\infty_T,0_T]}^{[T]} U_{2[-\infty,0]}^{[n]} U_{1[0,-\infty]}^{[n]} U_{1[0_T,\infty_T]}^{[T]} \mathcal{U}_{[\infty_T,0]}^{[-]} }_A \right. \\ & \langle P_2 | \Psi(0) \bar{\Psi}(\xi_2) \mathcal{U}_{[\xi_2,0]}^{[-]} | P_2 \rangle H \\ & \left. \underbrace{\mathcal{U}_{[0,\infty_T]}^{[-]} U_{1[\infty_T,\xi_1 T]}^{[T]} U_{1[-\infty,\xi_1]}^{[n]} \mathcal{U}_{[\xi_1,0]}^{[-]} \mathcal{U}_{[0,\xi_2]}^{[-]} U_{2[\xi_2,-\infty]}^{[n]} U_{2[\xi_2 T,\infty_T]}^{[T]} \mathcal{U}_{[\infty_T,0]}^{[-]} }_B \right], \quad (2.30) \end{aligned}$$

which looks worse than what we started with, but is in fact much simpler: the composite gauge links A and B , which are shown in figure 2.7, both start and stop at the same point and contain no loops, i.e., they are equal to unity. Using the fact that $A = B = 1$, we can write the cross

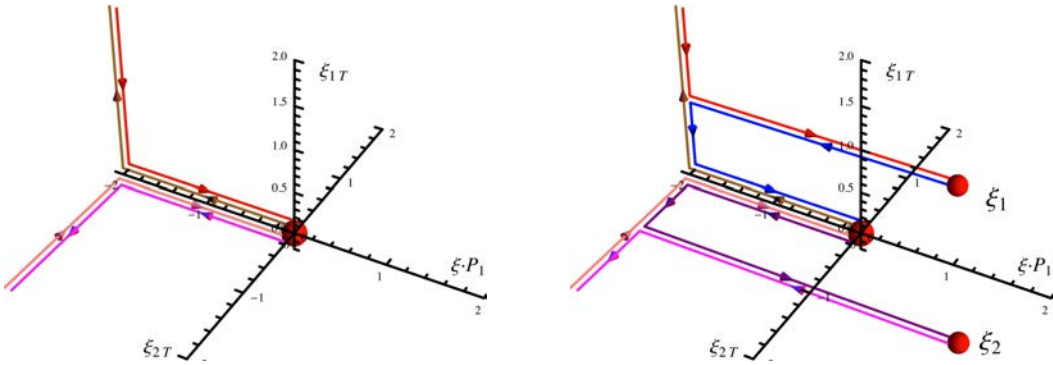


Figure 2.7: Structure of the composite gauge links A (left) and B (right) in Eq. (2.30).

section as

$$d\sigma_{DY} \sim \int d(p_1 \cdot P_1) d(p_2 \cdot P_2) d^4\xi_1 d^4\xi_2 e^{ip_1 \cdot \xi_1} e^{ip_2 \cdot \xi_2} \times \\ \text{Tr} \left[\langle P_1 | \mathcal{U}_{[0, \xi_1]}^{[-]} \Psi(\xi_1) \bar{\Psi}(0) | P_1 \rangle H^* \langle P_2 | \Psi(0) \bar{\Psi}(\xi_2) \mathcal{U}_{[\xi_2, 0]}^{[-]} | P_2 \rangle H \right], \quad (2.31)$$

which now has the right gauge link within both matrix elements. A correlator with the right gauge link is color gauge invariant, which one can see by inserting the unit operator, $1 = U^\dagger U$, with U a general gauge transformation, between all the operators in the matrix element, i.e.,

$$\langle P, S | \mathcal{U}_{[0, \xi]}^{[-]} \Psi(\xi) \bar{\Psi}(0) | P, S \rangle = \langle P, S | U^\dagger U \mathcal{U}_{[0, \xi]}^{[-]} U^\dagger U \Psi(\xi) \bar{\Psi}(0) U^\dagger U | P, S \rangle. \quad (2.32)$$

The proton state is color gauge invariant and, therefore,

$$U | P, S \rangle = | P, S \rangle, \\ \langle P, S | U^\dagger = \langle P, S |. \quad (2.33)$$

Furthermore, we know the gauge transformation properties of the link and quark fields,

$$U \mathcal{U}_{[0, \xi]}^{[-]} U^\dagger = V(0) \mathcal{U}_{[0, \xi]}^{[-]} V^\dagger(\xi), \\ U \Psi(\xi) = V(\xi) \Psi(\xi), \\ \bar{\Psi}(0) U^\dagger = \bar{\Psi}(0) V^\dagger(0), \quad (2.34)$$

where $V(\xi)$ is the gauge transformation at space-time point ξ in the fundamental representation. We can thus write

$$\langle P, S | \mathcal{U}_{[0, \xi]}^{[-]} \Psi(\xi) \bar{\Psi}(0) | P, S \rangle = \langle P, S | V(0) \mathcal{U}_{[0, \xi]}^{[-]} \underbrace{V^\dagger(\xi) V(\xi)}_{=1} \Psi(\xi) \bar{\Psi}(0) V^\dagger(0) | P, S \rangle \\ = V(0) \langle P, S | \mathcal{U}_{[0, \xi]}^{[-]} \Psi(\xi) \bar{\Psi}(0) | P, S \rangle V^\dagger(0), \quad (2.35)$$

which, in turn, implies that

$$\langle P, S | \mathcal{U}_{[0, \xi]}^{[-]} \Psi(\xi) \bar{\Psi}(0) | P, S \rangle \propto 1_c. \quad (2.36)$$

The trace in Eq. (2.31) can be split into a Dirac and color trace, of which the color trace can be split further, because of the correlators being proportional to the unit matrix in color space, i.e., we use the identity $\text{Tr}_c[1_c 1_c] = \frac{1}{N_c} \text{Tr}_c[1_c] \text{Tr}_c[1_c]$, to write

$$d\sigma_{DY} \sim \frac{1}{N_c} \text{Tr}_D \left[\text{Tr}_c \left[\int d(p_1 \cdot P_1) d^4\xi_1 e^{ip_1 \cdot \xi_1} \langle P_1 | \mathcal{U}_{[0, \xi_1]}^{[-]} \Psi(\xi_1) \bar{\Psi}(0) | P_1 \rangle \right] H^* \times \right. \\ \left. \text{Tr}_c \left[\int d(p_2 \cdot P_2) d^4\xi_2 e^{ip_2 \cdot \xi_2} \langle P_2 | \Psi(0) \bar{\Psi}(\xi_2) \mathcal{U}_{[\xi_2, 0]}^{[-]} | P_2 \rangle \right] H \right] \\ = \frac{1}{N_c} \text{Tr}_D \left[\Phi^{[-]}(x_1, \mathbf{p}_T, P_1, S_1) H^* \bar{\Phi}^{[-]}(x_2, \mathbf{k}_T, P_2, S_2) H \right]. \quad (2.37)$$

The final factorized expression we have arrived at, by including all the additional gluon exchanges, thus reads

$$\frac{d\sigma}{d\mathcal{R}} = \frac{(2\pi)^4}{S^2} \int d^2\mathbf{p}_T d^2\mathbf{k}_T \delta^2(\mathbf{p}_T + \mathbf{k}_T - \mathbf{q}_T) \times \frac{1}{N_c} \text{Tr}_D \left[\Phi^{[-]}(x_1, \mathbf{p}_T, P_1, S_1) H^* \bar{\Phi}^{[-]}(x_2, \mathbf{k}_T, P_2, S_2) H \right], \quad (2.38)$$

which has exactly the same form as the naive calculation in Eq. (2.17), but with the gauge-variant quark correlator replaced by a gauge *invariant* quark correlator with gauge link,

$$\begin{aligned} \Phi_{ij}^{[-]}(x, \mathbf{p}_T, P, S) &\equiv \int \frac{d(\xi \cdot P) d^2\xi_T}{(2\pi)^3} e^{ip \cdot \xi} \text{Tr}_c \left[\langle P, S | \mathcal{U}_{[0, \xi]}^{[-]} \Psi_i(\xi) \bar{\Psi}_j(0) | P, S \rangle \Big|_{n \cdot \xi = 0} \right] \\ &= \int \frac{d(\xi \cdot P) d^2\xi_T}{(2\pi)^3} e^{ip \cdot \xi} \langle P, S | \bar{\Psi}_j(0) \mathcal{U}_{[0, \xi]}^{[-]} \Psi_i(\xi) | P, S \rangle \Big|_{n \cdot \xi = 0}. \end{aligned} \quad (2.39)$$

There are still “subtleties” in the definition of the TMD correlator not discussed here, such as regularization of UV, IR and rapidity divergences. One can get rid of the latter one, by tilting the direction n of the gauge link to be not exactly on the light cone. The correlator gets in that case a dependence on the amount of tilt $\zeta = (p \cdot n)^2/n^2$, which serves as a rapidity cut-off on the gluons that are included in Figure 2.5. A full discussion on the operator definition of the TMD quark correlator is beyond the scope of this thesis, so for more information we refer to [6, 7, 8, 9, 10, 11, 12, 13].

Taking the subtleties in the operator definition into account, Eq. (2.39) gives a prescription to calculate the TMD correlator using lattice QCD, as has been done in, e.g., [14, 15]. Another way to handle the correlator is to parameterize the most general structure it can have, in terms of a limited set of distribution functions. These unknown functions are then considered as input, to be fitted from experimental data. This last route is the most common one and leads to the most accurate predictions. In section 2.2 the TMD correlation function is parameterized in terms of TMD distribution functions.

Process dependence

The quark correlator in Eq. (2.39), that has to be used for electroweak boson production in pp collisions, comes with the gauge link $\mathcal{U}_{[0, \xi]}^{[-]}$, which has its path running through minus infinity, as specified in Fig. 2.6. As it turns out to be, different processes need correlators with different gauge link paths. For example, in the process of Semi Inclusive Deep Inelastic Scattering (SIDIS) one has to use the $\Phi^{[+]}(x, \mathbf{p}_T)$ correlator [3, 4, 5], which has its link running through plus infinity (see figure 2.6). This process dependence is, in principle, a breaking of universality, because both correlators are, a priori, different. However, one can relate the two correlators by time reversal combined with parity inversion. To do so, add the unit operator² in the form of $(\mathcal{PT})^{-1}(\mathcal{PT})$, where \mathcal{P} is the parity inversion operator and \mathcal{T} the time reversal operator, between all operators

²Due to the anti-unitary character of \mathcal{T} , this will in fact produce the complex conjugate of the matrix element.

in the matrix element, i.e.,

$$\begin{aligned}
\Phi^{[-]}(x, \mathbf{p}_T, P, S) &= \int \frac{d(\xi \cdot P) d^2 \xi_T}{(2\pi)^3} e^{ip \cdot \xi} \langle P, S | \mathcal{U}_{[0, \xi]}^{[-]} \Psi(\xi) \bar{\Psi}(0) | P, S \rangle \Big|_{n \cdot \xi = 0} \\
&= \left(\int \frac{d(\xi \cdot P) d^2 \xi_T}{(2\pi)^3} e^{-ip \cdot \xi} \langle P, S | (\mathcal{PT})^{-1} (\mathcal{PT}) \mathcal{U}_{[0, \xi]}^{[-]} (\mathcal{PT})^{-1} \times \right. \\
&\quad \left. (\mathcal{PT}) \Psi(\xi) (\mathcal{PT})^{-1} (\mathcal{PT}) \bar{\Psi}(0) (\mathcal{PT})^{-1} (\mathcal{PT}) | P, S \rangle \Big|_{n \cdot \xi = 0} \right)^* \quad (2.40)
\end{aligned}$$

Due to the fact that QCD is parity and time reversal invariant, the \mathcal{PT} operation turns a proton state into a proton state, but with opposite spin, i.e.,

$$\mathcal{PT} | P, S \rangle = | P, -S \rangle. \quad (2.41)$$

The transformation rules for the field operators are given by

$$\begin{aligned}
(\mathcal{PT}) \Psi(\xi) (\mathcal{PT})^{-1} &= \gamma^0 \gamma^1 \gamma^3 \Psi(-\xi), \\
(\mathcal{PT}) \bar{\Psi}(0) (\mathcal{PT})^{-1} &= \bar{\Psi}(0) \gamma^3 \gamma^1 \gamma^0. \quad (2.42)
\end{aligned}$$

The \mathcal{PT} operation transforms a spatial coordinate as $\xi \rightarrow -\xi$ and, therefore, the gauge link behaves as

$$(\mathcal{PT}) \mathcal{U}_{[0, \xi]}^{[-]} (\mathcal{PT})^{-1} = \mathcal{U}_{[0, -\xi]}^{[+]}, \quad (2.43)$$

which has now its path running through plus infinity (see figure 2.6). Combining all those ingredients, we end up with

$$\boxed{\Phi^{[-]}(x, \mathbf{p}_T, P, S) = \gamma^0 \gamma^1 \gamma^3 \Phi^{[+]}(x, \mathbf{p}_T, P, -S)^* \gamma^3 \gamma^1 \gamma^0}, \quad (2.44)$$

which is a direct relation between the correlator one has to use in $pp \rightarrow VX$ and the correlator one has to use in SIDIS. Using this relation, measurements of the correlator in SIDS can be used to make predictions for vector boson production and vice versa.

Collinear case with link

If one is only interested in the total cross section, one can again use an expression in terms of collinear correlators,

$$\begin{aligned}
\frac{d\sigma}{dQ^2 dY} &= \frac{1}{2(2\pi)^4} \int d^2 \mathbf{q}_T \frac{d\sigma}{d\mathcal{R}} \\
&\cong \frac{1}{2S^2 N_c} \text{Tr}_D \left[H_0 \left[\int d^2 \mathbf{p}_T \Phi^{[-]}(x_1, \mathbf{p}_T, P_1, S_1) \right] H_0^* \left[\int d^2 \mathbf{k}_T \bar{\Phi}^{[-]}(x_2, \mathbf{k}_T, P_2, S_2) \right] \right] \\
&\cong \frac{1}{2S^2 N_c} \text{Tr}_D \left[H_0 \Phi(x_1, P_1, S_1) H_0^* \bar{\Phi}(x_2, P_2, S_2) \right], \quad (2.45)
\end{aligned}$$

where $\Phi(x, P, S)$ is the collinear correlator, defined by

$$\begin{aligned}\Phi(x, P, S) &\equiv \int d^2 \mathbf{p}_T \Phi^{[\pm]}(x, \mathbf{p}_T, P, S), \\ &= \int \frac{d(\xi \cdot P)}{2\pi} e^{ix\xi \cdot P} \text{Tr}_c \left[\langle P, S | \mathcal{U}_{[0, \xi]} \Psi(\xi) \bar{\Psi}(0) | P, S \rangle \Big|_{n \cdot \xi = \xi_T = 0} \right].\end{aligned}\quad (2.46)$$

The fields in the collinear correlator are evaluated at $n \cdot \xi = \xi_T = 0$, i.e., at zero transverse separation. Without transverse separation, the collinear correlator does not need a \pm superscript: the two different gauge links $\mathcal{U}_{[0, \xi]}^{[+]}$ and $\mathcal{U}_{[0, \xi]}^{[-]}$ in the TMD correlator, reduce to the same collinear gauge link $\mathcal{U}_{[0, \xi]}$ when $\xi_T = 0$. The reduction to a collinear gauge link is illustrated in Figure 2.8. Because the collinear correlator has the same gauge link for SIDIS and $pp \rightarrow VX$, there is no process dependence in the correlator. The total cross section of both processes can be described with the same set of distribution functions.

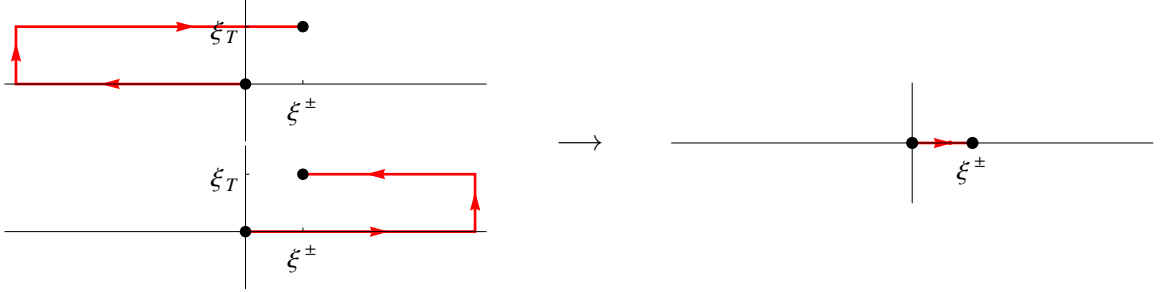


Figure 2.8: Both the plus and minus gauge link $\mathcal{U}_{[0, \xi]}^{[\pm]}$ (left) reduce to the same collinear gauge link $\mathcal{U}_{[0, \xi]}$ (right).

2.2 Parameterization of the quark correlator

In this section we will parameterize the quark correlation function with the most general structure that is allowed by the transformation properties we can infer from the matrix element structure. First of all, let us insert unit operators into the matrix element definition of the TMD correlator of the form $\Lambda^{-1}\Lambda$, where Λ is an arbitrary Lorentz transformation. This results in

$$\begin{aligned}\Phi^{[\pm]}(x, \mathbf{p}_T, P, S) &= \int d(p \cdot P) \frac{d^4 \xi}{(2\pi)^4} e^{ip \cdot \xi} \underbrace{\langle P, S | \Lambda^{-1}}_{\langle P', S' |} \underbrace{\Lambda \mathcal{U}_{[0, \xi]}^{[\pm]} \Lambda^{-1}}_{\mathcal{U}_{[0, \Lambda \xi]}^{[\pm]}} \underbrace{\Lambda \Psi(\xi)}_{\Lambda_{1/2} \Psi(\Lambda \xi)} \underbrace{\bar{\Psi}(0) \Lambda^{-1}}_{\bar{\Psi}(0) \Lambda_{1/2}^{-1}} \underbrace{\Lambda | P, S \rangle}_{| P', S' \rangle} \\ &= \int d(p' \cdot P') \frac{d^4 \xi}{(2\pi)^4} e^{ip' \cdot \xi} \Lambda_{\frac{1}{2}} \langle P', S' | \mathcal{U}_{[0, \xi]}^{[\pm]} \Psi(\xi) \bar{\Psi}(0) | P', S' \rangle \Lambda_{\frac{1}{2}}^{-1},\end{aligned}\quad (2.47)$$

where $\Lambda_{\frac{1}{2}}$ is the relevant spinor representation of the Lorentz transformation, and so

$$\boxed{\Phi^{[\pm]}(x, \mathbf{p}_T, P, S) = \Lambda_{\frac{1}{2}} \Phi^{[\pm]}(x, \mathbf{p}'_T, P', S') \Lambda_{\frac{1}{2}}^{-1}.}\quad (2.48)$$

This last relation implies that the correlator consists of the vectors at hand, P , p and S , dotted into γ matrices, possibly combined with γ_5 and scalar terms.

Another relation comes from the transformation properties of the matrix element under a Hermitian conjugation,

$$\begin{aligned}
\Phi^{[\pm]}(x, \mathbf{p}_T, P, S)^\dagger &= \int d(p \cdot P) \frac{d^4\xi}{(2\pi)^4} e^{-ip \cdot \xi} \langle P, S | \mathcal{U}_{[0, \xi]}^{[-]} \Psi(\xi) \bar{\Psi}(0) | P, S \rangle^\dagger \\
&= \int d(p \cdot P) \frac{d^4\xi}{(2\pi)^4} e^{-ip \cdot \xi} \langle P, S | \underbrace{\bar{\Psi}^\dagger(0)}_{\gamma^0 \Psi(0)} \underbrace{\Psi^\dagger(\xi)}_{\bar{\Psi}(\xi) \gamma^0} \underbrace{\mathcal{U}_{[0, \xi]}^{[-] \dagger}}_{\mathcal{U}_{[\xi, 0]}^{[-]}} | P, S \rangle \\
&= \int d(p \cdot P) \frac{d^4\xi}{(2\pi)^4} e^{-ip \cdot \xi} \gamma^0 \langle P, S | \mathcal{U}_{[0, -\xi]}^{[-]} \Psi(-\xi) \bar{\Psi}(0) | P, S \rangle \gamma^0, \tag{2.49}
\end{aligned}$$

and, therefore,

$$\boxed{\Phi^{[\pm]}(x, \mathbf{p}_T, P, S)^\dagger = \gamma^0 \Phi^{[\pm]}(x, \mathbf{p}_T, P, S) \gamma^0} \tag{2.50}$$

which implies that one can limit oneself to real-valued distribution functions.

The use of parity symmetry can further restrict the parameterization,

$$\begin{aligned}
\Phi^{[\pm]}(x, \mathbf{p}_T, P, S) &= \int d(p \cdot P) \frac{d^4\xi}{(2\pi)^4} e^{ip \cdot \xi} \langle P, S | \underbrace{\mathcal{P}^{-1}}_{\langle \bar{P}, -\bar{S} |} \underbrace{\mathcal{P} \mathcal{U}_{[0, \xi]}^{[\pm]} \mathcal{P}^{-1}}_{\mathcal{U}_{[0, \xi]}^{[\pm]}} \underbrace{\mathcal{P} \Psi(\xi)}_{\gamma^0 \Psi(\xi)} \underbrace{\bar{\Psi}(0) \mathcal{P}^{-1}}_{\bar{\Psi}(0) \gamma^0} \underbrace{\mathcal{P}}_{| \bar{P}, -\bar{S} \rangle} \\
&= \int d(\bar{p} \cdot \bar{P}) \frac{d^4\xi}{(2\pi)^4} e^{i\bar{p} \cdot \xi} \gamma^0 \langle \bar{P}, -\bar{S} | \mathcal{U}_{[0, \xi]}^{[\pm]} \Psi(\xi) \bar{\Psi}(0) | \bar{P}, \bar{S} \rangle \gamma^0, \tag{2.51}
\end{aligned}$$

where $\bar{P} \equiv (P^0, -\mathbf{P})$ and so

$$\boxed{\Phi^{[\pm]}(x, \mathbf{p}_T, P, S) = \gamma^0 \Phi^{[\pm]}(x, -\mathbf{p}_T, \bar{P}, -\bar{S}) \gamma^0} \tag{2.52}$$

which implies, e.g., that a term like $\gamma_5 \not{P}$ is forbidden, whereas \not{S} cannot come without a γ_5 or epsilon tensor.

Sudakov decomposition

The quark momentum p will be decomposed along the directions of the (almost) light-like vectors P and n and into a transverse piece orthogonal to P and n . The normalization of the n vector can be chosen freely, but we choose it to be normalized according to $n \cdot P = M^2$, where M is the proton mass, because then the decomposition

$$p = xP + p_T + \left(\frac{p \cdot P}{M^2} - x \right) n, \tag{2.53}$$

is such that both light-like directions have order 1 coefficients. In the process of Drell-Yan scattering, the vector

$$n = \frac{M^2 P'}{P \cdot P'}, \tag{2.54}$$

where P' is the momentum of the opposite proton, satisfies our requirements. The reason for doing this decomposition, is that we want to be able to rank all the possible different terms in

the correlator according to their importance in the high energy limit. We can now parameterize the correlator instead of with P and p (with basically equal size), with P , p_T and n , which, when contracted with the opposite correlator, produce terms with a clear ordering in size. The possible contractions, ordered according to their size, are

$$\begin{aligned} P \cdot P' &\sim S, \\ p_T \cdot k_T &\sim M^2, \\ P \cdot n' \sim P' \cdot n \sim n \cdot n' &\sim \frac{M^4}{S}. \end{aligned} \quad (2.55)$$

This ordering allows one to judge the importance of different terms in the parameterization of the correlator. For convenience, we will also separate the spin of the proton into a component along the proton direction and one perpendicular to it,

$$S = \lambda \frac{P}{M} + S_T - \lambda \frac{n}{M}, \quad (2.56)$$

such that $P \cdot S = 0$ and $S^2 = -\lambda^2 + \lambda^2 \frac{n^2}{M^2} + S_T^2 \cong -\lambda^2 + S_T^2$, where λ is the helicity of the proton and S_T its transverse spin.

2.2.1 TMD correlator

The most general structure we can write down for the transverse momentum dependent correlator in Eq. (2.39), given the constraints in Eq. (2.48), (2.50) and (2.52), is

$$\begin{aligned} \Phi^{q[\pm]}(x, \mathbf{p}_T) &= \frac{1}{2} \left\{ f_1^{q[\pm]}(x, \mathbf{p}_T^2) \not{P} + f_{1T}^{\perp q[\pm]}(x, \mathbf{p}_T^2) \frac{\epsilon_{\mu\nu\rho\sigma} \gamma^\mu P^\nu p_T^\rho S_T^\sigma}{M} + g_{1s}^{q[\pm]}(x, \mathbf{p}_T) \gamma_5 \not{P} \right. \\ &\quad + h_{1T}^{q[\pm]}(x, \mathbf{p}_T^2) \frac{\gamma_5 [\not{S}_T, \not{P}]}{2} + \lambda h_{1L}^{\perp q[\pm]}(x, \mathbf{p}_T^2) \frac{\gamma_5 [\not{p}_T, \not{P}]}{2M} \\ &\quad + h_{1T}^{\perp q[\pm]}(x, \mathbf{p}_T^2) \left(\frac{\mathbf{p}_T \cdot \mathbf{S}_T \gamma_5 [\not{p}_T, \not{P}]}{2M^2} - \frac{\mathbf{p}_T^2 \gamma_5 [\not{S}_T, \not{P}]}{4M^2} \right) \\ &\quad \left. + h_1^{\perp q[\pm]}(x, \mathbf{p}_T^2) \frac{i[\not{p}_T, \not{P}]}{2M} \right\} + \frac{1}{2} \left\{ e^{q[\pm]}(x, \mathbf{p}_T^2) M + f^{\perp q[\pm]}(x, \mathbf{p}_T^2) \not{p}_T \right. \\ &\quad - f_T^{q[\pm]}(x, \mathbf{p}_T^2) \frac{\epsilon_{\mu\nu\rho\sigma} P^\mu n^\nu \gamma^\rho S_T^\sigma}{M} - \lambda f_L^{\perp q[\pm]}(x, \mathbf{p}_T^2) \frac{\epsilon_{\mu\nu\rho\sigma} P^\mu n^\nu \gamma^\rho p_T^\sigma}{M^2} \\ &\quad - e_s^{q[\pm]}(x, \mathbf{p}_T) i \gamma_5 M + g_T^{\prime q[\pm]}(x, \mathbf{p}_T^2) \gamma_5 \not{S}_T M + g_s^{\perp q[\pm]}(x, \mathbf{p}_T) \gamma_5 \not{k}_T \\ &\quad + h_T^{\perp q[\pm]}(x, \mathbf{p}_T^2) \frac{\gamma_5 [\not{S}_T, \not{p}_T]}{2} + h_s^{q[\pm]}(x, \mathbf{p}_T) \frac{\gamma_5 [\not{P}, \not{p}]}{2M} \\ &\quad \left. + h^{q[\pm]}(x, \mathbf{p}_T^2) \frac{i[\not{P}, \not{p}]}{2M} \right\} + \dots \end{aligned} \quad (2.57)$$

where we have defined

$$g_{1s}^q(x, \mathbf{p}_T) \equiv \lambda g_{1L}^q(x, \mathbf{p}_T^2) + g_{1T}^q(x, \mathbf{p}_T^2) \frac{\mathbf{p}_T \cdot \mathbf{S}_T}{M} \quad (2.58)$$

and similarly for g_s^\perp , h_s and e_s . The quark flavor index on the correlator, which was suppressed, has now been made explicit. The antiquark correlator $\bar{\Phi}$ is parameterized in exactly the same way, but has an antiquark index on the distribution functions, e.g., $f_1^{\bar{q}}$.

The terms in the first curly brackets are called *leading twist* or *twist-2 terms*, because they will produce the largest terms in the cross section according to the ordering in Eq. (2.55). The terms in the second pair of curly brackets are called *next-to-leading twist* or *twist-3 terms*, because they can only produce the next-to-largest terms in the ordering of Eq. (2.55).

Interpretation of the distribution functions

The parameterization of the quark correlator has been done in Dirac space, which does not allow a very straightforward interpretation of the distribution functions. A more convenient choice for this is the spin basis, i.e., we like to find the quark production matrix C ,

$$\Phi(p) = u^\alpha(p) C_{\alpha\beta} \bar{u}^\beta(p) \delta(p^2), \quad (2.59)$$

that decomposes the correlator into the basis spanned by $u^\alpha(p)$, where $\alpha = L, R$ for the *chiral basis*

$$\gamma^5 u_\chi^{\text{R,L}}(p) = \pm u_\chi^{\text{R,L}}(p) \quad (2.60)$$

or $\alpha = \pm$ for the *transverse spin basis*

$$\hat{s}_T u_T^\pm(p) = \pm \frac{1}{2} u_T^\pm(p) \quad (2.61)$$

where the transverse spin operator is defined as

$$\hat{s}_T \equiv \frac{1}{2} \gamma^5 \not{s}_T, \quad (2.62)$$

with the transverse spin vector defined as (in light-cone coordinates $s = [s^-, s^+, \mathbf{s}_T]$)

$$s_T \equiv [0, 0, \cos \phi_{s_T}, \sin \phi_{s_T}]. \quad (2.63)$$

The TMD correlator reads, in terms of the production matrix,

$$\begin{aligned} \Phi(x, \mathbf{p}_T) &= \int d(p \cdot P) u^\alpha(p) C_{\alpha\beta} \bar{u}^\beta(p) \delta(p^2), \\ &= \frac{P^+}{2p^+} u^\alpha(x, \mathbf{p}_T) C_{\alpha\beta}(x, \mathbf{p}_T) \bar{u}^\beta(x, \mathbf{p}_T). \end{aligned} \quad (2.64)$$

We could create an explicit representation of each basis in Dirac space to project out the elements of C , but it is more convenient to work with the projection operators

$$\begin{aligned} \mathcal{P}_T^\kappa &\equiv \frac{1}{p^0} u_T^\kappa(p) u_T^\kappa(p)^\dagger = \frac{1 + \kappa \gamma^5 \not{s}_T}{2}, \\ \mathcal{P}_\chi^{\text{R,L}} &\equiv \frac{1}{p^0} u_\chi^{\text{R,L}}(p) u_\chi^{\text{R,L}}(p)^\dagger = \frac{1 \pm \gamma^5}{2}. \end{aligned} \quad (2.65)$$

The spinors are normalized according to

$$\begin{aligned}\bar{u}^\alpha(p)u^\beta(p) &= 2m\delta^{\alpha\beta}, \\ u^\alpha(p)^\dagger\gamma^0u^\beta(p) &= \bar{u}^\alpha(p)\gamma^0u^\beta(p) = 2p^0\delta^{\alpha\beta},\end{aligned}\quad (2.66)$$

so we can project out the elements of the quark production matrix C on the transverse basis using

$$C_{\kappa\kappa'}(x, \mathbf{p}_T)^2 = \frac{1}{2(P^+)^2} \text{Tr} \left[\mathcal{P}_T^\kappa \Phi(x, \mathbf{p}_T) \gamma^0 \mathcal{P}_T^{\kappa'} \Phi(x, \mathbf{p}_T) \gamma^0 \right]. \quad (2.67)$$

and likewise for the chiral basis. In the basis where the quark production matrix is diagonal it reads

$$C(x, \mathbf{p}_T) = P(x, \mathbf{p}_T) \frac{1}{2} \begin{pmatrix} 1 + \mathcal{P}(x, \mathbf{p}_T) & 0 \\ 0 & 1 - \mathcal{P}(x, \mathbf{p}_T) \end{pmatrix}, \quad (2.68)$$

with $P(x, \mathbf{p}_T)$ the probability of finding a quark with momentum fraction x and transverse momentum \mathbf{p}_T and $\mathcal{P}(x, \mathbf{p}_T)$ the degree of polarization at x and \mathbf{p}_T . Writing all the contributions from the different distribution functions in their diagonal basis, the correlator reads

$$\begin{aligned}\Phi(x, \mathbf{p}_T) &= \left(f_1(x, \mathbf{p}_T^2) + \frac{|\mathbf{p}_T||\mathbf{S}_T|}{M} \sin(\phi_{\mathbf{p}_T} - \phi_{\mathbf{S}_T}) f_{1T}^\perp(x, \mathbf{p}_T^2) \right) u_\chi \begin{pmatrix} \frac{1}{2} & 0 \\ 0 & \frac{1}{2} \end{pmatrix} \bar{u}_\chi \\ &\quad + \left(\lambda g_{1L}(x, \mathbf{p}_T^2) + \frac{\mathbf{p}_T \cdot \mathbf{S}_T}{M} g_{1T}(x, \mathbf{p}_T^2) \right) u_\chi \begin{pmatrix} \frac{1}{2} & 0 \\ 0 & -\frac{1}{2} \end{pmatrix} \bar{u}_\chi \\ &\quad + \left(|\mathbf{S}_T| h_{1T}(x, \mathbf{p}_T^2) - \frac{\mathbf{p}_T^2 |\mathbf{S}_T|}{2M^2} h_{1T}^\perp(x, \mathbf{p}_T^2) \right) u_{\mathbf{S}_T} \begin{pmatrix} \frac{1}{2} & 0 \\ 0 & -\frac{1}{2} \end{pmatrix} \bar{u}_{\mathbf{S}_T} \\ &\quad + \left(\frac{\lambda |\mathbf{p}_T|}{M} h_{1L}^\perp(x, \mathbf{p}_T^2) + \frac{|\mathbf{p}_T| \mathbf{p}_T \cdot \mathbf{S}_T}{M^2} h_{1T}^\perp(x, \mathbf{p}_T^2) \right) u_{\mathbf{p}_T} \begin{pmatrix} \frac{1}{2} & 0 \\ 0 & -\frac{1}{2} \end{pmatrix} \bar{u}_{\mathbf{p}_T} \\ &\quad + \frac{|\mathbf{p}_T|}{M} h_1^\perp(x, \mathbf{p}_T^2) u_{\mathbf{p}'_T} \begin{pmatrix} \frac{1}{2} & 0 \\ 0 & -\frac{1}{2} \end{pmatrix} \bar{u}_{\mathbf{p}'_T},\end{aligned}\quad (2.69)$$

where the transverse spin direction of $u_{\mathbf{S}_T}$ is the direction of \mathbf{S}_T , for $u_{\mathbf{p}_T}$ it is the direction of \mathbf{p}_T and for $u_{\mathbf{p}'_T}$ it is orthogonal to \mathbf{p}_T .

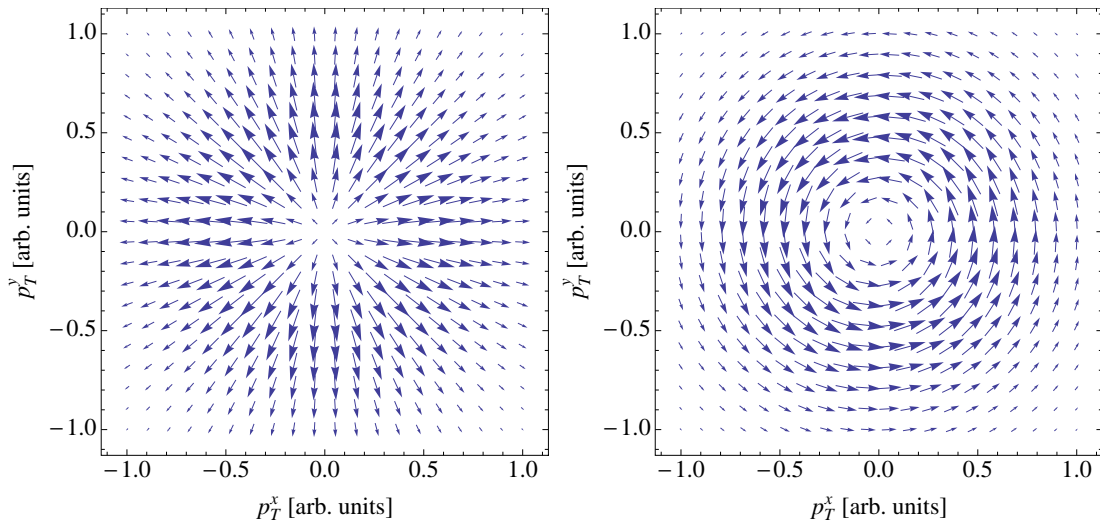
From the expansion in Eq. (2.69) it becomes clear how the naming convention of the distribution functions is chosen. The distribution functions describing unpolarized quarks (diagonal in any basis) are denoted by f and distributions describing longitudinally polarized quarks (diagonal in the chiral basis) are denoted by a g . The distribution functions denoted by a h are diagonal in a transverse basis of which the direction is shown in Figure 2.9 and 2.10. A subscript L or T indicates that the distribution is only relevant for longitudinal or transverse proton polarization and a subscript 1 indicates that is leading twist. The leading twist TMD distribution functions, together with their common names, are summarized in Table 2.1.

From the condition that $\mathcal{P} \leq 1$ one can derive the following upper bounds on the polarized distribution functions,

$$\begin{aligned}|g_{1L}(x, \mathbf{p}_T^2)|, |h_{1T}(x, \mathbf{p}_T^2)| &\leq f_1(x, \mathbf{p}_T^2), \\ |f_{1T}^\perp(x, \mathbf{p}_T^2)|, |g_{1T}(x, \mathbf{p}_T^2)|, |h_{1L}^\perp(x, \mathbf{p}_T^2)|, |h_1^\perp(x, \mathbf{p}_T^2)| &\leq \frac{M}{p_T} f_1(x, p_T^2), \\ |h_{1T}^\perp(x, \mathbf{p}_T^2)| &\leq \frac{M^2}{p_T^2} f_1(x, p_T^2).\end{aligned}\quad (2.70)$$

TMDs		quark polarization		
		U	L	T
nucleon polarization	U	f_1 TMD PDF		h_1^\perp Boer-Mulders
	L		g_{1L} helicity	h_{1L}^\perp worm-gear
	T	f_{1T}^\perp Siverts	g_{1T} worm-gear	h_{1T} transversity h_{1T}^\perp pretzelosity

Table 2.1: Table of leading twist TMD distribution functions and their common names.

Figure 2.9: Direction of quark polarization due to $h_{1L}^{\perp q}$ (left) and $h_1^{\perp q}$ (right) as a function of the transverse momentum of the quark.

Process dependence

The parameterizations of the plus (SIDIS) and minus (DY) correlator in Eq. (2.57) can be related by the use of Eq. (2.44). After inserting the two parameterizations and using

$$\begin{aligned}
\gamma^0 \gamma^1 \gamma^3 (\gamma^\mu)^* \gamma^3 \gamma^1 \gamma^0 &= \gamma^\mu, \\
\gamma^0 \gamma^1 \gamma^3 (\gamma_5 \gamma^\mu)^* \gamma^3 \gamma^1 \gamma^0 &= -\gamma_5 \gamma^\mu, \\
\gamma^0 \gamma^1 \gamma^3 (\sigma^{\mu\nu})^* \gamma^3 \gamma^1 \gamma^0 &= \sigma^{\mu\nu} \\
\gamma^0 \gamma^1 \gamma^3 (\gamma_5 \sigma^{\mu\nu})^* \gamma^3 \gamma^1 \gamma^0 &= -\gamma_5 \sigma^{\mu\nu},
\end{aligned} \tag{2.71}$$

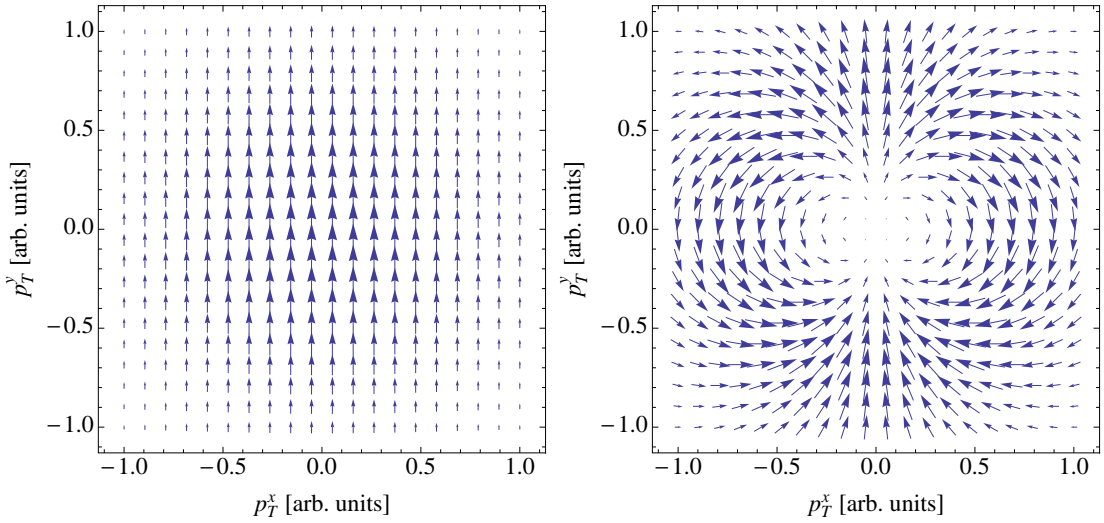


Figure 2.10: Direction of quark polarization due to h_{1T}^q (left) and $h_{1T}^{\perp q}$ (right) as a function of the transverse momentum of the quark for a proton polarized in the y -direction.

the following relations between the distribution functions can be derived,

$$\begin{aligned}
 f_1^{DY}(x, \mathbf{p}_T^2) &= f_1^{\text{SIDIS}}(x, \mathbf{p}_T^2), \\
 g_{1L}^{DY}(x, \mathbf{p}_T^2) &= g_{1L}^{\text{SIDIS}}(x, \mathbf{p}_T^2), \\
 g_{1T}^{DY}(x, \mathbf{p}_T^2) &= g_{1T}^{\text{SIDIS}}(x, \mathbf{p}_T^2), \\
 h_{1T}^{DY}(x, \mathbf{p}_T^2) &= h_{1T}^{\text{SIDIS}}(x, \mathbf{p}_T^2), \\
 h_{1L}^{\perp DY}(x, \mathbf{p}_T^2) &= h_{1L}^{\perp \text{SIDIS}}(x, \mathbf{p}_T^2), \\
 h_{1T}^{\perp DY}(x, \mathbf{p}_T^2) &= h_{1T}^{\perp \text{SIDIS}}(x, \mathbf{p}_T^2), \\
 f_{1T}^{\perp DY}(x, \mathbf{p}_T^2) &= -f_{1T}^{\perp \text{SIDIS}}(x, \mathbf{p}_T^2), \\
 h_1^{\perp DY}(x, \mathbf{p}_T^2) &= -h_1^{\perp \text{SIDIS}}(x, \mathbf{p}_T^2),
 \end{aligned} \tag{2.72}$$

i.e., all the plus and minus distributions are equal, except the Sivers function f_{1T}^{\perp} and Boer-Mulders function h_1^{\perp} , which are related by a minus sign. We can, therefore, drop all the DY/SIDIS superscripts, except for the Sivers and Boer-Mulders functions, for which one has to specify whether they have been obtained from a SIDIS or DY experiment. Note that processes other than SIDIS or DY (including more general vector boson production) might need different gauge links that cannot be related to these ones, see, e.g., [16].

2.2.2 Collinear correlator

The parameterization of the collinear correlator in Eq. (2.46) can be obtained in the same way as the TMD correlator in Eq. (2.57), except for the fact that we cannot use p_T . The most general structure fulfilling the constraints in Eq. (2.48), (2.50) and (2.52) is

$$\begin{aligned} \Phi^q(x) = & \frac{1}{2} \left\{ f_1^q(x) \not{P} + \lambda g_1^q(x) \gamma_5 \not{P} + h_1^q(x) \frac{\gamma_5 [\not{S}_T, \not{P}]}{2} \right\} \\ & + \frac{1}{2} \left\{ e^q(x) M + g_T^q(x) \gamma_5 \not{S}_T M + \lambda h_L^q(x) \frac{\gamma_5 [\not{P}, \not{M}]}{2M} - \lambda e_L^q(x) i \gamma_5 \right. \\ & \left. - f_T^q(x) \frac{\epsilon_{\mu\nu\rho\sigma} P^\mu n^\nu \gamma^\rho S_T^\sigma}{M} + h^q(x) \frac{\gamma_5 [\not{P}, \not{M}]}{2M} \right\} + \dots, \quad (2.73) \end{aligned}$$

where again the first and second pair of curly brackets contain the leading and next-to-leading twist terms respectively. The antiquark correlator is parameterized in the same way, but with distribution functions carrying antiquark indices, e.g., $f_1^{\bar{q}}$. The leading twist distributions are the *Parton Distribution Function* (PDF) $f_1^q(x)$, the *helicity distribution* $g_1^q(x)$ and the *transversity distribution* $h_1^q(x)$, which can be related to the TMDs (up to renormalization) by

$$\begin{aligned} f_1^q(x) &= \int d^2 \mathbf{p}_T f_1^q(x, \mathbf{p}_T^2), \\ g_1^q(x) &= \int d^2 \mathbf{p}_T g_{1L}^q(x, \mathbf{p}_T^2), \\ h_1^q(x) &= \int d^2 \mathbf{p}_T \left[h_{1T}^q(x, \mathbf{p}_T^2) - \frac{\mathbf{p}_T^2}{2M^2} h_{1T}^{\perp q}(x, \mathbf{p}_T^2) \right]. \quad (2.74) \end{aligned}$$

2.2.3 Evolution

At next-to-leading order in a perturbative expansion in the strong coupling constant, collinear divergences will appear in the hard scattering matrix element H . The divergences can be absorbed into the ‘bare’ parton distribution functions, as to arrive at *renormalized* distribution functions. Like the renormalization of coupling constants, also finite parts of the next-to-leading order corrections can be absorbed (see Figure 2.11), at the cost of introducing a scale dependence in the distribution functions. Just as there are different renormalization schemes, one also has different factorization schemes leading to different definitions of the hard part and distribution functions. The way we have defined the distribution functions (as parameterization of specific matrix elements) corresponds to the $\overline{\text{MS}}$ factorization scheme [17]. The factorization scale dependence of the renormalized collinear parton distribution functions is governed by the Gribov-Lipatov-Altarelli-Parisi evolution equation [18, 19]. Complete TMD factorization, including evolution of the TMD distribution functions is also established [20, 21, 22, 23, 10, 11].

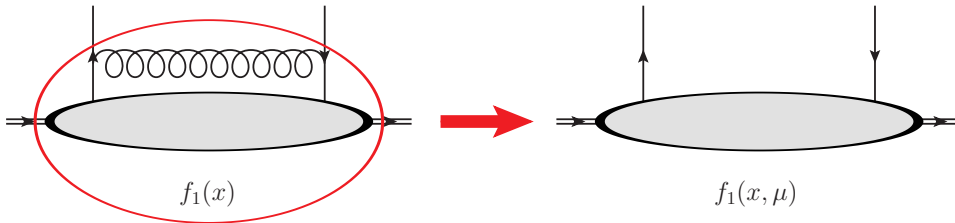


Figure 2.11: Diagram with additional real gluon emission that can be absorbed into the definition of the PDF.

2.3 Gluon-gluon fusion

The gluon-gluon fusion contribution to the inclusive production of a colorless final state V from a proton-proton collision is shown diagrammatically in Figure 2.12. The cross section for this

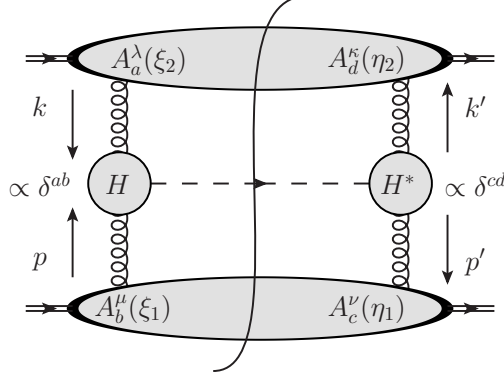


Figure 2.12: Diagrammatic representation of the gluon-gluon fusion contribution to the $pp \rightarrow VX$ cross section.

process can be written as

$$\begin{aligned}
 \frac{d\sigma}{d\mathcal{R}} &= \frac{(2\pi)^4}{2S} \int \frac{d^4k}{(2\pi)^4} \frac{d^4k'}{(2\pi)^4} \frac{d^4p}{(2\pi)^4} \frac{d^4p'}{(2\pi)^4} \delta^4(p+k-q) \times \\
 &\quad \text{Tr}_{c_8} \left[\Phi_g^{\mu\nu}(p, p', P_1, S_1) H_{\nu\kappa}^* \Phi_g^{\lambda\kappa}(k, k', P_2, S_2) H_{\mu\kappa} \right] \\
 &= \frac{(2\pi)^4}{2S} \int \frac{d^4k}{(2\pi)^4} \frac{d^4k'}{(2\pi)^4} \frac{d^4p}{(2\pi)^4} \frac{d^4p'}{(2\pi)^4} \delta^4(p+k-q) \times \\
 &\quad \frac{1}{8} \text{Tr}_{c_8} \left[\Phi_g^{\mu\nu}(p, p', P_1, S_1) \right] \text{Tr}_{c_8} \left[\Phi_g^{\lambda\kappa}(k, k', P_2, S_2) \right] H_{\mu\lambda} H_{\nu\kappa}^*,
 \end{aligned} \tag{2.75}$$

where we have defined the gluon correlator as

$$\Phi_{bc}^{\mu\nu}(p, p', P, S) \equiv \int d^4\xi d^4\eta e^{ip \cdot \xi - ip' \cdot \eta} \langle P, S | A_c^\nu(\eta) A_b^\mu(\xi) | P, S \rangle. \tag{2.76}$$

The color trace of the correlator can be written as

$$\begin{aligned}
 \text{Tr}_{c_8} \left[\Phi^{\mu\nu}(p, p', P, S) \right] &= \delta^{ab} \Phi_{ab}^{\mu\nu}(p, p', P, S) \\
 &= \int d^4\xi d^4\eta e^{ip \cdot \xi - ip' \cdot \eta} 2 \text{Tr}_c \left[\langle P, S | A^\nu(\eta) A^\mu(\xi) | P, S \rangle \right] \\
 &= \int d^4\xi d^4\eta \frac{e^{ip \cdot \xi - ip' \cdot \eta}}{(p \cdot n)(p' \cdot n)} 2 \text{Tr}_c \left[\langle P, S | \partial^n A^\nu(\eta) \partial^n A^\mu(\xi) | P, S \rangle \right],
 \end{aligned} \tag{2.77}$$

where the last step is for future convenience. Using translation invariance of the matrix element, we can write

$$\text{Tr}_{c_8} \left[\Phi^{\mu\nu}(p, p', P, S) \right] = \delta^4(p-p') (2\pi)^8 \text{Tr}_{c_8} \left[\Phi^{\mu\nu}(p, P, S) \right], \tag{2.78}$$

where

$$\text{Tr}_{c_8} [\Phi^{\mu\nu}(p, P, S)] \equiv \frac{1}{(2\pi)^4 (p \cdot n)^2} \int d^4 \xi e^{ip \cdot \xi} 2 \text{Tr}_c \left[\langle P, S | \partial^n A^\nu(0) \partial^n A^\mu(\xi) | P, S \rangle \right]. \quad (2.79)$$

The overall delta function can again be approximated as in Eq. (2.12) to (2.16), such that we can write the cross section in terms of $\int d(p \cdot P)$ integrated correlators. In the end the gluon-gluon fusion contribution to the $pp \rightarrow VX$ cross section is written in a factorized form similar to the quark-antiquark annihilation contribution in Eq. (2.17),

$$\frac{d\sigma}{d\mathcal{R}} = \frac{(2\pi)^4}{S^2} \frac{1}{8} \int d^2 \mathbf{p}_T d^2 \mathbf{k}_T \delta^2(\mathbf{p}_T + \mathbf{k}_T - \mathbf{q}_T) \times \\ \text{Tr}_{c_8} [\Phi_g^{\mu\nu}(x_1, \mathbf{p}_T, P_1, S_1)] \text{Tr}_{c_8} [\Phi_g^{\lambda\kappa}(x_2, \mathbf{k}_T, P_2, S_2)] H_{\mu\lambda} H_{\nu\kappa}^*, \quad (2.80)$$

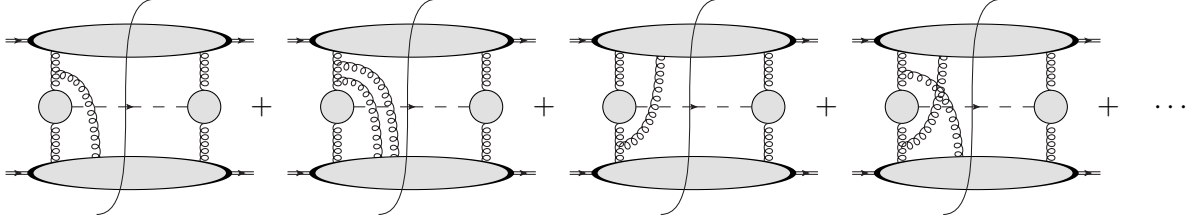
where the TMD correlator is defined as

$$\text{Tr}_{c_8} [\Phi_g^{\mu\nu}(x, \mathbf{p}_T, P, S)] = \int \frac{d(\xi \cdot P) d^2 \xi_T}{(p \cdot n)^2 (2\pi)^3} e^{ip \cdot \xi} 2 \text{Tr}_c \left[\langle P, S | \partial^n A^\nu(0) \partial^n A^\mu(\xi) | P, S \rangle \right]_{\xi \cdot n=0} \quad (2.81)$$

and should be evaluated at $x_1 = \frac{q \cdot P_2}{P_1 \cdot P_2}$ and $x_2 = \frac{q \cdot P_1}{P_1 \cdot P_2}$.

2.3.1 Inclusion of the gauge link

Just as in the quark-antiquark annihilation case, we should still include the contributions from additional gluon exchanges between the incoming legs and the soft parts, i.e.,



Kinematically these diagrams are, of course, the same as in the quark antiquark annihilation case, but also the color structure can again be written as a trace, provided that the gauge fields are in the adjoint representation. The sum of all diagrams can, therefore, again be written in an exponentiated form,

$$d\sigma \sim \text{Tr}_{c_8} \left[\Phi_g^{\mu\nu}(x_1, \mathbf{p}_T, P_1, S_1) U_-^{[n]}[p_2] U_-^{[n]\dagger}[p_1] \Phi_g^{\lambda\kappa}(x_2, \mathbf{k}_T, P_2, S_2) U_-^{[n]}[p_2] U_-^{[n]\dagger}[p_2] \right] H_{\mu\lambda} H_{\nu\kappa}^*. \quad (2.82)$$

The links in Eq. (2.82) can, just as in the quark-antiquark annihilation case, be eliminated by an appropriate gauge transformation, $V(\xi) \equiv \mathcal{U}_{[0,\xi]}^{[-]}$, where $\mathcal{U}_{[0,\xi]}^{[-]}$ is a *gauge link*, defined by

$$\mathcal{U}_{[0,\xi]}^{[\pm]} \equiv \mathcal{P} \exp \left(-ig \int_0^\xi dz_\mu A^\mu(z) \right), \quad (2.83)$$

in which the path should be taken as is indicated in figure 2.6. After the gauge transformation, the links are removed from the trace, i.e.,

$$\begin{aligned} d\sigma &\sim \text{Tr}_{c_8} \left[\Phi_g^{\mu\nu[-]}(x_1, \mathbf{p}_T, P_1, S_1) \Phi_g^{\lambda\kappa[-]}(x_2, \mathbf{k}_T, P_2, S_2) \right] H_{\mu\lambda} H_{\nu\kappa}^*, \\ &= \frac{1}{8} \text{Tr}_{c_8} \left[\Phi_g^{\mu\nu[-]}(x_1, \mathbf{p}_T, P_1, S_1) \right] \text{Tr}_{c_8} \left[\Phi_g^{\lambda\kappa[-]}(x_2, \mathbf{k}_T, P_2, S_2) \right] H_{\mu\lambda} H_{\nu\kappa}^*, \end{aligned} \quad (2.84)$$

but the correlators are modified. This modification is due to the fact that the A field transforms under a gauge transformation as

$$A^\mu \rightarrow \frac{i}{g} \mathcal{U}_{[0,\xi]}^{[-]} D^\mu \mathcal{U}_{[\xi,0]}^{[-]} \quad (2.85)$$

and, therefore, the combination $\partial^+ A^\mu$ transforms as

$$\begin{aligned} \partial^n A^\mu(\xi) &\rightarrow \partial^n \left(\mathcal{U}_{[0,\xi]}^{[-]} A^\mu(\xi) \mathcal{U}_{[\xi,0]}^{[-]} \right) + \frac{i}{g} \partial^n \left(\mathcal{U}_{[0,\xi]}^{[-]} \partial^\mu \mathcal{U}_{[\xi,0]}^{[-]} \right) \\ &= \mathcal{U}_{[0,\xi]}^{[-]} \left[-ig A^n(\xi) A^\mu(\xi) + ig A^\mu(\xi) A^n(\xi) + \partial^n(A^\mu(\xi)) \right] \mathcal{U}_{[\xi,0]}^{[-]} \\ &\quad + \mathcal{U}_{[0,\xi]}^{[-]} \left[A^n(\xi) \partial^\mu - \partial^\mu(A^n(\xi)) - A^n(\xi) \partial^\mu \right] \mathcal{U}_{[\xi,0]}^{[-]} \\ &= \mathcal{U}_{[0,\xi]}^{[-]} F^{n\mu}(\xi) \mathcal{U}_{[\xi,0]}^{[-]}, \end{aligned} \quad (2.86)$$

where $F^{\mu\nu}$ is the gluon field strength tensor. The modified correlator, which we define to always include the color trace, thus reads

$$\Phi_g^{\mu\nu[-,-]}(x, \mathbf{p}_T, P, S) \equiv \int \frac{d(\xi \cdot P) d^2 \xi_T}{(p \cdot n)^2 (2\pi)^3} e^{ip \cdot \xi} 2 \text{Tr}_c \left[\langle P, S | F^{n\nu}(0) \mathcal{U}_{[0,\xi]}^{[-]} F^{n\mu}(\xi) \mathcal{U}_{[\xi,0]}^{[-]} | P, S \rangle \right]_{\text{LF}}. \quad (2.87)$$

The correlator with gauge link is again a gauge invariant quantity, which could be calculated with lattice QCD or other models, or parameterized in terms of distribution functions. Parameterization of the gluon TMD correlator will be done in Section 2.4.1.

The factorized expression for the gluon-gluon fusion contribution to $pp \rightarrow VX$, including all the leading extra gluon exchanges, thus reads in terms of gauge invariant gluon field strength correlators with link,

$$\begin{aligned} \frac{d\sigma}{d\mathcal{R}} &= \frac{(2\pi)^4}{S^2} \frac{1}{8} \int d^2 \mathbf{p}_T d^2 \mathbf{k}_T \delta^2(\mathbf{p}_T + \mathbf{k}_T - \mathbf{q}_T) \times \\ &\quad \Phi_g^{\mu\nu[-,-]}(x_1, \mathbf{p}_T, P_1, S_1) \Phi_g^{\lambda\kappa[-,-]}(x_2, \mathbf{k}_T, P_2, S_2) H_{\mu\lambda} H_{\nu\kappa}^*, \end{aligned} \quad (2.88)$$

with $x_1 = \frac{q \cdot P_2}{P_1 \cdot P_2}$ and $x_2 = \frac{q \cdot P_1}{P_1 \cdot P_2}$.

Process dependence

The gauge invariant gluon correlator comes, in general, with *two* \pm superscripts, because it contains *two* gauge links, which could have different paths. For the case of gluon fusion, two minus links should be used, but other processes need different gauge links. The SIDIS process,

e.g., will need the $\Phi_g^{\mu\nu[+,+]}$ correlator. Following the same reasoning as in Section 2.1.1, the $\Phi_g^{\mu\nu[-,-]}$ and $\Phi_g^{\mu\nu[+,+]}$ correlators can be related by a \mathcal{PT} transformation. The field strength tensor F is invariant under this operation and, therefore, we come to the conclusion that

$$\Phi_g^{\mu\nu[-,-]}(x, \mathbf{p}_T, P, S) = \Phi_g^{\mu\nu[+,+]}(x, \mathbf{p}_T, P, -S)^*. \quad (2.89)$$

This relation between the $++$ and $--$ correlator can again be used to relate the distribution functions that have to be used in SIDIS to the functions that have to be used in gluon-gluon fusion. There are, however, also processes that need $+-$ correlators, which are not related to the $++$ and $--$ correlators. The $+-$ correlator should thus be parameterized in terms of independent distribution functions and universality is partially lost.

Collinear case

Just as for the quark–antiquark annihilation channel, one can write the \mathbf{q}_T integrated cross section in terms of collinear correlation functions,

$$\begin{aligned} \frac{d\sigma}{dQ^2 dY} &= \frac{1}{2(2\pi)^4} \int d^2 \mathbf{q}_T \frac{d\sigma}{d\mathcal{R}} \\ &\cong \frac{1}{16S^2} \left[\int d^2 \mathbf{p}_T \Phi_g^{\mu\nu[-,-]}(x_1, \mathbf{p}_T, P_1, S_1) \right] \left[\int d^2 \mathbf{k}_T \Phi_g^{\lambda\kappa[-,-]}(x_2, \mathbf{k}_T, P_2, S_2) \right] H_{\mu\lambda}^0 H_{\nu\kappa}^{0*} \\ &\cong \frac{1}{16S^2} \Phi_g^{\mu\nu}(x_1, P_1, S_1) \Phi_g^{\lambda\kappa}(x_2, P_2, S_2) H_{\mu\lambda}^0 H_{\nu\kappa}^{0*} \end{aligned} \quad (2.90)$$

where H^0 is the first order term in the collinear expansion of the hard matrix element,

$$H_{\mu\nu} = H_{\mu\nu}^0 + \mathbf{H}_{\mu\nu}^1 \cdot \mathbf{q}_T + \mathbf{q}_T \cdot H_{\mu\nu}^2 \mathbf{q}_T + \dots, \quad (2.91)$$

and $\Phi_g^{\mu\nu}(x, P, S)$ is the *collinear correlation function* defined by

$$\begin{aligned} \Phi_g^{\mu\nu}(x, P, S) &\equiv \int d^2 \mathbf{p}_T \Phi_g^{\mu\nu[\pm,\pm]}(x, \mathbf{p}_T, P, S), \\ &= \int \frac{d(\xi \cdot P)}{2\pi(p \cdot n)^2} e^{i x \xi \cdot P} 2 \text{Tr}_c [\langle P, S | F^{n\nu}(0) \mathcal{U}_{[0,\xi]} F^{n\mu}(\xi) \mathcal{U}_{[\xi,0]} | P, S \rangle]_{\xi \cdot n = \xi_T = 0}. \end{aligned} \quad (2.92)$$

Both plus and minus gauge links reduce to the same collinear gauge link (see Figure 2.8), just as for quarks. The collinear correlator does not need superscripts indicating the link direction and is not process dependent. In section 2.4.2, the collinear correlator will be parameterized in terms of distribution functions.

The convergences of the series in Eq. (2.91) is again determined by the available energy scales in the hard part. If the only compensating scale is Q , the higher order terms are suppressed q_T/Q . The correction terms in the collinear expansion can also be included, which will lead to expressions involving integrations of \mathbf{p}_T weighted TMD correlation functions, which are in general process dependent [16].

2.4 Parameterization of the gluon correlator

In this section we will parameterize the gluon correlation function with the most general structure that is allowed by the transformation properties we can infer from the matrix element structure.

2.4.1 TMD correlator

We will again make use of a Sudakov decomposition, but with a slightly different normalization for the n vector

$$n = \frac{P'}{P \cdot P'}, \quad (2.93)$$

such that the gluon momentum and proton spin read

$$\begin{aligned} p &= xP + p_T + (p \cdot P - xM^2) n, \\ S &= \lambda \frac{P}{M} + S_T - \lambda M n. \end{aligned} \quad (2.94)$$

Due to the anti-symmetric nature of the field strength tensor, the gluon correlator contracted with the n vector should be zero, i.e., $\Phi_g^{n\mu}(x, \mathbf{p}_T) = \Phi_g^{\mu n}(x, \mathbf{p}_T) = 0$, which means that the correlator can only have transverse components at leading twist. The parameterization should, therefore, only contain combinations of p_T , S_T and the transverse tensors defined by

$$\begin{aligned} g_T^{\mu\nu} &\equiv g^{\mu\nu} - P^\mu n^\nu - P^\nu n^\mu, \\ \epsilon_T^{\mu\nu} &\equiv \epsilon^{\mu\nu\rho\sigma} P_\rho n_\sigma. \end{aligned} \quad (2.95)$$

To exclude certain terms in the parameterization, we can again use symmetry properties of the matrix element. For example, Hermitian conjugation of the matrix element tells us that

$$\begin{aligned} \Phi_g^{\mu\nu[-,-]}(x, \mathbf{p}_T, P, S)^\dagger &= \int \frac{d(p \cdot P) d^4\xi}{(2\pi)^4 (p \cdot n)^2} e^{-ip \cdot \xi} 2 \text{Tr}_c \left[\langle P, S | F^{n\nu}(0) \mathcal{U}_{[0,\xi]}^{[-]} F^{n\mu}(\xi) \mathcal{U}_{[\xi,0]}^{[-]} | P, S \rangle \right]^\dagger \\ &= \int \frac{d(p \cdot P) d^4\xi}{(2\pi)^4 (p \cdot n)^2} e^{-ip \cdot \xi} 2 \text{Tr}_c \left[\langle P, S | \mathcal{U}_{[0,\xi]}^{[-]} F^{n\mu}(\xi) \mathcal{U}_{[\xi,0]}^{[-]} F^{n\nu}(0) | P, S \rangle \right] \\ &= \int \frac{d(p \cdot P) d^4\xi}{(2\pi)^4 (p \cdot n)^2} e^{-ip \cdot \xi} 2 \text{Tr}_c \left[\langle P, S | \mathcal{U}_{[-\xi,0]}^{[-]} F^{n\mu}(0) \mathcal{U}_{[0,-\xi]}^{[-]} F^{n\nu}(-\xi) | P, S \rangle \right] \\ &= \int \frac{d(p \cdot P) d^4\xi}{(2\pi)^4 (p \cdot n)^2} e^{ip \cdot \xi} 2 \text{Tr}_c \left[\langle P, S | \mathcal{U}_{[\xi,0]}^{[-]} F^{n\mu}(0) \mathcal{U}_{[0,\xi]}^{[-]} F^{n\nu}(\xi) | P, S \rangle \right] \\ &= \Phi_g^{\nu\mu[-,-]}(x, \mathbf{p}_T, P, S), \end{aligned} \quad (2.96)$$

and parity inversion implies

$$\begin{aligned} \Phi_g^{\mu\nu[-,-]}(x, \mathbf{p}_T, P, S) &= \int \frac{d(p \cdot P) d^4\xi}{(2\pi)^4 (p \cdot n)^2} e^{ip \cdot \xi} 2 \text{Tr}_c \left[\langle \bar{P}, -\bar{S} | F_{\nu}^{\bar{n}}(0) \mathcal{U}_{[0,\bar{\xi}]}^{[-]} F_{\mu}^{\bar{n}}(\bar{\xi}) \mathcal{U}_{[\bar{\xi},0]}^{[-]} | \bar{P}, -\bar{S} \rangle \right] \\ &= \int \frac{d(\bar{p} \cdot \bar{P}) d^4\xi}{(2\pi)^4 (\bar{p} \cdot \bar{n})^2} e^{i\bar{p} \cdot \xi} 2 \text{Tr}_c \left[\langle \bar{P}, -\bar{S} | F_{\nu}^{\bar{n}}(0) \mathcal{U}_{[0,\bar{\xi}]}^{[-]} F_{\mu}^{\bar{n}}(\bar{\xi}) \mathcal{U}_{[\bar{\xi},0]}^{[-]} | \bar{P}, -\bar{S} \rangle \right] \\ &= \Phi_{g\mu\nu}^{[-,-]}(x, -\mathbf{p}_T, \bar{P}, -\bar{S}) \Big|_{n \rightarrow \bar{n}}. \end{aligned} \quad (2.97)$$

The $n \rightarrow \bar{n}$ in the last relation implies that

$$\begin{aligned} g_T^{\mu\nu} &\rightarrow g_T^{\mu\nu}, \\ \epsilon_T^{\mu\nu} &\rightarrow -\epsilon_T^{\mu\nu}, \end{aligned} \quad (2.98)$$

in the parameterization. The most general parameterization³ of the gluon TMD correlator, consistent with the previously derived constraints, is given by

$$\begin{aligned} \Phi_g^{\mu\nu}(x, \mathbf{p}_T, P, S) = \frac{1}{2x} \left\{ -g_T^{\mu\nu} f_1^g(x, \mathbf{p}_T^2) + \left(\frac{p_T^\mu p_T^\nu}{M^2} + g_T^{\mu\nu} \frac{\mathbf{p}_T^2}{2M^2} \right) h_1^{\perp g}(x, \mathbf{p}_T^2) + i\epsilon_T^{\mu\nu} \lambda g_{1L}^g(x, \mathbf{p}_T^2) \right. \\ + i\epsilon_T^{\mu\nu} \frac{\mathbf{p}_T \cdot \mathbf{S}_T}{M} g_{1T}^g(x, \mathbf{p}_T^2) + g_T^{\mu\nu} \frac{\epsilon_T^{p_T S_T}}{M} f_{1T}^{\perp g}(x, \mathbf{p}_T^2) \\ - \frac{\epsilon_T^{p_T \{\mu} S_T^{\nu\}} + \epsilon_T^{S_T \{\mu} p_T^{\nu\}}}{4M} h_{1T}^g(x, \mathbf{p}_T^2) - \frac{\epsilon_T^{p_T \{\mu} p_T^{\nu\}}}{2M^2} h_{1L}^{\perp g}(x, \mathbf{p}_T^2) \\ \left. - \frac{\epsilon_T^{p_T \{\mu} p_T^{\nu\}}}{2M^2} \frac{\mathbf{p}_T \cdot \mathbf{S}_T}{M} h_{1T}^{\perp g}(x, \mathbf{p}_T^2) \right\} + \text{higher twist}, \end{aligned} \quad (2.99)$$

where higher twist stands for all terms that are proportional to Mn^μ , which, after contraction with the hard part, can only give M^2/S suppressed contributions to the cross section.

In principle all distribution functions carry an index indicating the type of gauge link in the correlator. However, using Eq. (2.89), we conclude that the first four distribution functions are equal in both the $[+, +]$ (used in SIDIS) and $[-, -]$ (used in gluon fusion) correlator and therefore do not need a specification of the link structure. The last four distribution functions differ in sign between the $[+, +]$ and $[-, -]$ correlator. A parameterization of these functions should therefore always specify whether it describes SIDIS or gluon fusion.

The naming of the distribution functions is chosen such that the f functions describe unpolarized gluons, the g functions circular polarization and the h functions linear polarization. The direction of the linear polarization, as a function of the gluonic transverse momentum, is shown in Figure 2.13 to 2.16. The plots are made with the particular h function at its *maximal* value, saturating the polarization at all values of p_T . The bounds on the distribution functions are

$$\begin{aligned} |g_{1L}^g(x, \mathbf{p}_T^2)| &\leq f_1^g(x, \mathbf{p}_T^2), \\ \frac{1}{4} |h_{1T}^g(x, \mathbf{p}_T^2)|, |f_{1T}^{\perp g}(x, \mathbf{p}_T^2)|, |g_{1T}^g(x, \mathbf{p}_T)| &\leq \frac{M}{p_T} f_1^g(x, \mathbf{p}_T^2), \\ \frac{1}{2} |h_1^{\perp g}(x, \mathbf{p}_T^2)|, \frac{1}{4} |h_{1L}^{\perp g}(x, \mathbf{p}_T^2)| &\leq \frac{M^2}{p_T^2} f_1^g(x, \mathbf{p}_T), \\ |h_{1T}^{\perp g}(x, \mathbf{p}_T^2)| &\leq \frac{4M^3}{p_T^3} f_1^g(x, \mathbf{p}_T^2). \end{aligned} \quad (2.100)$$

³We use the parameterization proposed in [24] and the naming convention introduced in [25].

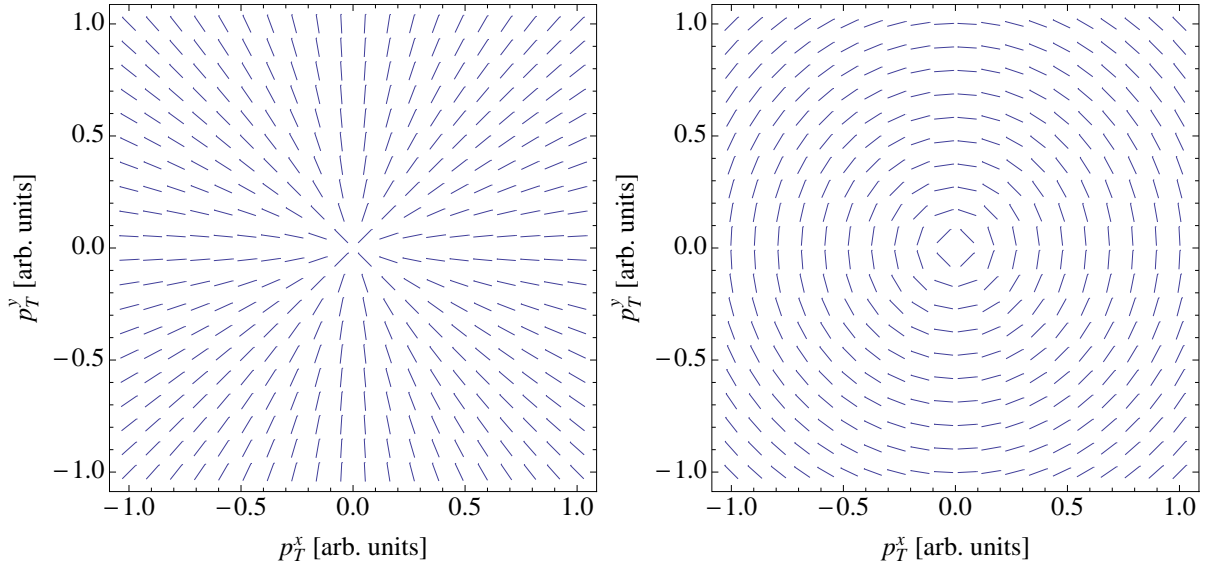


Figure 2.13: The effect of $h_1^{\perp g}$ on the gluon polarization inside a proton, for $h_1^{\perp g} > 0$ (left) and $h_1^{\perp g} < 0$ (right).

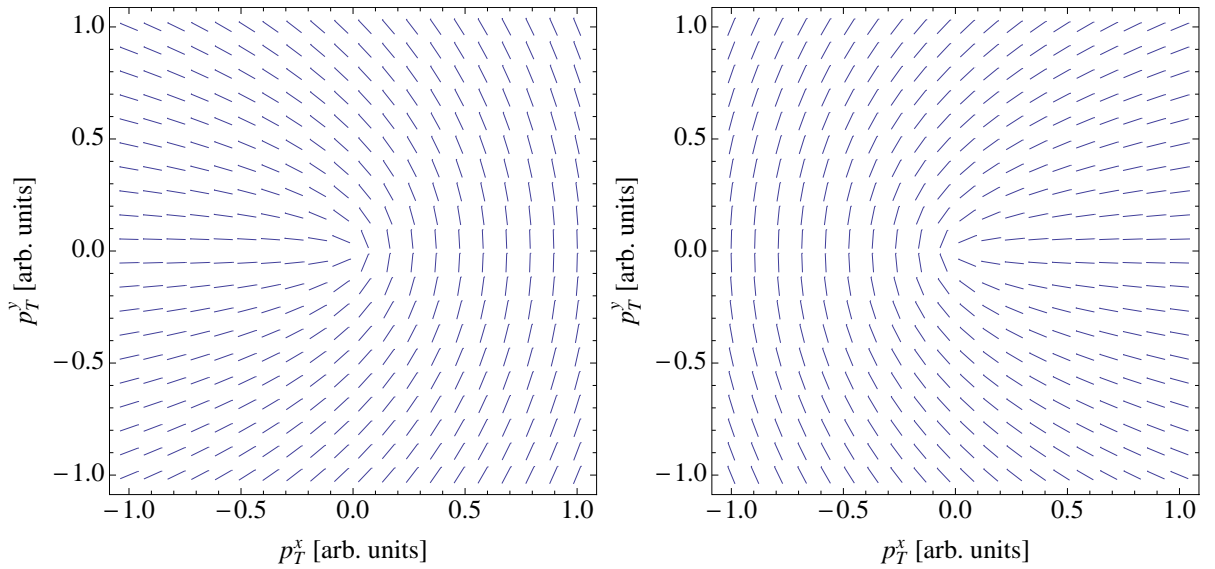


Figure 2.14: The effect of h_{1T}^g on the gluon polarization inside a proton, for $h_{1T}^g > 0$ (left) and $h_{1T}^g < 0$ (right). The y direction is set by the transverse spin direction \mathbf{S}_T .

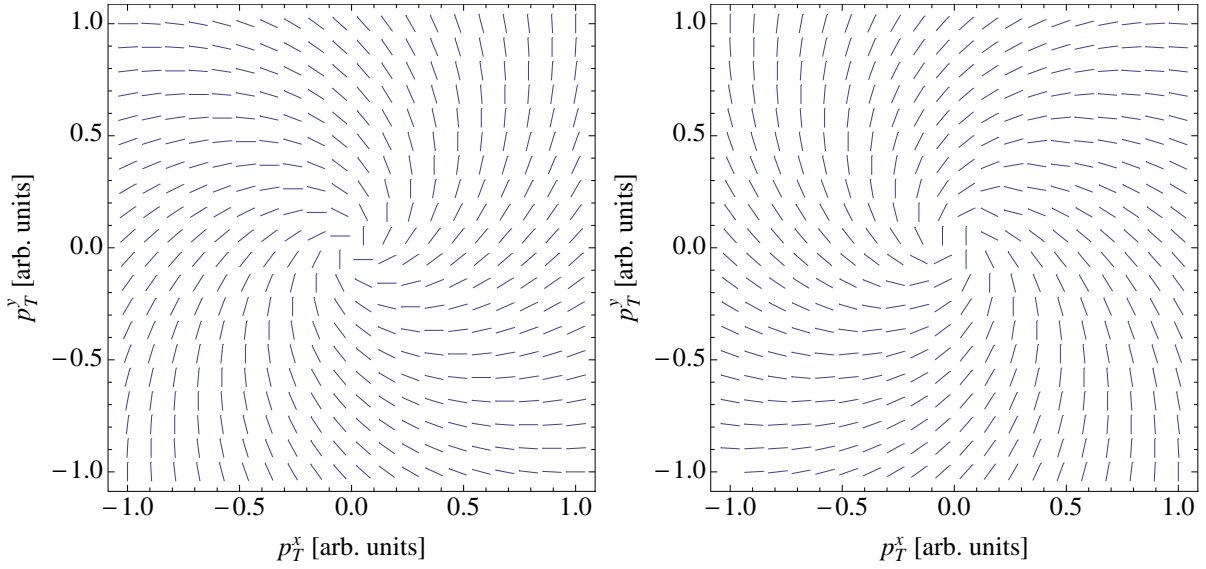


Figure 2.15: The effect of $h_{1L}^{\perp g}$ on the gluon polarization inside a proton, for $\lambda h_{1L}^{\perp g} > 0$ (left) and $\lambda h_{1L}^{\perp g} < 0$ (right).

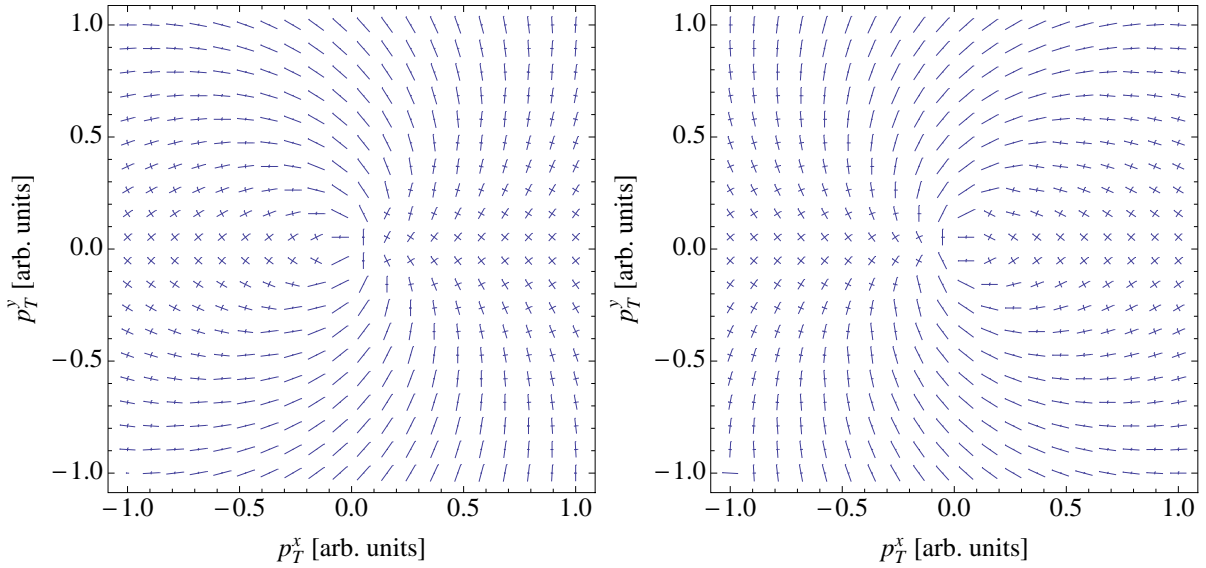


Figure 2.16: The effect of $h_{1T}^{\perp g}$ on the gluon polarization inside a proton, for $h_{1T}^{\perp g} > 0$ (left) and $h_{1T}^{\perp g} < 0$ (right). The y direction is set by the transverse spin direction \mathbf{S}_T . The degree of polarization is indicated by the length of the bar, i.e., a cross indicates no polarization.

2.4.2 Collinear correlator

The gluon collinear correlator as defined in Eq. (2.92) can be parameterized as

$$\boxed{\Phi_g^{\mu\nu}(x, P, S) = \frac{1}{2x} \left\{ -g_T^{\mu\nu} f_1^g(x) + i\epsilon_T^{\mu\nu} \lambda g_{1L}^g(x) \right\} + \text{higher twist.}} \quad (2.101)$$

Note that there is no equivalent of the quark transversity distribution for gluons. Other common names for the distribution functions are $g(x) = f_1^g(x)$ and $\Delta g(x) = g_{1L}^g(x)$.

2.5 Summary

In this chapter we have given a factorized description of the process $pp \rightarrow VX$, where V is an arbitrary colorless final state. The intrinsic transverse momentum of the proton constituents is not neglected, such that the cross section, differential in the transverse momentum of V , can be described correctly also at low values of q_T . In the remainder of this thesis we will use this factorized description to predict spin asymmetries in W boson production both in the Standard Model and beyond. We will also use the framework to predict the effect of the partonic transverse motion on Higgs production and show that it, in principle, can be used to distinguish scalar from pseudoscalar particles.

Chapter 3

Standard Model TMD effects in $p^\uparrow p^\uparrow \rightarrow VX$

3.1 Introduction

Within the collinear treatment of hadronic collisions, there can only be a correlation between the parton's polarization and that of the parent hadron. An unpolarized hadron consists of unpolarized partons. Also, a transversely polarized proton does not carry longitudinally polarized partons and vice versa.

This naive description works for total cross sections, but not necessarily for more differential cross sections as argued in the previous Chapter. A more complete treatment includes partonic transverse momentum in the description, which opens up the possibility of momentum-spin correlations. These can be correlations between the partonic momentum and the hadronic spin, between the partonic spin and partonic momentum, but also combinations. All correlations are described by in total 8 TMD distribution functions, which are summarized in Table 2.1.

An example TMD distribution is the Sivers function [26], which describes an asymmetry in the transverse momentum distribution of quarks with respect to the proton's transverse spin (displayed schematically in Figure 3.1). The effects of the Sivers function were first observed in Semi-Inclusive Deep Inelastic Scattering (SIDIS) [27, 28, 29] and will be studied in W production at RHIC from single transversely polarized proton-proton collisions as well, with the goal of measuring the predicted sign difference between the Sivers function for SIDIS and DY [30, 31].



Figure 3.1: The Sivers effect describes a transverse momentum distribution that is anti-symmetric with respect to the proton's spin direction.

Another example is the Worm-Gear (WG) distribution g_{1T} [32], which expresses a correlation between the quark's helicity and the angle between its transverse momentum and the

proton's transverse spin (displayed schematically in Figure 3.2). Data on double transverse spin asymmetries A_{LT} that receive contributions from the WG effect has become available only very recently [33, 34] and indicates that g_{1T} for the up-quark is not small [34].



Figure 3.2: The worm-gear effect describes a correlation between the quark chirality and the angle between its transverse momentum and the proton's transverse spin direction.

These TMD distributions can have a variety of observable effects in transversely polarized proton collisions. To investigate polarization effects one usually considers spin asymmetries, e.g., the *single transverse spin asymmetry*

$$A_T \equiv \frac{d\sigma^\uparrow - d\sigma^\downarrow}{d\sigma^\uparrow + d\sigma^\downarrow}, \quad (3.1)$$

or the *double transverse spin asymmetry*

$$A_{TT} \equiv \frac{d\sigma^{\uparrow\uparrow} - d\sigma^{\uparrow\downarrow} - d\sigma^{\downarrow\uparrow} + d\sigma^{\downarrow\downarrow}}{d\sigma^{\uparrow\uparrow} + d\sigma^{\uparrow\downarrow} + d\sigma^{\downarrow\uparrow} + d\sigma^{\downarrow\downarrow}}. \quad (3.2)$$

We will focus here on double transverse spin asymmetries in vector boson production, i.e., in Drell-Yan ($pp \rightarrow \gamma^* X \rightarrow \ell^+ \ell^- X$) and in W boson production with a leptonic decay ($pp \rightarrow WX \rightarrow \ell \nu_\ell X$).

Measuring the double transverse spin asymmetry A_{TT} in W boson production is in the future physics program of BNL's Relativistic Heavy Ion Collider (RHIC) [35] with the aim of finding physics Beyond the SM (BSM). Within the SM this spin asymmetry is zero at leading twist collinear factorization [36], because the W boson only couples to chiral left-handed quarks. A non-zero transverse spin asymmetry would indicate a mixed left- and right-handed coupling and thus BSM physics.

In the leptonic decay of a W boson, the neutrino goes unobserved making it very difficult to accurately determine the W boson's transverse momentum. It is therefore unlikely that $A_{TT}(q_T)$ will be measured, but instead an asymmetry differential in the charged lepton transverse momentum $A_{TT}(l_T)$. For $A_{TT}(l_T)$ it is possible to do a collinear expansion and express it in terms of collinear correlators. Higher order terms in the collinear expansion are in [35] dismissed on the basis of an expected M^2/M_W^2 suppression, where M is the hadronic scale and M_W the W boson mass.

Within the framework of TMD factorization the worm-gear and Sivers contribution to $A_{TT}(q_T)$ in W production was calculated in [37, 38], where it was found that the TMD and BSM effects give rise to asymmetries with different angular dependencies and thus can be separated from each other. These calculations use angles defined in the so called Collins-Soper (CS) frame, but in a realistic situation it is unlikely that this frame can be determined as it is necessary to accurately determine the W boson's transverse momentum for this.

We will therefore calculate¹ the double spin asymmetries in W boson production as a function

¹This Chapter is based on [39] and [40].

of the charged lepton momentum and azimuthal angle as measured in the laboratory frame, integrated over the neutrino momentum as that is the observable that actually *can* be measured. As it turns out, both BSM physics and TMD effects give rise to the *same* angular dependency if angles are measured in the lab frame. Besides that, we find that the asymmetries can be much larger than expected on the basis of the collinear higher twist suppression argument.

Using realistic assumptions for the Siverson and worm-gear distributions, we find that the asymmetries are below what could be measured at RHIC and thus do not form a real background for BSM studies. We stress, however, that even though \mathbf{q}_T is not observed and we can thus make a collinear expansion, the higher order corrections are not suppressed by M^2/M_W^2 and one should thus be very careful with dismissing TMD effects on the basis of not observing \mathbf{q}_T .

In contrast to W boson production, there *is* a double transverse spin asymmetry in the Drell-Yan process within the SM using collinear factorization. The DY double transverse spin asymmetry is proportional to the transversity distribution, more specifically it is of the form

$$A_{TT} \propto \cos\left(2\phi_S^\ell\right) \left[h_1^q(x_1)h_1^{\bar{q}}(x_2) + x_1 \leftrightarrow x_2\right], \quad (3.3)$$

where ϕ_S^ℓ is the angle between the lepton plane and the spin plane as shown in Figure 3.3 and it is planned to be measured at RHIC as a way to determine the transversity distribution [35].

One can also measure $A_{TT}(q_T)$, which is the double transverse spin asymmetry *at measured* q_T . The asymmetry as a function of q_T has been studied in Ref. [41] using a Collins-Soper-Sterman resummation approach (resumming large logs $\log^n q_T/Q$ to extend the collinear factorization regime down to small values of q_T , but neglecting intrinsic transverse momentum), showing it to be maximally of order 5% and fairly flat in q_T up to a few GeV. At measured q_T there will however be contributions from transverse momentum dependent effects.

Going beyond the collinear approximation, the leptons are not back-to-back anymore and one has to use another definition of the angle. Defining ϕ_S^ℓ as the angle between the momentum of one of the leptons and the spin plane as measured in the lab frame, there will again be contributions to A_{TT} from TMD effects with the same angular dependency as the contribution from transversity. We will calculate these contributions to see whether TMD effects will pose a substantial background for transversity measurements using spin asymmetries measured as a function of the lepton angle measured in the lab frame.

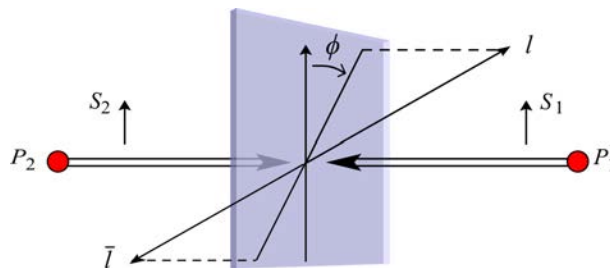


Figure 3.3: The azimuthal angle ϕ_S^ℓ is defined as the angle between the lepton plane and the spin plane. In the presence of partonic transverse momentum, the leptons are not back-to-back and do not form a plane with the beam axis and one has to use a more precise definition.

3.2 Drell-Yan and W boson production in TMD factorization

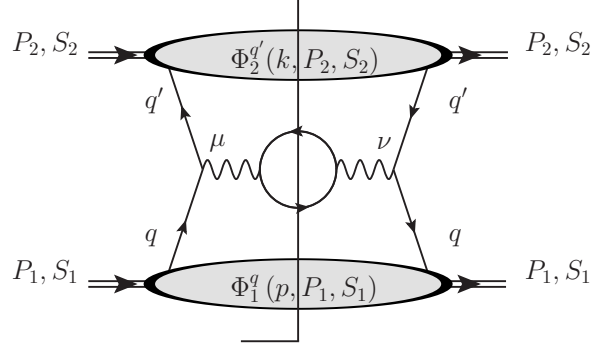


Figure 3.4: Leading diagram in Drell-Yan and W boson production.

In both processes we have to deal with vector-boson production from hadron-hadron collisions, with a subsequent leptonic decay. The cross section for such a process has its leading contribution coming from quark–antiquark annihilation diagram shown in Fig. 3.4. Using the factorization expression in Eq. (2.38) we can write the leading contribution to the cross section as

$$\frac{d\sigma}{d\mathcal{R}} = \frac{(2\pi)^4}{3S^2} \sum_{q,q'} \int d^2\mathbf{p}_T d^2\mathbf{k}_T \delta^2(\mathbf{p}_T + \mathbf{k}_T - \mathbf{q}_T) \times \\ \text{Tr}_D \left[\Phi^{[-]q}(x_1, \mathbf{p}_T, P_1, S_1) V_{qq'}^\nu \bar{\Phi}^{[-]q'}(x_2, \mathbf{k}_T, P_2, S_2) V_{qq'}^{\prime\mu} \right] D_{\mu\rho} D_{\nu\sigma}^* L^{\rho\sigma} + (1 \leftrightarrow 2), \quad (3.4)$$

in which $V_{qq'}^\mu$ is the vector-boson–quark interaction vertex (primed implies complex conjugated coupling strength), $D_{\mu\nu}$ is the vector boson propagator,

$$L^{\rho\sigma} = \text{Tr} [V_l^\rho \not{l} V_l^{\prime\sigma} l] \quad (3.5)$$

is the lepton tensor and

$$d\mathcal{R} = \frac{d^3\vec{l}}{(2\pi)^3 2E_l} \frac{d^3\vec{l}}{(2\pi)^3 2E_{\bar{l}}} \quad (3.6)$$

is the dilepton phase space element. We will define a spin flip symmetric and antisymmetric cross section by

$$\frac{d\sigma^S}{d\mathcal{R}} \equiv \frac{1}{4} \left(\frac{d\sigma^{\uparrow\uparrow}}{d\mathcal{R}} + \frac{d\sigma^{\uparrow\downarrow}}{d\mathcal{R}} + \frac{d\sigma^{\downarrow\uparrow}}{d\mathcal{R}} + \frac{d\sigma^{\downarrow\downarrow}}{d\mathcal{R}} \right), \\ \frac{d\sigma^A}{d\mathcal{R}} \equiv \frac{1}{4} \left(\frac{d\sigma^{\uparrow\uparrow}}{d\mathcal{R}} - \frac{d\sigma^{\uparrow\downarrow}}{d\mathcal{R}} - \frac{d\sigma^{\downarrow\uparrow}}{d\mathcal{R}} + \frac{d\sigma^{\downarrow\downarrow}}{d\mathcal{R}} \right). \quad (3.7)$$

3.3 Parameterization of the Sivers and worm-gear function

As often done, for our phenomenological studies we will assume factorization between \mathbf{k}_T and x dependence in the distribution functions, with a Gaussian dependence on \mathbf{k}_T . The unpolarized

TMD PDF $f_1^q(x, k_T)$ will thus read

$$f_1^q(x, k_T) = \frac{1}{\pi \langle k_T^2 \rangle} e^{-k_T^2 / \langle k_T^2 \rangle} f_1^q(x), \quad (3.8)$$

where $f_1^q(x)$ is the collinear parton distribution function, for which we use the global fit from [42]. Such a Gaussian dependence on \mathbf{k}_T has been shown to work very well [43]. We will use the value of the width,

$$\langle k_T^2 \rangle = 0.25 \text{ GeV}^2, \quad (3.9)$$

found by [44] based on the Cahn effect in unpolarized SIDIS. Although this value may differ from the $\langle k_T^2 \rangle$ in Drell-Yan, the deviation is not expected to matter for our purposes and to fall within the error in the estimates we will consider.

In SIDIS there are clear experimental observations of the asymmetries that would arise from the Siverts effect, offering strong support for the latter effect. Within that picture the current experimental data allows for a determination of the Siverts function for both the u and d quarks and antiquarks. In the recent extraction obtained by [45], the Siverts function for SIDIS is parameterized as

$$f_{1T}^{\perp q}(x, k_T) = -\mathcal{N}_q(x) h'(k_T) f_1^q(x, k_T) \quad (3.10)$$

with

$$h'(k_T) = \sqrt{2} e \frac{M_p}{M_1} e^{-k_T^2 / M_1^2}, \quad (3.11)$$

$$\mathcal{N}_q(x) = N_q x^{\alpha_q} (1-x)^{\beta_q} \frac{(\alpha_q + \beta_q)^{\alpha_q + \beta_q}}{\alpha_q^{\alpha_q} \beta_q^{\beta_q}}.$$

The numerical values found in the extraction are $M_1^2 = 0.34 \text{ GeV}^2$ for the flavor independent width of the distribution and the numbers in Table 3.1 for the parameters in the flavor dependent function that describes the x dependence. The resulting Siverts function is plotted in Figure 3.5. The current knowledge of the Siverts function at small x is limited, but the single spin asymmetry measurements at RHIC will certainly improve this. For the moment, we take what is known until a better determination will be available. Taking into account the error bars in [45] we come to the rough estimate that the effect of the Siverts function, as will be calculated in Section 3.4 and 3.5, could be maximally enhanced by an order of magnitude. As said before, the sign of the Siverts function for Drell-Yan is supposed to be opposite to the one for SIDIS, however in the *double* Siverts effect this has no influence.

	u	\bar{u}	d	\bar{d}
α_q	0.73	0.79	1.08	0.79
β_q	3.46	3.46	3.46	3.46
N_q	0.35	0.04	-0.9	-0.4

Table 3.1: Numerical values for the parameters in the Siverts function from [45].

A determination of the worm-gear function, based on fits of experimental data, is not available. Data on double transverse spin asymmetries A_{LT} that receive contributions from the WG

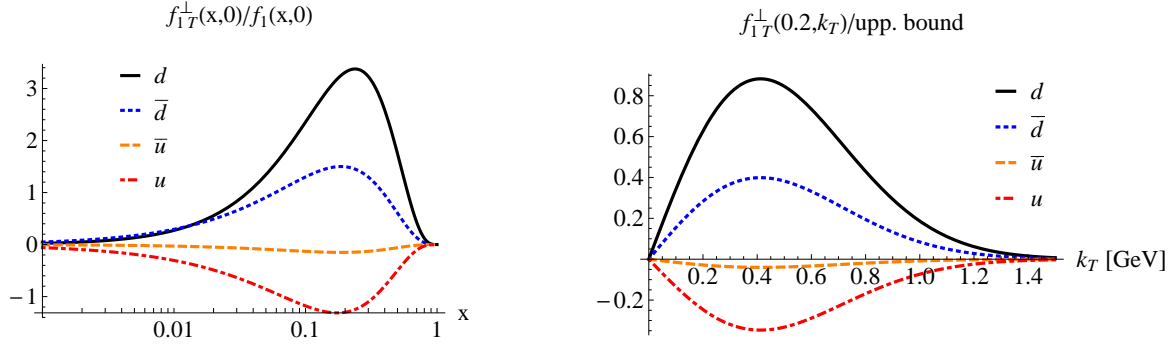


Figure 3.5: Plots of the Sivers function as extracted by [45] as a function of x (left) and k_T (right). The upper bound is as given in Eq. (2.70).

effect has become available only very recently [33, 34]. Recent measurements on ${}^3\text{He}$ indicate that g_{1T} for the up-quark is not small [34].

Given the fact that experimental extractions of the WG function are not available, we will employ a model for this function. Both the bag model [46] and the spectator model [47] agree quite well with a Gaussian approximation of the transverse momentum dependence for not too large values of the transverse momentum. We will therefore use a Gaussian Ansatz, which allows us to express the transverse momentum dependent distribution as

$$g_{1T}^q(x, k_T) = \frac{2M_p^2}{\pi \langle k_T^2 \rangle_{\text{WG}}^2} e^{-k_T^2 / \langle k_T^2 \rangle_{\text{WG}}} g_{1T}^{q(1)}(x), \quad (3.12)$$

in terms of its first transverse moment $g_{1T}^{q(1)}(x)$, which is defined as [48]

$$g_{1T}^{q(1)}(x) \equiv \int d^2 k_T \frac{k_T^2}{2M_p^2} g_{1T}^q(x, k_T). \quad (3.13)$$

For the width we will take a value in accordance with the bag model

$$\langle k_T^2 \rangle_{\text{WG}} = 0.71 \langle k_T^2 \rangle. \quad (3.14)$$

For the first moment, we will use a Wandzura-Wilczek (WW) type approximation [48, 49, 50] to express it in terms of the known helicity distribution $g_1(x)$ by

$$g_{1T}^{q(1)}(x) \approx x \int_x^1 dy \frac{g_1^q(y)}{y}. \quad (3.15)$$

For numerical estimates of this function the DSSV helicity distribution [51] will be used. The resulting worm-gear function is plotted in Figure 3.6. Deviations from the WW approximation can be considered [52], but the WW distribution is in fair agreement with the bag model, the spectator model, the light cone constituent quark model [53] and the light cone quark-diquark model [54]. Furthermore, a recent determination of target transverse spin asymmetries in SIDIS [55] is consistent with the theoretical prediction based on the WW type approximation of [56]. With all these ingredients the lowest Mellin moment $g_{1T}^{q(0,1)} \equiv \int dx g_{1T}^{q(1)}(x)$ of the first transverse

moment $g_{1T}^{q(1)}(x)$ can be calculated. We find $g_{1T}^{u(0,1)} = 0.091$ and $g_{1T}^{d(0,1)} = -0.026$. This is in excellent agreement with the evaluation on the lattice (at the scale 1.6 GeV): $g_{1T}^{u(0,1)} = 0.1055(66)$ and $g_{1T}^{d(0,1)} = -0.0235(38)$ from Ref. [57]. All this gives us confidence that the estimates below are sufficiently realistic.

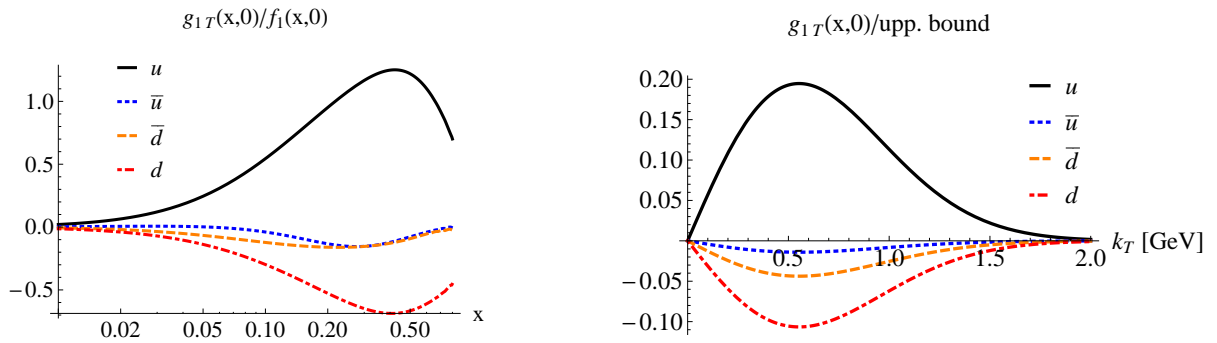


Figure 3.6: Plots of the worm-gear function obtained using the WW approximation in Eq. (3.15) as a function of x (left) and k_T (right). The upper bound is as given in Eq. (2.70).

3.4 Spin asymmetries in the Drell-Yan process

In the Drell-Yan process the virtual photon produces a lepton and anti-lepton, both of which can be detected. This allows a full determination of all the kinematic variables, such that one can transform to the Collins-Soper frame [58]. In that frame a double transverse spin asymmetry that depends on the lepton azimuthal angle can come solely from the transversity distribution, which makes this observable very suitable for an extraction of this distribution function from $A_{TT}(q_T)$. If one analyzes the lepton angular distribution in the lab frame, however, there can be a residual asymmetry coming from double Sivers and WG effects for the following reason. The Sivers and WG function both cause the photon transverse momentum and the proton spins to be correlated. When the virtual photon decays, the decay products are more inclined to move in the direction of the parent particle which, in turn, causes the direction of the decay products to be *also* correlated with the proton spin directions, albeit diluted.

In order to estimate the error that one would possibly make in the extraction of the transversity distributions from $A_{TT}(q_T)$ by not measuring the lepton angle ϕ_ℓ in the CS frame, we will calculate the double transverse spin asymmetries as a function of ϕ_ℓ measured in the laboratory frame coming from the Sivers and WG functions.

In the following analysis we will work towards an asymmetry differential in the photon's momentum squared Q^2 , transverse momentum length q_T , and rapidity $Y \equiv \frac{1}{2} \log q^+/q^-$. The other kinematic variables, which will be integrated over, are ϕ_q , which is the azimuthal angle of \mathbf{q}_T , and y , which is defined as $y \equiv l^-/q^-$. The final kinematic variable is the direction of the lepton transverse momentum ϕ_ℓ in the lab frame, which in the end will be integrated over with particular weights to select out the different contributions to the spin asymmetries. Rewriting

the phase space element into these lab frame coordinates, we get

$$d\mathcal{R} = \frac{Qq_T}{4(2\pi)^6} dq_T d\phi_q d\phi_\ell dQ dY dy \left(1 + \frac{q_T \cos(\phi_\ell - \phi_q)}{\sqrt{Q^2 \frac{1-y}{y} - q_T^2 \sin^2(\phi_\ell - \phi_q)}} \right), \quad (3.16)$$

such that the cross section we are interested in reads

$$\frac{d\sigma^{S,A}}{dQ dq_T d\phi_\ell dY} = \int dy d\phi_q \frac{q_T Q}{4(2\pi)^6} \left(1 + \frac{q_T \cos(\phi_\ell - \phi_q)}{\sqrt{Q^2 \frac{1-y}{y} - q_T^2 \sin^2(\phi_\ell - \phi_q)}} \right) \frac{d\sigma^{S,A}}{d\mathcal{R}}, \quad (3.17)$$

where $d\sigma/d\mathcal{R}$ is to be calculated according to Eq. (3.4). The vertices and propagator are, for the Drell-Yan process, given by

$$\begin{aligned} V_{qq'}^\nu &= ie_q e\gamma^\nu \delta_{qq'}, \\ V_l^\rho &= -ie\gamma^\rho, \\ D_{\mu\nu} &= -ig_{\mu\nu}/Q^2. \end{aligned} \quad (3.18)$$

Furthermore, the lepton (l) and anti-lepton (\bar{l}) momentum 4-vectors are specified in the lab frame by (in light cone notation $q = [q^-, q^+, \mathbf{q}_T]$)

$$\begin{aligned} l &= \left[\frac{1}{\sqrt{2}} \sqrt{\frac{y}{1-y}} e^{-Y} \sqrt{(1-y)l_T^2 + y\bar{l}_T^2}, \frac{\frac{1}{\sqrt{2}} \sqrt{\frac{1-y}{y}} l_T^2 e^Y}{\sqrt{(1-y)l_T^2 + y\bar{l}_T^2}}, l_T \cos \phi_\ell, l_T \sin \phi_\ell \right], \\ \bar{l} &= \left[\frac{1}{\sqrt{2}} \sqrt{\frac{1-y}{y}} e^{-Y} \sqrt{(1-y)l_T^2 + y\bar{l}_T^2}, \frac{\frac{1}{\sqrt{2}} \sqrt{\frac{y}{1-y}} \bar{l}_T^2 e^Y}{\sqrt{(1-y)l_T^2 + y\bar{l}_T^2}}, \right. \\ &\quad \left. q_T \cos \phi_q - l_T \cos \phi_\ell, q_T \sin \phi_q - l_T \sin \phi_\ell \right], \end{aligned} \quad (3.19)$$

where

$$l_T = q_T y \cos(\phi_\ell - \phi_q) + \sqrt{Q^2 y(1-y) - q_T^2 y^2 \sin^2(\phi_\ell - \phi_q)}. \quad (3.20)$$

The light cone momentum fractions are in terms of the lab-frame coordinates given by

$$x_{1,2} = e^{\pm Y} \sqrt{\frac{Q^2 + q_T^2}{S}}. \quad (3.21)$$

Having all these ingredients the cross section can be calculated using Eq. (3.4). The \mathbf{k}_T , \mathbf{p}_T and y integrals are performed, after which the resulting expression is expanded in powers of q_T/Q except for the Gaussian in the distributions, which delivers the high q_T suppression, and the expression for $x_{1,2}$ in the distribution functions. The expansion in q_T allows us to perform the ϕ_q integration analytically. After having done the ϕ_q integration we obtain the following approximate expression for the symmetric cross section,

$$\frac{d\sigma^S}{dq_T dQ d\phi_\ell dY} = \sum_q \frac{4\alpha^2 e_q^2 q_T}{9 \langle k_T^2 \rangle QS} e^{-q_T^2/2 \langle k_T^2 \rangle} F_1^q(x_1, x_2), \quad (3.22)$$

which is accurate up to leading order in $\mathcal{O}(q_T/Q)$. We have defined the following combination of distribution functions,

$$F_1^q(x_1, x_2) \equiv f_1^q(x_1)f_1^{\bar{q}}(x_2) + f_1^q(x_2)f_1^{\bar{q}}(x_1). \quad (3.23)$$

The symmetric cross section, integrated over ϕ_ℓ , is plotted as function of the three remaining variables in Fig. 3.7.

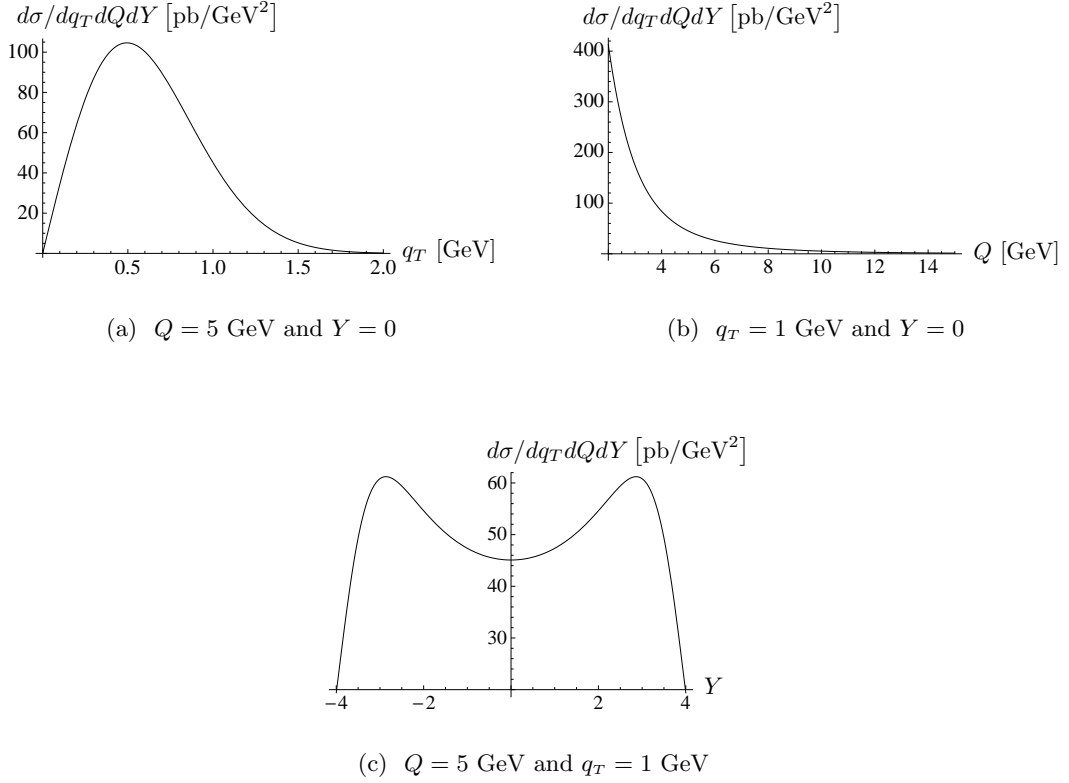


Figure 3.7: Differential cross section for the Drell-Yan process at RHIC energy $\sqrt{s} = 500$ GeV.

For the antisymmetric cross section we find the expression, keeping only leading order terms in q_T/Q for both the ϕ_ℓ dependent and independent part,

$$\begin{aligned} \frac{d\sigma^A}{dq_T dQ d\phi_\ell dY} = \sum_q \frac{\alpha^2 e_q^2 |\mathbf{S}_T|^2 q_T}{9M_p^2 QS} \left\{ e^{-q_T^2/2\langle k_T^2 \rangle_S} \left[1 - \frac{q_T^2}{2\langle k_T^2 \rangle_S} + \frac{q_T^4}{16Q^2 \langle k_T^2 \rangle_S} \cos 2\phi_S^\ell \right] F_{1T}^{\perp q}(x_1, x_2) \right. \\ \left. + e^{-q_T^2/2\langle k_T^2 \rangle_{WG}} \left[-1 + \frac{q_T^2}{2\langle k_T^2 \rangle_{WG}} + \frac{q_T^4}{16Q^2 \langle k_T^2 \rangle_{WG}} \cos 2\phi_S^\ell \right] G_{1T}^q(x_1, x_2) \right\}, \quad (3.24) \end{aligned}$$

where $\phi_S^\ell \equiv \phi_S - \phi_\ell$ is the angle between the spin plane and the lepton transverse momentum, and

$$\begin{aligned} F_{1T}^{\perp q}(x_1, x_2) &\equiv f_{1T}^{\perp q}(x_1)f_{1T}^{\perp \bar{q}}(x_2) + f_{1T}^{\perp q}(x_2)f_{1T}^{\perp \bar{q}}(x_1), \\ G_{1T}^q(x_1, x_2) &\equiv g_{1T}^q(x_1)g_{1T}^{\bar{q}}(x_2) + g_{1T}^q(x_2)g_{1T}^{\bar{q}}(x_1), \end{aligned} \quad (3.25)$$

in which $f_{1T}^{\perp q}(x)$ and $g_{1T}^q(x)$ are defined through the relation

$$\begin{aligned} f_{1T}^{\perp q}(x, k_T) &= \frac{1}{\pi \langle k_T^2 \rangle_S} e^{-k_T^2 / \langle k_T^2 \rangle_S} f_{1T}^{\perp q}(x), \\ g_{1T}^q(x, k_T) &= \frac{1}{\pi \langle k_T^2 \rangle_{\text{WG}}} e^{-k_T^2 / \langle k_T^2 \rangle_{\text{WG}}} g_{1T}^q(x), \end{aligned} \quad (3.26)$$

where the width of the Sivers function is given by

$$\langle k_T^2 \rangle_S \equiv \frac{\langle k_T^2 \rangle M_1^2}{\langle k_T^2 \rangle + M_1^2}. \quad (3.27)$$

We will define the three spin asymmetries

$$\begin{aligned} A_{TT}^0(q_T) &\equiv \frac{\int_0^{2\pi} d\phi_\ell d\sigma^A}{\int_0^{2\pi} d\phi_\ell d\sigma^S}, \\ A_{TT}^C(q_T) &\equiv \frac{\left(\int_{-\pi/4}^{\pi/4} - \int_{\pi/4}^{3\pi/4} + \int_{3\pi/4}^{5\pi/4} - \int_{5\pi/4}^{7\pi/4} \right) d\phi_\ell d\sigma^A}{\int_0^{2\pi} d\phi_\ell d\sigma^S}, \\ A_{TT}^S(q_T) &\equiv \frac{\left(\int_0^{\pi/2} - \int_{\pi/2}^{\pi} + \int_{\pi}^{3\pi/2} - \int_{3\pi/2}^{2\pi} \right) d\phi_\ell d\sigma^A}{\int_0^{2\pi} d\phi_\ell d\sigma^S}, \end{aligned} \quad (3.28)$$

which select out the ϕ_S^ℓ independent, cosine modulated and sine modulated terms, respectively. The latter, $A_{TT}^S(q_T)$, will be zero in this case, but not in W production (cf. next section) or γ - Z interference (not considered here, see, e.g., [37] or [38]). Both the $A_{TT}^C(q_T)$ asymmetry, to which transversity contributes, and the $A_{TT}^0(q_T)$ asymmetry receive a nonzero contribution from the double Sivers and WG effects and can be written as

$$\begin{aligned} A_{TT}^0(q_T) &= \frac{|\mathbf{S}_T|^2 \langle k_T^2 \rangle}{4M_p^2} \left\{ e^{-\frac{q_T^2}{2M_1^2}} \left(1 - \frac{q_T^2}{2\langle k_T^2 \rangle_S} \right) \frac{\sum_q e_q^2 F_{1T}^{\perp q}(x_1, x_2)}{\sum_q e_q^2 F_1^q(x_1, x_2)} \right. \\ &\quad \left. - e^{-q_T^2 \frac{\langle k_T^2 \rangle - \langle k_T^2 \rangle_{\text{WG}}}{2\langle k_T^2 \rangle \langle k_T^2 \rangle_{\text{WG}}}} \left(1 - \frac{q_T^2}{2\langle k_T^2 \rangle_{\text{WG}}} \right) \frac{\sum_q e_q^2 G_{1T}^q(x_1, x_2)}{\sum_q e_q^2 F_1^q(x_1, x_2)} \right\} \quad (3.29) \end{aligned}$$

and

$$\begin{aligned} A_{TT}^C(q_T) &= \frac{|\mathbf{S}_T|^2 \langle k_T^2 \rangle q_T^2}{32\pi M_p^2 Q^2} \left\{ e^{-\frac{q_T^2}{2M_1^2}} \frac{q_T^2}{\langle k_T^2 \rangle_S} \frac{\sum_q e_q^2 F_{1T}^{\perp q}(x_1, x_2)}{\sum_q e_q^2 F_1^q(x_1, x_2)} \right. \\ &\quad \left. + e^{-q_T^2 \frac{\langle k_T^2 \rangle - \langle k_T^2 \rangle_{\text{WG}}}{2\langle k_T^2 \rangle \langle k_T^2 \rangle_{\text{WG}}}} \frac{q_T^2}{\langle k_T^2 \rangle_{\text{WG}}} \frac{\sum_q e_q^2 G_{1T}^q(x_1, x_2)}{\sum_q e_q^2 F_1^q(x_1, x_2)} \right\}. \quad (3.30) \end{aligned}$$

We note that the bound on the $\cos 2\phi_S^\ell$ double transverse spin asymmetry as a function of q_T from transversity was estimated, within a collinear Collins-Soper-Sterman resummation approach [41], to be maximally of order 5% and fairly flat in q_T up to a few GeV at RHIC at a center of mass energy of 500 GeV. The first extraction of the quark transversity distribution h_1^q [59, 60], however,

indicates it to be about half its maximally allowed value at $Q^2 \sim 2 \text{ GeV}^2$. Therefore, if this also applies to the antiquark $h_1^{\bar{q}}$, an asymmetry of 1% or less should be expected at RHIC.

Asymmetries that are below the per mil level in the entire kinematic range of interest will generally not be shown. They will be below the detection limit at RHIC, which will be mainly restricted by systematic errors. For the case of Drell-Yan this will only leave the Siverson effect contribution to the asymmetry $A_{TT}^0(q_T)$, displayed in Fig. 3.8 as function of q_T , Q and Y . In the plot we also included, albeit completely negligible, the Siverson effect contribution to $A_{TT}^C(q_T)$, just in case the Siverson function at these values of x and Q turns out to be much larger.

The $A_{TT}^0(q_T)$ asymmetry reaches up to the percent level, but only for large Q^2 outside the range of interest. In the standard Drell-Yan range between the J/ψ and Υ , the asymmetry is on the per mil level for the double Siverson effect and far below that level for the double WG effect.

The $A_{TT}^C(q_T)$ asymmetry receives a contribution from the double Siverson effect at a level of 10^{-6} and from the g_{1T} function a contribution at a level of 10^{-8} . At small Q the asymmetry is small due to the smallness of the Siverson function with respect to the unpolarized distribution at low values of x , whereas at higher values of Q the q_T^2/Q^2 suppression becomes important. One way or the other, these magnitudes are far below the detection limit at RHIC, even if one takes into account a possible enhancement of the effect by an order of magnitude due to the uncertainty in the used parameterization of the Siverson function. Therefore, the TMD effects will not spoil a determination of the transversity distribution if those are determined from $A_{TT}^C(q_T)$ in the lab frame instead of in the Collins-Soper frame. As a cross-check, to assure that TMD effects are small, one could verify that the $A_{TT}^0(q_T)$ asymmetry is small. The $A_{TT}^C(q_T)$ asymmetry is bounded by the larger $A_{TT}^0(q_T)$ asymmetry due to the q_T^2/Q^2 suppression, irrespective of any assumptions on the Siverson function or the worm-gear distribution. We want to note that, considering asymmetries of this size, higher twist effects could become important. In case of incomplete averaging over the azimuthal angle, the ϕ_ℓ independent asymmetry $A_{TT}^0(q_T)$ may form a background for a determination of the ϕ_ℓ dependent $A_{TT}^C(q_T)$, but given its magnitude this should also not pose a problem.

The q_T -integrated asymmetries have also been calculated and A_{TT}^C is found to be a factor two smaller than $A_{TT}^C(q_T)$ and A_{TT}^0 a factor 1000 smaller than $A_{TT}^0(q_T)$. This agrees with the expectation that such effects are (at least) $\mathcal{O}(M_p^2/Q^2)$ power suppressed in this case. For completeness, we mention that the maximal q_T -integrated A_{TT}^C asymmetry from transversity is estimated to be at the few percent level at RHIC at a center of mass energy of 200 and 500 GeV [61, 62].

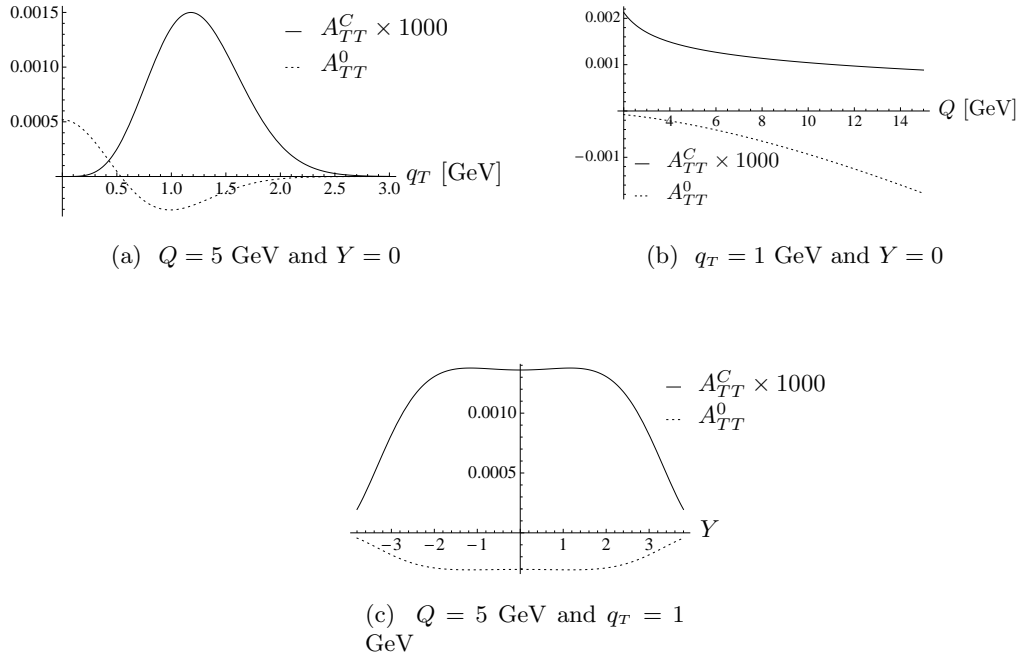


Figure 3.8: Contribution to $A_{TT}(q_T)$ in the Drell-Yan process from the double Sivers effect at RHIC energy $\sqrt{s} = 500$ GeV.

3.5 Spin asymmetries in W boson production

In the leptonic decay of a W boson the neutrino will go unobserved, which renders it impossible to determine the Collins-Soper frame. In that frame a double transverse spin asymmetry that depends on the lepton azimuthal angle can solely be caused by a non-zero right-handed coupling of the W boson in combination with a non-zero transversity distribution, which makes it a very suitable process for the determination of a possible $W - W'$ mixing as discussed in [36, 63, 64] and the next chapter. In the lab frame, however, there might again be a residual asymmetry coming from the double Sivers or WG effects. They can lead to a nonzero result in W production, which could be mistaken for physics beyond the Standard Model or simply spoil the opportunity to bound a possible $W - W'$ mixing.

In Ref. [64] the TMD background was dismissed on the basis of a dimensional counting argument. If the single Sivers effect is a 10% effect, a double Sivers effect asymmetry in W production would be on the percent level. However, as the Sivers asymmetry is an azimuthal asymmetry of \mathbf{q}_T , the lack of the knowledge of the W momentum prevents reconstruction of the asymmetry in W production directly. Instead, a lepton asymmetry can be measured (cf. [65]), which has a reduced magnitude. Naively one would expect from a dimensional analysis a large suppression of the size q_T^2/l_T^2 , where q_T denotes the size of the gauge boson transverse momentum ($\approx \langle k_T^2 \rangle$) and l_T of the lepton transverse momentum ($\approx M_W/2$). The reason being that the asymmetry should vanish in the limit $q_T \rightarrow 0$ and the only compensating scale is l_T . This would yield an asymmetry far below the per mil level. Another way to put it, is saying that since the transverse momentum of the W boson is not observed, collinear factorization applies.

Within collinear factorization, there are no spin asymmetries in W boson production at leading twist. Double transverse spin asymmetries can only be generated at next-to-next-to-leading twist, which is (naively) suppressed by M_p^2/Q^2 , i.e., M_p^2/M_W^2 in this case. A similar argument would suggest the single spin asymmetry $A_N(q_T)$ in W production arising from the Sivers effect to be q_T/l_T or M_p/M_W suppressed, leading to an asymmetry below the percent level. However, the Sivers effect in $A_N(q_T)$ in W production has recently been studied theoretically [30] and a large asymmetry (of order 10%) was predicted. Moreover, in Ref. [31] the lepton asymmetry $A_N(l_T)$ was evaluated numerically, which has a reduced magnitude, but still is around 3% for W^+ production. This is larger than expected from the dimensional argument and is because near resonance the width of the W boson becomes an important scale. The suppression can therefore be only as small as q_T/Γ_W , where Γ_W is the width of the W boson (≈ 2.1 GeV). In the language of collinear factorization, one should state that higher twist is not necessarily suppressed by factors of M_p/Q , because there is another scale in the hard part, being Γ_W in this case. Similarly, a double Sivers effect contribution to $A_{TT}(q_T)$ in W production is expected to be on the percent level and a factor q_T^2/Γ_W^2 smaller for the lepton asymmetry $A_{TT}(l_T)$ near resonance. When integrated over l_T instead, one can expect the asymmetry to be suppressed by a factor of q_T^2/M_W^2 , which implies an asymmetry well below the per mil level. Below we confirm these insights in an explicit calculation.

Rewriting the phase space element into the lab frame coordinates that will be observed, the lepton transverse momentum \mathbf{l}_T and its forward rapidity $Y_l \equiv \frac{1}{2} \log l^+/l^-$, and the remaining \mathbf{q}_T (or $\bar{\mathbf{l}}_T$) and $Y_{\bar{l}}$ that will be integrated over, we get

$$d\mathcal{R} = \frac{1}{4(2\pi)^6} d^2\mathbf{l}_T d^2\mathbf{q}_T dY_l dY_{\bar{l}} \quad (3.31)$$

such that the cross section we are interested in reads

$$\frac{d\sigma^{S,A}}{dl_T dY_l d\phi_\ell} = \frac{l_T}{4(2\pi)^6} \int dY_{\bar{l}} d^2\mathbf{q}_T \frac{d\sigma^{S,A}}{d\mathcal{R}}. \quad (3.32)$$

For W^- production, the interaction vertices and propagator read

$$\begin{aligned} V_{qq'}^\mu &= \frac{ig}{\sqrt{2}} (V_{CKM}^{ud})^* \gamma^\mu \mathcal{P}_L \delta_{uq'} \delta_{dq}, \\ V_l^\rho &= \frac{ig}{\sqrt{2}} \gamma^\rho \mathcal{P}_L, \\ D_{\mu\nu}^W &= \frac{-i}{q^2 - M_W^2 + i\Gamma_W M_W} \left(g_{\mu\nu} - \frac{q_\mu q_\nu}{M_W^2} \right), \end{aligned} \quad (3.33)$$

from which the W^+ coupling is obtained by $u \leftrightarrow d$ and $V_{CKM}^* \rightarrow V_{CKM}$. The charged lepton (l) and neutrino (\bar{l}) momentum 4-vectors can, in the lab frame, be expressed by (in light cone notation $l = [l^-, l^+, \mathbf{l}_T]$)

$$l = \left[\frac{l_T}{\sqrt{2}} e^{-Y_l}, \frac{l_T}{\sqrt{2}} e^{Y_l}, l_T \cos \phi_\ell, l_T \sin \phi_\ell \right], \quad \bar{l} = \left[\frac{\bar{l}_T}{\sqrt{2}} e^{-Y_{\bar{l}}}, \frac{\bar{l}_T}{\sqrt{2}} e^{Y_{\bar{l}}}, \mathbf{q}_T - \mathbf{l}_T \right], \quad (3.34)$$

in terms of the neutrino rapidity $Y_{\bar{l}}$, the charged lepton transverse momentum (in terms of l_T and ϕ_ℓ), the charged lepton rapidity Y_l , and the W boson transverse momentum \mathbf{q}_T . The light

cone momentum fractions can be expressed in terms of l_T through a power expansion in q_T as

$$\begin{aligned} x_1 &= \frac{l_T}{\sqrt{s}} (e^{Y_l} + e^{Y_{\bar{l}}}) - \frac{q_T}{\sqrt{s}} e^{Y_{\bar{l}}} \cos(\phi_\ell - \phi_q) + \mathcal{O}\left(\frac{q_T^2}{s}\right), \\ x_2 &= \frac{l_T}{\sqrt{s}} (e^{-Y_l} + e^{-Y_{\bar{l}}}) - \frac{q_T}{\sqrt{s}} e^{-Y_{\bar{l}}} \cos(\phi_\ell - \phi_q) + \mathcal{O}\left(\frac{q_T^2}{s}\right). \end{aligned} \quad (3.35)$$

As we are working at leading twist only, we can drop the non-leading terms in this expression as well. The advantage is that there will not be any \mathbf{q}_T dependence in the distribution functions, which allows us to perform the \mathbf{q}_T integration in the cross section analytically. After having done the \mathbf{q}_T integration, we expand in the cross section in parton transverse momentum up to order k_T^2 and p_T^2 . The integration with respect to \mathbf{k}_T and \mathbf{p}_T can then be done, which results in an expression in terms of the moments $g_{1T}^{(1)}(x)$, defined in Eq. (3.13), and $f_{1T}^{\perp(1)}(x)$, likewise defined as

$$f_{1T}^{\perp q(1)}(x) \equiv \int d^2\mathbf{k}_T \frac{k_T^2}{2M_p^2} f_{1T}^{\perp q}(x, k_T^2). \quad (3.36)$$

We find for the symmetric part of the cross section for W^- production

$$\frac{d\sigma^S}{dl_T dY_l d\phi_\ell} = \frac{g^4 |V_{CKM}^{ud}|^2 l_T^3}{48(2\pi)^2 S} \int dY_{\bar{l}} \frac{F}{D}, \quad (3.37)$$

and for the antisymmetric part

$$\frac{d\sigma^A}{dl_T dY_l d\phi_\ell} = \frac{g^4 M_p^2 |\mathbf{S}_T|^2 |V_{CKM}^{ud}|^2 l_T}{96(2\pi)^2 S} \int dY_{\bar{l}} \left\{ \frac{A}{D^3} F^O + \frac{B}{D^3} [F^C \cos 2\phi_s^\ell - F^S \sin 2\phi_s^\ell] \right\}, \quad (3.38)$$

where $\phi_s^\ell \equiv \phi_s - \phi_\ell$ is the angle between the spin plane and the charged lepton transverse momentum in the lab frame and

$$\begin{aligned} A &= 150l_T^8 - 32l_T^6 M_W^2 - 12l_T^4 M_W^4 + M_W^8 - 28l_T^4 M_W^2 \Gamma_W^2 + 2M_W^6 \Gamma_W^2 + M_W^4 \Gamma_W^4 \\ &\quad + 4l_T^2 \left[58l_T^6 - 9l_T^4 M_W^2 + M_W^4 (M_W^2 + \Gamma_W^2) - 2l_T^2 (3M_W^4 + 5M_W^2 \Gamma_W^2) \right] \cosh[Y_l - Y_{\bar{l}}] \\ &\quad + 4l_T^4 \left[26l_T^4 - 3M_W^2 (M_W^2 + \Gamma_W^2) \right] \cosh[2(Y_l - Y_{\bar{l}})] + (24l_T^8 + 4l_T^6 M_W^2) \cosh[3(Y_l - Y_{\bar{l}})] \\ &\quad + 2l_T^8 \cosh[4(Y_l - Y_{\bar{l}})], \\ B &= 130l_T^8 + 32l_T^6 M_W^2 + 16l_T^4 M_W^4 (M_W^2 + \Gamma_W^2) - M_W^4 (M_W^2 + \Gamma_W^2)^2 \\ &\quad - 4l_T^4 (15M_W^4 + 11M_W^2 \Gamma_W^2) + 6l_T^8 \cosh[4(Y_l - Y_{\bar{l}})] \\ &\quad + 4l_T^2 \left[54l_T^6 + 9l_T^4 M_W^2 + 3M_W^4 (M_W^2 + \Gamma_W^2) - 2l_T^2 (9M_W^4 + 7M_W^2 \Gamma_W^2) \right] \cosh[Y_l - Y_{\bar{l}}] \\ &\quad + 12l_T^4 \left[10l_T^4 - M_W^2 (M_W^2 + \Gamma_W^2) \right] \cosh[2(Y_l - Y_{\bar{l}})] + (40l_T^8 - 4l_T^6 M_W^2) \cosh[3(Y_l - Y_{\bar{l}})], \\ D &= 6l_T^4 - 4l_T^2 M_W^2 + M_W^4 + M_W^2 \Gamma_W^2 + (8l_T^4 - 4l_T^2 M_W^2) \cosh[Y_l - Y_{\bar{l}}] + 2l_T^4 \cosh[2(Y_l - Y_{\bar{l}})] \end{aligned} \quad (3.39)$$

and the distributions are contained in

$$\begin{aligned}
F &= e^{Y_i - Y_{\bar{i}}} f_1^d(x_1) f_1^{\bar{u}}(x_2) + e^{Y_{\bar{i}} - Y_i} f_1^d(x_2) f_1^{\bar{u}}(x_1), \\
F^0 &= e^{Y_i - Y_{\bar{i}}} \left[f_{1T}^{\perp d(1)}(x_1) f_{1T}^{\perp \bar{u}(1)}(x_2) - g_{1T}^{d(1)}(x_1) g_{1T}^{\bar{u}(1)}(x_2) \right] \\
&\quad + e^{Y_{\bar{i}} - Y_i} \left[f_{1T}^{\perp d(1)}(x_2) f_{1T}^{\perp \bar{u}(1)}(x_1) - g_{1T}^{d(1)}(x_2) g_{1T}^{\bar{u}(1)}(x_1) \right], \\
F^C &= e^{Y_i - Y_{\bar{i}}} \left[f_{1T}^{\perp d(1)}(x_1) f_{1T}^{\perp \bar{u}(1)}(x_2) + g_{1T}^{d(1)}(x_1) g_{1T}^{\bar{u}(1)}(x_2) \right] \\
&\quad + e^{Y_{\bar{i}} - Y_i} \left[f_{1T}^{\perp d(1)}(x_2) f_{1T}^{\perp \bar{u}(1)}(x_1) + g_{1T}^{d(1)}(x_2) g_{1T}^{\bar{u}(1)}(x_1) \right], \\
F^S &= e^{Y_i - Y_{\bar{i}}} \left[f_{1T}^{\perp \bar{u}(1)}(x_2) g_{1T}^{d(1)}(x_1) - f_{1T}^{\perp d(1)}(x_1) g_{1T}^{\bar{u}(1)}(x_2) \right] \\
&\quad + e^{Y_{\bar{i}} - Y_i} \left[f_{1T}^{\perp d(1)}(x_2) g_{1T}^{\bar{u}(1)}(x_1) - f_{1T}^{\perp \bar{u}(1)}(x_1) g_{1T}^{d(1)}(x_2) \right].
\end{aligned} \tag{3.40}$$

With the use of the expressions for the cross section in Eqs. (3.37) and (3.38), the spin asymmetries, as defined in Eq. (3.28), can be written as

$$\begin{aligned}
A_{TT}^0(l_T) &= \frac{|\mathbf{S}_T|^2 M_p^2 \int dY_{\bar{i}} \frac{A}{D^3} F^0}{2l_T^2 \int dY_{\bar{i}} \frac{F}{D}}, \\
A_{TT}^{C,S}(l_T) &= \frac{|\mathbf{S}_T|^2 M_p^2 \int dY_{\bar{i}} \frac{B}{D^3} F^{C,S}}{\pi l_T^2 \int dY_{\bar{i}} \frac{F}{D}}.
\end{aligned} \tag{3.41}$$

The results are easily modified for W^+ production by substituting $\bar{u} \rightarrow \bar{d}$, $d \rightarrow u$ in Eq. (3.40), substituting $l_T \rightarrow \bar{l}_T$, $\phi_{\ell} \rightarrow \phi_{\bar{\ell}}$ in all expressions and integrating over $Y_{\bar{i}}$ instead of Y_i in the cross sections and asymmetries. As a cross-check of the approximation method employed here, we calculated the single spin asymmetry A_N in W production and found reasonable agreement with the results in Refs. [30, 31] taking into account that different distribution functions were used.

The cross sections for W^{\pm} production are plotted in Fig. 3.9, in which numerical values for the parameters are taken from [66], the parameterization of the TMD distributions as discussed in Section 3.3 and the collinear PDFs from [42]. We have plotted the double spin asymmetries in

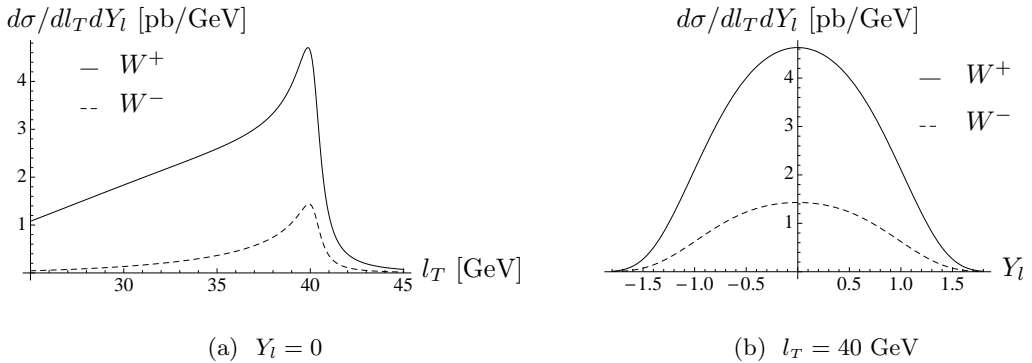


Figure 3.9: Differential cross section for W boson production at RHIC energy $\sqrt{s} = 500$ GeV.

W^+ production in Figs. 3.10 and 3.11 (the asymmetries in W^- production are smaller and will

therefore not be shown). The maximal asymmetry is near resonance and reaches up to 0.15%, which is already below the detection limit at RHIC. However, for a bound on a possible $W - W'$ mixing (discussed in the next Chapter), it is not the differential asymmetry that is relevant, but the asymmetry in the integrated cross section. In those asymmetries the contribution at $l_T < M_W/2$ largely cancels the contribution at $l_T > M_W/2$, resulting in very small asymmetries. We find the integrated asymmetry in W^- production around 10^{-7} and in W^+ production around 10^{-6} , far below detection limits at RHIC. This confirms the expectation expressed in Ref. [64] that the background from TMDs, is indeed negligible. However, the naive expectation that the TMD effects are of order 1% (because of the size of the distribution functions) times a suppression factor of $\langle k_T^2 \rangle / l_T^2$ does not hold.

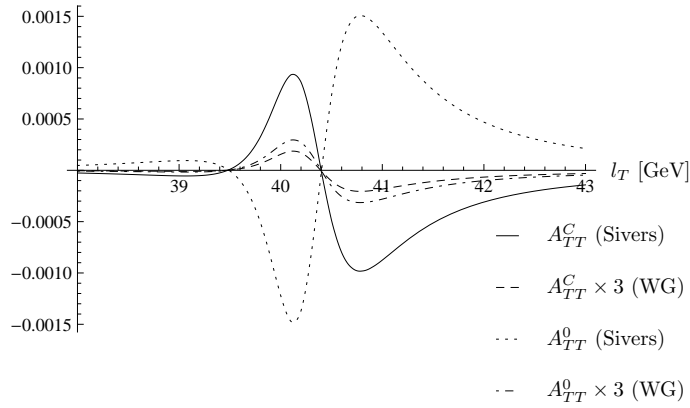


Figure 3.10: Double Sivers and worm-gear contributions to $A_{TT}(l_T)$ in W^+ boson production as a function of l_T at $Y = 0$ and RHIC energy $\sqrt{s} = 500$ GeV.

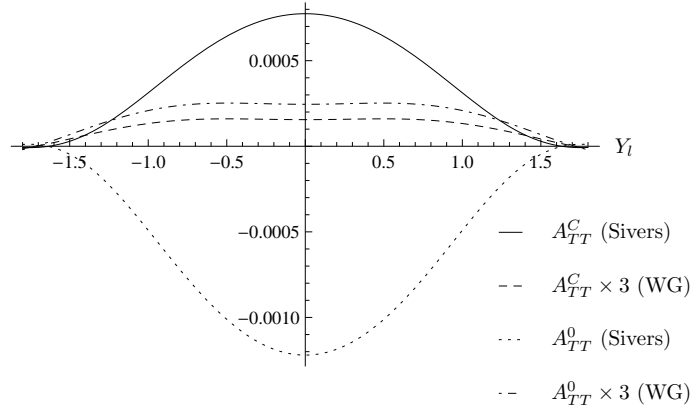


Figure 3.11: Double Sivers and worm-gear contributions to $A_{TT}(l_T)$ in W^+ boson production as a function of Y at $l_T = 40$ GeV at RHIC energy $\sqrt{s} = 500$ GeV.

The maximal effect from the TMDs can be estimated by taking the distribution equal to the

upper bound as given in Eq. (2.70), which leads to

$$f_{1T}^{\perp q(1)}(x) = g_{1T}^{q(1)}(x) = \frac{\sqrt{\pi \langle k_T^2 \rangle}}{4M_p} f_1^q(x). \quad (3.42)$$

In Figure 3.12, we show the maximal effect from the Sivers function, which is equal for W^+ and W^- production and independent of Y . The maximal effect from the WG function is exactly the same, but with the sign of A_{TT}^0 flipped. From the plot we can see that the maximal TMD effects are at the percent level and thus definitely not suppressed by a factor of $\langle k_T^2 \rangle / l_T^2 \sim 10^{-4}$. Due to the resonance effect, the suppression is only of order $\langle k_T^2 \rangle / \Gamma_W^2$.

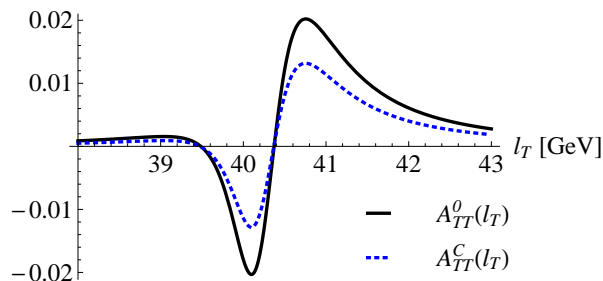


Figure 3.12: The maximal achievable $A_{TT}(l_T)$ in W^{\pm} boson production as a result of the Sivers effect.

3.6 Summary and conclusions

We calculated the transverse momentum dependent double transverse spin asymmetries in the laboratory frame for Drell-Yan and W production arising from the Sivers effect and from the worm-gear distribution function g_{1T} within transverse momentum dependent factorization. Those asymmetries were previously calculated only as a function of the lepton azimuthal angle measured in the Collins-Soper frame, where they are independent of it. The advantage being that one can, in that frame, easily distinguish them from the asymmetry coming from transversity, which *does* depend on the lepton azimuthal angle. If the lepton azimuthal angle is measured in the lab frame, however, a residual TMD effect survives and enters the double transverse spin asymmetry in exactly the same way as transversity does. This is in contrast to a collinear factorization approach where the effects from TMDs are absent to begin with. Therefore, a nonzero $\cos 2\phi_S^\ell$ asymmetry $A_{TT}(q_T)$ in Drell-Yan *in the lab frame* is *a priori* not a sufficient indication of a nonzero transversity distribution. However, from what is known about the magnitudes of the Sivers and worm-gear functions, our conclusion is that the TMD background is below the per mil level. Therefore, a percent level asymmetry *can* be viewed as coming from transversity. That is an important conclusion for the RHIC spin program. Transversity distributions can thus safely be determined from the transverse momentum dependent double spin asymmetry in the lab frame, like for the q_T -integrated asymmetry, assuming of course the antiquark transversity distributions are sufficiently large. As a cross-check of the smallness of

the TMD background, one can verify that the angular independent $A_{TT}^0(q_T)$ asymmetry that arises only from the mentioned TMD effects, is indeed much smaller.

We also obtained numerical estimates for the sizes of the double transverse spin asymmetries in W boson production at RHIC and found that they are below the detection limits. This is also an important conclusion as it means that the double Sivers and worm-gear effects do not hamper the investigation of a complex mixing of the W boson with a hypothetical W' boson using spin asymmetries as discussed in [64]. The asymmetries we find are, nonetheless, larger than one would naively expect on the basis of collinear factorization arguments. Even though the only dimensionful observable l_T is large (~ 40 GeV), the suppression of the TMD effects is not necessarily of the order $\langle k_T^2 \rangle / l_T^2$, but can be as large as $\langle k_T^2 \rangle / \Gamma_W^2$, due to the ‘hidden’ scale Γ_W . This is important to keep in mind when calculating hard scattering processes where intermediate particles can go on or nearly on-shell.

Chapter 4

BSM effects in $p^\uparrow p^\uparrow \rightarrow WX \rightarrow \ell\nu X$

In the previous Chapter, double transverse spin asymmetries in W boson production were investigated and it was concluded that they will be unmeasurably small at BNL's Relativistic Heavy Ion Collider (RHIC) even if transverse momentum dependent effects are taken into account. This strict prediction of the SM allows one to investigate physics Beyond the SM (BSM), in a way similar to neutron electric dipole moment measurements: any significant deviation from zero signals new physics

The idea of using double transverse spin asymmetries in W production to measure physics Beyond the Standard Model (BSM), was put forward in Ref. [63] and discussed further in Ref. [64]. Assuming that the W boson couples not only to the left-handed quarks, due to some as yet unknown physics beyond the SM, the following interesting double transverse spin asymmetries arises in the leptonic decay,

$$d\sigma^A \equiv \frac{1}{4} \left(d\sigma^{\uparrow\uparrow} - d\sigma^{\uparrow\downarrow} - d\sigma^{\downarrow\uparrow} + d\sigma^{\downarrow\downarrow} \right) \propto C_0 \cos 2\phi + C_1 \sin 2\phi, \quad (4.1)$$

where ϕ denotes the azimuthal angle of the outgoing charged lepton with respect to the spin plane, see figure 4.1.

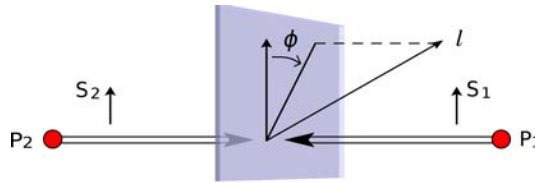


Figure 4.1: A leptonic decay of a W boson produced in a transversely polarized proton collision. The transverse momentum of the outgoing lepton l defines the azimuthal angle ϕ w.r.t. the transverse spins S_1 and S_2 of the colliding protons.

The reason for the asymmetries in the ϕ distribution is the following. Quarks in a transversely polarized proton are also to some extent transversely polarized, with a probability described by the transversity distribution [67]. A cross section is only sensitive to transverse polarization through the interference of left- and right-handed chirality states. Since the SM $V - A$ coupling of the W boson to the quarks only occurs for fixed (left-handed) chirality, no sensitivity to transverse polarization occurs in W -boson production [36], except through extremely small higher order quantum corrections. As a consequence, double transverse spin asymmetries due

to transversity will be negligibly small in the SM. Given the unmeasurably small contribution from TMD effects, as shown in the previous Chapter, a nonzero asymmetry would indicate a coupling of the W boson to right-handed quarks and thus BSM physics.

A small coupling of the W boson to right-handed quarks can, e.g., arise from the mixing with a hypothetical W' boson. Such a boson arises in theories in which a $SU(2)_R \otimes SU(2)_L$ gauge group is spontaneously broken to $SU(2)_L$ at some scale higher than the EW symmetry breaking scale. Examples are, besides others, left-right symmetric models [68, 69, 70, 71], Little(st) Higgs models [72], SUSY $SO(10)$ [73] and SUSY $E6$ [74]. We will consider a general model which is not specific to any of these scenarios. It consists of a W_L - and W_R boson coupling to left- and right-handed particles with strength g_L and g_R respectively. Those gauge eigenstates will mix to form two mass eigenstates

$$\begin{aligned} W_1^\pm &= \cos \zeta W_L^\pm + e^{\mp i\omega} \sin \zeta W_R^\pm, \\ W_2^\pm &= \sin \zeta W_L^\pm - e^{\pm i\omega} \cos \zeta W_R^\pm, \end{aligned} \quad (4.2)$$

where W_1 is identified with the observed W boson and W_2 with a hypothetical W' boson. As we will show, a nonvanishing mixing of the two bosons will cause the aforementioned asymmetries to appear. We find that, at RHIC energies, the amplitude of the $\cos 2\phi$ asymmetry is proportional to the real part of the mixing, whereas the amplitude of the $\sin 2\phi$ asymmetry is proportional to the imaginary part, i.e., with C_0 and C_1 defined as in Eq. (4.1), we find

$$\begin{aligned} C_0 &\propto \zeta \cos \omega, \\ C_1 &\propto \zeta \sin \omega. \end{aligned} \quad (4.3)$$

One or both of these asymmetries being nonzero (at detectable levels) implies physics beyond the Standard Model. The $\sin 2\phi$ asymmetry is even more interesting than the $\cos 2\phi$ asymmetry, because a non-zero value implies a new source of CP violation.

Bounds on the mixing angle ζ are often derived by measuring the right-handed coupling of the W boson to *leptons*. In any process a vanishing right-handed coupling to the leptons can result from the right-handed neutrino being too heavy to be produced or it may be leptophobic simply. Therefore, it is important to test the right-handed coupling of the W boson to leptons and quarks *independently*. As we will show, the method discussed here allows one to measure the right-handed coupling to quarks and is, therefore, independent of the as yet unknown right-handed neutrino mass.

This Chapter is partially based on [64], which was based on the best model independent bounds on the right-handed coupling of the W boson to quarks from the particle data group at that time. We have now extracted better model independent bounds on this coupling from the literature, which will be discussed in Section 4.2. Based on the new bounds, we will give updated numerical predictions for the asymmetries at RHIC and a possible future higher energy polarized collider in Sections 4.5 and 4.6. We will discuss and summarize the results in Sections 4.7 and 4.8, but we will first start with a general introduction to Left-Right models in the next Section.

4.1 Introduction Left-Right models

Left-Right (LR) models are extensions of the Standard Model (SM) which have an $SU(2)_R$ gauge symmetry, relating the right-handed up- and down-type fermions, just like the $SU(2)_L$ symmetry

the SM has between the left-handed up- and down-type fermions. The original proposal came in a series of papers [68, 75, 69, 70, 71] describing the maximal violation of parity in the weak interaction as a low-energy phenomenon. The idea was that at high energy the symmetry between left- and right-handed particles would be restored, hence the name of *left-right symmetric* models. The model can also incorporate exact CP symmetry, which then spontaneously breaks at low-energy [68, 76, 77] and, as a bonus, yield a viable Dark Matter (DM) candidate [78, 79]. Various GUT models, e.g., SUSY $SO(10)$ [73] or SUSY E_6 [74], *also* have the extra $SU(2)_R$ right-handed gauge group at some intermediate energy scale.

4.1.1 General framework

We will define a left-right model as any model that has, at some energy scale, higher than the electroweak scale, the gauge symmetry group

$$SU(2)_L \otimes SU(2)_R \otimes U(1)_{B-L}. \quad (4.4)$$

This gauge symmetry leads to two sets of charged gauge bosons, W_L^\pm and W_R^\pm , and three neutral gauge bosons. We will work with a general model in which the left- and right-handed gauge bosons can couple with different strengths g_L and g_R (a left-right *symmetric* model has, among other restrictive properties, equal left- and right-handed gauge strengths, i.e., $g_L = g_R$). The quarks are organized in doublets as follows

$$Q_L = \begin{pmatrix} u_L \\ d_L \end{pmatrix} \sim \left(\frac{1}{2}, 0, \frac{1}{3} \right), \quad Q_R = \begin{pmatrix} u_R \\ d_R \end{pmatrix} \sim \left(0, \frac{1}{2}, \frac{1}{3} \right), \quad (4.5)$$

where the row vector contains the $SU(2)_L \otimes SU(2)_R \otimes U(1)_{B-L}$ quantum numbers of the fields. The leptons doublets are likewise given by

$$\ell_L = \begin{pmatrix} \nu_L \\ e_L \end{pmatrix} \sim \left(\frac{1}{2}, 0, -1 \right), \quad \ell_R = \begin{pmatrix} \nu_R \\ e_R \end{pmatrix} \sim \left(0, \frac{1}{2}, -1 \right). \quad (4.6)$$

At some high energy scale v_R the gauge group is spontaneously broken to the SM gauge group. Usually this is done by introducing a left- and right-handed Higgs doublet [70] or triplet [71]. Choosing a triplet to break the $SU(2)_R$ symmetry has the advantage that one can incorporate, in a very natural way, a seesaw mechanism to give the left-handed neutrinos a light mass, e.g., $m_{\nu_e} \sim m_e^2/v_R$. At this stage the right-handed gauge boson W_R obtains a mass $M_{W_R} \sim g^2 v_R^2$, the exact value depending on the specific choice of breaking. We will focus on a first-stage breaking with triplets

$$\Delta_L \sim (1, 0, 2), \quad \Delta_R \sim (0, 1, 2). \quad (4.7)$$

In order to produce fermion masses and break the symmetry further down to $U(1)_{em}$ we also have to introduce a Higgs bi-doublet

$$\Phi = \begin{pmatrix} \phi_1^0 & \phi_2^+ \\ \phi_1^- & \phi_2^0 \end{pmatrix} \sim \left(\frac{1}{2}, \frac{1}{2}, 0 \right). \quad (4.8)$$

At least one bi-doublet is needed to generate the fermion masses, but more can be used. A model which accomplishes a second-stage breaking by just a *single* Higgs bi-doublet will be called a

minimal left-right model. In the rest of this chapter we will use such a minimal model as a prototype. The kinetic part of the Lagrangian, for the Higgs sector of the theory is given by

$$\mathcal{L}_{\text{HiggsKin}} = (D_\mu \Delta_R)^\dagger (D^\mu \Delta_R) + (D_\mu \Delta_L)^\dagger (D^\mu \Delta_L) + \text{Tr} \left[(D_\mu \Phi)^\dagger (D^\mu \Phi) \right], \quad (4.9)$$

in which

$$D^\mu \Delta_{L,R} = \left(\partial^\mu - ig_{L,R} \vec{T} \cdot \vec{W}_{L,R}^\mu - i2g' B^\mu \right) \Delta_{L,R} \quad (4.10)$$

and

$$D^\mu \Phi = \partial^\mu \Phi - ig_L \vec{\tau} \cdot \vec{W}_L^\mu \Phi + ig_R \Phi \vec{\tau} \cdot \vec{W}_R^\mu. \quad (4.11)$$

4.1.2 Gauge boson masses, mixing and couplings

The Higgs potential can be chosen in such a way that the Higgs triplet fields develop a Vacuum Expectation Value (VEV) of the form

$$\langle \Delta_L \rangle = 0, \quad \langle \Delta_R \rangle = \begin{pmatrix} 0 \\ 0 \\ v_R \end{pmatrix}, \quad (4.12)$$

and the Higgs bi-doublet a VEV of the form

$$\langle \Phi \rangle = \begin{pmatrix} k_1 & 0 \\ 0 & k_2 e^{i\omega} \end{pmatrix}, \quad (4.13)$$

where k_1 and k_2 are at the electroweak scale and v_R is some higher scale at which the $SU(2)_R$ symmetry is broken. At this minimum of the potential, all the physical Higgs particles (which are not eaten by the heavy gauge bosons) acquire a mass at the scale v_R except one, which obtains a mass proportional to the electroweak scale [70].

Spontaneous CP violation

The bi-doublet transforms under a CP transformation as $\Phi \rightarrow \Phi^*$ ¹, which implies that, if ω is not equal to 0 or π , then spontaneous violation of CP symmetry occurs. This spontaneous CP violation can, in principle, happen in the absence of explicit CP violation in the Lagrangian.

One might wonder whether one can construct a model with *just* spontaneous CP violation, but that turns out not to be possible with a *minimal* left-right symmetric model in a phenomenologically acceptable way. The problem being that, if the Higgs potential is CP symmetric, then either the vacuum phase ω is too small to explain the observed CP violation, or one needs to fine-tune the parameters in the Higgs potential, but then flavor changing neutral currents become too large [80, 81, 82, 83]. However, models with *two* Higgs bi-doublets *do* provide a phenomenologically acceptable model for spontaneous P and CP violation without explicit P and CP violation [77] and, as a bonus, also yield a viable Dark Matter (DM) candidate [78, 79].

¹one could define a different transformation, but a ‘standard’ mass term $\lambda \bar{q}_R \phi q_L + \text{h.c.}$ is CP even under this choice of transformation, given that λ is real.

Neutral gauge bosons

The non-zero VEVs of the Higgs fields will produce mass terms for the gauge bosons. We will first focus on the neutral gauge bosons $W_L^{3\mu}$, $W_R^{3\mu}$ and B^μ , which will mix to form one massless and two massive fields. The massless eigenstate (the photon) is given by

$$A = e \left(\frac{W_L^3}{g_L} + \frac{W_R^3}{g_R} + \frac{B}{2g'} \right), \quad (4.14)$$

which couples with strength eQ , where

$$e \equiv \frac{g'}{\sqrt{\frac{g_L^2}{g_L^2} + \frac{g_R^2}{g_R^2} + \frac{1}{4}}}, \quad (4.15)$$

to fermions with quantum number $Q = T_L^3 + T_R^3 + \frac{1}{2}(B-L)$. The quantum number Q corresponds to the electric charge of the fields. The SM relation $e/g = \sin \theta_W$ will in this model be replaced by the equivalent

$$\frac{e}{g_L} = \sin \theta_W, \quad (4.16)$$

which fixes the value of g' to be

$$g' = \frac{g_L g_R \sin \theta_W}{2\sqrt{g_R^2 - (g_L^2 + g_R^2) \sin^2 \theta_W}}. \quad (4.17)$$

The masses of the other neutral states are given by

$$\begin{aligned} M_{Z_1} &= \frac{g_L^2(k_1^2 + k_2^2)}{2 \cos^2 \theta_W} - \frac{g_L^2(k_1^2 + k_2^2)^2 (g_R^2 - (g_L^2 + g_R^2) \sin^2 \theta_W)^2}{8g_R^4 v_R^2 \cos^6 \theta_W} + \mathcal{O}\left(\frac{1}{v_R^4}\right), \\ M_{Z_2} &= \frac{2g_R^4 \cos^2 \theta_W v_R^2}{g_R^2 - (g_L^2 + g_R^2) \sin^2 \theta_W} + \frac{(k_1^2 + k_2^2)(g_R^2 - (g_L^2 + g_R^2) \sin^2 \theta_W)}{2 \cos^2 \theta_W} + \mathcal{O}\left(\frac{1}{v_R^2}\right), \end{aligned} \quad (4.18)$$

from which we can conclude that the Z_1 mass is at the electroweak scale and the Z_2 mass at the large scale v_R . The lowest mass eigenstate, which we identify with the Z boson, is given by

$$\begin{aligned} Z_1 = & + \cos \theta_W W_L^3 - g_L \sin \theta_W \tan \theta_W \left(\frac{W_R^3}{g_R} + \frac{B}{2g'} \right) \\ & - \frac{k_1^2 + k_2^2}{v_R^2} \left(-\frac{g_L z^2}{16g_R^5 \cos^5 \theta_W} W_R^3 + \frac{g_L^2 z^{3/2} \sin \theta_W}{8\sqrt{2}g_R^5 \cos^5 \theta_W} B \right) + \mathcal{O}(1/v_R^3), \end{aligned} \quad (4.19)$$

in which $z \equiv g_R^2(1 + \cos 2\theta_W) - g_L^2(1 - \cos 2\theta_W)$. From this we can deduce the coupling of Z boson to the fermions to be

$$V^{Z_1} = \frac{g_L}{\cos \theta_W} [T_L^3 - \sin^2 \theta_W Q] + \delta V^{Z_1}, \quad (4.20)$$

in which δV^{Z_1} is g_R times the $\mathcal{O}(1/v_R^2)$ part of Eq. (4.19). The coupling of the Z boson in a left-right model is thus identical to the coupling of the Z boson in the Standard Model except for a (very) small correction term. The important thing to note is that the correction term vanishes in both the limit $v_R \rightarrow \infty$ and $g_R \rightarrow \infty$, since that property holds for all the predicted corrections except the right-handed coupling of the W boson as will be shown in the next section.

Charged gauge bosons

The charged gauge bosons W_L^\pm and W_R^\pm will also mix to form mass eigenstates

$$\begin{aligned} W_1^\pm &= \cos \zeta W_L^\pm + e^{\mp i\omega} \sin \zeta W_R^\pm, \\ W_2^\pm &= \sin \zeta W_L^\pm - e^{\pm i\omega} \cos \zeta W_R^\pm, \end{aligned} \quad (4.21)$$

where the mixing angle ζ is given by

$$\tan \zeta = \frac{g_L k_1 k_2}{g_R v_R^2} + \frac{g_L k_1 k_2 (g_L^2 - g_R^2) (k_1^2 + k_2^2)}{2g_R^3 v_R^4} + \mathcal{O}\left(\frac{1}{v_R^6}\right). \quad (4.22)$$

The masses of those eigenstates are given by

$$\begin{aligned} M_{W_1}^2 &= \frac{1}{2} g_L^2 (k_1^2 + k_2^2) - \frac{g_L^2 k_1^2 k_2^2}{v_R^2} + \mathcal{O}\left(\frac{1}{v_R^4}\right), \\ M_{W_2}^2 &= g_R^2 v_R^2 + \frac{1}{2} g_R^2 (k_1^2 + k_2^2) + \mathcal{O}\left(\frac{1}{v_R^2}\right), \end{aligned} \quad (4.23)$$

from which we can again conclude that there is a low mass state proportional to the electroweak scale and a high mass state proportional to v_R . The couplings of the mass eigenstates are given by

$$\begin{aligned} V^{W_1^\pm} &= g_L \cos \zeta T_L^\pm + g_R e^{\mp i\omega} \sin \zeta T_R^\pm, \\ V^{W_2^\pm} &= g_L \sin \zeta T_L^\pm - g_R e^{\pm i\omega} \cos \zeta T_R^\pm, \end{aligned} \quad (4.24)$$

of which the W_1 coupling reduces to the purely left-handed coupling of the SM in the limit $v_R \rightarrow \infty$ (i.e., $\zeta \rightarrow 0$). However in the limit $g_R \rightarrow \infty$ the right-handed coupling remains, as

$$\lim_{g_R \rightarrow \infty} \zeta \propto 1/g_R. \quad (4.25)$$

One can now also look at the W to Z boson mass ratio,

$$\frac{M_{W_1}^2}{M_{Z_1}^2} = \cos^2 \theta_W + \delta_M, \quad (4.26)$$

which is equal to the SM prediction, apart from the mass correction term

$$\delta_M = \frac{k_1^2 + k_2^2}{4g_R^4 v_R^2 \cos^2 \theta_W} \left[-2g_R^2 \sin^2 \theta_W (g_L^2 + g_R^2 z_k) + \sin^4 \theta_W (g_L^4 + 2g_L^2 g_R^2 + g_R^4 z_k) + g_R^4 z_k \right], \quad (4.27)$$

where $z_k \equiv (k_1^4 - 6k_1 k_2 + k_2^4)/(k_1^2 + k_2^2)^2$. The correction vanishes in the limit $v_R \rightarrow \infty$, but not in the limit $g_R \rightarrow \infty$. However, if one wants to minimize the effect of the LR model on the SM mass relation, but retain a right-handed coupling of the W -boson, then the value of k_2 can be fine-tuned such that the mass correction term vanishes whereas the right-handed coupling of the W persists. For example, in the limit of $g_R \rightarrow \infty$ and $k_2 \rightarrow (1 + \sqrt{2})k_1$, the mass correction term vanishes, whereas the right-handed coupling of the W boson approaches $g_L(1 + \sqrt{2})k_1^2/v_R^2$. To put it briefly, the masses of the Z_2 and W_2 boson can be made arbitrarily large while retaining the mass relation between W_1 and Z_1 and keeping the coupling of the Z_1 boson at its SM value and yet introduce a right-handed coupling of the W_1 boson. This shows that bounds on the right-handed coupling of the W_1 boson should be set *independently* and not be derived from W_2 or Z_2 mass bounds, from determinations of the Z_1 boson coupling or the W_1 and Z_1 mass relation, at least in a *general* left-right model.

Connection between ζ and $M_W^2/M_{W'}^2$

One can derive an upper limit on the $W - W'$ mixing ζ in a minimal left-right model, in terms of the W and W' mass,

$$\tan \zeta \leq \frac{g_R M_{W_1}^2}{g_L M_{W_2}^2}, \quad (4.28)$$

which holds to leading order in $1/v_R^2$. This bound reduces in a left-right *symmetric* model to $\tan \zeta \leq M_{W_1}^2/M_{W_2}^2$, which is often used to translate bounds on the W' mass to bounds on the mixing angle ζ . However, in the case of unequal g_L and g_R these translated bounds are weakened. Especially bounds on the right-handed coupling of the W boson, being proportional to $g_R/g_L \zeta$, are strongly weakened. In the, not far fetched, case of $g_R = 2g_L$ the bounds are already weakened by a factor four. If one keeps g_R completely free, then the W' mass and the mixing angle ζ are *independent* parameters and it is necessary to obtain separate experimental bounds on them.

4.1.3 Quark masses, CKM matrices

In a minimal left-right model, the quarks get their mass through a Yukawa coupling of the form (following Ref. [84])

$$\bar{Q}_L \cdot (Y\Phi + \tilde{Y}\tilde{\Phi})Q_R + \text{h.c.}, \quad (4.29)$$

in which $\tilde{\Phi} \equiv \sigma_2 \Phi^* \sigma_2$ and Y and \tilde{Y} are two independent Yukawa coupling matrices. The quark mass matrices are then given by

$$\begin{aligned} M_u &= k_1 Y + k_2 e^{-i\omega} \tilde{Y}, \\ M_d &= k_1 \tilde{Y} + k_2 e^{i\omega} Y, \end{aligned} \quad (4.30)$$

which can be diagonalized as usual by

$$\begin{aligned} M_u &= U_{uL} m_u U_{uR}^\dagger, \\ M_d &= U_{dL} m_d U_{dR}^\dagger, \end{aligned} \quad (4.31)$$

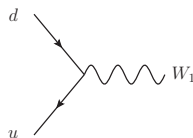
in which m_u and m_d are the diagonal quark mass matrices for the up- and down-type quarks. In the mass eigenstate basis we end up with flavor changing charged interactions governed by a left-handed CKM matrix

$$V_L = U_{uL}^\dagger U_{dL}, \quad (4.32)$$

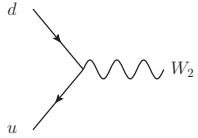
and its right-handed counterpart

$$V_R = U_{uR}^\dagger U_{dR}, \quad (4.33)$$

such that the coupling of the W bosons to the fermion mass eigenstates, are given by



$$= \frac{i}{\sqrt{2}} \left[\cos \zeta g_L V_L^{ud} \gamma^\mu \mathcal{P}_L + \sin \zeta e^{-i\omega} g_R V_R^{ud} \gamma^\mu \mathcal{P}_R \right] \quad (4.34)$$



$$= \frac{i}{\sqrt{2}} \left[\sin \zeta g_L V_L^{ud} \gamma^\mu \mathcal{P}_L - \cos \zeta e^{+i\omega} g_R V_R^{ud} \gamma^\mu \mathcal{P}_R \right] \quad (4.35)$$

One can utilize five rotations on the quark fields to remove five phases from the left-handed CKM matrix, however the right-handed CKM matrix will, in general, keep 6 non-zero complex phases. Furthermore, the mixing angles in the right-handed matrix are, in general, different from the ones in the left-handed matrix.

4.1.4 Manifest/Pseudo manifest

Within the class of left-right models, we can look at LR *symmetric* models. Those models have a discrete symmetry in the Lagrangian, relating chiral left and chiral right spinors. This discrete symmetry can be either parity P or charge conjugation C ², acting on the fields in the minimal left-right model as

$$P : \begin{cases} Q_L & \leftrightarrow Q_R \\ \Phi & \rightarrow \Phi^\dagger \end{cases} \quad C : \begin{cases} Q_L & \leftrightarrow (Q_R)^c \\ \Phi & \rightarrow \Phi^T \end{cases}, \quad (4.36)$$

which implies that the Lagrangian is symmetric under P , C or CP given that the Yukawa coupling matrices obey

$$P : Y = Y^\dagger, \quad C : Y = Y^T, \quad CP : Y = Y^*. \quad (4.37)$$

These constraints on the Yukawa couplings translate into a relation between the left and right CKM matrices. When one demands the Lagrangian to be P symmetric and $\omega = 0$ (i.e., no spontaneous CP violation) the mass matrices are Hermitian from which it follows that

$$V_{CKM}^R = S_u V_{CKM}^L S_d, \quad (4.38)$$

where $S_{u,d}$ are diagonal sign matrices. This is known as *manifest left-right symmetry*. It boils down to the fact that the mixing angles and CP violating Kobayashi-Maskawa (KM) phase δ_{13} are equal in the left and right matrix and the additional phases in the right matrix are either 0 or π . In the case that $\omega \neq 0$, relation (4.38) still approximately holds, because one needs either $\omega \sim \pi$ or $v_1/v_2 \sim 0$ to arrive at phenomenologically acceptable mass matrices, as explained in [84]. If one imposes C symmetry on the Lagrangian, the mass matrices are symmetric from which it follows that

$$V_{CKM}^R = K_u V_{CKM}^{L*} K_d, \quad (4.39)$$

where $K_{u,d}$ are diagonal phase matrices. This is known as *pseudo manifest left-right symmetry*. It says that the mixing angles are equal, the KM phase differs by a minus sign and the additional phases in the right matrix are unconstrained. If one demands CP symmetry on the Yukawa couplings, then there is, in general, no relation between the left and right CKM matrix, except for the case $\omega = 0$. In that situation the KM phases, as well as the additional phases in the right matrix, either vanish or are equal to π , resulting in no CP violation.

²There are two other transformations interchanging left and right, that one can define, $\Phi \leftrightarrow \tilde{\Phi}^\dagger$ and $\Phi \leftrightarrow \tilde{\Phi}^T$, but they lead to unrealistic mass matrices, respectively $M_u = M_d^\dagger$ in the first case and $M_u = M_d^T$ or $M_u = M_d^*$ in the second, see [84].

4.1.5 Non-universal coupling

In a *minimal* left-right model, as discussed so far, the right-handed CKM matrix is unitary, which can be seen directly from Eq. (4.33). However, we prefer to work in a completely model independent way and it, therefore, is interesting to see if and how a non-unitary CKM matrix could arise.

Suppose that the three different quark generations couple with different right-handed gauge strengths g_i . This would lead to problems constructing the standard Yukawa terms, but with the introduction of *three* bi-doublets, transforming under the right-handed gauge group with coupling strength g_i , this problem could be resolved. The Yukawa coupling matrices can be diagonalized in the ordinary way, but the expression for the right-handed CKM matrix in Eq. (4.33), will be modified to

$$V_R = U_{uR}^\dagger \begin{pmatrix} g_1/g_R & 0 & 0 \\ 0 & g_2/g_R & 0 \\ 0 & 0 & g_3/g_R \end{pmatrix} U_{dR}, \quad (4.40)$$

which produces, in general, a non-unitary right-handed CKM matrix.

It is thus possible to generate a non-unitary right-handed CKM matrix and, therefore, just as for the left-handed CKM matrix, unitarity tests should be carried out. This emphasizes the importance to determine the right-handed coupling of the W boson to all the different quark combinations *independently*.

4.1.6 Discussion

Lastly, we want to address several attractive features, despite the introduction of more parameters, of left-right models over the Standard Model. First, and common to all LR models, is the replacement of hypercharge by the $B - L$ quantum number. This reduces the amount of assignments of arbitrary hypercharge quantum numbers from 6 (for the right-handed up-type and down-type quarks and the left-handed quark doublet plus three for the leptons) to just two ($B = 1/3$ for all quarks and $L = 1$ for all leptons).

Secondly, the minimal left-right model predicts *naturally* almost diagonal CKM matrices when $k_1 \sim k_2$, irrespective of what is chosen for the Yukawa couplings. This nearly diagonal form of the CKM matrix is indeed what is observed in nature. In the SM, there is, *a priori*, no reason for small mixing between the quark families and one has to carefully choose the Yukawa couplings to arrive at an almost diagonal CKM matrix.

Thirdly, and specific to a P or CP symmetric Yukawa sector, is the correspondence between the number of Yukawa couplings and the total number of observable degrees of freedom in the CKM matrices and masses. With either Hermitian (P symmetric) or real (CP symmetric) Yukawa couplings, there are 9 real parameters per matrix plus the complex phase ω , totaling 19 real parameters (the absolute values of the VEVs k_1 and k_2 are measurable independently). Counting the observable degrees of freedom, there are three angles plus 6 phases in the right CKM matrix, plus three angles and one phase in the left CKM matrix, plus 6 masses, *also* totaling 19. This can be compared to the SM, which contains 36 real parameters in the Yukawa sector and just 10 observable degrees of freedom.

Lastly, and what was the original reason to propose the model, is that a left-right symmetric model can be explicitly parity conserving (and also CP conserving in a non-minimal model),

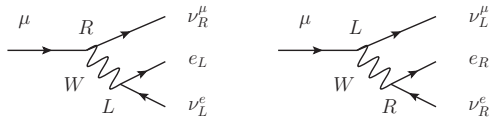
which is attractive in view of unification and the natural behavior of increasing symmetry with increasing energy.

4.2 Bounds on left-right models

The phenomenology of left-right models is very versatile. It involves the addition of new hypothetical neutral and charged gauge bosons and Higgs particles as well as a modification of the properties of the existing gauge bosons in the Standard Model. In principle all those new features can be used to exclude a left-right model.

However, as we have shown in the previous section, all modifications to the SM can be kept arbitrarily small while still introducing a right-handed coupling of the W boson. It is thus not sufficient to only look for the hypothetical W prime boson at the LHC. One has to *independently* verify that the W boson only couples to left-handed quarks and leptons.

It is also not sufficient to bound just the coupling to right-handed *leptons* as it is at present unclear whether a right-handed neutrino exists, let alone, what its mass will be. It might be that the neutrinos are ‘ordinary’ Dirac particles, such that there is no distinction between left- and right-handed neutrinos, but there might also be a Majorana mass term, which will lift this degeneracy and cause different masses for the left- and right-handed neutrinos. For example, in the theoretically attractive seesaw type models, the right-handed neutrino mass is at the GUT scale, whereas the left-handed neutrinos are at the eV scale. One way or another, if no right-handed neutrino exists or it is too heavy, a coupling of the W boson to it, will not be observed. If, e.g., one wants to see a right-handed coupling of the W boson in a muon decay experiment, the right-handed neutrino needs to be lighter than the muon for the process to be kinematically allowed, as there will always be a right-handed neutrino in the final state:



Bounds on the right-handed coupling to leptons can, therefore, not be translated into bounds on the right-handed coupling to quarks. The right-handed coupling of the W boson to quarks thus has to be investigated *independently*.

The right-handed coupling to quarks can be different for all pairs of quarks, because they all enter with their own right-handed CKM matrix element. So if one does not want to assume manifest or pseudo manifest left-right symmetry, i.e., work in a completely model independent way, one should give bounds on the right-handed coupling to the different quark pairs separately and not translate them into bounds on the mixing angle ζ , which is often done in the literature. We will give in this Chapter an overview of the best bounds on the right-handed coupling of the W boson to the different quarks pairs separately. We will specifically focus on the bounds on the coupling to the light quarks, as they will be important for the maximally expected size of the double transverse spin asymmetries at RHIC.

4.2.1 Bounds on the W_2 mass

First we will start with a brief overview of the bounds on the W_2 mass, as this we also be important to make predictions for polarized proton colliders with a higher center-of-mass energy than RHIC. Bounds on the heavy mass eigenstate of the charged gauge bosons W_2 , can be

divided into ‘direct’ and ‘indirect’ bounds. Direct bounds are derived from the absence of W_2 boson production in collider experiments, whereas indirect bounds are derived from the absence of quantum loop effects caused by a virtual W_2 boson.

Direct bounds

Most direct searches for a W' boson³ aim at seeing a mass resonance in either the $W' \rightarrow \ell\nu$ or $W' \rightarrow \text{jets}$ channel. The sensitivity to those resonances depends on the coupling of the hypothetical W' boson to the SM particles. Therefore, it is usually assumed that the W' boson couples in exactly the same way as the ordinary W boson. The ATLAS collaboration sets, using this assumption, the lower limit

$$M_{W'} > 2.2 \text{ TeV}, \quad (4.41)$$

at 95% confidence level in the $W' \rightarrow \ell\nu$ channel [85]. The CMS collaboration finds, under the same assumption, a lower limit of 2.3 TeV at 95% confidence level in the $W' \rightarrow e\nu, \mu\nu$ channel [86] and

$$M_{W'} > 1.5 \text{ TeV}, \quad (4.42)$$

in the $W' \rightarrow \text{jets}$ channel [87].

These bounds are not necessarily also bounds on the W_2 boson from a left-right model. For example, the bound found in the leptonic decay channel only holds if a right-handed neutrino exists and it has a mass smaller than 2.2 TeV. The bound obtained in the hadronic channel also needs caution when interpreting, because if, for example, the right-handed CKM matrix will be of the form

$$V_{\text{CKM}}^R \sim \begin{pmatrix} 0 & 0 & 1 \\ 0 & 1 & 0 \\ 1 & 0 & 0 \end{pmatrix}, \quad (4.43)$$

then bounds will be severely weakened, because the primary production channel in a hadron-hadron collider, $u\bar{d} \rightarrow W^+$, will not be available for the W_2 boson. Production of the W_2 will have to happen mainly through the process $c\bar{s} \rightarrow W_2^+$, which is heavily suppressed due to the small strange and charm distributions in the proton. It is therefore advisable to not accept these bounds at face value.

Indirect bounds

Indirect bounds are derived from the absence of the effects a virtual W_2 boson would cause in quantum loop corrections to an observable. Quantities which are very sensitive to the addition of a W_2 boson are found in the mixing of neutral mesons.

$K_L - K_S$ mass difference

The quantity most sensitive to the addition of a W_2 boson is the $K_L - K_S$ mass difference. In the original work [88], a bound of $M_{W_2} \gtrsim 1.6 \text{ TeV}$ was derived for the W_2 boson mass in a manifest left-right symmetric model, which is now updated to be

$$M_{W_2} \gtrsim 2.4 \text{ TeV}, \quad (4.44)$$

³We will use W' for a general heavy charged gauge boson.

valid for both a manifest and pseudo manifest left-right symmetric model [84]. Because the effect of the W_2 boson depends on the phase differences between the left- and right-handed CKM matrices, this bound can be evaded when all the right-handed phases can be chosen freely, i.e., when there is no specific left-right symmetry.

It is also important to note that indirect bounds get stronger as g_R is increased, in contrast to direct searches where the search range is kinematically limited by the energy of the collider. This property makes it possible to translate an indirect bound on the mass into a bound on the mixing angle ζ via Eq. (4.28). However, as this bound is only valid for (pseudo) manifest left-right symmetric models and we are looking for model independent bounds, we will not use this property.

$B_{d,s} - \bar{B}_{d,s}$ mixing

The observables in $B_{d,s} - \bar{B}_{d,s}$ mixing, such as the mass differences and indirect CP violation, are also sensitive to a virtual W_2 boson. The current data on B mixing is at tension with the SM, which can be resolved with a *pseudo manifest* left-right symmetric model with a M_{W_2} in the range $0.5 - 2$ TeV [84]. A *manifest* left-right symmetric model can only worsen the tension, and so a lower bound of $M_{W_2} \gtrsim 1.9$ TeV can be derived. In a model without any relation between the left- and right-handed CKM matrices, one should, most likely, also be able to resolve the tension, but this analysis has not been done yet.

4.2.2 Bounds on the W -boson coupling to right-handed leptons

To be complete, we will start with a brief discussion of the bounds on the right-handed coupling of the W boson to leptons, which are derived from either muon or tau decays. The TWIST collaboration obtains, from the muon decay process, $\mu^+ \rightarrow e^+ \nu_e \bar{\nu}_\mu$, a bound $|g_R^\mu/g_L^\mu| < 0.02$ at 90% CL [89], on the ratio of right- to left-handed coupling to muons, which, under the assumption of light right-handed neutrinos, translates to a bound on the mixing angle in a left-right model of

$$\left| \tan \zeta \frac{g_R}{g_L} \right| < 0.02, \quad (4.45)$$

at 90% CL. The OPAL collaboration finds from the leptonic tau decay processes, $\tau \rightarrow e \nu_e \nu_\tau$ and $\tau \rightarrow \mu \nu_\mu \nu_\tau$, the bound on the mixing angle

$$|\tan \zeta| < 0.12, \quad (4.46)$$

at 95% CL [90], assuming left-right symmetry and light right-handed neutrinos.

4.2.3 Bounds on the W -boson coupling to right-handed quarks

Bounds on the coupling of the W -boson to right-handed quarks do not suffer from the fact that the right-handed neutrino needs to be light enough for the bound to be valid. There are nevertheless complications when deriving bounds on these quark couplings as, e.g., different elements of the unknown right-handed CKM matrix will enter in different processes. As in a general LR model there is no relation between the left- and right-handed CKM matrices, one should measure the right-handed coupling of the W boson to all combinations of up- and

down-type quarks *independently*. Furthermore, some observables will just depend on the real part of the right-handed coupling, whereas other (CP violating observables) will measure the imaginary part and again others will measure just the absolute value of the coupling, such that many different observables will have to be combined in order to form a complete picture of the right-handed coupling (including V_R^{ij}) to the various quarks.

We will give an overview here of the bounds on the right-handed coupling to quarks, with a specific focus on the light quarks. As we do not want to assume anything for the right-handed CKM matrix nor for the right-handed gauge strength g_R , we will keep the dependence on these parameters in the bounds and do not try to translate them into a bound on the mixing angle ζ .

νN deep inelastic scattering

A possible way of constraining the right-handed coupling of the W boson to the light quarks u and d , lies in the process of νN and $\bar{\nu} N$ Deep Inelastic Scattering (DIS). Assuming only left (right) handed neutrinos (anti neutrinos) in the beam, the relative absence of charged current $\bar{\nu}_\mu$ induced events with respect to ν_μ induced events at large x and large y allows one to constrain the right-handed coupling. This can be seen from the leading order neutrino and anti-neutrino scattering cross sections

$$\begin{aligned}\frac{d\sigma^\nu}{dx dy} &= \frac{G^2 M E_\nu}{\pi} \{ [q(x) + (1-y)^2 \bar{q}(x)] + |\eta|^2 [\bar{q}(x) + (1-y)^2 q(x)] \}, \\ \frac{d\sigma^{\bar{\nu}}}{dx dy} &= \frac{G^2 M E_\nu}{\pi} \{ [\bar{q}(x) + (1-y)^2 q(x)] + |\eta|^2 [q(x) + (1-y)^2 \bar{q}(x)] \},\end{aligned}\quad (4.47)$$

where, $\eta \equiv g_R^{ud}/g_L^{ud}$, is defined as the ratio of the right- to left-handed coupling of the W boson to the u and d quarks. Within the LR model discussed in Chapter 4.1, this ratio can be written as

$$|\eta| = \left| \tan \zeta \frac{g_R V_R^{ud}}{g_L V_L^{ud}} \right|. \quad (4.48)$$

Defining the structure functions [91, 92]

$$\begin{aligned}q_R(x) &\equiv \frac{d\sigma^{\bar{\nu}}}{dx dy} - (1-y)^2 \frac{d\sigma^\nu}{dx dy} \Big|_{y \rightarrow 1} = \bar{q}(x) + |\eta|^2 q(x), \\ q_L(x) &\equiv \frac{d\sigma^\nu}{dx dy} - (1-y)^2 \frac{d\sigma^{\bar{\nu}}}{dx dy} \Big|_{y \rightarrow 1} = q(x) + |\eta|^2 \bar{q}(x),\end{aligned}\quad (4.49)$$

and using the fact that the distribution functions $q(x)$ and $\bar{q}(x)$ are non negative, one sees that in the large y limit, the ratio of q_R/q_L forms an *upper bound* on $|\eta|^2$. The size of q_R/q_L depends on x , and to make it as small as possible, one should look in the high x region, where the antiquark distribution is smallest. Using instead of the differential, the integrated cross sections with the cuts $x > 0.45$ and $y > 0.7$, the CCFR collaboration finds, using this method, the bound $|\eta|^2 < 0.0015$ at 90% CL, resulting in

$$\left| \tan \zeta \frac{g_R V_R^{ud}}{g_L V_L^{ud}} \right| < 0.04, \quad (4.50)$$

at 90% CL, which we translate to $\left| \tan \zeta \frac{g_R V_R^{ud}}{g_L V_L^{ud}} \right| < 0.024$ at 68% CL.

The error in the determination of $|\eta|^2$ is dominated by the statistical error, which is proportional to $\delta\sigma^{\bar{\nu}}/\sigma^\nu$. The event sample size of CCFR, which consists of $\sim 1.8 \times 10^6$ ν_μ events and 3.6×10^5 $\bar{\nu}_\mu$ events, has not been significantly improved since. The follow-up experiment, NuTeV, mainly reduced the systematic errors in the muon and hadronic energy measurements, which are irrelevant for the method discussed above. Also the CHORUS collaboration [93] has statistics in the same order of magnitude and significant improvements on the bound can therefore not be expected from their data. A future neutrino factory could, in principle, improve the bound, but it is difficult to say how much, e.g., one has to take into account that, using this method, the upper bound on $|\eta|^2$ cannot be smaller than $\bar{q}(x)/q(x)$.

Nuclear β -decay

Another process in which the coupling of the W boson to the light quarks shows up, is β -decay. Assuming that only a vector current participates (also scalar and tensor currents could be involved, but this is not the case in a left-right model), the dynamics of β -decay can be described by just four parameters. Those four parameters specify the coupling strength of the leptonic vector-current to the hadronic vector-current (axial-vector current) C_V (C_A) and the coupling strength of the leptonic axial-vector current to the hadronic vector-current (axial-vector current) C'_V (C'_A) (we will use the notation of [94]). The coupling strengths can be expressed as

$$\begin{aligned} C_V &= g_V (a_{LL} + a_{LR} + a_{RR} + a_{RL}), \\ C'_V &= g_V (a_{LL} + a_{LR} - a_{RR} - a_{RL}), \\ C_A &= g_A (a_{LL} - a_{LR} + a_{RR} - a_{RL}), \\ C'_A &= g_A (a_{LL} - a_{LR} - a_{RR} + a_{RL}), \end{aligned} \quad (4.51)$$

where a_{LR} is the product of the coupling to left-handed leptons and the coupling to right-handed quarks, etc. The SM prediction would be

$$\begin{aligned} a_{LL} &= \frac{g^2 V^{ud}}{8M_W^2} = \frac{G_F V^{ud}}{\sqrt{2}}, \\ a_{LR} &= a_{RL} = a_{RR} = 0, \end{aligned} \quad (4.52)$$

whereas a left-right model would predict

$$\begin{aligned} a_{LL} &= \frac{g_L^2 V_L^{ud}}{8M_{W_1}^2} \cos^2 \zeta + \frac{g_L^2 V_L^{ud}}{8M_{W_2}^2} \sin^2 \zeta, \\ a_{LR} &= \frac{g_L g_R V_R^{ud}}{8M_{W_1}^2} \cos \zeta \sin \zeta e^{-i\omega} - \frac{g_L g_R V_R^{ud}}{8M_{W_2}^2} \cos \zeta \sin \zeta e^{+i\omega}, \\ a_{RL} &= \frac{g_L g_R V_L^{ud}}{8M_{W_1}^2} \cos \zeta \sin \zeta e^{+i\omega} - \frac{g_L g_R V_L^{ud}}{8M_{W_2}^2} \cos \zeta \sin \zeta e^{-i\omega} \\ a_{RR} &= \frac{g_R^2 V_R^{ud}}{8M_{W_2}^2} \cos^2 \zeta + \frac{g_R^2 V_R^{ud}}{8M_{W_1}^2} \sin^2 \zeta. \end{aligned} \quad (4.53)$$

The couplings involving right-handed neutrinos will vanish, i.e., $a_{RL} = a_{RR} = 0$, if the mass of the right-handed neutrino is larger than the energy released in the β -decay (~ 0.8 MeV). The

constants g_V and g_A in Eq. (4.51) are the zero momentum limits of the hadronic form factors, which are defined by

$$\begin{aligned} g_V(q^2)\bar{p}\gamma_\mu n &= \langle p|\bar{u}\gamma_\mu d|n\rangle, \\ g_A(q^2)\bar{p}\gamma_\mu\gamma_5 n &= \langle p|\bar{u}\gamma_\mu\gamma_5 d|n\rangle. \end{aligned} \quad (4.54)$$

In a global least-squares fit to β -decay precision data, *without any extra assumptions*, the coupling strengths were found to be

$$\begin{aligned} 1.180 &< C_A/C_V < 1.372, \\ 0.857 &< C'_V/C_V < 1.169, \\ 0.868 &< C'_A/C_A < 1.153, \end{aligned} \quad (4.55)$$

at 90% confidence level [94], from which no significant bound on the right-handed coupling can be derived.

Imposing the constraint $C'_V/C_V = C'_A/C_A = 1$ (corresponding to $a_{RR} = a_{RL} = 0$, which is the case if the right-handed neutrino is heavy) makes the fit much more restrictive and results in

$$\begin{aligned} \text{Re}(C_A/C_V) &= 1.2699(7), \\ \text{Im}(C_A/C_V) &= 0.001(2). \end{aligned} \quad (4.56)$$

To determine the coupling of the W boson to the quarks, from C_A and C_V , one still needs the hadronic form factors as an input. These form factors need to be calculated theoretically, because the experimental determination is extracted precisely from these values of C_A and C_V , assuming a purely left-handed coupling of the W boson. The only way to get a theoretical estimate of these form factors is with lattice QCD, which is still rather inaccurate: the best determination is $g_A/g_V = 1.20(6)(4)$ [95]. Plugging in the lattice determination of the form factors, we can deduce, *assuming heavy right-handed neutrinos*, the coupling of the W -boson to the right-handed u and d quarks to be

$$\begin{aligned} \text{Re}\left(\tan\zeta e^{-i\omega}\frac{g_R V_R^{ud}}{g_L V_L^{ud}}\right) &= 0.03 \pm 0.04, \\ \text{Im}\left(\tan\zeta e^{-i\omega}\frac{g_R V_R^{ud}}{g_L V_L^{ud}}\right) &= -0.0004 \pm 0.0008. \end{aligned} \quad (4.57)$$

In the determination of the imaginary part of the right-handed coupling, it was assumed that hadronic form factors are real, i.e., no CP violation in the strong interaction. Under this assumptions β -decay provides a strong bound on the imaginary part of the right-handed W -boson coupling. It could, however, be that the QCD θ term (which is CP violating) generates a complex phase in the hadronic matrix elements that compensates the effect of the imaginary right-handed W boson coupling although this would be clear case of fine tuning.

Superaligned β -decay/ top-row unitarity

The large inaccuracy in the determination of the real part of the right-handed coupling from nuclear β -decay is entirely coming from the error in the lattice determination of g_A/g_V . A way

to circumvent this problem is by looking at superallowed Fermi decays (in which just the vector part of the hadronic current participates). The Conserved Vector Current (CVC) hypothesis states that $g_V = 1$, so no lattice calculations are needed. The decay rate for superallowed Fermi β -decay is given by [96]

$$\begin{aligned}\Gamma_\beta &\propto |C_V|^2 + |C'_V|^2, \\ &= |a_{LL} + a_{LR}|^2 + |a_{RL} + a_{RR}|^2, \\ &= |a_{LL}|^2 \left(1 + 2\text{Re} \left(\frac{a_{LR}}{a_{LL}} \right) + \dots \right),\end{aligned}\tag{4.58}$$

where in the last line only the leading order terms in the small quantities a_{LR} , a_{RL} and a_{RR} are kept. In the first line it is assumed that there is no vector–axial-vector interference on the lepton side, which is true if the right-handed neutrino mass is very large or very small with respect to the energy scales in β -decay ($\sim \text{MeV}$), such that left-right chirality flips do not occur on the lepton side. To get rid of the overall factor, one could take the ratio of the superallowed β -decay rate with the muon decay rate, which is given by

$$\begin{aligned}\Gamma_\mu &\propto |c_{LL}|^2 + |c_{LR}|^2 + |c_{RL}|^2 + |c_{RR}|^2, \\ &= |c_{LL}|^2(1 + \dots),\end{aligned}\tag{4.59}$$

where the c 's describe the leptonic couplings and are defined like the a 's in Eq. (4.53), but without the CKM matrix elements. This ratio is used in experiments to determine the CKM matrix element V^{ud} , and so we will define the experimentally obtained CKM matrix element, $|V_{\text{vec}}^{ud}|^2$ as the ratio of superallowed β -decay with respect to muon decay, i.e.,

$$|V_{\text{vec}}^{ud}|^2 \equiv \frac{\Gamma_\beta}{\Gamma_\mu} = |V_L^{ud}|^2 \left[1 + 2\text{Re} \left(\tan \zeta e^{-i\omega} \frac{g_R V_R^{ud}}{g_L V_L^{ud}} \right) + \dots \right].\tag{4.60}$$

The same thing can be done for the matrix elements V^{us} and V^{ub} if they are determined from pure vector transitions (this is the case for $K_{\ell 3}$ and $B_{\ell 3}$ decays). Summing those matrix elements squared one gets

$$\sum_i |V_{\text{vec}}^{ui}|^2 = \sum_i |V_L^{ui}|^2 + \sum_i 2\text{Re} \left(\tan \zeta e^{-i\omega} V_R^{ui} V_L^{ui*} g_R/g_L \right),\tag{4.61}$$

in which the left-hand side is what is tested in the so called CKM *top-row unitarity test* and the first term on the right-hand side should be equal to one assuming *three generation unitarity*. The experimental top-row unitarity test is satisfied to a very high level of accuracy, which leaves very little room for the second term on the right-hand side and can, therefore, be used to constrain a right-handed coupling. In the unitarity test in [96], the values used for V^{us} and V^{ub} were obtained from mixed vector and axial-vector transitions. Here we will stick to strictly vector transitions, i.e.,

$$|V_{\text{vec}}^{ud}| = 0.9743 \pm 0.0002,\tag{4.62}$$

from superallowed Fermi β -decay [96],

$$|V_{\text{vec}}^{us}| = 0.225 \pm 0.001,\tag{4.63}$$

from $K_{\ell 3}$ ($K \rightarrow \pi \ell \nu$) decays [97] and

$$|V_{\text{vec}}^{ub}| = (3.4 \pm 0.4) \cdot 10^{-3}, \quad (4.64)$$

from $B_{\ell 3}$ ($B \rightarrow \pi \ell \nu$) decays [98], which results in

$$|V_{\text{vec}}^{ud}|^2 + |V_{\text{vec}}^{us}|^2 + |V_{\text{vec}}^{ub}|^2 = 0.9999 \pm 0.0008, \quad (4.65)$$

which implies, assuming three generation unitarity, that

$$\text{Re} \left[\tan \zeta e^{-i\omega} \frac{g_R}{g_L} \sum_i V_R^{ui} V_L^{ui*} \right] = (-0.5 \pm 4) \cdot 10^{-4}. \quad (4.66)$$

In a manifest left-right symmetric model this would imply that

$$|\tan \zeta \cos \omega| < 4 \cdot 10^{-4}, \quad (4.67)$$

which is a strong limit on the mixing angle, but, in a model without any relation between the left- and right-handed CKM matrix, it might also just mean that the top-row of the right-handed matrix is almost perpendicular to the top-row of the left-handed matrix.

Meson decay

In the previous paragraph, the determination of the Standard Model CKM matrix elements V^{ud} , V^{us} and V^{ub} from pure vector decays was used, together with a unitarity constraint. Another way to obtain a bound on the right-handed coupling, which was put forward in [99], is to compare the determination of V^{ud} from pure vector transitions, to the determination of V^{ud} based on pure axial-vector transitions, coming from, e.g., leptonic pion decay.

Following [99], we will define the experimental extractions of the CKM matrix element based on a vector transition as V_{vec}^{ud} and the one based on an axial-vector transition as V_{ax}^{ud} . In the SM, both definitions are equal and, of course, correspond to the CKM matrix element V^{ud} , but beyond the SM they may be unequal and their difference is a measure for the right-handed coupling. This follows from the fact that V_{vec}^{ud} and V_{ax}^{ud} are measured by taking the ratio of respectively a vector and axial-vector decay rate to the muon decay rate, i.e.,

$$\begin{aligned} |V_{\text{vec}}^{ud}|^2 &= \frac{|C_V|^2 + |C_V'|^2}{|c_{LL}|^2 + |c_{LR}|^2 + |c_{RL}|^2 + |c_{RR}|^2} = \frac{|a_{LL} + a_{LR}|^2 + |a_{RL} + a_{RR}|^2}{|c_{LL}|^2 + |c_{LR}|^2 + |c_{RL}|^2 + |c_{RR}|^2}, \\ |V_{\text{ax}}^{ud}|^2 &= \frac{|C_A|^2 + |C_A'|^2}{|c_{LL}|^2 + |c_{LR}|^2 + |c_{RL}|^2 + |c_{RR}|^2} = \frac{|a_{LL} - a_{LR}|^2 + |a_{RL} - a_{RR}|^2}{|c_{LL}|^2 + |c_{LR}|^2 + |c_{RL}|^2 + |c_{RR}|^2}, \end{aligned} \quad (4.68)$$

which reduces in a left-right model to

$$\begin{aligned} |V_{\text{vec}}^{ud}| &= \left| V_L^{ud} + \tan \zeta e^{-i\omega} g_R V_R^{ud} / g_L + \dots \right|, \\ |V_{\text{ax}}^{ud}| &= \left| V_L^{ud} - \tan \zeta e^{-i\omega} g_R V_R^{ud} / g_L + \dots \right|, \end{aligned} \quad (4.69)$$

where the dots are higher order corrections in the small parameters ζ and $M_{W_1}^2/M_{W_2}^2$. Clearly, the difference of these two determinations gives the size of the right-handed currents in the weak decay,

$$\frac{|V_{\text{vec}}^{ud}| - |V_{\text{ax}}^{ud}|}{|V_{\text{vec}}^{ud}| + |V_{\text{ax}}^{ud}|} = \text{Re} \left[\tan \zeta e^{-i\omega} \frac{g_R V_R^{ud}}{g_L V_L^{ud}} \right]. \quad (4.70)$$

In principle V_{ax}^{ud} can be determined from pure axial-vector transitions in β -decay, i.e., Gamow-Teller transitions, but then the imprecisely known hadronic form factor g_A comes in. We will, therefore, extract V_{ax}^{ud} from leptonic pion decay $\pi^\pm \rightarrow \mu^\pm \nu[\gamma]$, for which the rate is given in [100]. Taking the branching ratio from the 2010 Particle Data Group (PDG) listing [66],

$$\Gamma(\pi^+ \rightarrow \mu^+ \nu_\mu[\gamma]) = (2.5281 \pm 0.0005) \cdot 10^{-14} \text{ MeV} \quad (4.71)$$

and the lattice determination of the pion decay constant,

$$f_\pi = 132 \pm 2 \text{ MeV}, \quad (4.72)$$

from [101], we come to the determination of

$$|V_{\text{ax}}^{ud}| = 0.962 \pm 0.015, \quad (4.73)$$

in which the error is dominated by the uncertainty in f_π . Note that we cannot use the more precise experimental determination of f_π from [102] as that is based precisely on this leptonic pion decay and uses V^{ud} as an input. A determination based on $\pi^0 \rightarrow 2\gamma$ decay, which does not depend on V^{ud} , would not improve the error margin of f_π as the π^0 lifetime is only known at 2% accuracy [102]. Using the determination of

$$|V_{\text{vec}}^{ud}| = 0.9743 \pm 0.0002, \quad (4.74)$$

from superallowed Fermi β -decay [96], we come to the determination of the right-handed coupling of the W -boson to the light quarks of ⁴

$$\text{Re} \left[\tan \zeta e^{-i\omega} \frac{g_R V_R^{ud}}{g_L V_L^{ud}} \right] = 0.006 \pm 0.008. \quad (4.75)$$

In the same way, we can use the difference between the determination of V_{vec}^{us} , coming from semi-leptonic kaon decay $K \rightarrow \pi \ell \nu$, and V_{ax}^{us} , coming from leptonic kaon decay $K \rightarrow \mu \nu$. Taking the value

$$|V_{\text{vec}}^{us}| = 0.2254 \pm 0.0013, \quad (4.76)$$

determined on the basis of $K \rightarrow \pi \ell \nu$ decay by [103] and the value

$$|V_{\text{ax}}^{us}| = 0.223 \pm 0.003, \quad (4.77)$$

determined from the branching ratio given in [103],

$$\Gamma(K^\pm \rightarrow \mu^\pm \nu[\gamma]) = (3.37 \pm 0.01) \cdot 10^{-14} \text{ MeV}, \quad (4.78)$$

the theoretical decay rate given in [104] and the lattice determination in [101],

$$f_K = 157 \pm 2 \text{ MeV}, \quad (4.79)$$

⁴In the original work [99] the determination of $|V_{\text{ax}}^{ud}|$ was mistakenly based on pion β -decay ($\pi^+ \rightarrow \pi^0 e^+ \nu_e$) which has a much smaller error, but is in fact a *vector* transition.

we calculate the right-handed coupling of the W -boson to the u and s quarks to be ⁵

$$\operatorname{Re} \left[\tan \zeta e^{-i\omega} \frac{g_R V_R^{us}}{g_L V_L^{us}} \right] = 0.005 \pm 0.007. \quad (4.80)$$

The same procedure works by comparing, close to the zero-recoil point limit, the $B \rightarrow D^* \ell \nu$ decay rate (axial) to the $B \rightarrow D \ell \nu$ decay rate (vector) [99], resulting in the determination

$$\operatorname{Re} \left[\tan \zeta e^{-i\omega} \frac{g_R V_R^{cb}}{g_L V_L^{cb}} \right] = 0.025 \pm 0.025. \quad (4.81)$$

Comparing leptonic $B \rightarrow \tau \nu$ to semi leptonic $B \rightarrow \pi \ell \nu$ decays, it is found in [99] that the coupling of the W -boson to the right-handed u and b quark is

$$\operatorname{Re} \left[\tan \zeta e^{-i\omega} \frac{g_R V_R^{ub}}{g_L V_L^{ub}} \right] = -0.19 \pm 0.07, \quad (4.82)$$

which is 2.7σ away from zero.

Neutron Electric Dipole Moment

The imaginary part of the right-handed coupling of the W boson is CP violating and contributes to the neutron Electric Dipole Moment (EDM). The present bound on the neutron EDM, quoted by the PDG [66], is

$$|d_n^e| < 2.9 \cdot 10^{-26} e \text{ cm}. \quad (4.83)$$

In [105], it was calculated that the contribution to the neutron EDM, from a non-zero CP -violating right-handed coupling of the W -boson, in a left-right symmetric model, is given by

$$|d_n^e| \simeq \left| \sin \zeta \operatorname{Im} \left[e^{-i\omega} V_R^{ud} V_L^{ud*} \right] \right| 3 \times 10^{-19} e \text{ cm}, \quad (4.84)$$

which, when combined with the bound on the EDM, translates to

$$\left| \sin \zeta \operatorname{Im} \left[e^{-i\omega} V_R^{ud} V_L^{ud*} \right] \right| < 10^{-7}. \quad (4.85)$$

Although this bound was originally derived for a left-right *symmetric* theory, it can easily be generalized to an arbitrary left-right model by inserting g_R/g_L . This is then by far the strongest bound on the imaginary part available. It is, however, possible that this contribution to the neutron EDM is canceled by the contribution from the QCD θ term. It would be best to rederive a combined bound on θ and the imaginary part of the right-handed W coupling, but that falls outside the scope of this thesis. For now, under the assumption that no large cancellations happen, Eq. (4.85) gives the best bound on the imaginary part.

⁵In the original work [99], the determination of $|V_{\text{ax}}^{us}|$ was based on the value of $|V_{\text{ax}}^{us}|/|V_{\text{ax}}^{ud}|$ found by [103] combined with the value of $|V_{\text{ax}}^{ud}|$ which was erroneously taken from pion β -decay.

4.2.4 Summary

In this section we have given an overview of the most important bounds on the right-handed coupling of the W -boson to the different quarks. We corrected the best model independent bound on the real part of the right-handed coupling of the W boson to the ud quarks, which is given in Eq. (4.75) and to the us quarks, which is given in Eq. (4.80). We derived an upper bound on the imaginary part of the right-handed coupling of the W boson to the ud quarks from nuclear β -decay, under the assumption of real hadronic matrix elements. The strongest bound, however, comes from the upper bound on the neutron EDM and is given in Eq. (4.85).

For easy comparison, we also translate the bounds on the right-handed coupling into bounds on the mixing angles $\zeta_g \equiv \frac{g_R}{g_L}\zeta$ and ω under the assumption $V_R^{ud} = V_L^{ud}$ in Figure 4.2.

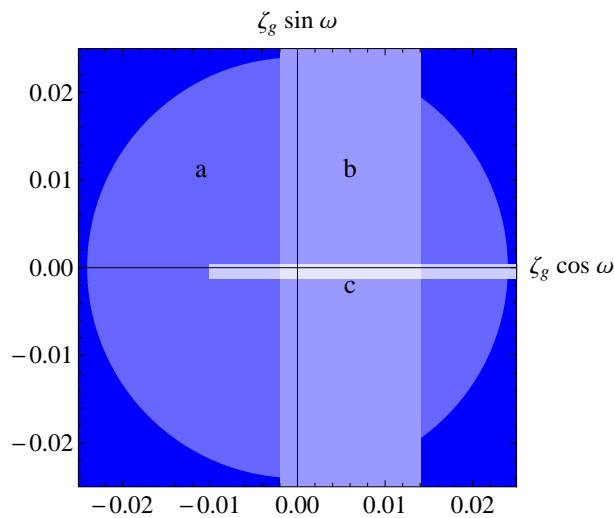


Figure 4.2: Translation of bounds on the right-handed W boson coupling to the u and d quarks into bounds (at 68% CL) on the mixing angles $\zeta_g \equiv g_R/g_L\zeta$ and ω under the assumption $V_R^{ud} = V_L^{ud}$. Bound (a) comes from νN DIS, whereas (b) from pion decay combined with superallowed β -decay and (c) from nuclear β -decay. The bound on the imaginary part from neutron EDM measurements is not visible on this scale.

4.3 Cross section and asymmetries in $p^\uparrow p^\uparrow \rightarrow (W_1 + W_2)X \rightarrow \ell\nu X$

Now that we have discussed the model and its current bounds, we will look at its consequences for $p^\uparrow p^\uparrow \rightarrow (W_1 + W_2)X \rightarrow \ell\nu X$ at RHIC. As said in the introduction, the SM predicts only negligibly small spin asymmetries in this process. We will now calculate the spin asymmetries in the general left-right model we have introduced in the previous sections.

In the leptonic decay of the W bosons, the neutrino will go unobserved and so we need the cross section integrated over the neutrino momentum. We choose to express the neutrino momentum in terms of $\mathbf{q}_T = \mathbf{l}_T + \bar{\mathbf{l}}_T$ and $z \equiv \bar{l}^-/l^-$. The z variable will be integrated over and does not need to be specified, but to get an idea of what it parameterizes one can relate it to the Collins-Soper angle θ by $z = \frac{1+\cos\theta}{1-\cos\theta}$. The charged lepton momentum will be specified by its

forward rapidity $Y \equiv \frac{1}{2} \log l^+/l^-$ and transverse momentum, both measured in the lab frame. The transverse momentum will be denoted by its length l_T and its azimuthal angle ϕ . The phase space element can, in these coordinates, be written as

$$d\mathcal{R} = \frac{d^3\mathbf{l}}{(2\pi)^3 2E_l} \frac{d^3\bar{\mathbf{l}}}{(2\pi)^3 2E_{\bar{l}}} = \frac{l_T}{4z(2\pi)^6} dz d^2\mathbf{q}_T dl_T dY d\phi. \quad (4.86)$$

The observable cross section thus reads

$$\frac{d\sigma}{dl_T dY d\phi} = \frac{l_T}{4(2\pi)^6} \int \frac{dz}{z} \int d^2\mathbf{q}_T \frac{d\sigma}{d\mathcal{R}}. \quad (4.87)$$

In the previous chapter (Section 3.5) we have shown that the Transverse Momentum Dependent (TMD) effects in W boson production are at the sub-percent level and so we will here use the collinear approximation for the \mathbf{q}_T integrated cross section in Eq. (2.45). In the collinear approximation, the cross section can be written as

$$\frac{d\sigma}{dl_T dY d\phi} = \frac{l_T}{4S^2(2\pi)^2} \int \frac{dz}{z} \frac{1}{N_c} \sum_{q,q'} \text{Tr}_D \left[\Phi^q(x_1, P_1, S_1) V_{jq'q'}^{\nu'} \Phi^{\bar{q}'}(x_2, P_2, S_2) V_{iqq'}^\mu \right] \times \\ D_{\mu\rho}^i D_{\nu\sigma}^{j*} L_{ij}^{\rho\sigma} + (1 \leftrightarrow 2), \quad (4.88)$$

where again $V_{qq'}^\mu$ is the vector-boson-quark interaction vertex (primed implies complex conjugated coupling strength), $D_{\mu\nu}$ is the vector boson propagator and L is the lepton tensor, given by

$$L_{ij}^{\rho\sigma} = \text{Tr} [V_{i\ell}^\rho \not{\ell} V_{j\ell}^{\sigma'} \not{\ell}]. \quad (4.89)$$

4.3.1 Cross section

We will calculate the general tree-level cross section for the process $p^\dagger p^\dagger \rightarrow (W_1^\pm + W_2^\pm)X \rightarrow \ell\nu X$, with the W bosons coupling through the vertices

$$V_{id\bar{u}}^\mu = \frac{i}{\sqrt{2}} \gamma^\mu [g_{L_i}^q \mathcal{P}_L + g_{R_i}^q \mathcal{P}_R], \\ V_{iu\bar{d}}^\mu = \frac{i}{\sqrt{2}} \gamma^\mu [(g_{L_i}^q)^* \mathcal{P}_L + (g_{R_i}^q)^* \mathcal{P}_R], \\ V_{i\ell}^\mu = \frac{i}{\sqrt{2}} \gamma^\mu [g_{L_i}^\ell \mathcal{P}_L + g_{R_i}^\ell \mathcal{P}_R], \quad (4.90)$$

with $\mathcal{P}_{R,L} = \frac{1}{2}(1 \pm \gamma^5)$ the right (left) chirality projection operator. For the boson propagators, we use the unitary gauge with a Breit-Wigner width, i.e.,

$$D_{\mu\rho}^i = -i \Pi_i(Q^2) \left[g_{\mu\rho} - \frac{q_\mu q_\rho}{M_{W_i}^2} \right], \quad (4.91)$$

with

$$\Pi_i(Q^2) \equiv \frac{1}{Q^2 - M_{W_i}^2 + i\Gamma_{W_i} M_{W_i}}. \quad (4.92)$$

Using Eq. (4.88), we obtain the following expression for the cross section

$$\begin{aligned} \frac{d\sigma}{dl_T dY d\phi} &= \frac{l_T^3}{192(2\pi)^2 S} \int dz \frac{(1+z)^2}{z^2} \left\{ A(z) \left(K_F^{++} F^{++} + K_F^{+-} F^{+-} \right) \right. \\ &+ C(z) \left(K_F^{-+} F^{-+} + K_F^{--} F^{--} \right) + B(z) |\mathbf{S}_{1T}| |\mathbf{S}_{2T}| \\ &\left. \left[\left(K_H^{++} H^{++} + K_H^{+-} H^{+-} \right) \cos(\phi_{S_1}^\ell + \phi_{S_2}^\ell) + \left(K_H^{-+} H^{-+} + K_H^{--} H^{--} \right) \sin(\phi_{S_1}^\ell + \phi_{S_2}^\ell) \right] \right\}, \end{aligned} \quad (4.93)$$

where we have defined the functions

$$A(z) \equiv \frac{1+z^2}{2(1+z)^2}, \quad B(z) \equiv \frac{z}{(1+z)^2}, \quad C(z) \equiv \frac{z-1}{2(1+z)}, \quad (4.94)$$

and the different combinations of distributions by

$$\begin{aligned} F^{\pm\pm}(x_1, x_2) &\equiv (f_1^d(x_1) f_1^{\bar{u}}(x_2) \pm x_1 \leftrightarrow x_2) \pm u \leftrightarrow d, \\ H^{\pm\pm}(x_1, x_2) &\equiv (h_1^d(x_1) h_1^{\bar{u}}(x_2) \pm x_1 \leftrightarrow x_2) \pm u \leftrightarrow d, \end{aligned} \quad (4.95)$$

furthermore, the couplings are contained in

$$\begin{aligned} K_F^{++} &\equiv G_{11}^l G_{11}^q |\Pi_1|^2 + G_{22}^l G_{22}^q |\Pi_2|^2 + \left(G_{12}^l G_{21}^q + G_{21}^l G_{12}^q \right) \text{Re}[\Pi_1 \Pi_2^*], \\ K_F^{+-} &\equiv i \left(G_{12}^l G_{21}^q - G_{21}^l G_{12}^q \right) \text{Im}[\Pi_1 \Pi_2^*], \\ K_F^{-+} &\equiv i \left(H_{12}^l H_{21}^q - H_{21}^l H_{12}^q \right) \text{Im}[\Pi_1 \Pi_2^*], \\ K_F^{--} &\equiv H_{11}^l H_{11}^q |\Pi_1|^2 + H_{22}^l H_{22}^q |\Pi_2|^2 + \left(H_{12}^l H_{21}^q + H_{21}^l H_{12}^q \right) \text{Re}[\Pi_1 \Pi_2^*], \\ K_H^{++} &\equiv G_{11}^l M_{11}^q |\Pi_1|^2 + G_{22}^l M_{22}^q |\Pi_2|^2 + \left(G_{12}^l M_{21}^q + G_{21}^l M_{12}^q \right) \text{Re}[\Pi_1 \Pi_2^*], \\ K_H^{+-} &\equiv i \left(G_{12}^l M_{21}^q - G_{21}^l M_{12}^q \right) \text{Im}[\Pi_1 \Pi_2^*], \\ K_H^{-+} &\equiv - \left(G_{12}^l N_{21}^q - G_{21}^l N_{12}^q \right) \text{Im}[\Pi_1 \Pi_2^*], \\ K_H^{--} &\equiv i G_{11}^l N_{11}^q |\Pi_1|^2 + i G_{22}^l N_{22}^q |\Pi_2|^2 + i \left(G_{12}^l N_{21}^q + G_{21}^l N_{12}^q \right) \text{Re}[\Pi_1 \Pi_2^*], \end{aligned} \quad (4.96)$$

in which we have defined

$$\begin{aligned} G_{ij}^s &\equiv 2 \left(g_{Li}^s g_{Lj}^{s*} + g_{Ri}^s g_{Rj}^{s*} \right), \\ H_{ij}^s &\equiv 2 \left(g_{Ri}^s g_{Rj}^{s*} - g_{Li}^s g_{Lj}^{s*} \right), \\ M_{ij}^s &\equiv 2 \left(g_{Li}^s g_{Rj}^{s*} + g_{Ri}^s g_{Lj}^{s*} \right), \\ N_{ij}^s &\equiv 2 \left(g_{Li}^s g_{Rj}^{s*} - g_{Ri}^s g_{Lj}^{s*} \right) \end{aligned} \quad (4.97)$$

The cross section is for summed W^\pm production from which specific W^+ or W^- production can be obtained by setting the appropriate parton distributions to zero. The angles $\phi_{S_1}^\ell$ and $\phi_{S_2}^\ell$ are defined as the azimuthal angle between the charged lepton and the transverse spin direction of

proton 1 and 2 respectively, with an increasing angle corresponding to the lepton being rotated in the clockwise direction if one looks in the direction of proton 1. The light cone momentum fractions and the vector boson momentum squared are in these coordinates given by

$$x_1 = \frac{l_T}{\sqrt{s}} e^Y \frac{1+z}{z}, \quad x_2 = \frac{l_T}{\sqrt{s}} e^{-Y} (1+z), \quad Q^2 = l_T^2 \frac{(1+z)^2}{z}. \quad (4.98)$$

The coupling strengths in a general Left-Right model can be read off from the vertices in Eq. (4.34) and (4.35). The coupling to quarks is given by

$$\begin{aligned} g_{L1}^q &= g_L \cos \zeta V_L^{ud} & g_{L2}^q &= g_L \sin \zeta V_L^{ud}, \\ g_{R1}^q &= g_R \sin \zeta e^{-i\omega} V_R^{ud} & g_{R2}^q &= -g_R \cos \zeta e^{i\omega} V_R^{ud}, \end{aligned} \quad (4.99)$$

whereas for the coupling to leptons one can use the same couplings, but without the CKM matrix element removed. In principle, one should include a PMNS matrix element in the coupling to leptons, but since the neutrino flavor is not observed one would end up with a cross section proportional to the sum over neutrino flavors $\sum_\nu |V_{PMNS}^{\ell\nu}|^2 = 1$ and so one can as well leave out the PMNS matrix element from the start. We will work with two different scenarios for the right-handed neutrinos: massless and no right-handed neutrinos. The massless ν_R scenario will be the default in the next equations, from which the no ν_R case can be obtained by setting the right-handed lepton coupling to zero.

4.3.2 Spin asymmetries

Next we consider asymmetries between the process with parallel and antiparallel proton spins. We will define a spin flip symmetric and antisymmetric cross section by

$$d\sigma^{S,A} \equiv \frac{1}{4} \left(d\sigma^{\uparrow\uparrow} \pm d\sigma^{\uparrow\downarrow} \pm d\sigma^{\downarrow\uparrow} + d\sigma^{\downarrow\downarrow} \right). \quad (4.100)$$

The anti-symmetric cross section $d\sigma^A$ is a function of ϕ , with two independent ϕ dependencies, $\cos 2\phi$ and $\sin 2\phi$. We will define two transverse spin asymmetries in the integrated cross section, that select out the two different angular dependencies by appropriate integration over the azimuthal angle,

$$\begin{aligned} A_{TT}^C &\equiv \frac{\int dl_T dY \left(\int_{-\pi/4}^{\pi/4} - \int_{\pi/4}^{3\pi/4} + \int_{3\pi/4}^{5\pi/4} - \int_{5\pi/4}^{7\pi/4} \right) d\phi d\sigma^A}{\int dl_T dY \int_0^{2\pi} d\phi d\sigma^S}, \\ A_{TT}^S &\equiv \frac{\int dl_T dY \left(\int_0^{\pi/2} - \int_{\pi/2}^{\pi} + \int_{\pi}^{3\pi/2} - \int_{3\pi/2}^{2\pi} \right) d\phi d\sigma^A}{\int dl_T dY \int_0^{2\pi} d\phi d\sigma^S}. \end{aligned} \quad (4.101)$$

The two spin asymmetries can, with the use of Eq. (4.93), be written as

$$\begin{aligned} A_{TT}^C &= \frac{2 \int dz dl_T dY \frac{l_T^3}{z} |\mathbf{S}_{1T}| |\mathbf{S}_{2T}| [K_H^{++} H^{++} + K_H^{+-} H^{+-}]}{\pi \int dz dl_T dY l_T^3 \left[\frac{z^2+1}{2z^2} (K_F^{++} F^{++} + K_F^{+-} F^{+-}) + \frac{z^2-1}{2z^2} (K_F^{-+} F^{-+} + K_F^{--} F^{--}) \right]}, \\ A_{TT}^S &= \frac{2 \int dz dl_T dY \frac{l_T^3}{z} |\mathbf{S}_{1T}| |\mathbf{S}_{2T}| [K_H^{-+} H^{-+} + K_H^{--} H^{--}]}{\pi \int dz dl_T dY l_T^3 \left[\frac{z^2+1}{2z^2} (K_F^{++} F^{++} + K_F^{+-} F^{+-}) + \frac{z^2-1}{2z^2} (K_F^{-+} F^{-+} + K_F^{--} F^{--}) \right]}, \end{aligned} \quad (4.102)$$

4.4 Transversity distribution

Since the asymmetries discussed here all are proportional to the quark transversity distribution functions (commonly denoted as $h_1, \delta q$ or $\Delta_T q$), we will briefly comment on what is known about them to date. Recent measurements by the HERMES experiment at DESY of a particular asymmetry (called the Collins asymmetry) in semi-inclusive DIS, in which electrons scattering off transversely polarized protons produce a spin direction dependent asymmetric azimuthal angular distribution of final state pions, indicate that the transversity distribution is nonzero [27]. Combining that data with measurements on the $e^+e^- \rightarrow h_1 h_2 X$ processes from the Belle Collaboration results in the first determination of the transversity functions [59] to be

$$h_1^q = x^\alpha (1-x)^\beta \frac{(\alpha + \beta)^{(\alpha + \beta)}}{\alpha^\alpha \beta^\beta} \frac{N_T^q}{2} (f_1^q(x) + g_1^q(x)), \quad (4.103)$$

where $\alpha = 1.14 \pm 0.68$, $\beta = 4.74 \pm 5.45$, $N_T^u = 0.48 \pm 0.09$ and $N_T^d = -0.62 \pm 0.3$. Concerning the errors in α and β , the function multiplying $(f_1 + g_1)$ in Eq. (4.103) can be peaked around any value. Therefore we will simply estimate $h_1^q(x) = f_1^q(x)/2$, when we turn to numerical predictions, which is slightly optimistic, but certainly compatible with (4.103) within errors.

The absence of experimental data on $h_1^{\bar{q}}$ prevents making absolute predictions for the asymmetries discussed here, but one can discuss upper bounds of the asymmetries. A source of suppression arises from the fact that this transversity distribution of antiquarks inside a proton is expected to be much smaller than that of quarks. As a consequence, the asymmetries may be considerably smaller at a proton-proton collider than at a proton-antiproton collider. For numerical predictions we will use the, possibly overestimated, antiquark transversity function $h_1^{\bar{q}}(x) = f_1^{\bar{q}}(x)/2$.

Estimates for RHIC based on the maximally possible magnitudes of the transversity distributions were found to be on the percent level for the $\cos(2\phi)$ asymmetry in the Drell-Yan process [106]. These were obtained by saturating the Soffer bound, $h_1^q(x) \leq \frac{1}{2}(f_1^q(x) + g_1^q(x))$, at a low energy scale and then evolving $h_1^q(x)$ to the appropriate scale by NLO evolution. At low Q and high x this method produces larger asymmetries than our simple choice for the transversity distributions. Whereas, at higher energies and low x their transversity distribution becomes smaller than ours. For the production of W -bosons at the RHIC energy the distribution functions at $Q \sim M_W$ and $x \sim 0.16$ are relevant. Comparing our predictions for the neutral current asymmetry with theirs at those values of Q and x , we find that our choices of the transversity distribution are compatible. In any case, the measurements of h_1^q and $h_1^{\bar{q}}$ will be essential if one wants to quantify the effects from new physics.

4.5 Numerical estimates for RHIC

At RHIC energy, $\sqrt{s} = 500$ GeV, the contributions from the W_2 boson will be negligible and we can thus approximate the K expressions in Eq. (4.96) as

$$\begin{aligned}
K_F^{++} &= G_{11}^l G_{11}^q |\Pi_1|^2, \\
K_F^{--} &= H_{11}^l H_{11}^q |\Pi_1|^2, \\
K_F^{+-} &= K_F^{-+} = 0, \\
K_H^{++} &= 4\text{Re}[g_{R1}^q g_{L1}^{q*}] G_{11}^l |\Pi_1|^2, \\
K_H^{--} &= 4\text{Im}[g_{R1}^q g_{L1}^{q*}] G_{11}^l |\Pi_1|^2, \\
K_H^{+-} &= K_H^{-+} = 0.
\end{aligned} \tag{4.104}$$

Within this approximation, the spin asymmetries read

$$\begin{aligned}
A_{TT}^C &= \text{Re}[g_{R1}^q g_{L1}^{q*}] \frac{8|\mathbf{S}_{1T}||\mathbf{S}_{2T}| \int dz dl_T dY \frac{l_T^3}{z} |\Pi_1(Q^2)|^2 G_{11}^l H^{++}}{\pi \int dz dl_T dY l_T^3 |\Pi_1(Q^2)|^2 \left[\frac{z^2+1}{2z^2} G_{11}^l G_{11}^q F^{++} + \frac{z^2-1}{2z^2} H_{11}^l H_{11}^q F^{--} \right]}, \\
A_{TT}^S &= \text{Im}[g_{R1}^q g_{L1}^{q*}] \frac{8|\mathbf{S}_{1T}||\mathbf{S}_{2T}| \int dz dl_T dY \frac{l_T^3}{z} |\Pi_1(Q^2)|^2 G_{11}^l H^{++}}{\pi \int dz dl_T dY l_T^3 |\Pi_1(Q^2)|^2 \left[\frac{z^2+1}{2z^2} G_{11}^l G_{11}^q F^{++} + \frac{z^2-1}{2z^2} H_{11}^l H_{11}^q F^{--} \right]}.
\end{aligned} \tag{4.105}$$

Expanding in the mixing angle ζ , we can write the spin asymmetries as

$$\begin{aligned}
A_{TT}^C &= |\mathbf{S}_{1T}||\mathbf{S}_{2T}| \text{Re} \left[\zeta \frac{g_R V_R^{ud}}{g_L V_L^{ud}} e^{-i\omega} \right] A, \\
A_{TT}^S &= |\mathbf{S}_{1T}||\mathbf{S}_{2T}| \text{Im} \left[\zeta \frac{g_R V_R^{ud}}{g_L V_L^{ud}} e^{-i\omega} \right] B,
\end{aligned} \tag{4.106}$$

where A and B are now numerical coefficients independent of the strengths of the couplings. The expressions in Eq. (4.106) are valid in both the massless and no right-handed neutrino scenario. From Eq. (4.106) we can conclude that a bound on A_{TT}^C can be translated directly into a bound on the real part of the mixing, whereas a bound on the A_{TT}^S asymmetry translates to a bound on the imaginary part of the mixing. Or, in other words, nonzero spin asymmetries imply physics beyond the Standard Model and, more specifically, a nonzero A_{TT}^S implies an extra source of CP violation beyond the Standard Model.

To get an idea of how large the spin asymmetries can be, given the constraints on a right-handed coupling of the W boson discussed in Section 4.2.3, we need to calculate the numerical values of A and B in Eq. (4.106). For all practical purposes one would like to look at asymmetries in the integrated cross section, but let us first look at the spin asymmetries in the differential cross section to get an idea of what the optimal integration range/experimental cuts could be. In Figure 4.3 and 4.4 we plotted A and B for W^+ and W^- production as function of l_T for different Y using our Ansatz for the transversity distribution as discussed in the previous Section and the numerical values for the unpolarized PDF from [42].

From the figures we can see that A grows with Y in W^+ production and shrinks with Y in W^- production. It will, therefore, be beneficial for the size of the asymmetry to exclude

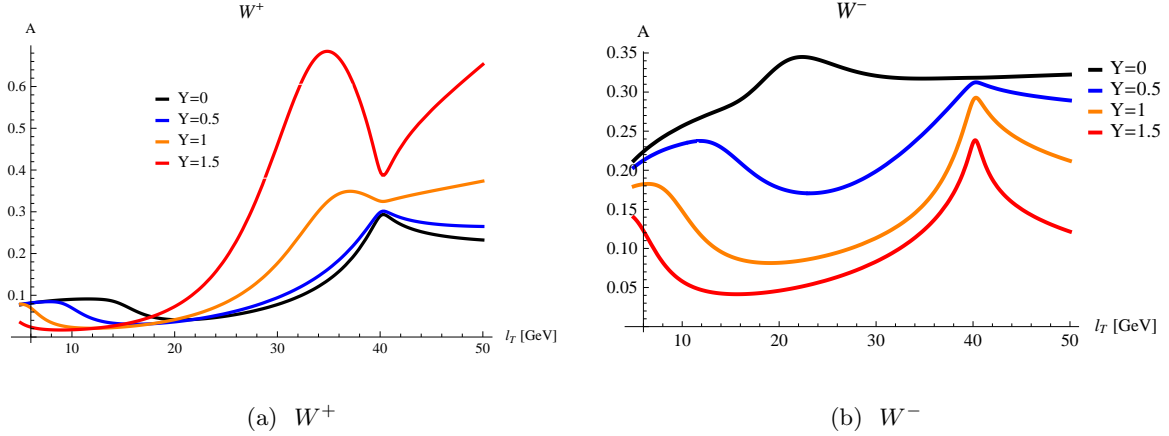


Figure 4.3: The A coefficient in Eq. (4.106) as a function of l_T for different Y .

the central region in W^+ production and the forward and backward region in W^- production, but it will go at the cost of lowering the number of events. It is impossible to determine the optimal experimental cuts as it will depend on the statistics available, the detector acceptance and systematic errors. Besides these experimental inputs, the optimal range will also depend on the parameterization of the transversity distribution and given its uncertainties, we think it is meaningless to try to optimize the range completely. Instead, we have calculated the A and B coefficients for a sample set of cuts and they are given in Table 4.1.

In our paper on spin asymmetries at RHIC [64] we based our estimates on the best model independent bound on the right-handed coupling at that time, which was from νN DIS. We will now update our analysis using the determination of the real part of the right-handed coupling in Eq. (4.75),

$$\text{Re} \left[\tan \zeta e^{-i\omega} \frac{g_R V_R^{ud}}{g_L V_L^{ud}} \right] = 0.006 \pm 0.008, \quad (4.107)$$

to be

$$\begin{aligned} W^- : \quad A_{TT}^C &= (0.2 \pm 0.2)\%, \\ W^+ : \quad A_{TT}^C &= (0.1 \pm 0.2)\%, \end{aligned} \quad (4.108)$$

which is most likely outside the reach of RHIC. However, it is not unlikely that, provided that the antiquark transversity turns out not to be too small, a competitive bound on the real part of the right-handed coupling can be set. Given the best bound on the imaginary part of the right-handed coupling in Eq. (4.85), the A_{TT}^S asymmetry will definitely be below what could be measured at RHIC.

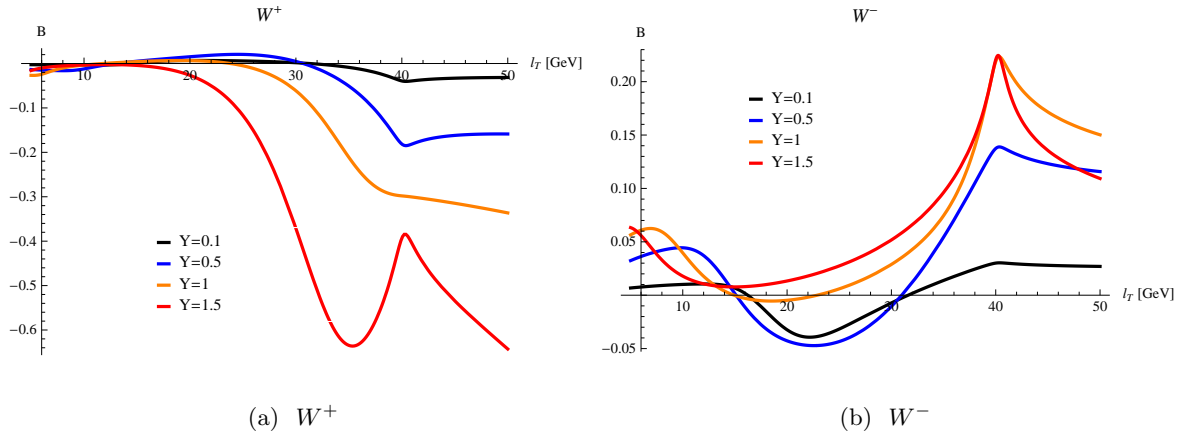


Figure 4.4: The B coefficient in Eq. (4.106) as a function of l_T for different Y . Not visible from the graphs, but important to note is that the B coefficient is odd in Y .

$30 < l_T < 45$ GeV		W^+	W^-
$0 < Y < 1$	A	0.22	0.27
$0.5 < Y < 1$	B	-0.15	0.11

Table 4.1: The coefficients A and B in Eq. (4.106) that set the size of the spin asymmetries in the integrated cross section.

4.6 Numerical estimates for a higher energy collider

Although it is unlikely that there will be a polarized proton collider with a higher center of mass energy than RHIC in the foreseen future, it is still interesting to see how the spin asymmetries behave in the energy range where the W_2 boson becomes important. In Figure 4.5 to 4.7 numerical estimates for the spin asymmetries are given at a center of mass energy of $\sqrt{s} = 14$ TeV assuming $M_{W_2} = 2.5$ TeV, $\Gamma_{W_2} = 20$ GeV and a mixing angle of $\zeta = 0.01$, various values of g_R , $\omega = 0, \pi/2$ and for both the massless and no right-handed neutrino scenario. One can see from the plots that in the absence of right-handed neutrinos, the spin asymmetries become large around $l_T \sim M_{W_2}/2$ even for a small mixing angle. The cross section for observing such a high l_T lepton is however very small, as the leptonic decay of the W_2 boson is suppressed by two factors of the mixing angle ζ when there is no right-handed neutrino. It is also interesting to note that even in the absence of a complex mixing, i.e., given $\omega = 0$, there is still a large A_{TT}^S asymmetry around $l_T \sim M_{W_2}/2$ in the no ν_R case, contrary to what was found around $l_T \sim M_{W_1}/2$, where a nonzero A_{TT}^S implies CP violation beyond the SM.

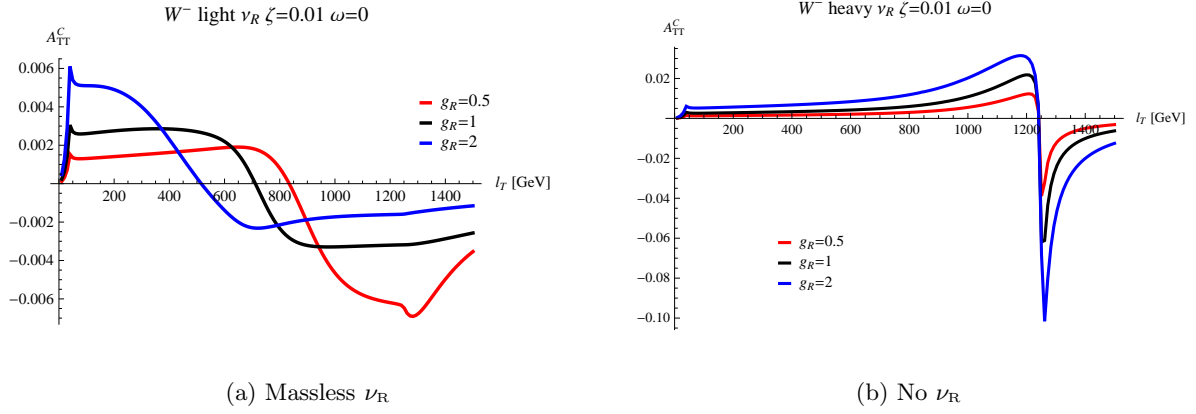


Figure 4.5: The spin asymmetry A_{TT}^C at $Y = 0$ as a function of the lepton transverse momentum at a center of mass energy $\sqrt{s} = 14$ TeV.

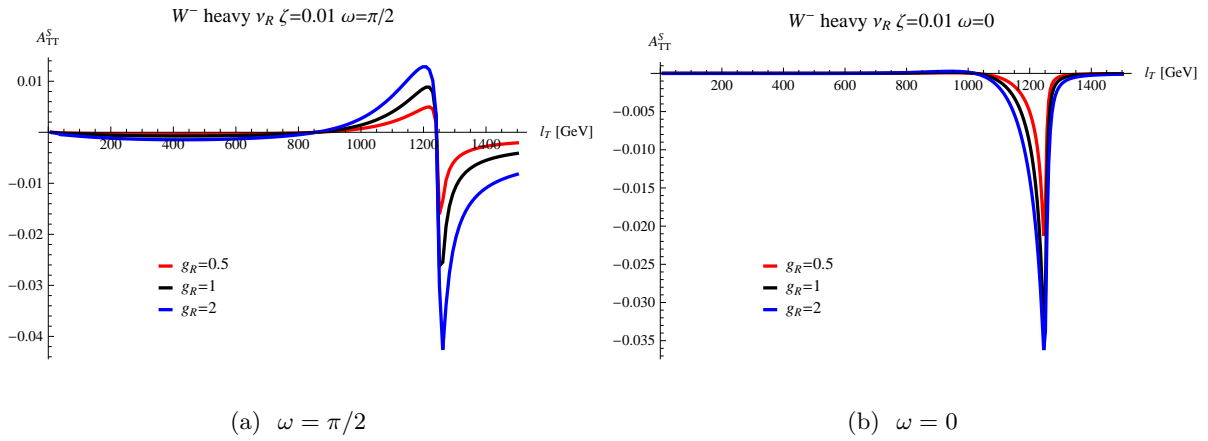


Figure 4.6: The spin asymmetry A_{TT}^S at $Y = 0.5$ as a function of the lepton transverse momentum at a center of mass energy $\sqrt{s} = 14$ TeV assuming there is no right-handed neutrino.

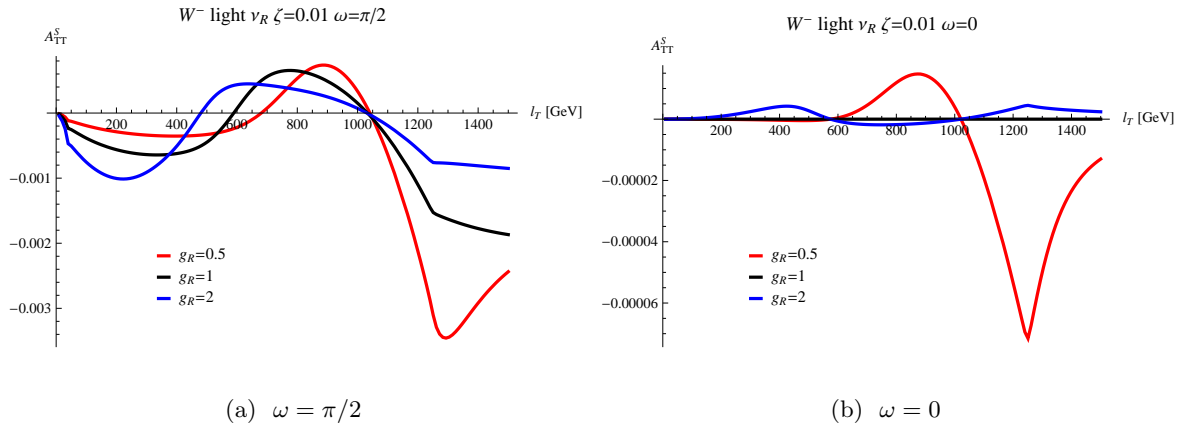


Figure 4.7: The spin asymmetry A_{TT}^S at $Y = 0.5$ as a function of the lepton transverse momentum at a center of mass energy $\sqrt{s} = 14$ TeV assuming a massless right-handed neutrino.

4.7 Discussion

We end with a discussion on the expected background. Deviations from the left-handed SM coupling may be generated effectively in higher orders in α or α_s , for instance by the exchange of a Higgs boson or gluon between the annihilating $q\bar{q}$ pair. Such higher order corrections are all suppressed by a factor of $\alpha_{(s)}m_um_d/M_W^2$ producing unmeasurably small asymmetries. Transverse momentum dependent effects generate residual double transverse spin asymmetries within the SM, but these were found in the previous Chapter to be well below detection limits at RHIC.

We expect the largest experimental background to come from misidentified events. This can be caused by missing a lepton from a neutral current event interpreted as a neutrino from a charged current event. The cross section for such a missing lepton with $|Y| > 1$ is in the order of a picobarn, leading to false A_{TT} asymmetries smaller than 10^{-3} . For A_{TT}^\perp the only neutral current contribution comes from the interference of photon and Z -boson contributions. It is proportional to the Z -boson width. Again this contribution can be safely ignored. Another type of misidentified event can come from heavy quark decays, but this background is largely removed together with the cuts that remove dijet events [107].

One might wonder how well an analogous asymmetry in neutral gauge boson production might serve as probe for a modified Z coupling, caused by, e.g., mixing with a hypothetical Z' -boson. The analogous A_{TT}^C asymmetry in neutral gauge boson production is already present in the SM due to the mixed left-right coupling of the Z boson. As the size of the asymmetry is proportional to the transversity distributions, it is impossible to give an accurate prediction. An additional Z' boson would alter the asymmetry, but it would be a correction (per cent level) that is smaller than the inaccuracy of the SM prediction due to the unknown transversity distributions. Without a determination of the transversity distributions at the percent level, an A_{TT}^C asymmetry in the neutral current would be useless in the search for an anomalous Z coupling.

The situation is different for an analogous A_{TT}^S asymmetry in the neutral current. It is, strictly speaking, present in the SM as well due to the interference of the photon and the Z -boson contributions, but at $Q^2 \sim M_Z^2$ this interference effect can be ignored. The A_{TT}^S asymmetry in Z boson production is thus, in principle, suited as a probe for new CP -violation. However, it is questionable whether the accuracy at which this asymmetry can be determined at RHIC is sufficient, concerning the small cross section for Z boson production.

4.8 Summary

We have given an introduction to general left-right models, which do not necessarily have a symmetry relating left-handed and right-handed particles (as opposed to left-right *symmetric* models). In these models it is possible to have a non-zero right-handed coupling of the ordinary W boson, while all other SM relations are kept intact and the masses of the extra gauge bosons can be made arbitrarily large. This makes it necessary to set independent bounds on the right-handed coupling of the W boson and not infer bounds from, e.g., lower bounds on the mass of a W' boson. Apart from that, it is also necessary to bound the coupling to all 9 different combinations of up- and down-type quarks independently as they all enter with their own right-handed CKM matrix element which, in a general left-right model, is not related to the left-handed CKM matrix. We listed and, when necessary, corrected bounds on the right-handed

W boson coupling from the literature. We calculated the double transverse spin asymmetries that arise in the process $p^\uparrow p^\uparrow \rightarrow (W_1 + W_2)X \rightarrow \ell\nu X$, in our general left-right model. Two asymmetries are found, one proportional to $\cos 2\phi$ and one proportional to $\sin 2\phi$, where ϕ is the angle between the spin plane and the charged lepton's transverse momentum. Both of these asymmetries vanish in the SM and can be used to set a bound on (or measure) a right-handed W boson coupling to the ud quark combination. We found that at RHIC energy, $\sqrt{s} = 500$ GeV, the $\cos 2\phi$ asymmetry is proportional to the real part of the right-handed coupling, whereas the $\sin 2\phi$ asymmetry is proportional to the CP -violating imaginary part.

Numerical estimates for the size of the spin asymmetries were made using reasonable assumptions on the transversity distributions for the quarks and antiquarks. Given the current bounds on the right-handed coupling of the W boson, we estimate the the $\sin 2\phi$ asymmetry to be negligibly small and the $\cos 2\phi$ asymmetry to be around 0.1%. The latter asymmetry can therefore, when design goals are met (800 pb⁻¹ at 70% polarization), be used to set a somewhat weaker but *independent* bound on the real part of the right-handed coupling. The bounds on the imaginary part of the right-handed W boson coupling are not free of assumptions and we therefore argue that also the $\sin 2\phi$ asymmetry is an interesting observable even though it will definitely not reach the bound set by the neutron EDM, it is independent of assumptions on the QCD θ term.

At higher energy, the dependence of the two spin asymmetries on the mixing parameters is more complicated. We give numerical estimates of the spin asymmetries at an imagined polarized collider with $\sqrt{s} = 14$ TeV, for some specific choices of the mixing parameters and in the limit of massless and no right-handed neutrinos. It is shown that, in the no right-handed neutrino scenario, substantial asymmetries can arise at high lepton energy even in the case of small mixing.

Chapter 5

TMD effects in Higgs production

The ATLAS and CMS collaboration have recently discovered a new boson with a mass around 126 GeV [108, 109] decaying into $\gamma\gamma$, ZZ^* and WW^* . This newly found particle could be the Standard Model (SM) Higgs boson, but it might also be something else. Before one can be sure, all its properties need to be checked against the SM predictions. Therefore, the next task is the determination of the spin and CP quantum numbers of this new boson.

Due to the Landau-Yang theorem [110, 111] and the observation of the $\gamma\gamma$ decay mode, a spin-1 boson is already ruled out. This leaves the possibility of a spin-0 or spin-2 boson, which can be distinguished from each other by considering the angular distributions in $\gamma\gamma$ or WW^* decays [112] or in the $ZZ^* \rightarrow 4\ell$ decay [113, 114].

Given that the new boson turns out to be a spin-0 boson, it can have two possible CP quantum numbers¹. The two possibilities are $CP = 1$ (for a *scalar* boson) or $CP = -1$ (for a *pseudoscalar* boson). The SM Higgs boson is a *scalar* boson and the identification of the new particle as a *pseudoscalar* boson would thus immediately rule out the possibility that the newly found particle is the SM Higgs boson.

To determine the CP quantum number experimentally, one can look at kinematical distributions in $H \rightarrow VV^*$ decays [115], the angular distribution of the jets in Higgs + 2 jet production [116, 117] or the spin distribution in τ pair decays [118, 119]. We will show in this Chapter that the difference between a scalar and pseudoscalar coupling is *also* visible in the *transverse momentum distribution* of the scalar particle if it is produced through gluon-gluon fusion.

The Higgs transverse momentum distribution has been calculated in the framework of collinear factorization with q_T resummation at Next-to-Leading Logarithmic (NLL) accuracy at low q_T matched to a fixed order calculation at Next-to-Leading Order accuracy (NLO) at large q_T [120, 121, 122, 123] and at Next-to-Next-to-Leading Logarithmic (NNLL) accuracy matched to a fixed order calculation at NLO [124, 125, 126].

It was noted [127] that in the q_T resummation of gluon-gluon fusion so called “gluon spin correlations” become important, which cause the standard Drell-Yan transverse momentum resummation to fail for the gluon-gluon fusion process. This effect first appears in the computation of the Next-to-Next-to-Leading Order (NNLO) QCD radiative corrections to the Higgs boson q_T cross section and is properly taken into account in [128] and [129].

¹Provided that CP is conserved, which is the case in the SM, where CP violation is limited to the charged current interaction. In the absence of CP symmetry, one cannot assign a CP quantum number and the coupling to fermions is, in principle, a linear combination of the two interaction terms $\bar{\Psi}\Psi$ and $\bar{\Psi}\gamma_5\Psi$.

We claim² that the fact that these “gluon spin correlations” only contribute at NNLO in Higgs production (and thus have a small impact), is due to the use of the collinear factorization framework, in which the polarized gluons have to be generated from the unpolarized distribution by gluon radiation. Within the framework of Transverse Momentum Dependent (TMD) factorization, the effect of polarized gluons is already present at tree-level and described by a non-perturbative input function $h_1^{\perp g}$. A significant influence of linearly polarized gluons on the Higgs transverse momentum distribution can therefore not be excluded.

As TMD factorization is the only framework that can properly describe the Higgs transverse momentum distribution at low values of q_T , we will calculate the Higgs boson transverse momentum distribution using this framework. We will do this for both a scalar and pseudoscalar boson and investigate the differences. Important background processes in the study of the Higgs boson are $\gamma\gamma$ and ZZ^* continuum production (from gluon fusion through a quark box). The effects of linearly polarized gluons on these processes will also be investigated. We find that effect on the q_T distribution for scalar, pseudoscalar and background processes have distinct features, which can, at least in principle, be used to differentiate a scalar from a pseudoscalar boson.

5.1 The Higgs transverse momentum distribution

At the LHC, the leading contribution to Higgs production is through gluon fusion, in which two gluons couple via a top quark loop to a Higgs boson. The reason for the dominance of this channel is twofold, the coupling of the Higgs to the top quark is large due its large mass and secondly, the gluon density is large compared to the quark density at high energies, which favors gg over $q\bar{q}$ initiated processes. The next to largest contribution to Higgs production is vector boson fusion [115], which will not be considered here. The leading contribution to Higgs

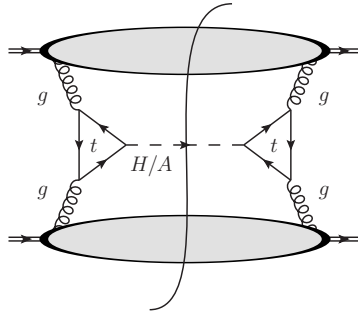


Figure 5.1: The gluon-gluon fusion contribution to Higgs production.

production can thus diagrammatically be written as in Figure 5.1, which, in accordance with Eq. (2.88), can be expressed in a factorized form as

$$\frac{d\sigma}{d\mathcal{R}} = \frac{(2\pi)^4}{S^2} \frac{1}{8} \int d^2\mathbf{p}_T d^2\mathbf{k}_T \delta^2(\mathbf{p}_T + \mathbf{k}_T - \mathbf{q}_T) \Phi_g^{\mu\nu[-,-]}(x_1, \mathbf{p}_T, P_1, S_1) \Phi_g^{\lambda\kappa[-,-]}(x_2, \mathbf{k}_T, P_2, S_2) H_{\mu\lambda} H_{\nu\kappa}^*, \quad (5.1)$$

with the momentum fractions $x_1 = \frac{q \cdot P_2}{P_1 \cdot P_2}$ and $x_2 = \frac{q \cdot P_1}{P_1 \cdot P_2}$ and H the partonic $gg \rightarrow H/A$ scattering amplitude. The partonic amplitude will be calculated for Standard Model (SM)

²This Chapter is based on [130] and [131].

Higgs boson production and for pseudoscalar Higgs production for which the SM is extended with a pseudoscalar boson coupling to fermions via the vertex in Figure 5.2. The gluon TMD

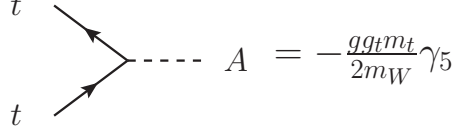


Figure 5.2: The $t\bar{t}A$ interaction vertex.

correlator is parameterized in Eq. (2.99) and reads, for an unpolarized proton,

$$\Phi_g^{\mu\nu}(x, \mathbf{p}_T) = -\frac{1}{2x} \left\{ g_T^{\mu\nu} f_1^g(x, \mathbf{p}_T^2) - \left(\frac{p_T^\mu p_T^\nu}{M^2} + g_T^{\mu\nu} \frac{\mathbf{p}_T^2}{2M^2} \right) h_1^{\perp g}(x, \mathbf{p}_T^2) \right\} + \text{higher twist}, \quad (5.2)$$

with $p_T^2 = -\mathbf{p}_T^2$, $g_T^{\mu\nu} = g^{\mu\nu} - P^\mu n^\nu / P \cdot n - n^\mu P^\nu / P \cdot n$, and M the proton mass. The function $f_1^g(x, \mathbf{p}_T^2)$ represents the unpolarized gluon distribution and $h_1^{\perp g}(x, \mathbf{p}_T^2)$ represents the distribution of linearly polarized gluons.

For Higgs production, we need the 1-particle on-shell phase space element, which reads

$$d\mathcal{R} = \frac{d^3\mathbf{q}}{(2\pi)^3 2E_q} = \frac{dY d^2\mathbf{q}_T}{2(2\pi)^3}, \quad (5.3)$$

where Y is the Higgs boson's forward rapidity, $Y \equiv \frac{1}{2} \log q^+ / q^-$, and \mathbf{q}_T its transverse momentum in the laboratory frame. Using the TMD factorization expression in Eq. (5.1) and the phase space element, we can write the cross section for on-shell Higgs boson production as

$$\frac{d\sigma}{dY d^2\mathbf{q}_T} = \frac{\pi}{8S^2} \int d^2\mathbf{p}_T d^2\mathbf{k}_T \delta^2(\mathbf{p}_T + \mathbf{k}_T - \mathbf{q}_T) \Phi_g^{\mu\nu}(x_1, \mathbf{p}_T) \Phi_g^{\rho\sigma}(x_2, \mathbf{k}_T) \left(\hat{\mathcal{M}}^{\mu\rho} \right) \left(\hat{\mathcal{M}}^{\nu\sigma} \right)^* \Big|_{p=x_1 P_1}^{k=x_2 P_2} + \mathcal{O}\left(\frac{q_T}{m_H}\right), \quad (5.4)$$

where

$$x_{1,2} = \frac{m_H}{\sqrt{S}} e^{\pm Y} \quad (5.5)$$

and the $\mathcal{O}(q_T/m_H)$ corrections are due to the fact that we evaluate the hard scattering matrix element using the collinear approximation for the momenta.

In principle one can now calculate the $gg \rightarrow H$ hard scattering matrix element, which has two Lorentz indices, $\mathcal{M}^{\mu\nu}$, but for future convenience we would like to switch to the helicity amplitude formalism, in which scattering amplitudes are calculated for particles with definite helicity. To write the Higgs production cross section in terms of helicity amplitudes, insert the gluon polarization sum

$$\sum_{\lambda=\pm} \epsilon_\lambda^\mu (\epsilon_\lambda^\nu)^* = -g^{\mu\nu}. \quad (5.6)$$

into Eq. (5.4) to get

$$\frac{d\sigma}{dY d^2\mathbf{q}_T} = \frac{\pi}{8S^2} \int d^2\mathbf{p}_T d^2\mathbf{k}_T \delta^2(\mathbf{p}_T + \mathbf{k}_T - \mathbf{q}_T) \sum_{\lambda_1 \lambda_2 \lambda_3 \lambda_4 = \pm} \Phi_{g_1}^{\lambda_1 \lambda_3}(x_1, \mathbf{p}_T) \Phi_{g_2}^{\lambda_2 \lambda_4}(x_2, \mathbf{k}_T) \mathcal{M}^{\lambda_1 \lambda_2} \left(\mathcal{M}^{\lambda_3 \lambda_4} \right)^* \Big|_{\substack{k=x_2 P_2 \\ p=x_1 P_1}} + \mathcal{O}\left(\frac{q_T}{m_H}\right), \quad (5.7)$$

in terms of the *helicity correlators*

$$\begin{aligned} \Phi_{g_1}^{\lambda_1 \lambda_4} &\equiv \Phi_g^{\mu\nu} \epsilon_\mu^{\lambda_1}(p) \epsilon_\nu^{\lambda_4}(p)^*, \\ \Phi_{g_2}^{\lambda_2 \lambda_3} &\equiv \Phi_g^{\mu\nu} \epsilon_\mu^{\lambda_2}(k) \epsilon_\nu^{\lambda_3}(k)^* \end{aligned} \quad (5.8)$$

and the *helicity amplitude*

$$\mathcal{M}^{\lambda_1 \lambda_2} \equiv \mathcal{M}^{\mu\nu} \epsilon_\mu^{\lambda_1}(p)^* \epsilon_\nu^{\lambda_2}(k)^*. \quad (5.9)$$

The helicity correlators read (see Appendix C)

$$\begin{aligned} \Phi_{g_1}^{\lambda_1 \lambda_2}(x, \mathbf{p}_T) &= \frac{1}{2x} \begin{cases} f_1^g(x, \mathbf{p}_T^2) & ++ \\ f_1^g(x, \mathbf{p}_T^2) & -- \\ w(\mathbf{p}_T) h_1^{\perp g}(x, \mathbf{p}_T^2) & +- \\ w(\mathbf{p}_T)^* h_1^{\perp g}(x, \mathbf{p}_T^2) & -+ \end{cases} \\ \Phi_{g_2}^{\lambda_1 \lambda_2} &= \left(\Phi_{g_1}^{\lambda_1 \lambda_2} \right)^* \end{aligned} \quad (5.10)$$

in which we have defined $w(\mathbf{p}_T)$ as

$$w(\mathbf{p}_T) \equiv -\frac{p_T^2}{2M^2} e^{i2(\phi_{\mathbf{p}_T} - \phi_{\mathbf{q}_T} - \phi)}. \quad (5.11)$$

The appearance of the angles $\phi_{\mathbf{q}_T}$ and ϕ is due to our choice for the polarization vectors, which is very convenient for calculations of the matrix element that include the decay of the Higgs boson, but for on-shell Higgs boson production the choice of polarization vectors is arbitrary. For uniformity we choose to use the same vectors here. The partonic helicity amplitudes read (see Appendix E for details on the calculation of the partonic amplitudes \mathcal{M} and expressions for $\mathcal{A}_{gg \rightarrow H/A}$.)

$$\mathcal{M}_{gg \rightarrow H}^{\lambda_1 \lambda_2} = \mathcal{A}_{gg \rightarrow H} \begin{cases} -1 & ++ \\ & -- \\ 0 & +- \\ & -+ \end{cases} \quad (5.12)$$

for a scalar boson and

$$\mathcal{M}_{gg \rightarrow A}^{\lambda_1 \lambda_2} = \mathcal{A}_{gg \rightarrow A} \begin{cases} -1 & ++ \\ 1 & -- \\ 0 & +- \\ & -+ \end{cases}. \quad (5.13)$$

for a pseudoscalar boson. Using the fact that the $+-$ amplitudes are zero, we can simplify the cross section to (from here on we will drop the $\mathcal{O}(q_T/m_H)$ for clarity)

$$\begin{aligned} \frac{d\sigma}{dY d^2\mathbf{q}_T} &= \frac{\pi}{8S^2} \int d^2\mathbf{p}_T d^2\mathbf{k}_T \delta^2(\mathbf{p}_T + \mathbf{k}_T - \mathbf{q}_T) \left[\Phi_{g_1}^{++} \Phi_{g_2}^{++} \mathcal{M}^{++} (\mathcal{M}^{++})^* \right. \\ &\quad \left. + \Phi_{g_1}^{--} \Phi_{g_2}^{--} \mathcal{M}^{--} (\mathcal{M}^{--})^* + \Phi_{g_1}^{+-} \Phi_{g_2}^{+-} \mathcal{M}^{++} (\mathcal{M}^{--})^* + \Phi_{g_1}^{-+} \Phi_{g_2}^{-+} \mathcal{M}^{--} (\mathcal{M}^{++})^* \right], \end{aligned} \quad (5.14)$$

which, by using the explicit expressions for the correlator and amplitudes, can be further reduced to

$$\frac{d\sigma}{dY d^2\mathbf{q}_T} = \frac{\pi \mathcal{A}_{gg \rightarrow H/A}}{16m_H^2 S} \left(\mathcal{C}[f_1^g f_1^g] \pm \mathcal{C}[w_H h_1^{\perp g} h_1^{\perp g}] \right), \quad (5.15)$$

where \pm stands for scalar/pseudoscalar. The convolution \mathcal{C} is defined as

$$\mathcal{C}[w f f] \equiv \int d^2\mathbf{p}_T \int d^2\mathbf{k}_T \delta^2(\mathbf{p}_T + \mathbf{k}_T - \mathbf{q}_T) w(\mathbf{p}_T, \mathbf{k}_T) f(x_a, \mathbf{p}_T^2) f(x_b, \mathbf{k}_T^2) \quad (5.16)$$

and the weight for the $h_1^{\perp g} h_1^{\perp g}$ term, w_H , is given by

$$w_H = \frac{2(\mathbf{k}_T \cdot \mathbf{p}_T)^2 - \mathbf{k}_T^2 \mathbf{p}_T^2}{4M^4}. \quad (5.17)$$

The linearly polarized gluon term, $\mathcal{C}[w_H h_1^{\perp g} h_1^{\perp g}]$, has the model independent property that both the \mathbf{q}_T integral and the second moment in \mathbf{q}_T vanish,

$$\begin{aligned} \int d^2\mathbf{q}_T \mathcal{C}[w_H h_1^{\perp g} h_1^{\perp g}] &= 0, \\ \int d^2\mathbf{q}_T \mathbf{q}_T^2 \mathcal{C}[w_H h_1^{\perp g} h_1^{\perp g}] &= 0, \end{aligned} \quad (5.18)$$

irrespective of the functional form of $h_1^{\perp g}$ (see Appendix D). This implies that the total cross section is not influenced by the effect of linearly polarized gluons. The \mathbf{q}_T integral of the $\mathcal{C}[f_1^g f_1^g]$ term can be expressed in terms of collinear distribution functions, i.e.,

$$\int d^2\mathbf{q}_T \mathcal{C}[f_1^g f_1^g] = f_1^g(x_1) f_1^g(x_2). \quad (5.19)$$

Furthermore, we note that both $\mathcal{C}[f_1^g f_1^g]$ and $\mathcal{C}[w_H h_1^{\perp g} h_1^{\perp g}]$ do not depend on the direction of \mathbf{q}_T and we can thus integrate out this degree of freedom to get

$$\frac{d\sigma}{dY dq_T^2} = \pi \frac{d\sigma}{dY d^2\mathbf{q}_T}. \quad (5.20)$$

Normalizing that cross section to the \mathbf{q}_T -integrated one, which we can write, using Eq. (5.19), as

$$\frac{d\sigma}{dY} = \frac{\pi \mathcal{A}_{gg \rightarrow H/A}}{16m_H^2 S} f_1^g(x_1) f_1^g(x_2), \quad (5.21)$$

we get

$$\frac{1}{d\sigma/dY} \frac{d\sigma}{dY dq_T^2} = [1 \pm R(q_T)] \frac{\pi \mathcal{C}[f_1^g f_1^g]}{f_1^g(x_1) f_1^g(x_2)}, \quad (5.22)$$

where the $R(q_T)$ function is defined as

$$R(q_T) \equiv \frac{\mathcal{C}[w_H h_1^{\perp g} h_1^{\perp g}]}{\mathcal{C}[f_1^g f_1^g]}. \quad (5.23)$$

The functional form of Eq. (5.22) tells us that the transverse momentum distribution of a scalar and pseudoscalar boson resembles what one would expect on the basis of unpolarized gluons plus or minus a correction due to the linear polarization of the gluons, with a size given by $R(q_T)$. We can already give some generic properties of $R(q_T)$, without any specific assumption on the distribution of linearly polarized gluons, $h_1^{\perp g}$: given the properties in Eq. (5.18) we know that $R(q_T)$ should have at least two nodes and in the limit $q_T \rightarrow 0$, the function is positive. Given these two properties, we know that the effect of linearly polarized gluons will be such that for a scalar boson, as a function of q_T , it enhances, suppresses and enhances again the production, whereas for pseudoscalar boson this is reversed.

5.1.1 Parameterization of the linearly polarized gluon distribution

As a first step, to study the effects of linearly polarized gluons, we follow a standard approach for TMDs in the literature and assume a simple Gaussian dependence of the gluon TMDs on transverse momentum:

$$f_1^g(x, \mathbf{p}_T^2) = \frac{f_1^g(x)}{\pi \langle p_T^2 \rangle} \exp\left(-\frac{\mathbf{p}_T^2}{\langle p_T^2 \rangle}\right), \quad (5.24)$$

where $f_1^g(x)$ is the collinear gluon distribution, $f_1^g(x) = \int d^2\mathbf{p}_T f_1^g(x, \mathbf{p}_T)$. The width, $\langle p_T^2 \rangle$, depends on the energy scale, Q , and should be experimentally determined. We will estimate $\langle p_T^2 \rangle = 7 \text{ GeV}^2$, at $Q = m_H = 125 \text{ GeV}$, in rough agreement with the Gaussian fit to $f_1^u(x, \mathbf{p}_T^2)$ evolved to $Q = M_Z$ of Ref. [22].

No experimental data on $h_1^{\perp g}$ is available, but a positivity bound has been derived in Ref. [24]:

$$\frac{\mathbf{p}_T^2}{2M^2} |h_1^{\perp g}(x, \mathbf{p}_T^2)| \leq f_1^g(x, \mathbf{p}_T^2). \quad (5.25)$$

Models may also shed light on the size of $h_1^{\perp g}$. In the simple perturbative quark target model of gluon TMDs of Ref. [25] the function $h_1^{\perp g}$ is found to possess the same characteristic $1/x$ increase as the distribution of unpolarized gluons f_1^g , which suggests that linearly polarized gluons may be as relevant at small x as unpolarized ones. Other recent model calculations [132, 133] show saturation of the positivity bound of the relevant (Weizsäcker-Williams) $h_1^{\perp g}$ distribution in heavy nuclei for large transverse momentum. Given these model calculations we expect the linearly polarized gluon distribution to be substantial. The functional form is however hard to tell, so, as a first Ansatz, we will use a Gaussian distribution for $h_1^{\perp g}$, with a width of $r \langle p_T^2 \rangle$ and a normalization such that it satisfies the upper bound for all \mathbf{p}_T , i.e.,

$$h_1^{\perp g}(x, \mathbf{p}_T^2) = \frac{M^2 f_1^g(x)}{\pi \langle p_T^2 \rangle^2} \frac{2e(1-r)}{r} \exp\left(-\frac{\mathbf{p}_T^2}{r \langle p_T^2 \rangle}\right). \quad (5.26)$$

We will keep r a free parameter as much as possible and, only when numerical values are necessary, use either $r = 1/3$ or $r = 2/3$. In Figure 5.3, $f_1^g(x, p_T)$ and $\frac{p_T^2}{2M^2}h_1^{\perp g}(x, p_T)$ are plotted as a function of p_T .

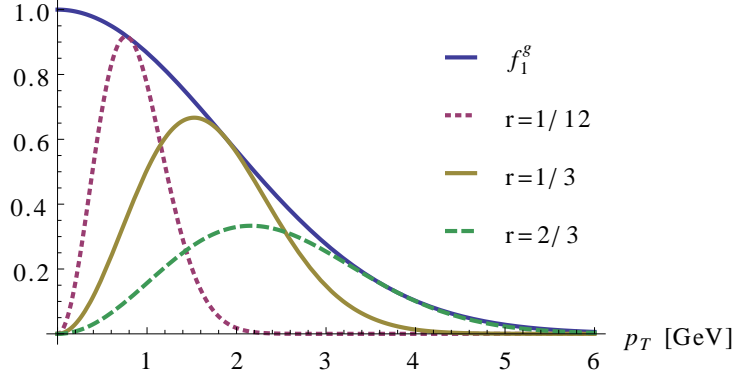


Figure 5.3: The p_T dependence of $f_1^g(x, p_T)$ and $\frac{p_T^2}{2M^2}h_1^{\perp g}(x, p_T)$ for the choice of $r = 1/12$, $r = 1/3$ and $r = 2/3$. All distributions are normalized with respect to $f_1^g(x, 0)$.

5.1.2 Numerical predictions

To give more insight into the effect of linear gluon polarization we will now plug in our Ansatz for the TMDs f_1^g and $h_1^{\perp g}$. Using the Gaussian Ansatz for f_1^g , we can write

$$\mathcal{C}[f_1^g f_1^g] = \frac{f_1^g(x_1)f_1^g(x_2)}{2\pi\langle p_T^2 \rangle} e^{-\frac{q_T^2}{2\langle p_T^2 \rangle}} \quad (5.27)$$

and the transverse momentum distribution in Eq. (5.22) thus as

$$\frac{1}{d\sigma/dY} \frac{d\sigma}{dY dq_T^2} = [1 \pm R(q_T)] \frac{1}{2\langle p_T^2 \rangle} e^{-q_T^2/2\langle p_T^2 \rangle}. \quad (5.28)$$

The $R(q_T)$ function can, with our model for the linearly polarized gluon distribution in Eq. (5.26), be evaluated to

$$R(q_T) = \frac{r}{2}(1-r)^2 \left(1 - \frac{q_T^2}{r\langle p_T^2 \rangle} + \frac{q_T^4}{8r^2\langle p_T^2 \rangle^2} \right) \exp \left[2 - \frac{1-r}{r} \frac{q_T^2}{2\langle p_T^2 \rangle} \right], \quad (5.29)$$

which is plotted in Figure 5.4 together with the *maximal achievable* $R(q_T)$, which is obtained for $h_1^{\perp g}$ saturating the bound for all x and p_T , i.e., $h_1^{\perp g}(x, \mathbf{p}_T^2) = \frac{2M^2}{p_T^2} f_1^g(x, \mathbf{p}_T^2)$. The resulting transverse momentum distribution is plotted in Figure 5.5 for $r = 2/3$ and $r = 1/3$ and in Figure 5.6 for the maximal gluon polarization.

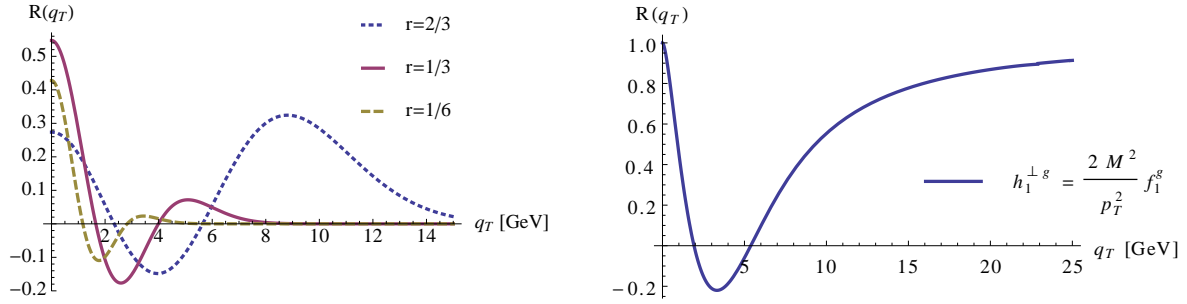


Figure 5.4: The function $R(q_T)$ in Eq. (5.29) plotted as function of q_T for different choices of r (left) and the *maximal achievable* $R(q_T)$, which is obtained for $h_1^{\perp g}(x, \mathbf{p}_T^2) = \frac{2M^2}{p_T^2} f_1^g(x, \mathbf{p}_T^2)$ (right).

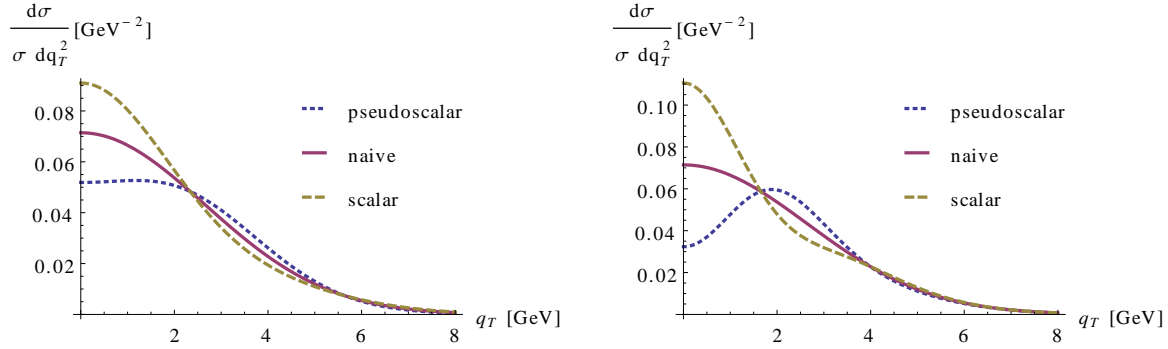


Figure 5.5: Transverse momentum distribution of the Higgs, using the parameterization of $h_1^{\perp g}$ in Eq. (5.26) with $r = 2/3$ (left) and $r = 1/3$ (right). The naive curve is the prediction for both scalar and pseudoscalar in the absence of linear gluon polarization, i.e., $h_1^{\perp g} = 0$.

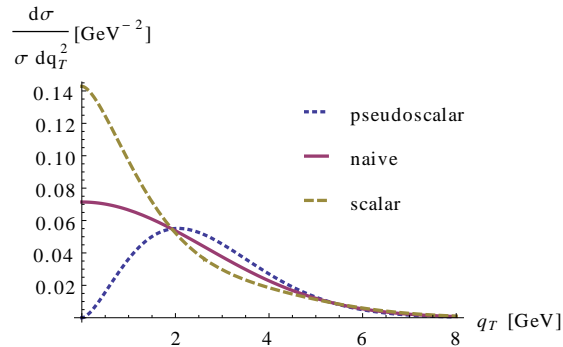


Figure 5.6: Transverse momentum distribution of the Higgs, assuming maximal gluon polarization, i.e., $h_1^{\perp g}(x, \mathbf{p}_T^2) = \frac{2M^2}{p_T^2} f_1^g(x, \mathbf{p}_T^2)$. The naive curve is the prediction for both scalar and pseudoscalar in the absence of linear gluon polarization, i.e., $h_1^{\perp g} = 0$.

5.1.3 Discussion

Looking at Figure 5.5 and 5.6 one sees a clear difference between the transverse momentum distribution of a scalar and pseudoscalar boson. The effect is as expected, showing an enhancement at low q_T , followed by suppression, followed by enhancement again for a scalar and reversed for a pseudoscalar. However, as long as $h_1^{\perp g}$ is not measured, the absolute size of the effect will be unknown, but, as said before, it will always show the same qualitative behavior. Higher order perturbative corrections will also modify the exact form and width of our tree-level q_T distribution, as well as the size of the modulation. The effects of this remain to be investigated. Although corrections to this leading order result have still to be taken into account, we think this is an interesting proof of concept, that the transverse momentum distribution can, in principle, be used to determine the parity of a scalar boson.

5.2 The diphoton transverse momentum distribution

In practice, one can not directly study the transverse momentum distribution of the Higgs boson, but only that of the decay products. There will inevitably be processes other than just the creation and annihilation of a Higgs boson that contribute to the same final state of particles. For example, in the channel most important to the discovery of the new 126 GeV boson, the $H \rightarrow \gamma\gamma$ channel, a background process that contributes to the same final state is $gg \rightarrow \text{quark box} \rightarrow \gamma\gamma$. In order to distinguish a scalar from a pseudoscalar using the transverse momentum distribution, one also needs a prediction for the background transverse momentum distribution, as it might have a shape similar to that of a scalar or pseudoscalar boson and be mistaken for it. Besides differentiating scalar from pseudoscalar, the transverse momentum distribution might also be used to separate signal from background, provided that the signal and background distributions differ enough. For these reasons, we will calculate the diphoton transverse momentum distribution and compare the contributions from the different partonic sub channels.

We will look at diphoton production from pp collisions initiated by gluon-gluon fusion, which can be represented diagrammatically as in Figure 5.7. In accordance with Eq. (2.88), this can

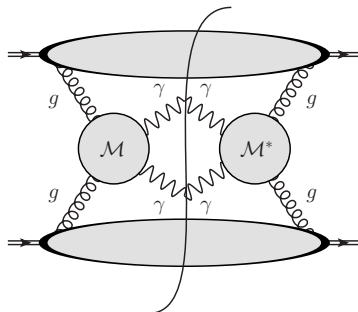


Figure 5.7: General diagram for diphoton production through gluon fusion.

be expressed in a factorized form in terms of helicity amplitudes and correlators as

$$\frac{d\sigma}{d^4q d\Omega} = \frac{1}{256\pi^2 S^2} \int d^2\mathbf{p}_T d^2\mathbf{k}_T \delta^2(\mathbf{p}_T + \mathbf{k}_T - \mathbf{q}_T) \sum_{\lambda_1 \lambda_2 \lambda_3 \lambda_4 \kappa_1 \kappa_2 = \pm} \Phi_{g_1}^{\lambda_1 \lambda_3}(x_1, \mathbf{p}_T) \Phi_{g_2}^{\lambda_2 \lambda_4}(x_2, \mathbf{k}_T) \mathcal{M}^{\lambda_1 \lambda_2 \kappa_1 \kappa_2} \left(\mathcal{M}^{\lambda_3 \lambda_4 \kappa_1 \kappa_2} \right)^*, \quad (5.30)$$

where we have used the phase space element

$$d\mathcal{R} \equiv \frac{d^3\vec{q}_1}{(2\pi)^3 2q_1^0} \frac{d^3\vec{q}_2}{(2\pi)^3 2q_2^0} = \frac{d^4q}{(2\pi)^4} \frac{d\Omega}{32\pi^2} \quad (5.31)$$

and the gluon/photon polarization sum

$$\sum_{\lambda=\pm} \epsilon_\lambda^\mu (\epsilon_\lambda^\nu)^* = -g^{\mu\nu} \quad (5.32)$$

to write the cross section terms of the helicity amplitude, which is defined as

$$\mathcal{M}^{\lambda_1 \lambda_2 \kappa_1 \kappa_2} \equiv \mathcal{M}^{\mu\nu\rho\sigma} \left(\epsilon_\mu^{\lambda_1}(p) \right)^* \left(\epsilon_\nu^{\lambda_2}(k) \right)^* \epsilon_\rho^{\kappa_1}(q_1) \epsilon_\sigma^{\kappa_2}(q_2). \quad (5.33)$$

Inserting the expression for the helicity correlator in Eq. (5.10) (which is correct up to leading order in q_T/Q), we get

$$\begin{aligned} \frac{d\sigma}{d^4q d\Omega} = \frac{1}{1024\pi^2 Q^2 S} & \left\{ F_1 \mathcal{C} [f_1^g f_1^g] + F_2 \mathcal{C} \left[\text{Re}[w_p w_k^*] h_1^{\perp g} h_1^{\perp g} \right] + F_2' \mathcal{C} \left[\text{Im}[w_p w_k^*] h_1^{\perp g} h_1^{\perp g} \right] \right. \\ & + F_3^\pm \mathcal{C} \left[\text{Re}[w_p] h_1^{\perp g} f_1^g \pm \text{Re}[w_k] f_1^g h_1^{\perp g} \right] + F_3'^\pm \mathcal{C} \left[\text{Im}[w_p] h_1^{\perp g} f_1^g \pm \text{Im}[w_k] f_1^g h_1^{\perp g} \right] \\ & \left. + F_4 \mathcal{C} \left[\text{Re}[w_p w_k] h_1^{\perp g} h_1^{\perp g} \right] + F_4' \mathcal{C} \left[\text{Im}[w_p w_k] h_1^{\perp g} h_1^{\perp g} \right] \right\} + \mathcal{O}(q_T/Q), \quad (5.34) \end{aligned}$$

in which the F_i are defined in terms of the partonic helicity amplitudes in Appendix E. The F_i functions only depend on the partonic Mandelstam variables \hat{s} , \hat{t} and \hat{u} , which can be expressed in terms of the Collins-Soper angle θ and Q , see Appendix B (there is also a minor \mathbf{p}_T and \mathbf{k}_T dependence, but that is irrelevant as we are working at leading order in q_T/Q).

The partonic processes contributing to $gg \rightarrow \gamma\gamma$ that we include are ‘direct’ $gg \rightarrow \gamma\gamma$ scattering via a quark box and Higgs (H) and pseudoscalar boson (A) production. The Higgs production and quark box contributions are calculated within the Standard Model and for the pseudoscalar boson contribution, the SM is again extended with a pseudoscalar, coupling via the vertex in Figure 5.2. We can write the partonic amplitude diagrammatically as in Figure 5.8, in which the $H \rightarrow \gamma\gamma$ decay diagrams that occur through W and Goldstone boson loops are not shown, but are included in the calculation. The pseudoscalar boson A is assumed *not* to couple to W or Goldstone bosons at tree level and so the top quark triangle really is the only contribution we take into account. In Appendix E, more details on the calculation of the partonic amplitudes can be found.

From the general property of the helicity amplitudes

$$\mathcal{M}^{\lambda_1 \lambda_2 \lambda_3 \lambda_4} = \mathcal{M}^{-\lambda_1 - \lambda_2 - \lambda_3 - \lambda_4}, \quad (5.35)$$

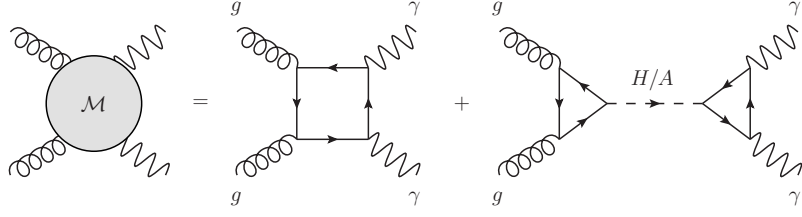


Figure 5.8: Partonic sub-channels that contribute to $gg \rightarrow \gamma\gamma$ scattering. In the $gg \rightarrow H \rightarrow \gamma\gamma$ channel also W and Goldstone boson loops contribute in the decay, but are not shown.

which is a consequence of parity conservation, it follows that the primed F_i 's in Eq. (5.34) are zero,

$$F_2' = F_3'^{\pm} = F_4' = 0. \quad (5.36)$$

Using this constraint, the general structure of the cross section in Eq. (5.34), simplifies to

$$\begin{aligned} \frac{d\sigma}{d^4q d\Omega} = & \frac{1}{1024\pi^2 Q^2 S} \left\{ F_1 \mathcal{C} [f_1^g f_1^g] + F_2 \mathcal{C} [w_H h_1^{\perp g} h_1^{\perp g}] \right. \\ & \left. + F_3^{\pm} \mathcal{C} [w_3(\mathbf{p}_T) h_1^{\perp g} f_1^g \pm w_3(\mathbf{k}_T) f_1^g h_1^{\perp g}] \cos(2\phi) + F_4 \mathcal{C} [w_4 h_1^{\perp g} h_1^{\perp g}] \cos(4\phi) \right\} + \mathcal{O}(q_T/Q), \end{aligned} \quad (5.37)$$

with the weights defined as (see Appendix D)

$$\begin{aligned} w_H & \equiv \frac{2(\mathbf{k}_T \cdot \mathbf{p}_T)^2 - \mathbf{k}_T^2 \mathbf{p}_T^2}{4M^4}, \\ w_3(\mathbf{p}_T) & \equiv \frac{2(\mathbf{q}_T \cdot \mathbf{p}_T)^2 - \mathbf{q}_T^2 \mathbf{p}_T^2}{2\mathbf{q}_T^2 M^2}, \\ w_4 & \equiv \frac{[\mathbf{k}_T^2 \mathbf{q}_T^2 - 2(\mathbf{q}_T \cdot \mathbf{k}_T)^2] [\mathbf{p}_T^2 \mathbf{q}_T^2 - 2(\mathbf{q}_T \cdot \mathbf{p}_T)^2]}{4M^4 \mathbf{q}_T^4}. \end{aligned} \quad (5.38)$$

The cross section does not explicitly depend on $\phi_{\mathbf{q}_T}$ (it does implicitly depend on the direction of \mathbf{q}_T through the Collins-Soper angle ϕ) and so we will integrate it out by first rewriting the phase space element using

$$d^4q d\Omega = \frac{1}{2} Q dQ dY dq_T^2 d\phi_{\mathbf{q}_T}, \quad (5.39)$$

to get

$$\frac{d\sigma}{dQ dY dq_T^2 d\Omega} = \frac{Q}{2} \int d\phi_{\mathbf{q}_T} \frac{d\sigma}{d^4q d\Omega} = Q\pi \frac{d\sigma}{d^4q d\Omega}. \quad (5.40)$$

We define a q_T and ϕ dependent distribution by normalizing the cross section to the \mathbf{q}_T and ϕ integrated one, which reads

$$\frac{d\sigma}{dQ dY d\cos\theta} = \frac{F_1 f_1^g(x_1) f_1^g(x_2)}{512\pi QS}, \quad (5.41)$$

to get (from here on we will drop the $\mathcal{O}(q_T/Q)$ for clarity)

$$\frac{1}{\frac{d\sigma}{dQdYd\cos\theta}} \frac{d\sigma}{dQdYdq_T^2d\Omega} = \left[1 + \frac{F_2}{F_1} R(q_T) + \frac{F_3^\pm}{F_1} R_3^\pm(q_T) \cos 2\phi + \frac{F_4}{F_1} R_4(q_T) \cos 4\phi \right] \times \frac{\mathcal{C}[f_1^g f_1^g]}{2f_1^g(x_1)f_1^g(x_2)}, \quad (5.42)$$

with $R(q_T)$ defined as before in Eq. (5.23) and the two additional R functions as

$$R_3^\pm(q_T) \equiv \frac{\mathcal{C}[w_3(\mathbf{p}_T)h_1^{\perp g}f_1^g \pm w_3(\mathbf{k}_T)f_1^g h_1^{\perp g}]}{\mathcal{C}[f_1^g f_1^g]},$$

$$R_4(q_T) \equiv \frac{\mathcal{C}[w_4 h_1^{\perp g} h_1^{\perp g}]}{\mathcal{C}[f_1^g f_1^g]}. \quad (5.43)$$

We will also define a q_T distribution by taking the ratio of the $\phi_{\mathbf{q}_T}$ and ϕ integrated cross section to the cross section integrated over \mathbf{q}_T and ϕ , to get

$$\frac{1}{\frac{d\sigma}{dQdYd\cos\theta}} \frac{d\sigma}{dQdYd\cos\theta dq_T^2} = \left[1 + \frac{F_2}{F_1} R(q_T) \right] \frac{\pi \mathcal{C}[f_1^g f_1^g]}{f_1^g(x_1)f_1^g(x_2)}, \quad (5.44)$$

which has the same form as the on-shell Higgs q_T distribution in Eq. (5.22), but with the size of the linearly polarized gluon effect modified by a factor F_2/F_1 .

5.2.1 Numerical predictions

Using a Gaussian Ansatz for $f_1^g(x, \mathbf{p}_T^2)$, the diphoton q_T distribution can be written as

$$\frac{1}{\frac{d\sigma}{dQdYd\cos\theta}} \frac{d\sigma}{dQdYd\cos\theta dq_T^2} = \left[1 + \frac{F_2}{F_1} R(q_T) \right] \frac{1}{2\langle p_T^2 \rangle} e^{-q_T^2/2\langle p_T^2 \rangle}. \quad (5.45)$$

The ratio F_2/F_1 is plotted in the left graph of Fig. 5.9. At the Higgs mass we reproduce Eq. (5.28), i.e. $F_2/F_1 \rightarrow \pm 1$, for a scalar/pseudoscalar, but away from the pole, the background quickly dominates. To mimic a finite detector resolution in the determination of Q , we also plot the ratio F_2/F_1 in which both numerator and denominator are separately weighted with a Gaussian distribution. From the graph we see that the continuum background reduces the effect to approximately 30% or 20% of the maximal size with a 0.5 or 1 GeV resolution, respectively. The signal and background transverse momentum distributions in Eq. (5.45) are plotted in Figure 5.10.

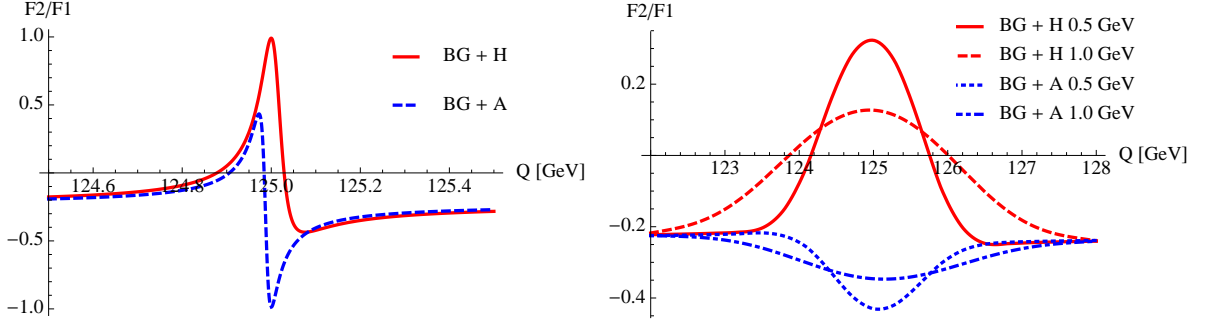


Figure 5.9: The ratio F_2/F_1 in Eq. (5.45) plotted as function of Q at $\theta = \pi/2$ for a 125 GeV scalar (H) or pseudoscalar (A) boson (left) and the same curves including a detector resolution of 0.5 and 1 GeV (right).

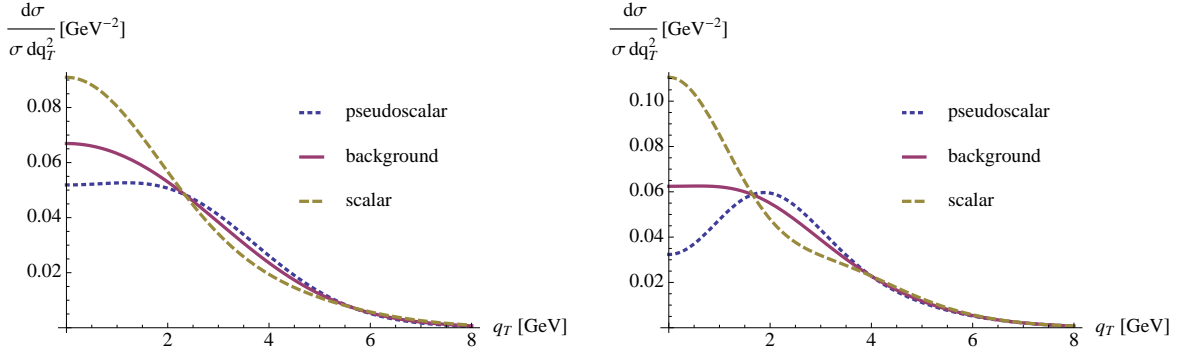


Figure 5.10: The diphoton transverse momentum distribution due to scalar and pseudoscalar boson production and $gg \rightarrow$ quark box $\rightarrow \gamma\gamma$ continuum production. For the linearly polarized gluon distribution, the parameterization in Eq. (5.26) is used with $r = 2/3$ (left) and $r = 1/3$ (right).

Using the Gaussian Ansatz for f_1^g , the q_T and ϕ distribution can be written as

$$\frac{1}{\frac{d\sigma}{dQdYd\cos\theta}} \frac{d\sigma}{dQdYdq_T^2d\Omega} = \left[1 + \frac{F_2}{F_1} R(q_T) + \frac{F_3^\pm}{F_1} R_3^\pm(q_T) \cos 2\phi + \frac{F_4}{F_1} R_4(q_T) \cos 4\phi \right] \times \frac{e^{-q_T^2/2\langle p_T^2 \rangle}}{4\pi \langle p_T^2 \rangle}. \quad (5.46)$$

The additional R functions, as defined in Eq. (5.43), are evaluated, using the parameterization of $h_1^{\perp g}$ in Eq. (5.26), to

$$\begin{aligned} R_3^-(q_T) &= 0, \\ R_3^+(q_T) &= 4r^2 \frac{1-r}{(1+r)^3} \frac{q_T^2}{\langle p_T^2 \rangle} \exp \left[1 - \frac{1-r}{1+r} \frac{q_T^2}{2\langle p_T^2 \rangle} \right], \\ R_4(q_T) &= \frac{(1-r)^2 (2r\langle p_T^2 \rangle - q_T^2)^2}{16r \langle p_T^2 \rangle^2} \exp \left[2 - \frac{1-r}{r} \frac{q_T^2}{2\langle p_T^2 \rangle} \right]. \end{aligned} \quad (5.47)$$

The functions $R_3^+(q_T)$ and $R_4(q_T)$ are plotted in Figure 5.11 as a function of q_T for $r = 2/3$ and $r = 1/3$. The ratios F_3/F_1 and F_4/F_1 for background + scalar boson production and background + pseudoscalar boson production are plotted in Figure 5.12 and 5.13. For scalar and pseudoscalar boson only production one has $F_3 = F_4 = 0$ resulting in a ϕ -independent distribution, as it should be for a spin-0 particle. For just the background process $gg \rightarrow \text{quark box} \rightarrow \gamma\gamma$ the F ratios, which are independent of Q , are plotted as function of θ in Figure 5.14. The resulting q_T and ϕ distribution for the background process is plotted in Figure 5.15 for $\theta = \pi/2$.

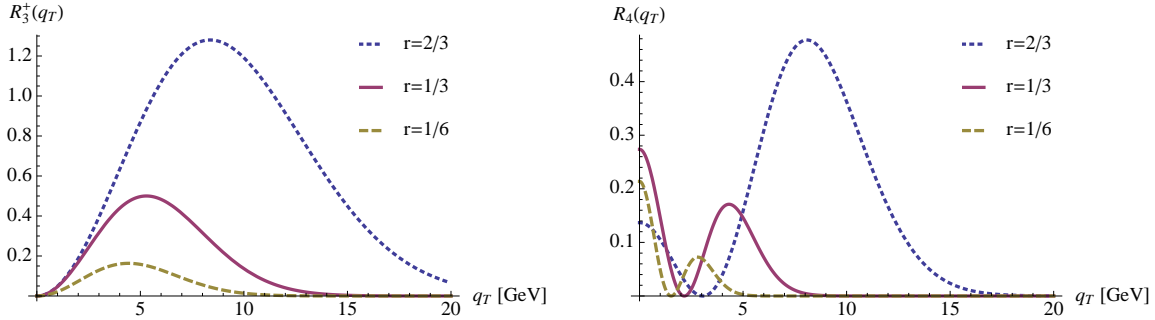


Figure 5.11: The functions $R_3^+(q_T)$ (left) and $R_4(q_T)$ (right) in Eq. (5.47) plotted as function of q_T for different choices of r .

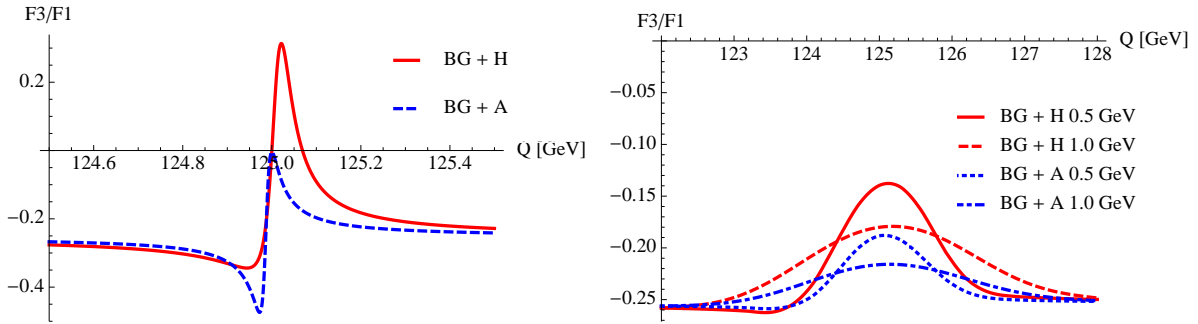


Figure 5.12: The ratio F_3^+/F_1 in Eq. (5.46) plotted as function of Q at $\theta = \pi/2$ for a 125 GeV scalar (H) or pseudoscalar (A) boson (left) and the same curves including a detector resolution of 0.5 and 1 GeV (right).

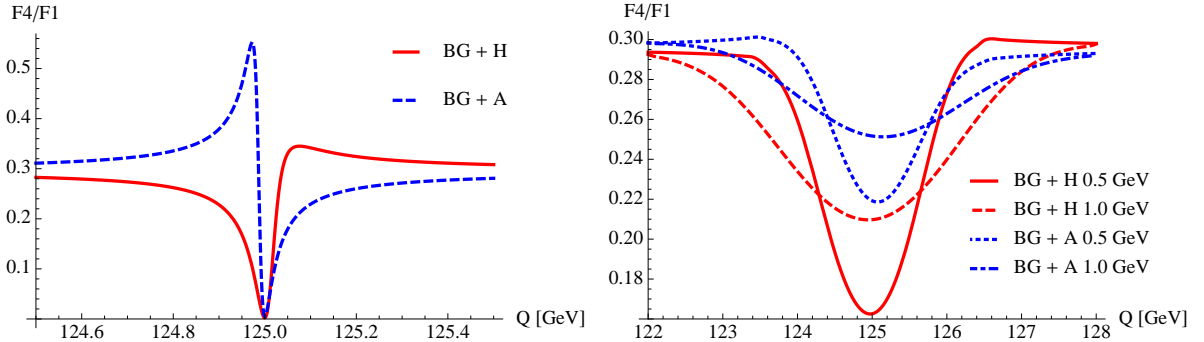


Figure 5.13: The ratio F_4/F_1 in Eq. (5.46) plotted as function of Q at $\theta = \pi/2$ for a 125 GeV scalar (H) or pseudoscalar (A) boson (left) and the same curves including a detector resolution of 0.5 and 1 GeV (right).

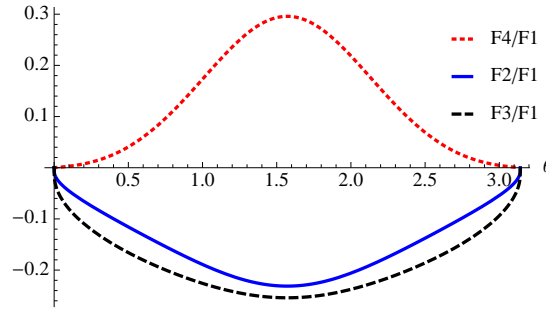


Figure 5.14: The F ratios for the background process $gg \rightarrow \text{quark box} \rightarrow \gamma\gamma$, which are independent of Q , as a function of θ .

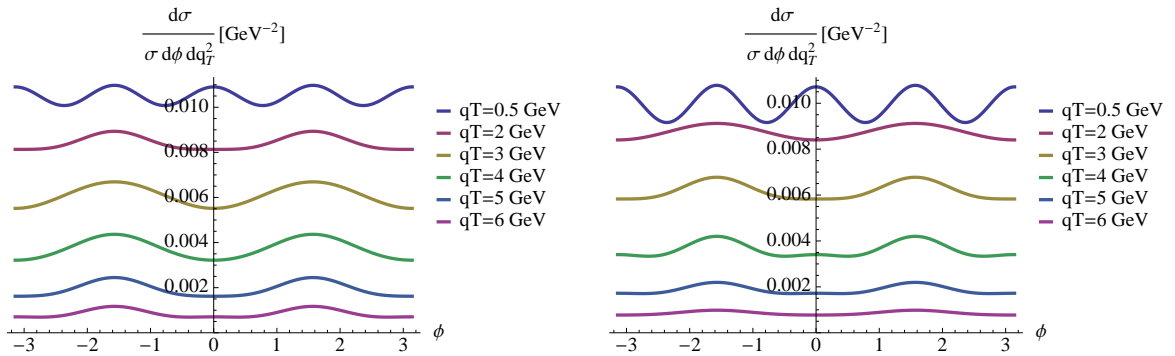


Figure 5.15: The distribution of photon pairs from the background process $gg \rightarrow \text{quark box} \rightarrow \gamma\gamma$ as a function of ϕ for different values of q_T at $\theta = \pi/2$ for $r = 2/3$ (left) and $r = 1/3$ (right). The distribution for the process $gg \rightarrow H(A) \rightarrow \gamma\gamma$ is independent of ϕ .

5.2.2 Discussion

Looking at Figure 5.9, we see that if the diphoton pair's invariant mass is close to the Higgs mass, the characteristic modification of the transverse momentum distribution is the same as for the Higgs itself. However, as little as 0.1 GeV away from the Higgs mass, the modification of the transverse momentum distribution is severely altered by the background process. With a detector resolution of $\gtrsim 0.5$ GeV, as expected for ATLAS and CMS, one may thus expect not to see anything. However, emulating an experimental resolution of 1 GeV in the determination of Q shows that the effect is reduced to 20% of its original size. That implies that the difference between the Higgs and background transverse momentum distribution as shown in Figure 5.10, will reduce to 20% of its size. The difference between the scalar/pseudoscalar boson and background q_T distribution will be smaller, but the characteristic feature that scalar boson production is enhanced at low q_T , suppressed at moderate q_T and enhanced again at high q_T as compared to the background (and reversed for a pseudoscalar), will remain. Although it may not be easy to get enough statistics to claim that the Higgs transverse momentum distribution is enhanced-suppressed-enhanced as compared to the background (or reversed), this method is conceptually straightforward.

Looking at the ϕ distribution of the continuum $\gamma\gamma$ production in Figure 5.15 we see that there is a clear modulation due to linearly polarized gluons as already noted in [134], which was aimed at the RHIC center of mass energy $\sqrt{s} = 500$ GeV. Although the size of the effect is not too large ($\sim 10\%$), using our model for $h_1^{\perp g}$, the relatively large numbers in which $\gamma\gamma$ pairs from continuum production are produced might make measuring this modulation very well feasible. Observing the ϕ modulation in continuum $\gamma\gamma$ production could serve as a proof-of-concept that the effect of linearly polarized gluons exists and to establish the fact that $h_1^{\perp g}$ is nonzero.

5.3 The $pp \rightarrow ZZ^*X \rightarrow 4\ell X$ transverse momentum distribution

The next to most important decay channel in the search for a light Higgs boson is $H \rightarrow ZZ^* \rightarrow 4\ell$, in which the Higgs boson decays to one on-shell Z boson and one off-shell Z boson or virtual photon of which both decay to a lepton pair.

In most of the extensions of the SM that predict a pseudoscalar boson, it does not couple to vector bosons at tree level because of P and CP conservation. In that case, one could think that one could easily distinguish scalar from pseudoscalar: the size of the *total* cross section should be enough, as it should be much smaller for a pseudoscalar than for a scalar. For example, the fact both ATLAS [108] and CMS [109] *do* observe the $H \rightarrow ZZ^*$ decay, would imply that it is a scalar. It is, however, not *that* easy as there are two ways to enhance the pseudoscalar coupling to Z (and/or W) bosons: one could either drop the demand of P and CP symmetry and introduce a tree-level coupling to the vector bosons or introduce a higher dimensional (non-renormalizable) operator (as for example done in [135]) that couples the pseudoscalar to the vector bosons in a P and CP invariant way.

For now, we will calculate the $pp \rightarrow ZZ^*X \rightarrow 4\ell X$ transverse momentum distribution assuming a SM Higgs and our earlier discussed model for a pseudoscalar boson that couples only to quarks, which will have a strongly suppressed cross section in this channel as compared to the scalar Higgs boson. We leave it for future work to calculate the ZZ^* transverse momentum distribution for a pseudoscalar boson that does have a P and CP violating tree level coupling to the Z boson or a P and CP even non-renormalizable coupling. Also the WW^* transverse

momentum distribution will be treated in future work.

The gluon-gluon fusion contribution to $pp \rightarrow ZZ^*X \rightarrow 4\ell X$ can be represented diagrammatically as in Figure 5.16 and, in accordance with Eq. (2.88), be expressed in a factorized form

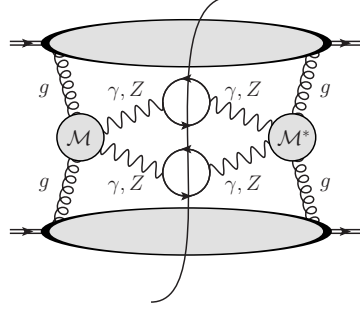


Figure 5.16: General diagram for $pp \rightarrow ZZ^*X \rightarrow 4\ell X$ production through gluon fusion.

as

$$\frac{d\sigma}{d\mathcal{R}} = \frac{(2\pi)^4}{8S^2} \int d^2\mathbf{p}_T d^2\mathbf{k}_T \delta^2(\mathbf{p}_T + \mathbf{k}_T - \mathbf{q}_T) \Phi_g^{\lambda_1\kappa_1[-,-]}(x_1, \mathbf{p}_T, P_1, S_1) \times \\ \Phi_g^{\lambda_2\kappa_2[-,-]}(x_2, \mathbf{k}_T, P_2, S_2) \sum_{i,j,k,l=\gamma,Z} \mathcal{M}_{\lambda_1\lambda_2\mu_1\mu_2}^{gg\rightarrow ik} \Pi_i^{\mu_1\nu_1}(q_1) L_{1\nu_1\rho_1}^{ij} \left(\Pi_j^{\rho_1\sigma_1}(q_1) \right)^* \times \\ \Pi_k^{\mu_2\nu_2}(q_2) L_{2\nu_2\rho_2}^{kl} \left(\Pi_l^{\rho_2\sigma_2}(q_2) \right)^* \left(\mathcal{M}_{\kappa_1\kappa_2\sigma_1\sigma_2}^{gg\rightarrow jl} \right)^*, \quad (5.48)$$

with the momentum fractions evaluated at $x_{1,2} = \frac{q \cdot P_{2,1}}{P_1 \cdot P_2}$ and $\mathcal{M}_{gg \rightarrow ik}^{\mu\nu\rho\sigma}$ the $gg \rightarrow ik$ matrix element, with $i, j = \gamma, Z$, Π_γ and Π_Z the γ and Z propagators,

$$\Pi_\gamma^{\mu\nu}(q) \equiv g^{\mu\nu} \frac{-i}{q^2}, \\ \Pi_Z^{\mu\nu}(q) \equiv \left(g^{\mu\nu} - \frac{q_1^\mu q_1^\nu}{m_Z^2} \right) \frac{-i}{q^2 - m_Z^2 + i\Gamma_Z m_Z} \quad (5.49)$$

and $L_n^{ij\mu\nu}$ the lepton tensor for lepton pair n

$$L_n^{ij\mu\nu} = \text{Tr} \left[\gamma^\mu \left(g_V^{\ell_n i} + g_A^{\ell_n i} \gamma^5 \right) \bar{l}_n \gamma^\nu \left(g_V^{\ell_n j*} + g_A^{\ell_n j*} \gamma^5 \right) l_n \right] \\ = \left(g_V^{\ell_n i} g_V^{\ell_n j*} + g_A^{\ell_n i} g_A^{\ell_n j*} \right) \text{Tr} \left[\gamma^\mu \bar{l}_n \gamma^\nu l_n \right] + \left(g_A^{\ell_n i} g_V^{\ell_n j*} + g_V^{\ell_n i} g_A^{\ell_n j*} \right) \text{Tr} \left[\gamma^\mu \gamma^5 \bar{l}_n \gamma^\nu l_n \right] \\ = 4G_{\ell_n}^{ij} \left[\bar{l}_n^\mu l_n^\nu + l_n^\mu \bar{l}_n^\nu - g^{\mu\nu} \right] - 4i \left(g_A^{\ell_n i} g_V^{\ell_n j*} + g_V^{\ell_n i} g_A^{\ell_n j*} \right) \epsilon^{\mu\nu\rho\sigma} \bar{l}_{n\rho} l_{n\sigma}, \quad (5.50)$$

where, in the last step, we have defined

$$G_{\ell_n}^{ij} \equiv \left(g_V^{\ell_n i} g_V^{\ell_n j*} + g_A^{\ell_n i} g_A^{\ell_n j*} \right). \quad (5.51)$$

We want to calculate the cross section integrated over the polar and azimuthal angles of the lepton pair in their rest frame, so let us first rewrite the phase space element

$$d\mathcal{R} = \frac{d^3l_1}{(2\pi)^3 2E_{l_1}} \frac{d^3\bar{l}_1}{(2\pi)^3 2E_{\bar{l}_1}} \frac{d^3l_2}{(2\pi)^3 2E_{l_2}} \frac{d^3\bar{l}_2}{(2\pi)^3 2E_{\bar{l}_2}}, \quad (5.52)$$

by using

$$\frac{d^3 l_n}{(2\pi)^3 2E_{l_n}} \frac{d^3 \bar{l}_n}{(2\pi)^3 2E_{\bar{l}_n}} = \frac{d^4 q_n}{(2\pi)^4} \frac{d\Omega_n}{32\pi^2}, \quad (5.53)$$

as

$$d\mathcal{R} = \frac{d^4 q_1}{(2\pi)^4} \frac{d\Omega_1}{32\pi^2} \frac{d^4 q_2}{(2\pi)^4} \frac{d\Omega_2}{32\pi^2}, \quad (5.54)$$

where $d\Omega_n$ contains the angles θ_n and ϕ_n of lepton pair n . The next step is to rewrite the lepton tensor in terms of

$$\begin{aligned} \Delta q_n &\equiv l_n - \bar{l}_n, \\ q_n &\equiv l_n + \bar{l}_n, \end{aligned} \quad (5.55)$$

i.e.

$$L^{ij\mu\nu} = 2G_\ell^{ij} [q^\mu q^\nu + \Delta q^\mu \Delta q^\nu - q^2 g^{\mu\nu}] - 2i \left(g_A^{\ell i} g_V^{\ell j*} + g_V^{\ell i} g_A^{\ell j*} \right) \epsilon^{\mu\nu\rho\sigma} q_\rho \Delta q_\sigma, \quad (5.56)$$

in which the subscript n has now been suppressed. The vectors q and Δq can be expressed in the lepton pair rest frame by

$$\begin{aligned} \Delta q &= (0, q \sin \theta \cos \phi, q \sin \theta \sin \phi, q \cos \theta), \\ q &= (q, 0, 0, 0). \end{aligned} \quad (5.57)$$

Now we can perform the integration over $d\Omega$, i.e.

$$\begin{aligned} \int d\Omega \Delta q^\mu \Delta q^\nu &= \frac{4\pi}{3} (q^\mu q^\nu - q^2 g^{\mu\nu}), \\ \int d\Omega \Delta q^\mu &= 0, \end{aligned} \quad (5.58)$$

which allows us to write the lepton tensor as

$$\int d\Omega L^{ij\mu\nu} = \frac{32\pi G_\ell^{ij}}{3} (q^\mu q^\nu - q^2 g^{\mu\nu}). \quad (5.59)$$

Using the fact that

$$q_\mu \int d\Omega L^{ij\mu\nu} = q_\nu \int d\Omega L^{ij\mu\nu} = 0, \quad (5.60)$$

we can write the cross section, integrated over both lepton pair's $d\Omega$, as

$$\begin{aligned} d\sigma &= \frac{(2\pi)^4}{8S^2} \frac{d^4 q_1}{(2\pi)^4} \frac{d^4 q_2}{(2\pi)^4} \frac{1}{(3\pi)^2} \int d^2 \mathbf{p}_T d^2 \mathbf{k}_T \delta^2(\mathbf{p}_T + \mathbf{k}_T - \mathbf{q}_T) \Phi_g^{\lambda_1 \kappa_1}(x_1, \mathbf{p}_T) \Phi_g^{\lambda_2 \kappa_2}(x_2, \mathbf{k}_T) \times \\ &\sum_{i,j,k,l=\gamma,Z} G_{\ell_1}^{ij} G_{\ell_2}^{kl} \mathcal{M}_{\lambda_1 \lambda_2 \mu_1 \mu_2}^{gg \rightarrow ik} \Pi_i(q_1^2) (q_1^2 g^{\mu_1 \sigma_1} - q_1^{\mu_1} q_1^{\sigma_1}) \Pi_j(q_1^2)^* \times \\ &\Pi_k(q_2^2) (q_2^2 g^{\mu_2 \sigma_2} - q_2^{\mu_2} q_2^{\sigma_2}) \Pi_l(q_2^2)^* (\mathcal{M}_{\kappa_1 \kappa_2 \sigma_1 \sigma_2}^{gg \rightarrow jl})^*, \end{aligned} \quad (5.61)$$

where Π_i denotes the non-tensorial part of the propagator, i.e.

$$\begin{aligned}\Pi_\gamma(q) &\equiv \frac{-i}{q^2}, \\ \Pi_Z(q) &\equiv \frac{-i}{q^2 - m_Z^2 + i\Gamma_Z m_Z}.\end{aligned}\quad (5.62)$$

We will write the cross section in terms of helicity amplitudes, because they are easier to calculate. This can be done by using the general polarization sum

$$\sum_{\epsilon^\mu q_\mu=0} \epsilon^\mu (\epsilon^\nu)^* = -g^{\mu\nu} + \frac{q^\mu q^\nu}{q^2}, \quad (5.63)$$

which reduces to the transverse polarization sum for the gluons by virtue of the Ward identity, i.e.

$$\sum_{\lambda=\pm} \epsilon_\lambda^\mu (\epsilon_\lambda^\nu)^* = -g^{\mu\nu}. \quad (5.64)$$

Inserting the polarization sum, the cross section can be written as

$$\begin{aligned}d\sigma &= \frac{q_1^2 q_2^2 d^4 q_1 d^4 q_2}{18S^2(2\pi)^6} \int d^2 \mathbf{p}_T d^2 \mathbf{k}_T \delta^2(\mathbf{p}_T + \mathbf{k}_T - \mathbf{q}_T) \sum_{\lambda_i=\pm} \sum_{\kappa_i=0,\pm} \sum_{i,j,k,l=\gamma,Z} \\ &\left[\Phi_g^{\mu\nu}(x_1, \mathbf{p}_T) \epsilon_\mu^{\lambda_1}(p) \left(\epsilon_\nu^{\lambda_4}(p) \right)^* \right] \left[\Phi_g^{\mu\nu}(x_2, \mathbf{k}_T) \epsilon_\mu^{\lambda_2}(k) \left(\epsilon_\nu^{\lambda_3}(k) \right)^* \right] \times \\ &\left[\mathcal{M}_{gg \rightarrow ik}^{\mu\nu\rho\sigma} \left(\epsilon_\mu^{\lambda_1}(p) \right)^* \left(\epsilon_\nu^{\lambda_2}(k) \right)^* \epsilon_\rho^{\kappa_1}(q_1) \epsilon_\sigma^{\kappa_2}(q_2) \right] \left[\mathcal{M}_{gg \rightarrow jl}^{\mu\nu\rho\sigma} \left(\epsilon_\mu^{\lambda_4}(p) \right)^* \left(\epsilon_\nu^{\lambda_3}(k) \right)^* \epsilon_\rho^{\kappa_1}(q_1) \epsilon_\sigma^{\kappa_2}(q_2) \right]^* \times \\ &\Pi_i(q_1^2) \Pi_j(q_1^2)^* \Pi_k(q_2^2) \Pi_l(q_2^2)^* G_{\ell_1}^{ij} G_{\ell_2}^{kl}. \quad (5.65)\end{aligned}$$

Expressing the phase space element as (see Appendix B)

$$d^4 q_1 d^4 q_2 = \frac{\tilde{Q}}{4} dQ dM_1^2 dM_2^2 dY d\Omega d^2 \mathbf{q}_T, \quad (5.66)$$

the cross section can be written as

$$\begin{aligned}\frac{d\sigma}{dQ dM_1^2 dM_2^2 dY d\Omega d^2 \mathbf{q}_T} &= \frac{M_1^2 M_2^2 \tilde{Q}}{72S^2(2\pi)^6} \int d^2 \mathbf{p}_T d^2 \mathbf{k}_T \delta^2(\mathbf{p}_T + \mathbf{k}_T - \mathbf{q}_T) \times \\ &\sum_{i,j,k,l=\gamma,Z} \Pi_i(M_1^2) \Pi_j(M_1^2)^* \Pi_k(M_2^2) \Pi_l(M_2^2)^* G_{\ell_1}^{ij} G_{\ell_2}^{kl} \times \\ &\sum_{\lambda_i=\pm} \sum_{\kappa_i=0,\pm} \Phi_1^{\lambda_1 \lambda_4}(x_1, \mathbf{p}_T) \Phi_1^{\lambda_2 \lambda_3}(x_2, \mathbf{k}_T) \mathcal{M}_{gg \rightarrow ik}^{\lambda_1 \lambda_2 \kappa_1 \kappa_2} \left(\mathcal{M}_{gg \rightarrow jl}^{\lambda_4 \lambda_3 \kappa_1 \kappa_2} \right)^*, \quad (5.67)\end{aligned}$$

where the helicity correlator is defined as in Eq. (5.10) and the helicity amplitude as in Eq. (5.33).

Contracting the helicity correlator (see Appendix C) with the helicity amplitudes, the most general structure of the cross section is again

$$\frac{d\sigma}{dQ dM_1^2 dM_2^2 dY d\Omega d^2\mathbf{q}_T} = \frac{M_1^2 M_2^2 \tilde{Q}}{288Q^2 S(2\pi)^6} \left\{ F_1 \mathcal{C} [f_1^g f_1^g] + F_2 \mathcal{C} \left[\text{Re}[w_p w_k^*] h_1^{\perp g} h_1^{\perp g} \right] + F_2' \mathcal{C} \left[\text{Im}[w_p w_k^*] h_1^{\perp g} h_1^{\perp g} \right] \right. \\ \left. + F_3^{\pm} \mathcal{C} \left[\text{Re}[w_p] h_1^{\perp g} f_1^g \pm \text{Re}[w_k] f_1^g h_1^{\perp g} \right] + F_3'^{\pm} \mathcal{C} \left[\text{Im}[w_p] h_1^{\perp g} f_1^g \pm \text{Im}[w_k] f_1^g h_1^{\perp g} \right] \right. \\ \left. + F_4 \mathcal{C} \left[\text{Re}[w_p w_k] h_1^{\perp g} h_1^{\perp g} \right] + F_4' \mathcal{C} \left[\text{Im}[w_p w_k] h_1^{\perp g} h_1^{\perp g} \right] \right\} + \mathcal{O}\left(\frac{q_T}{Q}\right), \quad (5.68)$$

where we now work at leading order in q_T/Q as the expressions for the helicity correlator are only correct up to that order as well as that \hat{s} , \hat{t} and \hat{u} do not depend on \mathbf{p}_T and \mathbf{k}_T at that order and the F_n can thus be pulled out of the convolution. The F_n functions are defined by

$$F_n \equiv \sum_{i,j,k,l=\gamma,Z} \Pi_i(M_1^2) \Pi_j(M_1^2)^* \Pi_k(M_2^2) \Pi_l(M_2^2)^* G_{\ell_1}^{ij} G_{\ell_2}^{kl} \tilde{F}_n^{ijkl} \quad (5.69)$$

in terms of the \tilde{F}_n^{ijkl} functions, which are defined in Appendix E in terms of the partonic amplitudes. Working at leading order in q_T/Q , the momentum fractions can be expressed as $x_{1,2} = \frac{Q}{\sqrt{S}} e^{\pm Y}$.

The partonic amplitude consists again of three partonic sub channels: ‘direct’ scattering via a quark box and through scalar/pseudoscalar Higgs production and decay. For now we take the same model as used before, in which the pseudoscalar couples only to fermions, such that the decay to ZZ^* will have to go through a top triangle, i.e., we take the partonic diagrams that are shown in Figure 5.17. More details on the calculation of the partonic amplitudes can be found

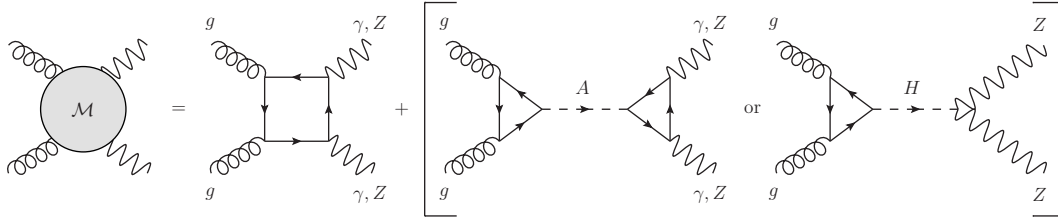


Figure 5.17: Partonic sub-channels that contribute to $gg \rightarrow ZZ^*$ scattering. In the scalar Higgs decay there are, in principle, also loop diagrams that contribute to $H \rightarrow Z\gamma$, but their contribution is much smaller than the tree-level $H \rightarrow ZZ$ contribution.

in Appendix E.

From the property of the $gg \rightarrow ZZ^*$ helicity amplitudes (see Appendix E)

$$\mathcal{M}^{\lambda_1 \lambda_2 \lambda_3 \lambda_4} = \pm \mathcal{M}^{-\lambda_1 - \lambda_2 - \lambda_3 - \lambda_4}, \quad (5.70)$$

with \pm depending on whether the number of longitudinal polarizations is even/odd, it follows that the primed F_i 's are zero,

$$F_2' = F_3'^{\pm} = F_4' = 0. \quad (5.71)$$

Using this constraint and rewriting the weights in the convolution (see Appendix D), the general structure of the cross section in Eq. (5.68) simplifies to (from here on we drop again the $\mathcal{O}(q_T/Q)$ for clarity)

$$\begin{aligned} \frac{d\sigma}{dQ dM_1^2 dM_2^2 dY d\Omega d^2\mathbf{q}_T} &= \frac{M_1^2 M_2^2 \tilde{Q}}{288Q^2 S(2\pi)^6} \left\{ F_1 \mathcal{C} [f_1^g f_1^g] + F_2 \mathcal{C} [w_H h_1^{\perp g} h_1^{\perp g}] \right. \\ &\quad \left. + F_3^\pm \mathcal{C} [w_3(\mathbf{p}_T) h_1^{\perp g} f_1^g \pm w_3(\mathbf{k}_T) f_1^g h_1^{\perp g}] \cos(2\phi) + F_4 \mathcal{C} [w_4 h_1^{\perp g} h_1^{\perp g}] \cos(4\phi) \right\}, \end{aligned} \quad (5.72)$$

We again normalize the cross section to the \mathbf{q}_T and ϕ integrated one, which reads

$$\frac{d\sigma}{dQ dM_1^2 dM_2^2 dY d\cos\theta} = \frac{M_1^2 M_2^2 \tilde{Q}}{24Q^2 S(2\pi)^5} F_1 f_1^g(x_1) f_1^g(x_2), \quad (5.73)$$

to get the q_T and ϕ distribution

$$\begin{aligned} \frac{1}{\frac{d\sigma}{dQ dM_1^2 dM_2^2 dY d\cos\theta}} \frac{d\sigma}{dQ dM_1^2 dM_2^2 dY d\Omega dq_T^2} \\ = \left[1 + \frac{F_2}{F_1} R(q_T) + \frac{F_3^\pm}{F_1} R_3^\pm(q_T) \cos 2\phi + \frac{F_4}{F_1} R_4(q_T) \cos 4\phi \right] \frac{\mathcal{C}[f_1^g f_1^g]}{2f_1^g(x_1) f_1^g(x_2)}, \end{aligned} \quad (5.74)$$

with the R functions defined as before. We also define a q_T distribution, by taking the ratio of the $\phi_{\mathbf{q}_T}$ and ϕ integrated cross section to the cross section integrated over \mathbf{q}_T and ϕ , to get

$$\frac{1}{\frac{d\sigma}{dQ dM_1^2 dM_2^2 dY d\cos\theta}} \frac{d\sigma}{dQ dM_1^2 dM_2^2 dY d\cos\theta dq_T^2} = \left[1 + \frac{F_2}{F_1} R(q_T) \right] \frac{\pi \mathcal{C}[f_1^g f_1^g]}{f_1^g(x_1) f_1^g(x_2)}. \quad (5.75)$$

Both distributions have the same form as the diphoton distribution, but with different F functions, which now also depend on the invariant masses squared of the lepton pairs, M_1^2 and M_2^2 .

5.3.1 Numerical predictions

Using the Gaussian Ansatz, the q_T and ϕ distribution again reads

$$\begin{aligned} \frac{1}{\frac{d\sigma}{dQ dM_1^2 dM_2^2 dY d\cos\theta}} \frac{d\sigma}{dQ dM_1^2 dM_2^2 dY d\Omega dq_T^2} \\ = \left[1 + \frac{F_2}{F_1} R(q_T) + \frac{F_3^\pm}{F_1} R_3^\pm(q_T) \cos 2\phi + \frac{F_4}{F_1} R_4(q_T) \cos 4\phi \right] \frac{e^{-q_T^2/2\langle p_T^2 \rangle}}{4\pi \langle p_T^2 \rangle}. \end{aligned} \quad (5.76)$$

with the R functions as given in Eq. 5.29 and 5.47. The ratios F_2/F_1 , F_3/F_1 and F_4/F_1 are plotted in Figure 5.18 for background + scalar Higgs production and background + pseudoscalar Higgs production. In Figure 5.19 the distribution of Z boson pairs from the different subprocesses are plotted as function of q_T and ϕ . The F ratios for the process $gg \rightarrow \text{box} \rightarrow ZZ$ are plotted in Figure 5.20 together with the distribution of on-shell Z bosons from this process at a fixed value of Q .

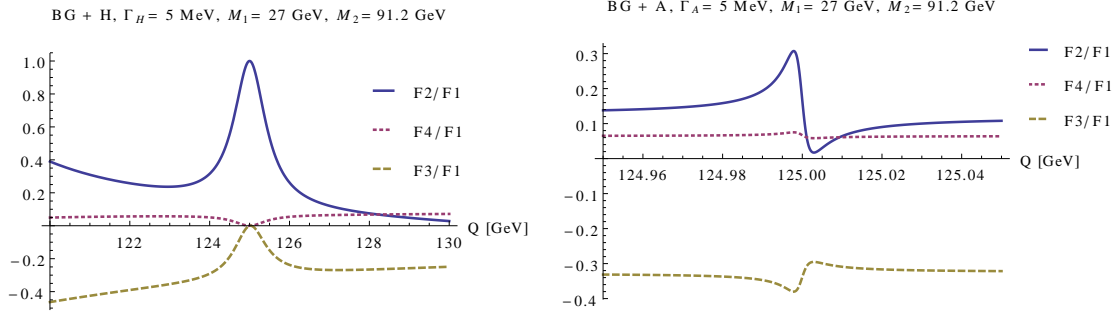


Figure 5.18: The ratios F_2/F_1 , F_3/F_1 and F_4/F_1 in Eq. (5.74) plotted as function of Q at $\theta = \pi/2$, $M_1 = 27$ GeV, $M_2 = M_Z$ and assuming a 125 GeV scalar (left) or pseudoscalar (right) Higgs, with a 5 MeV width.

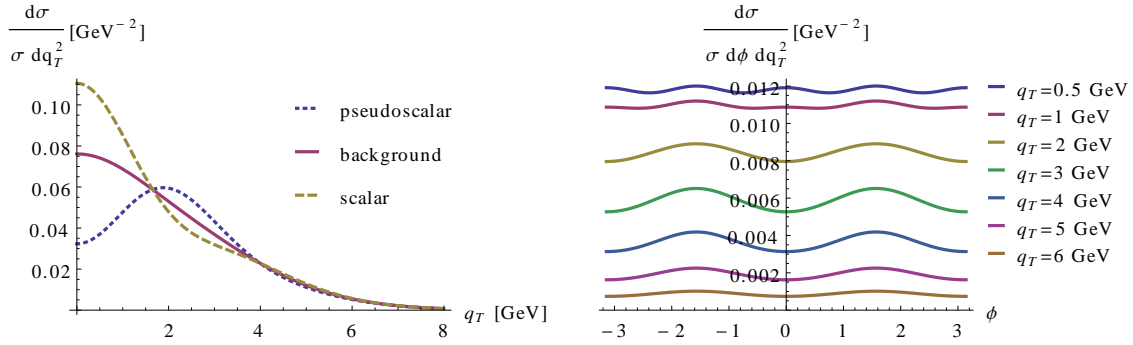


Figure 5.19: Left: the distribution of Z boson pairs with $M_1 = 27$ GeV and $M_2 = M_Z$, from scalar/pseudoscalar Higgs production and the background process $gg \rightarrow \text{box} \rightarrow ZZ^*$ as a function of q_T at $Q = 125$ GeV and $\theta = \pi/2$, assuming $r = 1/3$ in the parameterization of $h_1^{\perp g}$. Right: the distribution of Z boson pairs with $M_1 = 27$ GeV and $M_2 = M_Z$, from the background process $gg \rightarrow \text{box} \rightarrow ZZ^*$ as a function of ϕ for different values of q_T at $Q = 125$ GeV and $\theta = \pi/2$, assuming $r = 1/3$ in the parameterization of $h_1^{\perp g}$.

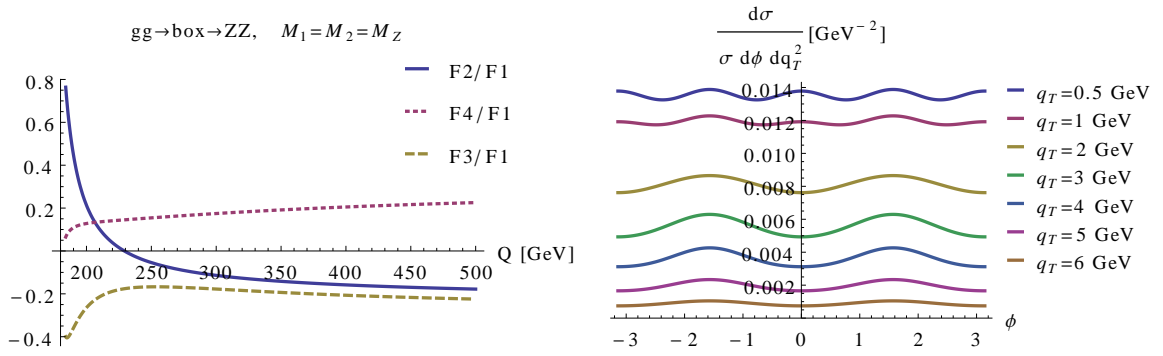


Figure 5.20: Left: the ratios F_2/F_1 , F_3/F_1 and F_4/F_1 in Eq. (5.74) for the $gg \rightarrow \text{box} \rightarrow ZZ$ contribution to on-shell Z boson pair production as function of Q at $\theta = \pi/2$. Right: the distribution of on-shell Z boson pairs from the process $gg \rightarrow \text{box} \rightarrow ZZ$ as a function of ϕ for different values of q_T at $Q = 190$ GeV and $\theta = \pi/2$, assuming $r = 1/3$ in the parameterization of $h_1^{\perp g}$.

5.3.2 Discussion

Looking at Figure 5.18, we see that the effect of a pseudoscalar Higgs in the ZZ^* transverse momentum distribution is negligible. This is not surprising, as under the assumption of no tree-level coupling to the Z boson, the signal to background ratio is very poor. Increasing the $A \rightarrow ZZ^*$ decay rate (by adding either a tree-level P and CP violating coupling or a P and CP conserving non-renormalizable coupling) would enhance the effect.

The effect of a scalar Higgs is, in this channel, larger than in the $\gamma\gamma$ channel, which shows itself in the fact that the width of the peak in F_2/F_1 is much wider. This means that the invariant mass of the ZZ^* pair does not have to be selected with such great accuracy to keep a substantial difference between the transverse momentum distribution of the Higgs (+ small amount of background) and the background. The discriminating power between scalar and pseudoscalar is thus, in principle, *larger* in this channel. However, seen the effective event rate of $H \rightarrow ZZ^*$ in [108, 109], it will take much more integrated luminosity to determine the transverse momentum distribution in this decay channel.

5.4 Summary and conclusions

We calculated the effect of linear gluon polarization on the production of scalar and pseudoscalar bosons through gluon-gluon fusion in pp collisions. Even in the absence of polarization of the proton, the gluons inside the proton are expected to be polarized. The amount of polarization cannot perturbatively be calculated, but model calculations show that it is most likely substantial. Within transverse momentum dependent factorization, the linear gluon polarization is treated as a non-perturbative input and described by the TMD $h_1^{\perp g}$.

Linear gluon polarization does not have an effect on the *total* cross section. However, the *transverse momentum distribution* is altered by linearly polarized gluons and in *distinct ways* for scalar and pseudoscalar bosons. We find that the effect is always such that scalar boson production is enhanced at low q_T , suppressed at moderate q_T and enhanced again at high q_T with respect to the distribution expected on the basis of unpolarized gluons. This effect is exactly *reversed* for a pseudoscalar, so there one should expect a suppression-enhancement-suppression with respect to the unpolarized q_T distribution. This characteristic modulation is *independent* of the sign of $h_1^{\perp g}$, which opens up the possibility to *use* the transverse momentum distribution to determine the CP quantum number of a scalar particle.

We made numerical predictions for the transverse momentum distribution of a scalar and pseudoscalar boson assuming a simple Gaussian functional form for $h_1^{\perp g}$ and a normalization such that the upper bound on $h_1^{\perp g}$ is satisfied for all \mathbf{p}_T and x . Depending on the width of the Gaussian, the effect on the transverse momentum distribution (shown in Figure 5.5) is large, in the order of 20-50% at low q_T . If this Ansatz for $h_1^{\perp g}$ turns out to be realistic, then an identification of a spin-0 boson as a scalar or pseudoscalar on the basis of the transverse momentum distribution is very well feasible.

An important decay channel in the investigation of the newly found boson at the LHC is the decay to two photons. There are background processes that also contribute to this final state, e.g., continuum production through $gg \rightarrow \text{quark box} \rightarrow \gamma\gamma$. We calculated the transverse momentum distribution of this background process and found it to be modified only slightly due to gluon polarization (shown in Figure 5.10). This implies that, if one compares the boson's transverse momentum distribution to the background's one, either an enhancement-suppression-

enhancement or a suppression-enhancement-suppression will be observed depending on the boson being a scalar or pseudoscalar respectively.

In practice, it will be difficult to separate the background q_T distribution from the boson's q_T distribution due to finite detector resolution. Assuming that one tries to isolate the boson's contribution from the continuum background on the basis of the invariant mass Q with a detector resolution of 1 GeV, the effect of linearly polarized gluons is reduced to 20% of the size shown in Figure 5.10. This will make it more difficult, but not impossible to distinguish scalar from pseudoscalar in this channel.

Another important decay channel is the $H \rightarrow ZZ^* \rightarrow 4\ell$, for which there is also a $gg \rightarrow$ quark box $\rightarrow ZZ^*$ continuum production background process. The size of the effect of linearly polarized gluons on this background process depends on Q and the invariant masses of the lepton pairs and is for values relevant in Higgs decay small (see Figure 5.18), which allows one to do the same analysis as in the $\gamma\gamma$ case to distinguish scalar from pseudoscalar. The effect in Higgs boson production + background around $Q = m_H$ is larger than in the $\gamma\gamma$ channel due to the better signal to background ratio. Within our model of a pseudoscalar boson (that does not couple to the Z boson at tree level) the effect is negligible in pseudoscalar production + background due to the poor signal to background ratio. This model is, however, not realistic for the newly found boson at the LHC and to describe that boson well an enhanced coupling to the Z boson should be introduced by either a P and CP violating tree-level coupling or a higher-dimensional non-renormalizable coupling. Calculating the pseudoscalar + background transverse momentum distribution in such a model is left for future work.

Continuum production does not only form a background, but can also be used to determine the *size* of the linearly polarized gluon distribution. This can be done by measuring $\cos 2\phi$ and $\cos 4\phi$ modulations in the cross section, where ϕ is the azimuthal Collins-Soper angle. The angular modulation is expected to be substantial ($\pm 10\%$) in diphoton continuum production at low q_T using our model for $h_1^{\perp g}$ (shown in Figure 5.15), which makes that process well suited to measure the size of the linearly polarized gluon distribution.

A measurement of a ϕ modulation in either $\gamma\gamma$ or ZZ^* continuum production is highly desirable as it would establish a nonzero linearly polarized gluon distribution $h_1^{\perp g}$ at that energy scale. Model calculations indicate that $h_1^{\perp g}$ is substantial at low energy, but that does not necessarily mean that this is also true at a higher energy scale, e.g., around m_H . The evolution of $h_1^{\perp g}$ with the energy scale Q is as yet unknown, but as gluons get linearly polarized by radiating of another gluon, we think evolution will not kill $h_1^{\perp g}$.

Recently, it was put forward that the transverse momentum distribution of scalar and pseudoscalar quarkonia will be influenced by the effect of linearly polarized gluons as well [136] and in the same way as discussed here. This provides *another* way to measure the linearly polarized gluon distribution and at a *different* energy scale, making it possible to explore the evolution of $h_1^{\perp g}$.

Chapter 6

Summary

Proton-proton collisions pose some serious challenges for theoreticians, because the exact structure of the proton is unknown and cannot be calculated within perturbation theory. Although it *is* possible to write many observables in hadronic collisions in terms of a *calculable* and a *measurable* (non-perturbative) part, this is not necessarily true for every observable and has to be checked for each case. Besides that, different observables need different factorization formulas. For example, the *total cross section* for a given process is well described within *collinear factorization*, but a *transverse momentum distribution* can only properly be described at all scales using *Transverse Momentum Dependent* (TMD) factorization. Another complication arises from the *process dependence* of some of the non-perturbative parts, which makes the distribution functions measured in one process not necessarily usable in another process. To put it briefly, proton-proton collisions do not form a totally impassable ground, but caution needs to be taken when calculating observables.

Transverse momentum dependent factorization expresses observables in terms of calculable hard parts and (perturbatively) non-calculable matrix elements that do not only depend on the momentum fraction of the parton, but also on its transverse momentum. The non-calculable matrix elements are parameterized in terms of distribution functions, of which 8 are needed to parameterize the structure that contributes at leading order in $1/Q$ (as compared to three for the collinear correlator). The extra distribution functions describe spin-momentum correlations. For example, the Sivers function describes the asymmetry of the parton transverse momentum distribution with respect to the nucleon's transverse spin. Another example is the Worm-Gear (WG) function, which describes a correlation between the parton's helicity and the angle between its transverse momentum and the nucleon's spin.

These two TMD distributions can have a variety of observable effects in transversely polarized proton-proton collisions. We have focused in this thesis on double transverse spin asymmetries in vector boson production, i.e., in Drell-Yan ($pp \rightarrow \gamma^* X \rightarrow \ell^+ \ell^- X$) and in W boson production with a leptonic decay ($pp \rightarrow WX \rightarrow \ell \nu_\ell X$). Both of these asymmetries can and will be measured at BNL's Relativistic Heavy Ion Collider (RHIC).

The double transverse spin asymmetry in Drell-Yan is interesting as it can be used to measure the quark *transversity* distribution, which measures the extent to which quarks are transversely polarized inside a transversely polarized hadron. The asymmetry can be defined in the q_T *integrated* or *differential* cross section, of which the latter one needs the TMD factorization framework to be described properly. The TMD contributions to the asymmetry in the differential cross section were already calculated in the literature, where it was found that both the Sivers and

worm-gear distributions contribute to a double transverse spin asymmetry that is *independent* of the lepton angle ϕ measured in the Collins-Soper (CS) frame, whereas the asymmetry due to the transversity distribution has a characteristic $\cos 2\phi$ dependence. Using this fact, contributions from TMD effects can be separated from the transversity contribution and they thus do not form a background for transversity measurements.

The situation, however, is different if one measures the lepton angle in the laboratory frame. The lepton direction is, in that frame, slightly correlated with the direction of the pair as a whole and the TMD effects can, therefore, *also* produce asymmetries that depend on the lepton angle. This is important to note, as TMD effects thus, in principle, form a background for measurements that try to extract the transversity distribution from asymmetries measured in the lab frame.

We, therefore, estimated the size of the Sivers and WG contribution to these asymmetries as a function of the lepton angle *measured in the laboratory frame* and found that the resulting background for transversity measurements is *negligible*. The contribution of TMD effects to the integrated (non q_T dependent) spin asymmetry is *also negligible*, as one would expect, because collinear factorization should apply for that observable. Transversity measurements at RHIC can thus safely be performed using angular measurements in the laboratory frame, which simplifies the analysis.

Measuring the double transverse spin asymmetry A_{TT} in W boson production is also in the future physics program of RHIC, with the aim of finding physics Beyond the SM (BSM). Within the SM, this spin asymmetry is zero at leading twist *collinear factorization*, because the W boson only couples to chiral left-handed quarks. A non-zero transverse spin asymmetry would then indicate a mixed left- and right-handed coupling and thus BSM physics.

However, collinear factorization is not necessarily applicable to double transverse spin asymmetries in W boson production. Using the framework of TMD factorization the worm-gear and Sivers contribution to $A_{TT}(q_T)$ in W production was calculated in [37, 38], where it was found that the TMD and BSM effects give rise to asymmetries with different angular dependencies. TMD effects can thus, in principle, be split from BSM effects, but these calculations use again angles defined in the Collins-Soper frame. In W boson production, however, it is very unlikely that one can perform the analysis in the CS frame, as one needs an accurate determination of the W boson's transverse momentum for this and in the leptonic decay of a W boson, the neutrino goes unobserved making this very difficult.

A secondary effect of the difficulty measuring the W boson transverse momentum, is that it is unlikely that $A_{TT}(q_T)$ will be measured, but instead an asymmetry differential in the charged lepton transverse momentum $A_{TT}(l_T)$. For $A_{TT}(l_T)$ it is possible to do a collinear expansion and express it in terms of collinear correlators. Higher order terms in the collinear expansion (TMD effects) are expected to be M^2/M_W^2 suppressed, where M is the hadronic scale and M_W the W boson mass. Naively, one would thus conclude that TMD effects can be of no influence in $A_{TT}(l_T)$.

To be completely sure about the TMD backgrounds in BSM studies through double transverse spin asymmetries in W boson production at RHIC, we have calculated the asymmetries, within the TMD framework, as a function of the charged lepton momentum and azimuthal angle *as measured in the laboratory frame*, integrated over the neutrino momentum as that is the observable that actually *can* be measured. As it turns out, both BSM physics and TMD effects give rise to the *same* angular dependency if angles are measured in the lab frame and can thus not be separated from each other. Besides that, we find that the asymmetries can be much

larger (max 2%) than expected on the basis of the collinear higher twist suppression argument.

Using realistic assumptions for the Siverson and worm-gear distributions, however, we find that the asymmetries are below what could be measured at RHIC and thus do not form a real background for BSM studies. We stress, nonetheless, that even though \mathbf{q}_T is not observed and we can thus make a collinear expansion, the higher order corrections are not suppressed by M^2/M_W^2 and one should thus be very careful with dismissing TMD effects on the basis of not observing \mathbf{q}_T .

A nonzero spin asymmetry in W boson production will thus only arise as an effect of BSM physics, in particular a right-handed coupling of the W boson to quarks. A right-handed coupling can arise in, e.g., Left-Right (LR) models, in which the SM is extended with a $SU(2)_R$ symmetry. Such models also predict additional W_R gauge bosons, which mix under an angle ζ with the W_L boson to form the mass eigenstates W_1 and W_2 . The W_1 boson corresponds almost to W_L , but the small admixture of the W_R provides a small coupling to the right-handed fermions. In Chapter 4, it is argued that in a general LR model the extra gauge bosons can be made arbitrarily heavy while keeping the right-handed W boson coupling constant. Independent bounds on the masses of the new gauge bosons and the right-handed coupling of the W boson should therefore be set.

Many bounds on the mixing angle ζ in LR models are set by using the assumption of *manifest* or *pseudomanifest* left-right symmetry, which provides a relation between the left- and right-handed CKM matrix, but in this way only a very limited subset of models is bounded. We argue that it is important to give model independent (assumption free) bounds on the right-handed coupling to all different quarks individually. We have extracted from the literature what we think are the most stringent bounds currently available. The list is not necessarily complete as not all model dependent bounds can straightforwardly be translated into model independent ones.

Using the best model independent bounds on the right-handed W boson coupling, we estimate in Chapter 4 the transverse spin asymmetries that can be expected at RHIC. In principle, two independent spin asymmetries can be measured, one with a $\sin 2\phi$ and one with a $\cos 2\phi$ angular dependence, where ϕ is the angle between the spin plane and the charged lepton's transverse momentum. The sizes of the two asymmetries are proportional to the imaginary and real part of the right-handed W boson coupling respectively. We estimated the size of these asymmetries and concluded that, at design integrated luminosity, the bounds most likely cannot be improved, but a competitive and entirely independent bound on the real part of the coupling *can* be set.

Transverse momentum dependent effects can also show up in *unpolarized* proton-proton collisions. TMD factorization, for example, allows for a nonzero linear gluon polarization, even if the proton itself is not polarized. The direction of the linear polarization is in the direction of the transverse momentum of the gluon, and the extent of polarization is described by the non-perturbative distribution function $h_1^{\perp g}$. The exact size of this distribution is unknown, but model calculations indicate that it might saturate its upper bound, at least in specific kinematical regions.

The linear polarization of gluons inside an unpolarized hadron can have observable effects at the Large Hadron Collider (LHC). For example, in Higgs production, which happens mainly through gluon-gluon fusion, the transverse momentum distribution is altered. Also the $\gamma\gamma$ and ZZ^* continuum production that occurs via $gg \rightarrow$ quark box is influenced by gluon polarization. This is important to note as calculations of the transverse momentum distribution based on

collinear factorization with q_T resummation or event generator based distributions that use parton shower techniques do not incorporate this effect and the use of these predictions might lead to misinterpretation of the data.

The effect of linearly polarized gluons is in fact such that it can be used to distinguish a scalar boson from a pseudoscalar one as the transverse momentum distribution of a scalar boson is enhanced at low q_T , suppressed at moderate q_T and enhanced again at large q_T as compared to the background, whereas for a pseudoscalar one has the opposite. The transverse momentum distribution is thus, in principle, sufficient to determine the parity of the newly found scalar boson at the LHC.

Higher order corrections and evolution of the relevant TMD distributions will have to be included to make more realistic predictions of the Higgs transverse momentum distribution. The size of the effect can be affected by this, but the qualitative behavior will always be such that a scalar boson has enhancement-suppression-enhancement with respect to the background, whereas a pseudoscalar has a suppression-enhancement-suppression. This prediction of TMD factorization allows one to turn the complex structure of a proton, involving parton polarization, into a tool to investigate or exclude physics beyond the Standard Model.

Appendix A

Polarization vectors

A.1 Covariant form

When calculating helicity amplitudes it is often very convenient to have covariant expressions for the polarization vectors in terms of the external momenta instead of an explicit representation in components. In this Appendix, we give a covariant representation of the polarization vectors for $2 \rightarrow 2$ scattering. We make use of the Mandelstam variables, defined as

$$\begin{aligned}\hat{s} &\equiv (p+k)^2, \\ \hat{t} &\equiv (p-q_1)^2, \\ \hat{u} &\equiv (k-q_1)^2.\end{aligned}\tag{A.1}$$

The most general way to write the polarization vectors in a $2 \rightarrow 2$ scattering process is

$$\begin{aligned}\epsilon_\lambda^\mu(p) &= \frac{1}{2\sqrt{\Delta}}(\chi^\mu - i\lambda L^\mu), \\ \epsilon_\lambda^\mu(k) &= \frac{1}{2\sqrt{\Delta}}(\chi^\mu + i\lambda L^\mu), \\ \epsilon_\lambda^\mu(q_1) &= \frac{1}{2\sqrt{\Delta}}(\chi^\mu - i\lambda K^\mu), \\ \epsilon_\lambda^\mu(q_2) &= \frac{1}{2\sqrt{\Delta}}(\chi^\mu + i\lambda K^\mu),\end{aligned}\tag{A.2}$$

in which χ^μ is a pseudovector and K^μ and L^μ vectors. The only pseudovector we can construct is

$$\chi^\mu \equiv \epsilon^{\mu\nu\rho\sigma} p_\nu k_\rho q_{1\sigma}.\tag{A.3}$$

To get the right normalization and orthogonality relation, $(\epsilon_{\lambda_1}^\mu)^* \epsilon_{\lambda_2\mu} = -\delta_{\lambda_1\lambda_2}$, we have to demand that

$$K^2 = L^2 = \chi^2 = -2\Delta.\tag{A.4}$$

A further constraint on L and K comes from the orthogonality of the polarization vectors to the momenta, which results in

$$q_1 \cdot K = q_2 \cdot K = p \cdot L = k \cdot L = 0.\tag{A.5}$$

Those two relations can be solved for K and L .

A.1.1 Massless final state

Assuming all particles to be massless,

$$p^2 = k^2 = q_1^2 = q_2^2 = 0, \quad (\text{A.6})$$

the constraints can be solved to get

$$\Delta = \frac{1}{8} \hat{s} \hat{t} \hat{u} \quad (\text{A.7})$$

and

$$\begin{aligned} K^\mu &= -\frac{\hat{u}}{2} p^\mu + \frac{\hat{t}}{2} k^\mu + \frac{\hat{u} - \hat{t}}{2} q_1^\mu, \\ L^\mu &= -\frac{\hat{u}}{2} p^\mu - \frac{\hat{t}}{2} k^\mu - \hat{s} q_1^\mu. \end{aligned} \quad (\text{A.8})$$

A.1.2 Massive final state (with equal masses)

Assuming the final state particles to be heavy, with equal mass, i.e.,

$$\begin{aligned} p^2 &= k^2 = 0, \\ q_1^2 &= q_2^2 = (p + k - q_1)^2 = M^2, \end{aligned} \quad (\text{A.9})$$

the constraints can be solved to get

$$\Delta = \frac{1}{8} \hat{s} (\hat{t} \hat{u} - M^4) \quad (\text{A.10})$$

and

$$\begin{aligned} K^\mu &= A \left[-(\hat{u} + M^2) p^\mu + (\hat{t} + M^2) k^\mu + (\hat{u} - \hat{t}) q_1^\mu \right], \\ L^\mu &= \frac{1}{2} \left[(M^2 - \hat{u}) p^\mu + (M^2 - \hat{t}) k^\mu - \hat{s} q_1^\mu \right], \end{aligned} \quad (\text{A.11})$$

in which

$$A \equiv \frac{1}{2} \sqrt{\frac{s}{s - 4M^2}}. \quad (\text{A.12})$$

The last step is to construct the longitudinal polarization vectors from the conditions

$$\begin{aligned} \epsilon_0^\mu(q_i)^* \epsilon_{0\mu}(q_i) &= -1, \\ \epsilon_0^\mu(q_i)^* \epsilon_{\pm\mu}(q_i) &= 0, \\ \epsilon_0^\mu(q_i) q_{i\mu} &= 0, \end{aligned} \quad (\text{A.13})$$

which results in

$$\begin{aligned} \epsilon_0^\mu(q_1) &= \frac{i2A}{\hat{s}M} \left[2M^2(k^\mu + p^\mu) - \hat{s} q_1^\mu \right], \\ \epsilon_0^\mu(q_2) &= \frac{i2A}{\hat{s}M} \left[(\hat{t} + \hat{u})(k^\mu + p^\mu) + \hat{s} q_1^\mu \right]. \end{aligned} \quad (\text{A.14})$$

A.1.3 Massive final state (with unequal masses)

Assuming the final state particles to be heavy with two different masses, i.e.,

$$\begin{aligned} p^2 &= k^2 = 0 \\ q_1^2 &= M_1^2 \\ q_2^2 &= (p + k - q_1)^2 = M_2^2 \end{aligned} \tag{A.15}$$

the constraints can be solved to get

$$\Delta = \frac{1}{8}s (\hat{t}\hat{u} - M_1^2 M_2^2) \tag{A.16}$$

and

$$\begin{aligned} K^\mu &= A \left\{ [M_1^2 (2M_2^2 + t - u) - t(t + u)] k^\mu \right. \\ &\quad \left. + [M_1^2 (-2M_2^2 + t - u) + u(t + u)] p^\mu + s(u - t) q_1^\mu \right\}, \\ L^\mu &= \frac{1}{2} (M_1^2 - t) k^\mu + \frac{1}{2} (M_1^2 - u) p^\mu - \frac{s}{2} q_1^\mu, \end{aligned} \tag{A.17}$$

in which

$$A \equiv \frac{1}{2\sqrt{(t + u)^2 - 4M_1^2 M_2^2}}. \tag{A.18}$$

The last step is to construct the longitudinal polarization vectors from the conditions in Eq. (A.13), which results in

$$\begin{aligned} \epsilon_0^\mu(q_1) &= A \left(4iM_1 k^\mu - \frac{2i(2M_1^2 - t - u)}{M_1} q_1^\mu + 4iM_1 p^\mu \right), \\ \epsilon_0^\mu(q_2) &= A \left(\frac{2i(t + u)}{M_2} k^\mu + \frac{2i(2M_2^2 - t - u)}{M_2} q_1^\mu + \frac{2i(t + u)}{M_2} p^\mu \right). \end{aligned} \tag{A.19}$$

A.2 Useful contractions of polarization vectors

A couple useful contractions of polarization vectors is

$$\epsilon^{\lambda_1}(p)^* \cdot \epsilon^{\lambda_2}(k)^* = \begin{cases} -1 & ++ \\ -1 & -- \\ 0 & \text{rest} \end{cases} \tag{A.20}$$

and (assuming the most general case of unequal masses in the final state)

$$\epsilon^{\lambda_3}(q_1) \cdot \epsilon^{\lambda_4}(q_2) = \begin{cases} -1 & ++ \\ -1 & -- \\ \frac{-\hat{s} + M_1^2 + M_2^2}{2M_1 M_2} & 00 \\ 0 & \text{rest} \end{cases} \tag{A.21}$$

Contractions involving epsilon tensors can be written as

$$\epsilon^{pk\epsilon(p)^*\epsilon(k)^*} = -\frac{i}{2}\hat{s} \begin{cases} 1 & ++ \\ -1 & -- \\ 0 & \text{rest} \end{cases} \quad (\text{A.22})$$

for the in-state and

$$\epsilon^{q_1q_2\epsilon(q_1)\epsilon(q_2)} = \frac{i}{2}\sqrt{(\hat{s} - M_1^2 - M_2^2)^2 - 4M_1^2M_2^2} \begin{cases} 1 & ++ \\ -1 & -- \\ 0 & \text{rest} \end{cases} \quad (\text{A.23})$$

for the out-state.

Appendix B

Frames

It is often useful to have explicit representations of the momentum vectors in components. We will give explicit representations in three different frames: the hadronic Center Of Mass (COM) frame, the ‘intermediate frame’, which we will define below and the Collins-Soper frame. The incoming hadronic momenta are given by P_1 and P_2 , the incoming partonic momenta by p and k and the outgoing by q_1 and q_2 of which the sum is denoted by q . The hadronic center of mass energy is given by S and the partonic one by s . The vectors p_T , k_T and q_T are the transverse projections of p , k and q in the hadronic center of mass frame.

B.1 Equal mass final state

The incoming partons are taken to be massless, the protons to have mass M_p and we will first consider the outgoing momenta to have equal mass M , i.e.,

$$\begin{aligned} p^2 &= k^2 = 0, \\ (p+k)^2 &= s, \\ q_1^2 = q_2^2 &= (p+k-q_1)^2 = M^2, \\ P_1^2 = P_2^2 &= M_p^2, \\ (P_1 + P_2)^2 &= S. \end{aligned}$$

(B.1)

Hadronic COM frame

In this frame the hadronic center of mass is stationary, i.e., $P_1 + P_2 = (\sqrt{S}, 0, 0, 0)$ and P_1 and P_2 have no transverse components, i.e., $P_1^1 = P_1^2 = P_2^1 = P_2^2 = 0$.

$$\begin{aligned}
P_1 &= \left(\frac{1}{2}\sqrt{S}, \mathbf{0}, \frac{1}{2}\sqrt{S - 4M_p^2} \right), \\
P_2 &= \left(\frac{1}{2}\sqrt{S}, \mathbf{0}, -\frac{1}{2}\sqrt{S - 4M_p^2} \right), \\
q &= \left(\sqrt{s + q_T^2} \cosh Y, \mathbf{q}_T, \sqrt{s + q_T^2} \sinh Y \right), \\
p_T &= (0, \mathbf{p}_T, 0), \\
k_T &= (0, \mathbf{q}_T - \mathbf{p}_T, 0), \\
\epsilon_\lambda^\mu(p) &\equiv \frac{1}{2\sqrt{\Delta}} (\chi^\mu - i\lambda L^\mu) = \left(0, \frac{-i\lambda}{\sqrt{2}} e^{-i\lambda(\phi + \phi_{\mathbf{q}_T})}, \frac{1}{\sqrt{2}} e^{-i\lambda(\phi + \phi_{\mathbf{q}_T})}, 0 \right) + \mathcal{O}\left(\frac{q_T, p_T}{\sqrt{s}}\right) \quad (\text{B.2})
\end{aligned}$$

Intermediate frame

In the intermediate frame

- the partonic COM only moves in the transverse direction (set to be the x direction) and
- the hadronic COM only moves along the beam direction,

i.e., $p^3 = -k^3$ and P_1 and P_2 have no transverse components. The frame is obtained from the hadronic COM frame by a boost along the z -direction.

$$\begin{aligned}
p &= \left(\frac{s + 2\mathbf{q}_T \cdot \mathbf{p}_T}{2\sqrt{s + q_T^2}}, \mathbf{p}_T, \frac{1}{2} \sqrt{\frac{s^2 - 4s(p_T^2 - \mathbf{p}_T \cdot \mathbf{q}_T) - 4(p_T^2 q_T^2 - (\mathbf{p}_T \cdot \mathbf{q}_T)^2)}{s + q_T^2}} \right) \\
k &= \left(\frac{s + 2q_T^2 - \mathbf{q}_T \cdot \mathbf{p}_T}{2\sqrt{s + q_T^2}}, \mathbf{q}_T - \mathbf{p}_T, -\frac{1}{2} \sqrt{\frac{s^2 - 4s(p_T^2 - \mathbf{p}_T \cdot \mathbf{q}_T) - 4(p_T^2 q_T^2 - (\mathbf{p}_T \cdot \mathbf{q}_T)^2)}{s + q_T^2}} \right) \\
q &= p + k = \left(\sqrt{s + q_T^2}, \mathbf{q}_T, 0 \right) \\
q_1 &= \left(\frac{1}{2}\sqrt{s + q_T^2} + \frac{q_T}{2\sqrt{s}}\sqrt{s - 4M^2} \sin \theta \cos \phi, \frac{1}{2\sqrt{s}}\sqrt{(s + q_T^2)(s - 4M^2)} \sin \theta \cos \phi \right. \\
&\quad \left. + \frac{1}{2}q_T, \frac{1}{2}\sqrt{s - 4M^2} \sin \theta \sin \phi, \frac{1}{2}\sqrt{s - 4M^2} \cos \theta \right) \\
p_T &= (0, \mathbf{p}_T, 0) \\
k_T &= (0, \mathbf{q}_T - \mathbf{p}_T, 0) \\
P_1 &= \left(\frac{1}{2}\sqrt{S} \cosh Y - \frac{1}{2}\sqrt{S - 4M_p^2} \sinh Y, \mathbf{0}, \frac{1}{2}\sqrt{S - 4M_p^2} \cosh Y - \frac{1}{2}\sqrt{S} \sinh Y \right) \\
P_2 &= \left(\frac{1}{2}\sqrt{S} \cosh Y + \frac{1}{2}\sqrt{S - 4M_p^2} \sinh Y, \mathbf{0}, -\frac{1}{2}\sqrt{S - 4M_p^2} \cosh Y - \frac{1}{2}\sqrt{S} \sinh Y \right) \\
\epsilon_\lambda^\mu(p) &\equiv \frac{1}{2\sqrt{\Delta}} (\chi^\mu - i\lambda L^\mu) = \left(0, \frac{-i\lambda}{\sqrt{2}} e^{-i\lambda(\phi + \phi_{\mathbf{q}_T})}, \frac{1}{\sqrt{2}} e^{-i\lambda(\phi + \phi_{\mathbf{q}_T})}, 0 \right) + \mathcal{O}\left(\frac{q_T, p_T}{\sqrt{s}}\right) \quad (\text{B.3})
\end{aligned}$$

Collins-Soper frame

The Collins-Soper frame is a partonic COM frame with a particular choice for the orientation of the spatial axes. One can define the CS frame in two different ways

- The frame that is obtained by boosting the above mentioned ‘‘Intermediate frame’’ in the direction of \mathbf{q}_T until q has no transverse component left and is purely time-like.
- The partonic rest frame in which the \hat{z} and \hat{x} unit vectors are given by

$$\begin{aligned}\hat{z} &= \frac{Z}{\sqrt{-Z^2}} & \text{with} & & Z &\equiv \frac{P_2 \cdot q}{P_1 \cdot P_2} P_1 - \frac{P_1 \cdot q}{P_1 \cdot P_2} P_2 \\ \hat{x} &= \frac{X}{\sqrt{-X^2}} & \text{with} & & X &\equiv \frac{P_1}{P_1 \cdot Z} - \frac{P_2}{P_2 \cdot Z} - \left(\frac{P_1 \cdot q}{P_1 \cdot Z} - \frac{P_2 \cdot q}{P_2 \cdot Z} \right) \frac{q}{q^2}\end{aligned}\quad (\text{B.4})$$

The momenta are in this frame given by

$$\begin{aligned}q_1 &= \left(\frac{1}{2}\sqrt{s}, \frac{1}{2}\sqrt{s-4M^2} \sin \theta \cos \phi, \frac{1}{2}\sqrt{s-4M^2} \sin \theta \sin \phi, \frac{1}{2}\sqrt{s-4M^2} \cos \theta \right), \\ q_2 &= \left(\frac{1}{2}\sqrt{s}, -\frac{1}{2}\sqrt{s-4M^2} \sin \theta \cos \phi, -\frac{1}{2}\sqrt{s-4M^2} \sin \theta \sin \phi, -\frac{1}{2}\sqrt{s-4M^2} \cos \theta \right), \\ p &= \left(\frac{1}{2}\sqrt{s}, -\frac{1}{2}(q_T - 2\mathbf{p}_T^x) \sqrt{\frac{s}{s+q_T^2}}, \mathbf{p}_T^y, \right. \\ &\quad \left. \frac{1}{2} \sqrt{\frac{s^2 + 4s(\mathbf{p}_T \cdot \mathbf{q}_T - \mathbf{p}_T^2) + 4[(\mathbf{p}_T \cdot \mathbf{q}_T)^2 - \mathbf{p}_T^2 q_T^2]}{s+q_T^2}} \right), \\ k &= \left(\frac{1}{2}\sqrt{s}, \frac{1}{2}(q_T - 2\mathbf{p}_T^x) \sqrt{\frac{s}{s+q_T^2}}, -\mathbf{p}_T^y, \right. \\ &\quad \left. -\frac{1}{2} \sqrt{\frac{s^2 + 4s(\mathbf{p}_T \cdot \mathbf{q}_T - \mathbf{p}_T^2) + 4[(\mathbf{p}_T \cdot \mathbf{q}_T)^2 - \mathbf{p}_T^2 q_T^2]}{s+q_T^2}} \right), \\ q &= p + k = (\sqrt{s}, 0, 0, 0),\end{aligned}\quad (\text{B.5})$$

in which the x -direction of \mathbf{p}_T is set by the direction of \mathbf{q}_T in the lab and intermediate frame. To leading order in \mathbf{p}_T and \mathbf{q}_T , the polarization vectors are, in this frame, given by

$$\begin{aligned}\epsilon_\lambda(p) &= \left(0, \frac{-i\lambda e^{-i\lambda\phi}}{\sqrt{2}}, \frac{e^{-i\lambda\phi}}{\sqrt{2}}, 0 \right), \\ \epsilon_{\lambda=\pm 1}(q_1) &= \left(0, \frac{-\sin \phi - i\lambda \cos \theta \cos \phi}{\sqrt{2}}, \frac{\cos \phi - i\lambda \cos \theta \sin \phi}{\sqrt{2}}, \frac{i\lambda \sin \theta}{\sqrt{2}} \right), \\ \epsilon_0(q_1) &= \left(\frac{-i\sqrt{s-4M^2}}{2M}, \frac{i\sqrt{s}}{2M} \sin \theta \cos \phi, \frac{i\sqrt{s}}{2M} \sin \theta \sin \phi, \frac{i\sqrt{s}}{2M} \cos \theta \right), \\ \epsilon_0(q_2) &= \left(\frac{-i\sqrt{s-4M^2}}{2M}, -\frac{i\sqrt{s}}{2M} \sin \theta \cos \phi, -\frac{i\sqrt{s}}{2M} \sin \theta \sin \phi, -\frac{i\sqrt{s}}{2M} \cos \theta \right).\end{aligned}\quad (\text{B.6})$$

Mandelstam variables

The Mandelstam variables are, in these coordinates, given by

$$\begin{aligned} t &\equiv (p - q_1)^2 = \frac{1}{2} \cos \theta \sqrt{s(s - 4M^2)} + M^2 - \frac{s}{2} + \mathcal{O}(\mathbf{p}_T, \mathbf{q}_T), \\ u &\equiv (k - q_1)^2 = -\frac{1}{2} \cos \theta \sqrt{s(s - 4M^2)} + M^2 - \frac{s}{2} + \mathcal{O}(\mathbf{p}_T, \mathbf{q}_T). \end{aligned} \quad (\text{B.7})$$

Momentum fractions

The momentum fractions are, in these coordinates, given by

$$x_{1,2} \equiv \frac{q \cdot P_{2,1}}{P_1 \cdot P_2} = e^{\pm Y} \sqrt{\frac{s + q_T^2}{S}} + \mathcal{O}(M_p^2/S). \quad (\text{B.8})$$

B.2 Unequal mass final state

In this section we will take the outgoing particles to be massive, with two different masses M_1 and M_2 , i.e.,

$$\begin{aligned} p^2 &= k^2 = 0, \\ (p + k)^2 &= s, \\ q_1^2 &= M_1^2, \\ q_2^2 &= (p + k - q_1)^2 = M_2^2, \\ P_1^2 &= P_2^2 = M_p^2, \\ (P_1 + P_2)^2 &= S. \end{aligned} \quad (\text{B.9})$$

Collins-Soper frame

The outgoing momenta are in this frame given by

$$\begin{aligned} q_1 &= \left(\sqrt{M_1^2 + \tilde{Q}^2}, \tilde{Q} \sin \theta \cos \phi, \tilde{Q} \sin \theta \sin \phi, \tilde{Q} \cos \theta \right), \\ q_2 &= \left(\sqrt{M_2^2 + \tilde{Q}^2}, -\tilde{Q} \sin \theta \cos \phi, -\tilde{Q} \sin \theta \sin \phi, -\tilde{Q} \cos \theta \right), \\ q &= p + k = q_1 + q_2 = (\sqrt{s}, 0, 0, 0) \\ \Delta q &= q_1 - q_2 = \left(\frac{M_1^2 - M_2^2}{\sqrt{s}}, 2\tilde{Q} \sin \theta \cos \phi, 2\tilde{Q} \sin \theta \sin \phi, 2\tilde{Q} \cos \theta \right) \end{aligned} \quad (\text{B.10})$$

where

$$\tilde{Q} \equiv \frac{1}{2\sqrt{s}} \sqrt{(M_1^2 - M_2^2)^2 - 2s(M_1^2 + M_2^2) + s^2}. \quad (\text{B.11})$$

The polarization vectors read, to leading order in \mathbf{q}_T and \mathbf{p}_T ,

$$\begin{aligned}
\epsilon_\lambda(p) &= \left(0, \frac{-i\lambda e^{-i\lambda\phi}}{\sqrt{2}}, \frac{e^{-i\lambda\phi}}{\sqrt{2}}, 0 \right) \\
\epsilon_{\lambda=\pm 1}(q_1) &= \left(0, \frac{-\sin\phi - i\lambda \cos\theta \cos\phi}{\sqrt{2}}, \frac{\cos\phi - i\lambda \cos\theta \sin\phi}{\sqrt{2}}, \frac{i\lambda \sin\theta}{\sqrt{2}} \right), \\
\epsilon_0(q_1) &= \left(-i\sqrt{\frac{M_1^4 - 2M_1^2(M_2^2 + s) + (M_2^2 - s)^2}{4sM_1^2}}, \frac{i\sin(\theta)\cos(\phi)(M_1^2 - M_2^2 + s)}{2M_1\sqrt{s}}, \right. \\
&\quad \left. \frac{i\sin(\theta)\sin(\phi)(M_1^2 - M_2^2 + s)}{2M_1\sqrt{s}}, \frac{i\cos(\theta)(M_1^2 - M_2^2 + s)}{2M_1\sqrt{s}} \right), \\
\epsilon_0(q_2) &= \left(-i\sqrt{\frac{M_1^4 - 2M_1^2(M_2^2 + s) + (M_2^2 - s)^2}{4sM_2^2}}, \frac{i\sin(\theta)\cos(\phi)(M_1^2 - M_2^2 - s)}{2M_2\sqrt{s}}, \right. \\
&\quad \left. \frac{i\sin(\theta)\sin(\phi)(M_1^2 - M_2^2 - s)}{2M_2\sqrt{s}}, \frac{i\cos(\theta)(M_1^2 - M_2^2 - s)}{2M_2\sqrt{s}} \right). \tag{B.12}
\end{aligned}$$

Mandelstam variables

The Mandelstam variables are, in these coordinates and to leading order in \mathbf{q}_T and \mathbf{p}_T , given by

$$\begin{aligned}
t \equiv (p - q_1)^2 &= \frac{M_1^2 + M_2^2 - s}{2} + \frac{1}{2} \cos\theta + \sqrt{s^2 - 2s(M_1^2 + M_2^2) + (M_1^2 + M_2^2)^2}, \\
u \equiv (k - q_1)^2 &= \frac{M_1^2 + M_2^2 - s}{2} + \frac{1}{2} \cos\theta - \sqrt{s^2 - 2s(M_1^2 + M_2^2) + (M_1^2 + M_2^2)^2}. \tag{B.13}
\end{aligned}$$

B.3 Phase space

We like to rewrite the 2-particle phase space element in terms of the kinematic variables that we have used to parameterize the outgoing momenta, being Q , Y , \mathbf{q}_T , M_1 , M_2 , θ and ϕ . To do so, we first rewrite the element as

$$d^4q_1 d^4q_2 = \frac{1}{16} d^4q d^4\Delta q. \tag{B.14}$$

Then we will express d^4q in terms of dY , dQ and $d\mathbf{q}_T$, where Y is the forward rapidity, Q the COM energy and \mathbf{q}_T the transverse momentum of the pair. This is done by using

$$q \equiv q_1 + q_2 \stackrel{\text{LAB}}{=} \left(\sqrt{Q^2 + \mathbf{q}_T^2} \cosh Y, \mathbf{q}_T, \sqrt{Q^2 + \mathbf{q}_T^2} \sinh Y \right), \tag{B.15}$$

from which it follows that

$$d^4q = Q dQ dY d^2\mathbf{q}_T, \tag{B.16}$$

where $Q \equiv \sqrt{s}$.

The second step is to express $d^4\Delta q$ in terms of dM_1^2 , dM_2^2 , $d\Omega$, where $M_i^2 \equiv q_i^2$ and $d\Omega$ contains the Collins-Soper angles θ and ϕ of the Z^*Z^* pair. For $d^4\Delta q$ we can use the the

expression for Δq in the CS frame, because the transformation from the LAB to the CS frame does not depend on M_1 , M_2 , θ or ϕ . (note: for e.g. d^4q one cannot take the CS frame expression, although d^4q is frame independent, it should be calculated in a fixed frame and not one that depends on (in this case) Q , Y and \mathbf{q}_T .) The momenta q_1 and q_2 are parameterized in the Collins-Soper (CS) frame by

$$\begin{aligned} q_1^{\text{CS}} &\equiv \left(\sqrt{M_1^2 + \tilde{Q}^2}, \tilde{Q} \sin \theta \cos \phi, \tilde{Q} \sin \theta \sin \phi, \tilde{Q} \cos \theta \right), \\ q_2^{\text{CS}} &\equiv \left(\sqrt{M_2^2 + \tilde{Q}^2}, -\tilde{Q} \sin \theta \cos \phi, -\tilde{Q} \sin \theta \sin \phi, -\tilde{Q} \cos \theta \right), \end{aligned} \quad (\text{B.17})$$

i.e.

$$\Delta q \equiv q_1 - q_2 \stackrel{\text{CS}}{=} \left(\frac{M_1^2 - M_2^2}{\sqrt{s}}, 2\tilde{Q} \sin \theta \cos \phi, 2\tilde{Q} \sin \theta \sin \phi, 2\tilde{Q} \cos \theta \right), \quad (\text{B.18})$$

where

$$\tilde{Q} \equiv \frac{1}{2Q} \sqrt{(M_1^2 - M_2^2)^2 - 2Q^2(M_1^2 + M_2^2) + Q^4}. \quad (\text{B.19})$$

From this parameterization it follows that

$$d^4\Delta q = \frac{4\tilde{Q}}{Q} d\Omega dM_1^2 dM_2^2, \quad (\text{B.20})$$

and therefore

$$d^4q_1 d^4q_2 = \frac{\tilde{Q}}{4} dQ dM_1^2 dM_2^2 dY d\Omega d^2\mathbf{q}_T. \quad (\text{B.21})$$

Appendix C

Helicity correlator

The helicity correlators are defined as

$$\begin{aligned}\Phi_{g1}^{\lambda_1\lambda_4} &\equiv \Phi_g^{\mu\nu} \epsilon_\mu^{\lambda_1}(p) \epsilon_\nu^{\lambda_4}(p)^*, \\ \Phi_{g2}^{\lambda_2\lambda_3} &\equiv \Phi_g^{\mu\nu} \epsilon_\mu^{\lambda_2}(k) \epsilon_\nu^{\lambda_3}(k)^*.\end{aligned}\tag{C.1}$$

To calculate the contraction with the polarization vectors, we use an explicit representation of the polarization vectors in component form in the LAB frame,

$$\epsilon_\lambda^\mu(p) = (\epsilon_\lambda^\mu(k))^* = \left(0, \frac{-i\lambda}{\sqrt{2}} e^{-i\lambda(\phi+\phi_{\mathbf{q}_T})}, \frac{1}{\sqrt{2}} e^{-i\lambda(\phi+\phi_{\mathbf{q}_T})}, 0\right) + \mathcal{O}\left(\frac{p_T, k_T}{\sqrt{s}}\right).\tag{C.2}$$

This form follows from the covariant definition we use to calculate the helicity amplitudes, see Appendix A and B. We will neglect the $\mathcal{O}(p_T, k_T/\sqrt{s})$ corrections. Contracting the polarization vectors with the leading twist gluon correlator for an unpolarized hadron,

$$\Phi_g^{\mu\nu}(x, \mathbf{p}_T) = -\frac{1}{2x} \left\{ g_T^{\mu\nu} f_1^g(x, \mathbf{p}_T^2) - \left(\frac{p_T^\mu p_T^\nu}{M^2} + g_T^{\mu\nu} \frac{\mathbf{p}_T^2}{2M^2} \right) h_1^{\perp g}(x, \mathbf{p}_T^2) \right\},\tag{C.3}$$

we end up with the helicity correlators,

$$\begin{aligned}\Phi_{g1}^{\lambda_1\lambda_2}(x, \mathbf{p}_T) &= \frac{1}{2x} \begin{pmatrix} f_1^g(x, \mathbf{p}_T^2) & ++ \\ w(\mathbf{p}_T) h_1^{\perp g}(x, \mathbf{p}_T^2) & +- \\ w(\mathbf{p}_T)^* h_1^{\perp g}(x, \mathbf{p}_T^2) & -+ \end{pmatrix} \\ \Phi_{g2}^{\lambda_1\lambda_2}(x, \mathbf{k}_T) &= \frac{1}{2x} \begin{pmatrix} f_1^g(x, \mathbf{p}_T^2) & ++ \\ w(\mathbf{k}_T)^* h_1^{\perp g}(x, \mathbf{k}_T^2) & +- \\ w(\mathbf{k}_T) h_1^{\perp g}(x, \mathbf{k}_T^2) & -+ \end{pmatrix}\end{aligned}\tag{C.4}$$

in which we have defined $w(\mathbf{p}_T)$ as

$$w(\mathbf{p}_T) \equiv -\frac{p_T^2}{2M^2} e^{i2(\phi_{\mathbf{p}_T} - \phi_{\mathbf{q}_T} - \phi)}.\tag{C.5}$$

Appendix D

Weights & Convolutions

The weights that appear in the contraction of helicity correlator with helicity amplitudes, can be rewritten as

$$\begin{aligned}
\text{Re}[w(\mathbf{p}_T)w(\mathbf{k}_T)^*] &= \frac{\mathbf{p}_T^2 \mathbf{k}_T^2}{4M^4} \cos 2(\phi_{\mathbf{p}_T} - \phi_{\mathbf{k}_T}) = \frac{2(\mathbf{k}_T \cdot \mathbf{p}_T)^2 - \mathbf{k}_T^2 \mathbf{p}_T^2}{4M^4}, \\
\text{Im}[w(\mathbf{p}_T)w(\mathbf{k}_T)^*] &= 0, \\
\text{Re}[w(\mathbf{p}_T)] &= -\frac{\mathbf{p}_T^2}{2M^2} \cos 2(\phi_{\mathbf{p}_T} - \phi_{\mathbf{q}_T} - \phi) = \frac{2(\mathbf{q}_T \cdot \mathbf{p}_T)^2 - \mathbf{q}_T^2 \mathbf{p}_T^2}{2\mathbf{q}_T^2 M^2} \cos(2\phi) \\
\text{Im}[w(\mathbf{p}_T)] &= -\frac{\mathbf{p}_T^2}{2M^2} \sin 2(\phi_{\mathbf{p}_T} - \phi_{\mathbf{q}_T} - \phi) = -\frac{2(\mathbf{q}_T \cdot \mathbf{p}_T)^2 - \mathbf{q}_T^2 \mathbf{p}_T^2}{2\mathbf{q}_T^2 M^2} \sin(2\phi), \\
\text{Re}[w(\mathbf{p}_T)w(\mathbf{k}_T)] &= \frac{\mathbf{p}_T^2 \mathbf{k}_T^2}{4M^4} \cos 2(\phi_{\mathbf{p}_T} + \phi_{\mathbf{k}_T} - 2\phi_{\mathbf{q}_T} - 2\phi) \\
&= \frac{[\mathbf{k}_T^2 \mathbf{q}_T^2 - 2(\mathbf{q}_T \cdot \mathbf{k}_T)^2] [\mathbf{p}_T^2 \mathbf{q}_T^2 - 2(\mathbf{q}_T \cdot \mathbf{p}_T)^2]}{4M^4 \mathbf{q}_T^4} \cos(4\phi), \\
\text{Im}[w(\mathbf{p}_T)w(\mathbf{k}_T)] &= \frac{\mathbf{p}_T^2 \mathbf{k}_T^2}{4M^4} \sin 2(\phi_{\mathbf{p}_T} + \phi_{\mathbf{k}_T} - 2\phi_{\mathbf{q}_T} - 2\phi) \\
&= -\frac{[\mathbf{k}_T^2 \mathbf{q}_T^2 - 2(\mathbf{q}_T \cdot \mathbf{k}_T)^2] [\mathbf{p}_T^2 \mathbf{q}_T^2 - 2(\mathbf{q}_T \cdot \mathbf{p}_T)^2]}{4M^4 \mathbf{q}_T^4} \sin(4\phi). \tag{D.1}
\end{aligned}$$

We will introduce shorthands for the following combinations of momenta

$$\begin{aligned}
w_H &\equiv \frac{2(\mathbf{k}_T \cdot \mathbf{p}_T)^2 - \mathbf{k}_T^2 \mathbf{p}_T^2}{4M^4}, \\
w_3(\mathbf{p}_T) &\equiv \frac{2(\mathbf{q}_T \cdot \mathbf{p}_T)^2 - \mathbf{q}_T^2 \mathbf{p}_T^2}{2\mathbf{q}_T^2 M^2}, \\
w_4 &\equiv \frac{[\mathbf{k}_T^2 \mathbf{q}_T^2 - 2(\mathbf{q}_T \cdot \mathbf{k}_T)^2] [\mathbf{p}_T^2 \mathbf{q}_T^2 - 2(\mathbf{q}_T \cdot \mathbf{p}_T)^2]}{4M^4 \mathbf{q}_T^4}. \tag{D.2}
\end{aligned}$$

Some general properties of convolutions of distributions functions are

$$\begin{aligned}
\int d^2\mathbf{q}_T \mathcal{C}[f_1^g f_1^g] &= \int d^2\mathbf{p}_T f_1^g(x_1, \mathbf{p}_T^2) \int d^2\mathbf{k}_T f_1^g(x_2, \mathbf{k}_T^2) = f_1^g(x_1) f_1^g(x_2), \\
\int d^2\mathbf{q}_T \mathcal{C}[w_H h_1^{\perp g} h_1^{\perp g}] &= \int d^2\mathbf{p}_T \int d^2\mathbf{k}_T \frac{\mathbf{p}_T^2 \mathbf{k}_T^2}{4M^4} \cos\left(2\phi_{\mathbf{p}_T}^{\mathbf{k}_T}\right) h_1^{\perp g}(x_1, \mathbf{p}_T^2) h_1^{\perp g}(x_2, \mathbf{k}_T^2) \\
&= 0, \\
\int d^2\mathbf{q}_T \mathbf{q}_T^2 \mathcal{C}[w_H h_1^{\perp g} h_1^{\perp g}] &= \int d^2\mathbf{p}_T \int d^2\mathbf{k}_T \frac{\mathbf{p}_T^2 \mathbf{k}_T^2}{4M^4} (\mathbf{p}_T + \mathbf{k}_T)^2 \cos\left(2\phi_{\mathbf{p}_T}^{\mathbf{k}_T}\right) \times \\
&\quad h_1^{\perp g}(x_1, \mathbf{p}_T^2) h_1^{\perp g}(x_2, \mathbf{k}_T^2) \\
&= 0.
\end{aligned} \tag{D.3}$$

Using the following parameterization of the distribution functions

$$f_1^g(x, \mathbf{p}_T^2) = \frac{f_1^g(x)}{\pi \langle p_T^2 \rangle} \exp\left(-\frac{\mathbf{p}_T^2}{\langle p_T^2 \rangle}\right), \tag{D.4}$$

and

$$h_1^{\perp g}(x, \mathbf{p}_T^2) = \frac{M^2 f_1^g(x)}{\pi \langle p_T^2 \rangle^2} \frac{2e(1-r)}{r} \exp\left(-\frac{\mathbf{p}_T^2}{r \langle p_T^2 \rangle}\right), \tag{D.5}$$

the R functions can be evaluated to

$$\begin{aligned}
R(q_T) &\equiv \frac{\mathcal{C}[w_H h_1^{\perp g} h_1^{\perp g}]}{\mathcal{C}[f_1^g f_1^g]} = \frac{r}{2} (1-r)^2 \left(1 - \frac{q_T^2}{r \langle p_T^2 \rangle} + \frac{q_T^4}{8 r^2 \langle p_T^2 \rangle^2}\right) \exp\left[2 - \frac{1-r}{r} \frac{q_T^2}{2 \langle p_T^2 \rangle}\right], \\
R_3^-(q_T) &\equiv \frac{\mathcal{C}[w_3(\mathbf{p}_T) h_1^{\perp g} f_1^g - w_3(\mathbf{k}_T) f_1^g h_1^{\perp g}]}{\mathcal{C}[f_1^g f_1^g]} = 0, \\
R_3^+(q_T) &\equiv \frac{\mathcal{C}[w_3(\mathbf{p}_T) h_1^{\perp g} f_1^g + w_3(\mathbf{k}_T) f_1^g h_1^{\perp g}]}{\mathcal{C}[f_1^g f_1^g]} = 4r^2 \frac{1-r}{(1+r)^3} \frac{q_T^2}{\langle p_T^2 \rangle} \exp\left[1 - \frac{1-r}{1+r} \frac{q_T^2}{2 \langle p_T^2 \rangle}\right], \\
R_4(q_T) &\equiv \frac{\mathcal{C}[w_4 h_1^{\perp g} h_1^{\perp g}]}{\mathcal{C}[f_1^g f_1^g]} = \frac{(1-r)^2}{16r} \frac{(2r \langle p_T^2 \rangle - q_T^2)^2}{\langle p_T^2 \rangle^2} \exp\left[2 - \frac{1-r}{r} \frac{q_T^2}{2 \langle p_T^2 \rangle}\right].
\end{aligned} \tag{D.6}$$

Appendix E

Partonic amplitudes

In all calculations of the helicity amplitudes we use FeynCalc [137] for tracing and tensor reduction to scalar integrals, which are evaluated using LoopTools [138].

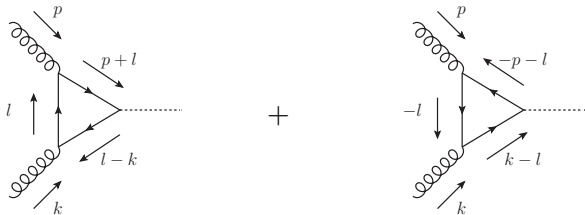
E.1 On-shell Higgs production

The definition of the helicity amplitude is

$$\mathcal{M}^{\lambda_1 \lambda_2} \equiv \mathcal{M}^{\mu\nu} \epsilon_{\mu}^{\lambda_1}(p)^* \epsilon_{\nu}^{\lambda_2}(k)^*. \quad (\text{E.1})$$

E.1.1 The process $gg \rightarrow H$

The diagrams contributing to the $gg \rightarrow H$ process are



The corresponding amplitude is

$$\begin{aligned}
\mathcal{M}_{gg \rightarrow H}^{\lambda_1 \lambda_2} &= \frac{1}{i} (\epsilon_{1\mu}^{\lambda_1})^* (\epsilon_{2\nu}^{\lambda_2})^* (ig_s)^2 \left(\frac{-igm_t}{2m_W} \right) (-1)(i)^3 \times \\
&\int \frac{d^D l}{(2\pi)^D} \frac{1}{(l^2 - m_t^2 + i\epsilon)((l+p)^2 - m_t^2 + i\epsilon)((l-k)^2 - m_t^2 + i\epsilon)} \times \\
&\left\{ \text{Tr}[\gamma^\mu (\not{l} + m_t) \gamma^\nu (\not{l} - \not{k} + m_t) (\not{l} + \not{p} + m_t)] \right. \\
&\quad \left. + \text{Tr}[\gamma^\mu (-\not{p} - \not{l} + m_t) (\not{k} - \not{l} + m_t) \gamma^\nu (-\not{l} + m_t)] \right\} \\
&= \mathcal{A}_{gg \rightarrow H} g^{\mu\nu} (\epsilon_{1\mu}^{\lambda_1})^* (\epsilon_{2\nu}^{\lambda_2})^* \\
&= \mathcal{A}_{gg \rightarrow H} \begin{cases} -1 & ++ \\ & -- \\ 0 & +- \\ & -+ \end{cases} \tag{E.2}
\end{aligned}$$

with

$$\mathcal{A}_{gg \rightarrow H} \equiv -\frac{2^{5/4} \sqrt{G_F} \alpha_s m_t^2}{\pi} \left[\left(2m_t^2 - \frac{1}{2} \hat{s} \right) C_0(0, 0, \hat{s}, m_t^2, m_t^2, m_t^2) + 1 \right], \tag{E.3}$$

where C_0 is the scalar triangle integral defined in Appendix F.

E.1.2 The process $gg \rightarrow A$

For pseudoscalar Higgs production, we have the same diagrams, but with the $t\bar{t}A$ -vertex being

$$t \quad \swarrow \quad \text{---} A = -\frac{gg_t m_t}{2m_W} \gamma_5 \quad \searrow \quad t$$

This results in the amplitude

$$\begin{aligned}
\mathcal{M}_{gg \rightarrow A}^{\lambda_1 \lambda_2} &= \frac{2^{5/4} \sqrt{G_F} \alpha_s g_t m_t}{(2\pi)^3} (\epsilon_{1\mu}^{\lambda_1})^* (\epsilon_{2\nu}^{\lambda_2})^* \\
&\int d^D l \frac{1}{(l^2 - m_t^2 + i\epsilon)((l+p)^2 - m_t^2 + i\epsilon)((l-k)^2 - m_t^2 + i\epsilon)} \times \\
&\left\{ \text{Tr}[\gamma^\mu (\not{l} + m_t) \gamma^\nu (\not{l} - \not{k} + m_t) \gamma^5 (\not{l} + \not{p} + m_t)] \right. \\
&\quad \left. + \text{Tr}[\gamma^\mu (-\not{p} - \not{l} + m_t) \gamma^5 (\not{k} - \not{l} + m_t) \gamma^\nu (-\not{l} + m_t)] \right\} \\
&= -\frac{2^{5/4} \sqrt{G_F} \alpha_s g_t m_t^2}{\pi} C_0(0, 0, \hat{s}, m_t^2, m_t^2, m_t^2) (\epsilon_{1\mu}^{\lambda_1})^* (\epsilon_{2\nu}^{\lambda_2})^* p_\rho k_\sigma \epsilon^{\rho\sigma\mu\nu} \\
&= \mathcal{A}_{gg \rightarrow A} \begin{cases} -1 & ++ \\ 1 & -- \\ 0 & +- \\ & -+ \end{cases} \tag{E.4}
\end{aligned}$$

with

$$\mathcal{A}_{gg \rightarrow A} \equiv -i \frac{\hat{s} 2^{5/4} \sqrt{G_F} \alpha_s g_t m_t^2}{2\pi} C_0(0, 0, \hat{s}, m_t^2, m_t^2, m_t^2). \quad (\text{E.5})$$

E.2 Diphoton production $gg \rightarrow \gamma\gamma$

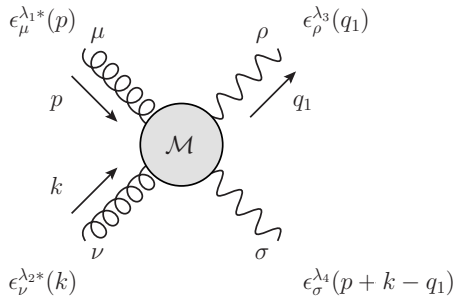
The F functions for diphoton production are expressed in terms of the partonic helicity amplitudes by

$$\begin{aligned} F_1 &= \sum_{\lambda_1, \lambda_2, \lambda_3, \lambda_4} \mathcal{M}^{\lambda_1 \lambda_2 \lambda_3 \lambda_4} \left(\mathcal{M}^{\lambda_1 \lambda_2 \lambda_3 \lambda_4} \right)^* \\ F_2 &= 2 \sum_{\lambda_3, \lambda_4} \text{Re} \left[\mathcal{M}^{++\lambda_3 \lambda_4} \left(\mathcal{M}^{--\lambda_3 \lambda_4} \right)^* \right] \\ F_2' &= 2 \sum_{\lambda_3, \lambda_4} \text{Im} \left[\mathcal{M}^{++\lambda_3 \lambda_4} \left(\mathcal{M}^{--\lambda_3 \lambda_4} \right)^* \right] \\ F_3^\pm &= 2 \sum_{\lambda, \lambda_3, \lambda_4} \text{Re} \left[\mathcal{M}^{\lambda - \lambda_3 \lambda_4} \left(\mathcal{M}^{\lambda + \lambda_3 \lambda_4} \right)^* \pm \mathcal{M}^{+\lambda \lambda_3 \lambda_4} \left(\mathcal{M}^{-\lambda \lambda_3 \lambda_4} \right)^* \right] \\ F_3'^\pm &= 2 \sum_{\lambda, \lambda_3, \lambda_4} \text{Im} \left[\mathcal{M}^{\lambda - \lambda_3 \lambda_4} \left(\mathcal{M}^{\lambda + \lambda_3 \lambda_4} \right)^* \pm \mathcal{M}^{+\lambda \lambda_3 \lambda_4} \left(\mathcal{M}^{-\lambda \lambda_3 \lambda_4} \right)^* \right] \\ F_4 &= 2 \sum_{\lambda_3, \lambda_4} \text{Re} \left[\mathcal{M}^{+-\lambda_3 \lambda_4} \left(\mathcal{M}^{-+\lambda_3 \lambda_4} \right)^* \right] \\ F_4' &= 2 \sum_{\lambda_3, \lambda_4} \text{Im} \left[\mathcal{M}^{+-\lambda_3 \lambda_4} \left(\mathcal{M}^{-+\lambda_3 \lambda_4} \right)^* \right] \end{aligned} \quad (\text{E.6})$$

The definition of the helicity amplitudes is

$$\mathcal{M}^{\lambda_1 \lambda_2 \lambda_3 \lambda_4} \equiv \mathcal{M}^{\mu\nu\rho\sigma} \left(\epsilon_\mu^{\lambda_1}(p) \right)^* \left(\epsilon_\nu^{\lambda_2}(k) \right)^* \epsilon_\rho^{\lambda_3}(q_1) \epsilon_\sigma^{\lambda_4}(q_2), \quad (\text{E.7})$$

or graphically



E.2.1 The sub-process $gg \rightarrow H \rightarrow \gamma\gamma$

We first calculate the amplitude for the Higgs decay process $H \rightarrow \gamma\gamma$. In this decay, there is a contribution from top-quark and W -boson loops, i.e.,

$$\mathcal{M}_{H \rightarrow \gamma\gamma}^{\lambda_3\lambda_4} = \mathcal{M}_{H \rightarrow \text{top loop} \rightarrow \gamma\gamma}^{\lambda_3\lambda_4} + \mathcal{M}_{H \rightarrow W \text{ loop} \rightarrow \gamma\gamma}^{\lambda_3\lambda_4}. \quad (\text{E.8})$$

The top quark contribution to the decay can be related to the $gg \rightarrow H$ production process by

$$\mathcal{M}_{H \rightarrow \text{top loop} \rightarrow \gamma\gamma}^{\lambda_1\lambda_2} = Q_t^2 N_c \mathcal{M}_{gg \rightarrow H}^{\lambda_1\lambda_2} \Big|_{\alpha_s \rightarrow \alpha}. \quad (\text{E.9})$$

The W -boson loop contribution we will take from [139], where it is given to be

$$\begin{aligned} \mathcal{M}_{H \rightarrow W \text{ loop} \rightarrow \gamma\gamma}^{\lambda_3\lambda_4} &= \frac{2^{1/4} \sqrt{G_F} \alpha}{2\pi} \times \\ & [m_H^2 + 6m_W^2 - 6m_W^2(m_H^2 - 2m_W^2)C_0(0, 0, m_H^2, m_W^2, m_W^2, m_W^2)] \epsilon_{3\mu}^{\lambda_3} \epsilon_{4\nu}^{\lambda_4} g^{\mu\nu} \\ &= \frac{2^{1/4} \sqrt{G_F} \alpha}{2\pi} [m_H^2 + 6m_W^2 - 6m_W^2(m_H^2 - 2m_W^2)C_0(0, 0, m_H^2, m_W^2, m_W^2, m_W^2)] \times \\ & \begin{cases} -1 & ++ \\ & -- \\ 0 & +- \\ & -+ \end{cases} \end{aligned} \quad (\text{E.10})$$

which holds for an on-shell Higgs boson only, but that should be accurate enough.

The amplitude for the total process can now be obtained from the previous results,

$$\begin{aligned} \mathcal{M}_{gg \rightarrow H \rightarrow \gamma\gamma}^{\lambda_1\lambda_2\lambda_3\lambda_4} &= \frac{1}{i} \left(i \mathcal{M}_{gg \rightarrow H}^{\lambda_1\lambda_2} \right) \frac{i}{\hat{s} - m_H^2 + i\Gamma_H m_H} \left(i \mathcal{M}_{H \rightarrow \gamma\gamma}^{\lambda_3\lambda_4} \right) \\ &= - \frac{\mathcal{M}_{gg \rightarrow H}^{\lambda_1\lambda_2} \mathcal{M}_{H \rightarrow \gamma\gamma}^{\lambda_3\lambda_4}}{\hat{s} - m_H^2 + i\Gamma_H m_H} \\ &= \alpha_s \alpha_H \begin{cases} + + + + \\ + + -- \\ - - ++ \\ - - - - \\ 0 \quad \text{rest} \end{cases} \end{aligned} \quad (\text{E.11})$$

with

$$\begin{aligned} A_H &\equiv \frac{2\sqrt{2}G_F m_t^2}{\pi^2} \left[\left(2m_t^2 - \frac{\hat{s}}{2} \right) C_0(0, 0, \hat{s}, m_t^2, m_t^2, m_t^2) + 1 \right] \frac{1}{\hat{s} - m_H^2 + i\Gamma_H m_H} \times \\ & \left[-2m_t^2 Q_t^2 N_c \left\{ \left(2m_t^2 - \frac{\hat{s}}{2} \right) C_0(0, 0, \hat{s}, m_t^2, m_t^2, m_t^2) + 1 \right\} + \frac{1}{2} m_H^2 + 3m_W^2 \right. \\ & \quad \left. - 3m_W^2(m_H^2 - 2m_W^2)C_0(0, 0, m_H^2, m_W^2, m_W^2, m_W^2) \right]. \end{aligned} \quad (\text{E.12})$$

E.2.2 The sub-process $gg \rightarrow A \rightarrow \gamma\gamma$

We first calculate the $A \rightarrow \gamma\gamma$ decay amplitude. In the decay of the pseudoscalar Higgs, we assume that only the top quark loop contributes. Again, this top quark contribution can be related to the $gg \rightarrow A$ production process by

$$\mathcal{M}_{A \rightarrow \gamma\gamma}^{\lambda_3 \lambda_4} = -Q_t^2 N_c \mathcal{M}_{gg \rightarrow A}^{\lambda_3 \lambda_4} \Big|_{\alpha_s \rightarrow \alpha} \quad (\text{E.13})$$

Note the sign flip, which is caused by the fact that the production amplitude has to be contracted with complex conjugated polarization vectors, whereas the decay matrix element is contracted with ‘normal’ polarization vectors.

Production and decay amplitudes can be combined as before to obtain the full $gg \rightarrow A \rightarrow \gamma\gamma$ amplitude, i.e.,

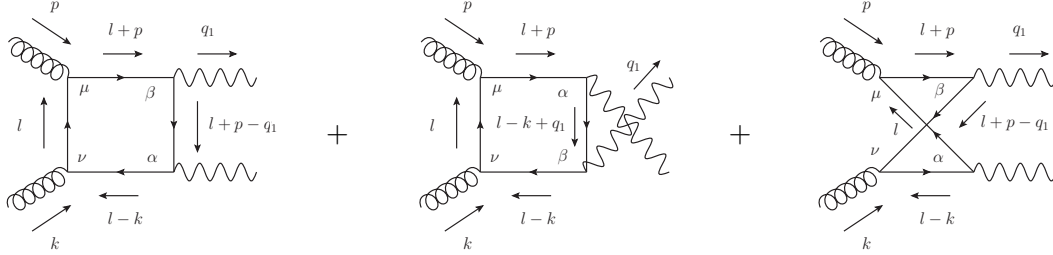
$$\begin{aligned} \mathcal{M}_{gg \rightarrow A \rightarrow \gamma\gamma}^{\lambda_1 \lambda_2 \lambda_3 \lambda_4} &= -\mathcal{M}_{gg \rightarrow A}^{\lambda_1 \lambda_2} \mathcal{M}_{A \rightarrow \gamma\gamma}^{\lambda_3 \lambda_4} \frac{1}{\hat{s} - m_H^2 + i\Gamma_H m_H} \\ &= \alpha_s \alpha A_A \begin{cases} 1 & ++++ \\ & ---- \\ -1 & ++-- \\ & --++ \\ 0 & \text{rest} \end{cases} \end{aligned} \quad (\text{E.14})$$

with

$$A_A \equiv -\alpha_s \alpha \frac{\sqrt{2} G_F m_t^4 g_T^2}{\pi^2} Q_t^2 N_c [\hat{s} C_0(0, 0, \hat{s}, m_t^2, m_t^2, m_t^2)]^2 \frac{1}{\hat{s} - m_H^2 + i\Gamma_H m_H} \quad (\text{E.15})$$

E.2.3 The sub-process $gg \rightarrow \text{box} \rightarrow \gamma\gamma$

The diagrams contributing to the process $gg \rightarrow \text{box} \rightarrow \gamma\gamma$ are



The corresponding amplitude is

$$\begin{aligned} \mathcal{M}_{gg \rightarrow \text{box} \rightarrow \gamma\gamma}^{\lambda_1 \lambda_2 \lambda_3 \lambda_4} &= -4\pi\alpha_s 4\pi\alpha \sum_{q=u,d,s,c,b} Q_q^2 (\epsilon_{1\mu}^{\lambda_1})^* (\epsilon_{2\nu}^{\lambda_2})^* (\epsilon_{3\beta}^{\lambda_3}) (\epsilon_{4\alpha}^{\lambda_4}) \int \frac{d^D l}{i(2\pi)^D} \\ &\quad \left\{ \frac{\text{Tr}[\gamma^\mu l \gamma^\nu (l - \not{k}) \gamma^\alpha (l + \not{p} - \not{q}_1) \gamma^\beta (l + \not{p})]}{l^2 (l+p)^2 (l-k)^2 (l+p-q_1)^2} \right. \\ &\quad + \frac{\text{Tr}[\gamma^\mu l \gamma^\nu (l - \not{k}) \gamma^\beta (l - \not{k} + \not{q}_1) \gamma^\alpha (l + \not{p})]}{l^2 (l+p)^2 (l-k)^2 (l-k+q_1)^2} \\ &\quad \left. + \frac{\text{Tr}[\gamma^\mu l \gamma^\alpha (l + \not{p} + \not{k} - \not{q}_1) \gamma^\nu (l + \not{p} - \not{q}_1) \gamma^\beta (l + \not{p})]}{l^2 (l+p)^2 (l+p-q_1)^2 (l+p+k-q_1)^2} \right\}. \end{aligned} \quad (\text{E.16})$$

Inserting the covariant expression for the polarization vectors as defined in Appendix A, calculating the trace and canceling factors between numerators and denominators until only scalar integrals are left, we come to the result

$$\mathcal{M}_{gg \rightarrow \text{box} \rightarrow \gamma\gamma}^{\lambda_1 \lambda_2 \lambda_3 \lambda_4} = 8\alpha_s \alpha \sum_{q=u,d,s,c,b} Q_q^2 M^{\lambda_1 \lambda_2 \lambda_3 \lambda_4} \quad (\text{E.17})$$

with

$$\begin{aligned} M^{++++} &= -\frac{t^3 + tu^2}{s^2} C_0(0, 0, t, 0, 0, 0) - \frac{u^3 + ut^2}{s^2} C_0(0, 0, u, 0, 0, 0) \\ &\quad + \frac{t^3 u + tu^3}{2s^2} D_0(0, 0, 0, 0, t, u, 0, 0, 0, 0) + \frac{t-u}{s} B_0(t, 0, 0) + \frac{u-t}{s} B_0(u, 0, 0) - 1, \\ M^{++++-} &= 1, \\ M^{++--} &= 1, \end{aligned} \quad (\text{E.18})$$

where B_0 , C_0 and D_0 are scalar integrals as defined in Appendix F. The others helicity amplitudes can be obtained using the relations

$$\begin{aligned} M^{\lambda_1 \lambda_2 \lambda_3 \lambda_4} &= M^{-\lambda_1 - \lambda_2 - \lambda_3 - \lambda_4}, \\ M^{++++-} &= M^{++-+-} = M^{+-+--} = M^{-++++}, \\ M^{+---+} &= M^{+++++} \Big|_{t \leftrightarrow s}, \\ M^{+--+} &= M^{+++++} \Big|_{u \leftrightarrow s}. \end{aligned} \quad (\text{E.19})$$

The first relation can be inferred from the structure of the polarization vectors by first realizing that the tensor structure of the amplitude can be written only in terms of p^μ , k^μ , q_1^μ and $g^{\mu\nu}$'s. The only way a χ^μ can be contracted with this in a non-zero way, is with a $g^{\mu\nu}$ and another χ^μ . The amplitude will thus always have an even number of λ 's in every term and so if all $\lambda_i \rightarrow -\lambda_i$ the amplitude is unchanged. For this $\gamma\gamma$ case, one could also directly argue that this is a consequence of parity conservation.

The second relation comes from the fact that the sum of diagram is unchanged by flipping them all upside down or flipping left and right. The third and fourth relation are obtained from flipping two endpoints of the box, combined with the relation

$$M^{+--+} = M^{++++}. \quad (\text{E.20})$$

The scalar integrals can be expressed in terms of logs (see Appendix F) to write the $++++$ helicity amplitude as

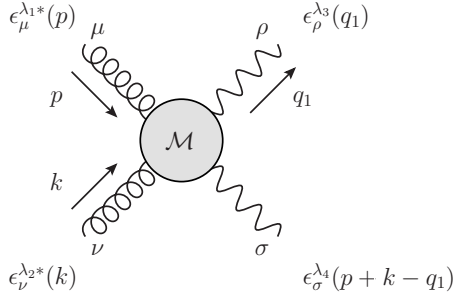
$$\begin{aligned} M^{++++} &= -1 + \frac{u-t}{s} \log|t/u| - \frac{t^2 + u^2}{2s^2} [\log^2|t/u| + \pi^2 \theta(t/u)] \\ &\quad + i\pi[\theta(t) - \theta(u)] \left(\frac{t-u}{s} + \frac{t^2 + u^2}{s^2} \log|t/u| \right). \end{aligned} \quad (\text{E.21})$$

E.3 Z boson pair production $gg \rightarrow ZZ^*$

We need to calculate the helicity amplitudes for the process $gg \rightarrow ZZ^*$, where it is understood that Z stands for both the Z boson and the photon. The definition of the helicity amplitudes is

$$\mathcal{M}_{gg \rightarrow ik}^{\lambda_1 \lambda_2 \lambda_3 \lambda_4} \equiv \mathcal{M}_{gg \rightarrow ik}^{\mu\nu\rho\sigma} \left(\epsilon_\mu^{\lambda_1}(p) \right)^* \left(\epsilon_\nu^{\lambda_2}(k) \right)^* \epsilon_\rho^{\lambda_3}(q_1) \epsilon_\sigma^{\lambda_4}(q_2), \quad (\text{E.22})$$

where $i, j = \gamma, Z$. Graphically we have



The \tilde{F} functions for ZZ^* production are expressed in terms of the partonic helicity amplitudes by

$$\begin{aligned}
\tilde{F}_1^{ijkl} &= \sum_{\lambda_1, \lambda_2, \lambda_3, \lambda_4} \mathcal{M}_{gg \rightarrow ik}^{\lambda_1 \lambda_2 \lambda_3 \lambda_4} \left(\mathcal{M}_{gg \rightarrow jl}^{\lambda_1 \lambda_2 \lambda_3 \lambda_4} \right)^* \\
\tilde{F}_2^{ijkl} &= 2 \sum_{\lambda_3, \lambda_4} \text{Re} \left[\mathcal{M}_{gg \rightarrow ik}^{++\lambda_3 \lambda_4} \left(\mathcal{M}_{gg \rightarrow jl}^{--\lambda_3 \lambda_4} \right)^* \right], \\
\tilde{F}_{2'}^{ijkl} &= 2 \sum_{\lambda_3, \lambda_4} \text{Im} \left[\mathcal{M}_{gg \rightarrow ik}^{++\lambda_3 \lambda_4} \left(\mathcal{M}_{gg \rightarrow jl}^{--\lambda_3 \lambda_4} \right)^* \right], \\
\tilde{F}_{3\pm}^{ijkl} &= 2 \sum_{\lambda, \lambda_3, \lambda_4} \text{Re} \left[\mathcal{M}_{gg \rightarrow ik}^{\lambda - \lambda_3 \lambda_4} \left(\mathcal{M}_{gg \rightarrow jl}^{\lambda + \lambda_3 \lambda_4} \right)^* \pm \mathcal{M}_{gg \rightarrow ik}^{+\lambda \lambda_3 \lambda_4} \left(\mathcal{M}_{gg \rightarrow jl}^{-\lambda \lambda_3 \lambda_4} \right)^* \right], \\
\tilde{F}_{3'\pm}^{ijkl} &= 2 \sum_{\lambda, \lambda_3, \lambda_4} \text{Im} \left[\mathcal{M}_{gg \rightarrow ik}^{\lambda - \lambda_3 \lambda_4} \left(\mathcal{M}_{gg \rightarrow jl}^{\lambda + \lambda_3 \lambda_4} \right)^* \pm \mathcal{M}_{gg \rightarrow ik}^{+\lambda \lambda_3 \lambda_4} \left(\mathcal{M}_{gg \rightarrow jl}^{-\lambda \lambda_3 \lambda_4} \right)^* \right], \\
\tilde{F}_4^{ijkl} &= 2 \sum_{\lambda_3, \lambda_4} \text{Re} \left[\mathcal{M}_{gg \rightarrow ik}^{+-\lambda_3 \lambda_4} \left(\mathcal{M}_{gg \rightarrow jl}^{-+\lambda_3 \lambda_4} \right)^* \right], \\
\tilde{F}_{4'}^{ijkl} &= 2 \sum_{\lambda_3, \lambda_4} \text{Im} \left[\mathcal{M}_{gg \rightarrow ik}^{+-\lambda_3 \lambda_4} \left(\mathcal{M}_{gg \rightarrow jl}^{-+\lambda_3 \lambda_4} \right)^* \right].
\end{aligned} \tag{E.23}$$

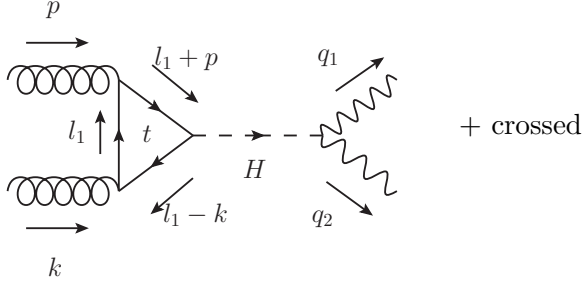
$$\begin{aligned}
\hat{s} &\equiv (p+k)^2, \\
\hat{t} &\equiv (p-q_1)^2, \\
\hat{u} &\equiv (k-q_1)^2, \\
p^2 &= k^2 = 0, \\
q_1^2 &= M_1^2, \\
q_2^2 &= (p+k-q_1)^2 = M_2^2.
\end{aligned} \tag{E.24}$$

E.3.1 The sub-process $gg \rightarrow H \rightarrow ij$

There is a tree-level coupling of the Z -boson to the Higgs, so the dominant contribution in $gg \rightarrow H \rightarrow ij$ is given by $gg \rightarrow H \rightarrow ZZ$ and so, as a first approximation, we will take

$$\mathcal{M}_{gg \rightarrow H \rightarrow \gamma Z}^{\lambda_1 \lambda_2 \lambda_3 \lambda_4} = \mathcal{M}_{gg \rightarrow H \rightarrow Z \gamma}^{\lambda_1 \lambda_2 \lambda_3 \lambda_4} = \mathcal{M}_{gg \rightarrow H \rightarrow \gamma \gamma}^{\lambda_1 \lambda_2 \lambda_3 \lambda_4} = 0. \tag{E.25}$$

The dominant contribution to $gg \rightarrow H \rightarrow ZZ$ process is given by the diagram



The corresponding helicity amplitude can be written as

$$\mathcal{M}_{gg \rightarrow H \rightarrow ZZ}^{\lambda_1 \lambda_2 \lambda_3 \lambda_4} = C_H \epsilon^{\lambda_3}(q_1) \cdot \epsilon^{\lambda_4}(q_2) \epsilon_{\mu}^{\lambda_1}(p) \epsilon_{\nu}^{\lambda_2}(k)^* \int d^D l \frac{\text{Tr} [\gamma^{\mu}(\not{l} + m_t) \gamma^{\nu}(\not{l} - \not{k} + m_t)(\not{l} + \not{p} + m_t)]}{(l^2 - m_t^2 + i\delta)((l+p)^2 - m_t^2 + i\delta)((l-k)^2 - m_t^2 + i\delta)} + (p \leftrightarrow k), \quad (\text{E.26})$$

where the overall factor C_H is given by

$$C_H = \frac{1}{i} (-1) (ig_s)^2 \frac{1}{2} \delta^{ab} i^3 \left(\frac{-igm_t}{2m_W} \right) \frac{1}{(2\pi)^4} \frac{i}{\hat{s} - m_H^2 + i\Gamma_H m_H} \frac{igm_Z}{\cos \theta_W} \quad (\text{E.27})$$

$$= -i\alpha_s \delta^{ab} 2\sqrt{2} G_F m_Z^2 m_t \frac{1}{(2\pi)^3} \frac{1}{\hat{s} - m_H^2 + i\Gamma_H m_H}. \quad (\text{E.28})$$

After performing the trace and tensor reduction the amplitude can be written as

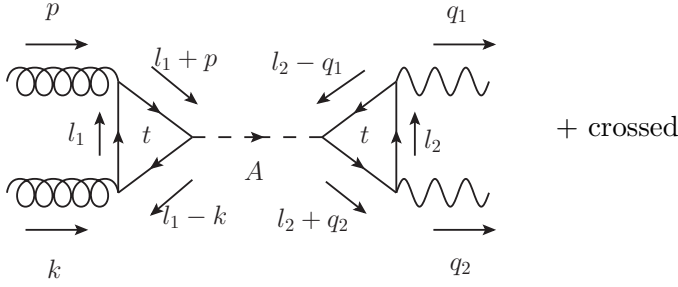
$$\mathcal{M}_{gg \rightarrow H \rightarrow ZZ}^{\lambda_1 \lambda_2 \lambda_3 \lambda_4} = 4i\pi^2 m_t C_H \left[(4m_t^2 - \hat{s}) C_0(0, 0, \hat{s}, m_t^2, m_t^2, m_t^2) + 2 \right] \begin{cases} 1 & \begin{matrix} +++ \\ ++-- \\ --++ \\ ---- \end{matrix} \\ \frac{\hat{s} - M_1^2 - M_2^2}{2M_1 M_2} & \begin{matrix} ++00 \\ --00 \end{matrix} \\ 0 & \text{rest} \end{cases} \quad (\text{E.29})$$

E.3.2 The sub-process $gg \rightarrow A \rightarrow ij$

We assume that the pseudoscalar Higgs couples only to fermions and with a vertex

$$t \begin{array}{c} \nearrow \\ \searrow \\ \nearrow \\ \searrow \end{array} \text{---} A = -\frac{gg_t m_t}{2m_W} \gamma_5$$

The main contribution to the process $gg \rightarrow A \rightarrow ij$ will therefore be given by



The corresponding helicity amplitude can be written as

$$\begin{aligned} \mathcal{M}_{gg \rightarrow A \rightarrow ij}^{\lambda_1 \lambda_2 \lambda_3 \lambda_4} &= C_A \int d^D l_1 \frac{\epsilon_\mu^{\lambda_1}(p)^* \epsilon_\nu^{\lambda_2}(k)^* \text{Tr} [\gamma^\mu (\not{l}_1 + m_t) \gamma^\nu (\not{l}_1 - \not{k} + m_t) \gamma^5 (\not{l}_1 + \not{p} + m_t)]}{(l_1^2 - m_t^2 + i\delta)((l_1 + p)^2 - m_t^2 + i\delta)((l_1 - k)^2 - m_t^2 + i\delta)} \times \\ &\int d^D l_2 \\ &\frac{\epsilon_\mu^{\lambda_3}(q_1) \epsilon_\nu^{\lambda_4}(q_2) \text{Tr} [\gamma^\mu (g_V^{ti} + g_A^{ti} \gamma^5) (\not{l}_2 + m_t) \gamma^\nu (g_V^{tj} + g_A^{tj} \gamma^5) (\not{l}_2 + \not{q}_2 + m_t) \gamma^5 (\not{l}_2 - \not{q}_1 + m_t)]}{(l_2^2 - m_t^2 + i\delta)((l_2 - q_1)^2 - m_t^2 + i\delta)((l_2 + q_2)^2 - m_t^2 + i\delta)} \\ &+ \left(\begin{array}{c} p \leftrightarrow k \\ \lambda_1 \leftrightarrow \lambda_2 \end{array} \right) + \left(\begin{array}{c} q_1 \leftrightarrow q_2 \\ \lambda_3 \leftrightarrow \lambda_4 \end{array} \right), \quad (\text{E.30}) \end{aligned}$$

where the overall factor C_A is given by

$$\begin{aligned} C_A &= \frac{1}{i} (-1) (i g_s)^2 i^3 \left(\frac{-g g_t m_t}{2m_W} \right) \frac{1}{(2\pi)^4} \frac{i}{\hat{s} - m_H^2 + i\Gamma_H m_H} (-1) N_c i^3 \left(\frac{-g g_t m_t}{2m_W} \right) \frac{1}{(2\pi)^4} \\ &= \frac{2\sqrt{2} G_F \alpha_s N_c g_t^2}{(2\pi)^7} \frac{m_t^2}{\hat{s} - m_H^2 + i\Gamma_H m_H}. \quad (\text{E.31}) \end{aligned}$$

After performing the traces and tensor reduction, the amplitude can be written as

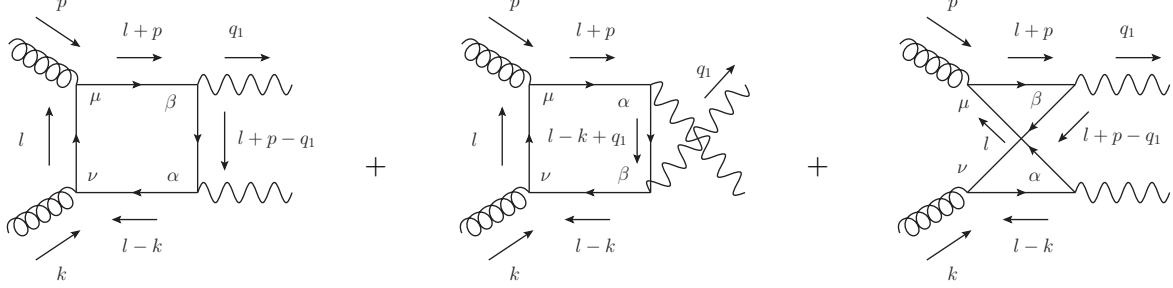
$$\begin{aligned} \mathcal{M}_{gg \rightarrow A \rightarrow ij}^{\lambda_1 \lambda_2 \lambda_3 \lambda_4} &= C_A \left[-8\pi^2 m_t \epsilon^{pk\epsilon(p)*\epsilon(k)*} C_0(0, 0, \hat{s}, m_t^2, m_t^2, m_t^2) \right] \frac{-8\pi^2 m_t \epsilon^{q_1 q_2 \epsilon(q_1) \epsilon(q_2)}}{(\hat{s} - M_1^2 - M_2^2)^2 - 4M_1^2 M_2^2} \\ &\left\{ \left[\left(g_V^{ti} g_V^{tj} + g_A^{ti} g_A^{tj} \right) (M_1^2 - M_2^2)^2 + \hat{s}^2 \left(g_V^{ti} g_V^{tj} - g_A^{ti} g_A^{tj} \right) - 2g_V^{ti} g_V^{tj} \hat{s} (M_1^2 + M_2^2) \right] \times \right. \\ &C_0(M_1^2, M_2^2, \hat{s}, m_t^2, m_t^2, m_t^2) + 2g_A^{ti} g_A^{tj} (M_1^2 - M_2^2 + s) B_0(M_1^2, m_t^2, m_t^2) \\ &\left. + 2g_A^{ti} g_A^{tj} (M_2^2 - M_1^2 + s) B_0(M_2^2, m_t^2, m_t^2) - 4g_A^{ti} g_A^{tj} \hat{s} B_0(\hat{s}, m_t^2, m_t^2) \right] \}. \quad (\text{E.32}) \end{aligned}$$

The vector and axial-vector coupling strengths are given by

$$\begin{aligned} g_A^{tZ} &= -\frac{ig}{4 \cos \theta_W}, \\ g_V^{tZ} &= \frac{ig}{4 \cos \theta_W} \left(1 - \frac{8}{3} \sin^2 \theta_W \right), \\ g_A^{t\gamma} &= 0, \\ g_V^{t\gamma} &= ie \frac{2}{3}, \\ g &= 2^{5/4} M_W \sqrt{G_F}. \quad (\text{E.33}) \end{aligned}$$

E.3.3 The sub-process $gg \rightarrow \text{box} \rightarrow ij$

The diagrams contributing to the process $gg \rightarrow \text{fermion box} \rightarrow ZZ$ are



plus the diagrams with a reversed charge flow.

The helicity amplitudes can be written as

$$\begin{aligned}
\mathcal{M}_{gg \rightarrow \text{Box} \rightarrow ij}^{\lambda_1 \lambda_2 \lambda_3 \lambda_4} &= \frac{1}{i} 4\pi \alpha_s \sum_{q=u,d,s,c,b} \epsilon_\mu^{\lambda_1}(p)^* \epsilon_\nu^{\lambda_2}(k)^* \epsilon_\beta^{\lambda_3}(q_1) \epsilon_\alpha^{\lambda_4}(q_2) \int \frac{d^D l}{(2\pi)^D} \times \\
&\left\{ \frac{\text{Tr}[\gamma^\mu \not{l} \gamma^\nu (\not{l} - \not{k}) \gamma^\alpha (g_V^{qj} + g_A^{qj} \gamma^5) (\not{l} + \not{p} - \not{q}_1) \gamma^\beta (g_V^{qi} + g_A^{qi} \gamma^5) (\not{l} + \not{p})]}{l^2 (l+p)^2 (l-k)^2 (l+p-q_1)^2} \right. \\
&+ \frac{\text{Tr}[\gamma^\mu \not{l} \gamma^\nu (\not{l} - \not{k}) \gamma^\beta (g_V^{qj} + g_A^{qj} \gamma^5) (\not{l} - \not{k} + \not{q}_1) \gamma^\alpha (g_V^{qi} + g_A^{qi} \gamma^5) (\not{l} + \not{p})]}{l^2 (l+p)^2 (l-k)^2 (l-k+q_1)^2} \\
&\left. + \frac{\text{Tr}[\gamma^\mu \not{l} \gamma^\alpha (g_V^{qj} + g_A^{qj} \gamma^5) (\not{l} + \not{p} + \not{k} - \not{q}_1) \gamma^\nu (\not{l} + \not{p} - \not{q}_1) \gamma^\beta (g_V^{qi} + g_A^{qi} \gamma^5) (\not{l} + \not{p})]}{l^2 (l+p)^2 (l+p-q_1)^2 (l+p+k-q_1)^2} \right\} + \text{rev}
\end{aligned} \tag{E.34}$$

The reversed charge flow diagrams produce the same traces, but with $g_A \rightarrow -g_A$. This implies that there will be no terms proportional to $g_A g_V$, but only g_V^2 and g_A^2 . The latter two will be equal, which you can see by moving the second γ^5 to the left. The matrix element can therefore be written as

$$\mathcal{M}_{gg \rightarrow \text{Box} \rightarrow ij}^{\lambda_1 \lambda_2 \lambda_3 \lambda_4} = -\frac{\alpha_s}{\pi} \sum_{q=u,d,s,c,b} \left(g_V^{qi} g_V^{qj} + g_A^{qi} g_A^{qj} \right) M^{\lambda_1 \lambda_2 \lambda_3 \lambda_4}, \tag{E.35}$$

where M is defined as

$$\begin{aligned}
M^{\lambda_1 \lambda_2 \lambda_3 \lambda_4} &\equiv \epsilon_\mu^{\lambda_1}(p)^* \epsilon_\nu^{\lambda_2}(k)^* \epsilon_\beta^{\lambda_3}(q_1) \epsilon_\alpha^{\lambda_4}(q_2) \frac{(2\pi)^{4-D}}{-i4\pi^2} \int d^D l \\
&\left\{ \frac{\text{Tr}[\gamma^\mu \not{l} \gamma^\nu (\not{l} - \not{k}) \gamma^\alpha (\not{l} + \not{p} - \not{q}_1) \gamma^\beta (\not{l} + \not{p})]}{l^2 (l+p)^2 (l-k)^2 (l+p-q_1)^2} + \frac{\text{Tr}[\gamma^\mu \not{l} \gamma^\nu (\not{l} - \not{k}) \gamma^\beta (\not{l} - \not{k} + \not{q}_1) \gamma^\alpha (\not{l} + \not{p})]}{l^2 (l+p)^2 (l-k)^2 (l-k+q_1)^2} \right. \\
&\left. + \frac{\text{Tr}[\gamma^\mu \not{l} \gamma^\alpha (\not{l} + \not{p} + \not{k} - \not{q}_1) \gamma^\nu (\not{l} + \not{p} - \not{q}_1) \gamma^\beta (\not{l} + \not{p})]}{l^2 (l+p)^2 (l+p-q_1)^2 (l+p+k-q_1)^2} \right\}. \tag{E.36}
\end{aligned}$$

The coupling strengths are given by

$$\begin{aligned}
g_A^{dZ} &= -g_A^{uZ} = \frac{ig}{4 \cos \theta_W}, \\
g_V^{uZ} &= \frac{ig}{4 \cos \theta_W} \left(1 - \frac{8}{3} \sin^2 \theta_W \right), \\
g_V^{dZ} &= \frac{ig}{4 \cos \theta_W} \left(1 + \frac{4}{3} \sin^2 \theta_W \right), \\
g_A^{q\gamma} &= 0, \\
g_V^{q\gamma} &= ieQ_q, \\
g &= 2^{5/4} M_W \sqrt{G_F}.
\end{aligned} \tag{E.37}$$

From the structure of the polarization vectors we can infer that

$$M^{\lambda_1 \lambda_2 \lambda_3 \lambda_4} = \pm M^{-\lambda_1 - \lambda_2 - \lambda_3 - \lambda_4}, \tag{E.38}$$

where \pm is for even/odd number of longitudinal polarizations. This can be seen by first realizing that the tensor structure of the amplitude can be written only in terms of p^μ , k^μ , q_1^μ and $g^{\mu\nu}$'s. The only way a χ^μ can be contracted with this in a non-zero way is with a $g^{\mu\nu}$ and another χ^μ . Therefore, an amplitude with just \pm polarizations, will always have an even number of λ 's in every term, and so $\lambda \rightarrow -\lambda$ will leave the amplitude unchanged. If there is a single longitudinal polarization in the amplitude, the number of λ 's will always be odd, etc. The structure of the polarization vectors also implies that

$$M^{\lambda_1 \lambda_2 \lambda_3 \lambda_4} = M^{\lambda_1 \lambda_2 - \lambda_3 - \lambda_4} \Big|_{A \rightarrow -A}. \tag{E.39}$$

Another relation comes from the fact that the diagrammatic structure is unchanged by flipping all diagrams upside down and therefore

$$M^{\lambda_1 \lambda_2 \lambda_3 \lambda_4} = M^{\lambda_2 \lambda_1 \lambda_4 \lambda_3}. \tag{E.40}$$

By combining those relations, one gets that

$$\begin{aligned}
M^{++--} &= M^{++++} \Big|_{A \rightarrow -A} \\
M^{+++-} &= M^{+++-} \\
M^{+---} &= M^{+---} \\
M^{+--+} &= M^{+--+} \Big|_{A \rightarrow -A} \\
M^{++0+} &= M^{++0+} \\
M^{++-0} &= M^{++-0} = M^{++0+} \Big|_{A \rightarrow -A} \\
M^{+-0-} &= -M^{+-0-} \\
M^{+--0} &= -M^{+--0} = M^{+-+0} \Big|_{A \rightarrow -A}
\end{aligned} \tag{E.41}$$

With the use of the relations between the box amplitudes, there are only 8 independent amplitudes left that have to be calculated, being M^{++++} , M^{+++-} , M^{+---} , M^{+--+} , M^{++0+} , M^{+-+0} , M^{+-0-} and M^{+--0} .

Appendix F

Scalar integrals

The definitions of the scalar integrals are

$$B_0(p_1^2, m_1^2, m_2^2) \equiv \frac{(2\pi\mu)^{4-D}}{i\pi^2} \int d^D l \frac{1}{[l^2 - m_1^2 + i\delta][(l + p_1)^2 - m_2^2 + i\delta]}, \quad (\text{F.1})$$

$$C_0(p_1^2, p_2^2, (p_1 + p_2)^2, m_1^2, m_2^2, m_3^2) \equiv \frac{(2\pi\mu)^{4-D}}{i\pi^2} \int d^D l \times \frac{1}{[l^2 - m_1^2 + i\delta][(l + p_1)^2 - m_2^2 + i\delta][(l + p_1 + p_2)^2 - m_3^2 + i\delta]} \quad (\text{F.2})$$

and

$$D_0(p_1^2, p_2^2, p_3^2, p_4^2, (p_1 + p_2)^2, (p_2 + p_3)^2, m_1^2, m_2^2, m_3^2, m_4^2) \equiv \frac{(2\pi\mu)^{4-D}}{i\pi^2} \int \frac{d^D l}{[l^2 - m_1^2 + i\delta]} \times \frac{1}{[(l + p_1)^2 - m_2^2 + i\delta][(l + p_1 + p_2)^2 - m_3^2 + i\delta][(l + p_1 + p_2 + p_3)^2 - m_4^2 + i\delta]}. \quad (\text{F.3})$$

Some analytical expressions are

$$B_0(\hat{s}, m^2, m^2) = \left(\frac{\mu^2}{m^2}\right)^\epsilon \left[\frac{1}{\epsilon} + 2 + \sqrt{1 - \frac{4m^2}{\hat{s}}} \log \left(\frac{\sqrt{1 - \frac{4m^2}{\hat{s}}} - 1}{\sqrt{1 - \frac{4m^2}{\hat{s}}} + 1} \right) \right] \quad (\text{F.4})$$

and

$$C_0(0, 0, \hat{s}, m^2, m^2, m^2) = \frac{1}{2\hat{s}} \log^2 \left(\frac{\sqrt{1 - \frac{4m^2}{\hat{s}}} - 1}{\sqrt{1 - \frac{4m^2}{\hat{s}}} + 1} \right). \quad (\text{F.5})$$

In general the scalar integrals are evaluated numerically using LoopTools [138].

Polarisatie-effecten in proton-protonbotsingen binnen het Standaardmodel en daar voorbij

Nederlandse samenvatting

Alle 60 miljoen bekende scheikundige stoffen kunnen worden opgebouwd uit niet meer dan 118 bouwstenen, atomen genaamd. Door atomen op verschillende manieren met elkaar te verbinden ontstaat materie met totaal verschillende eigenschappen, van water en zand tot geneesmiddelen als ibuprofen. Net zoals legosteentjes is maar een zeer beperkt aantal verschillende bouwstenen nodig om een gigantisch grote verscheidenheid aan producten te kunnen maken.

Als we kijken naar waar de atomen zelf uit opgebouwd zijn, dan zien we dat slechts drie verschillende bouwstenen nodig zijn: elektronen, up-quarks en down-quarks. De quarks vormen protonen en neutronen waaruit de atoomkern bestaat. De elektronen vormen vervolgens een wolk om deze atoomkern heen. Door de materie op kleinere en kleinere lengteschalen te bekijken, hebben we 60 miljoen stoffen gereduceerd tot slechts *drie* bouwstenen.

In de deeltjesfysica, de wetenschappelijke discipline die zich bezighoudt met onderzoek naar de kleinste bouwstenen van de natuur, is daarom de leidende gedachte dat de natuur eenvoudiger wordt door te kijken op steeds kleinere lengteschalen wat overeenkomt met hogere energie. Hoe kleiner de lengteschaal (en dus hoe hoger de energie) waarop de natuur onderzocht wordt, hoe minder verschillende vormen van materie er zijn en hoe meer symmetrie de natuur heeft. Men verwacht daarom dat de natuur bij zeer hoge energie (korte afstandsschalen) te beschrijven valt met een eenvoudige theorie waaruit alle fenomenen die plaatsvinden bij lage energie (en lange afstandsschalen) af te leiden zijn.

In hun poging om de natuur te onderzoeken bij voortdurend hogere energie maken deeltjesfysici gebruik van deeltjesversnellers die deeltjes versnellen in tegenovergestelde richtingen tot elkaar dicht bij de lichtsnelheid om ze vervolgens op elkaar te laten botsen. Door te onderzoeken welke verschillende nieuwe deeltjes gemaakt worden in de botsingen kunnen conclusies getrokken worden over hoe de natuur zich gedraagt bij grote energie. Vooruitgang in de deeltjesfysica heeft voornamelijk geleund op steeds hoog-energetischere (en grotere) deeltjesversnellers.

De deeltjesversnellers die de hoogste energie kunnen behalen maken gebruik van protonen om te versnellen. De reden hiervoor is dat protonen veel minder energie verliezen dan elektronen als ze worden afgebogen. Protonversnellers hebben daarom bijna altijd het energierecord in handen gehad en momenteel is dit record in handen van een protonversneller met de naam Large Hadron Collider (LHC) die deel uitmaakt van het onderzoekscentrum CERN in Genève.

Een notoir probleem met protonversnellers is de moeilijkheid om protonbotsingen theoretisch nauwkeurig te beschrijven. Zulke theoretische beschrijvingen van wat er in een botsing gebeurt zijn noodzakelijk om de gegevens die uit de experimenten komen te interpreteren. De moeilijkheid van de beschrijving zit hem in het feit dat protonen geen elementaire deeltjes zijn, maar gebonden toestanden van quarks waarvan de exacte structuur, tot op heden, niet uitgerekend kan worden.

Om toch een beschrijving te kunnen geven van de botsingen, kan het proton voorgesteld worden als een collectie partonen (quarks, anti-quarks en gluonen) die allemaal in dezelfde richting bewegen als het proton en daarbij een fractie x van de impuls van het proton bij zich dragen. De hoeveelheid partonen bij een gegeven impulsfractie x wordt beschreven door een zogenaamde partondistributiefunctie, die niet te berekenen is en daarom in experimenten gemeten moet worden. Dit simpele empirische model is bedacht door de natuurkundige Feynman en wordt het partonmodel genoemd. Inmiddels is dit empirische model uitgebreid en op een solide theoretische basis gebracht binnen het raamwerk van de quantumveldentheorie. Er wordt nu aan gerefereerd als *collineaire factorisatie* en het vormt de basis voor de meeste theoretische beschrijvingen van proton-protonbotsingen.

De daadwerkelijke beweging van de partonen binnenin een proton is echter complexer en een beschrijving waarin alle partonen collineair met het proton bewegen volstaat dan ook niet altijd. Voor sommige observabelen in een protonbotsing is het noodzakelijk om ook de transversale beweging van de partonen te beschouwen. Het theoretische raamwerk waarin dit gebeurt is de zogenaamde *Transverse Momentum Dependent (TMD) factorization*, wat voornamelijk gebruikt zal worden in dit proefschrift.

Binnen het kader van de TMD-factorisatie is er ruimte voor allerlei ‘nieuwe’ effecten die niet aanwezig zijn in de collineaire beschrijving van het proton. Zo zou het bijvoorbeeld kunnen dat up-quarks meer naar rechts bewegen en de down-quarks meer naar links binnen een gepolariseerd proton (als we de spinrichting omhoog kiezen en kijken in de richting waarin het proton beweegt), een effect dat bekend staat als het Sivers effect. Ook kan het zijn dat de quarks meer gepolariseerd zijn naarmate ze meer bewegen in de richting van de spin van het proton, wat we het worm-gear effect zullen noemen. Weer een ander effect dat afwezig is in de collineaire beschrijving is de lineaire polarisatie van gluonen in een ongepolariseerd proton. In dit proefschrift zijn een aantal van deze nieuwe effecten onderzocht die relevant kunnen zijn voor experimenten die momenteel gedaan worden bij CERNs LHC en bij de Relativistic Heavy Ion Collider (RHIC) op Brookhaven National Laboratory.

Zo is onderzocht wat de invloed is van het genoemde Sivers en worm-gear effect op zogenaamde transversale spin asymmetrieën die gemeten gaan worden bij RHIC. Deze effecten waren al eerder onderzocht, maar daarbij werd ervan uitgegaan dat de analyse uitgevoerd zou worden in een bepaald referentiestelsel, genaamd het Collins-Soperstelsel. Het gebruik van dat specifieke referentiestelsel is echter niet altijd even praktisch en soms zelfs onmogelijk. We hebben daarom de effecten uitgerekend in het zogenaamde laboratoriumstelsel dat *wel* altijd makkelijk te gebruiken is.

We hebben de invloed van de nieuwe TMD-effecten op spin asymmetrieën in twee verschillende processen berekend, zijnde het Drell-Yan process waarin via een virtueel foton een muonpaar geproduceerd wordt en productie van W -bosonen met een verval naar neutrinos en geladen leptonen. Het eerste proces gaat gebruikt worden om de transversale spindistributie van quarks te bepalen. Onze berekeningen tonen aan dat de invloed van TMD-effecten klein is. Dit is gunstig, omdat dit betekent dat de analyse uitgevoerd kan worden in het laboratoriumstelsel in

plaats van het moeilijker te bepalen Collins-Soperstelsel, wat de analyse vereenvoudigt.

Het andere proces, W -boson productie, kan gebruikt worden om te zoeken naar nieuwe deeltjes die niet eerder ontdekt zijn. Onze berekeningen laten zien dat de TMD-effecten in principe eenzelfde signaal kunnen genereren als een nieuw deeltje, maar dat de grootte van het signaal zodanig klein is dat het niet gemeten kan worden bij RHIC. Ook dit is gunstig, omdat deze effecten dus niet de zoektocht naar nieuwe deeltjes kunnen verstoren. Ondanks dat de effecten klein zijn, blijken ze wel vele malen groter te zijn dan wat je in eerste instantie zou verwachten. Dit is een belangrijke gegeven dat van pas kan komen bij toekomstige berekeningen van TMD-effecten.

Gegeven het feit dat TMD-effecten klein zijn, kan het W -boson productieproces dus gebruikt worden om naar nieuwe deeltjes, ofwel natuurkunde voorbij het Standaardmodel te zoeken bij RHIC. De vraag die dan rest is natuurlijk: hoe gevoelig zullen deze metingen bij RHIC zijn voor nieuwe fysica? Om dit te beantwoorden hebben we gekeken naar experimentele observabelen die gelijksoortige nieuwe fysica begrenzen. We hebben samengevat wat de sterkste, modelonafhankelijke grenzen hierop zijn en concluderen dat RHIC op ontwerpcapaciteit de grenzen niet zal verbeteren. Wel kan op een onafhankelijke manier de bestaande grens geverifieerd worden. Deze conclusies kunnen relevant zijn voor het bepalen welke experimenten bij de RHIC versneller prioriteit dienen te krijgen.

Binnen het raamwerk van de TMD-factorisatie kunnen, zoals eerder gezegd, de gluonen binnenin het proton lineair gepolariseerd zijn, zelfs als het proton zelf niet gepolariseerd is. Dit is van belang voor de LHC waar, door ongepolariseerde protonen op elkaar te laten botsen, gezocht wordt naar het Higgsdeeltje. We hebben daarom onderzocht wat de invloed van gluonpolarisatie op de productie van Higgsdeeltjes zal zijn.

Onze berekeningen tonen aan dat de totale hoeveelheid Higgsdeeltjes die geproduceerd zal worden in de LHC niet verandert, maar dat de snelheid die ze zullen hebben *wel* verandert. Ook hebben we laten zien dat de snelheidsverdeling voor een Higgsdeeltje zoals voorspeld door het Standaardmodel *anders* is dan die van een zogenaamd pseudoscalair Higgsdeeltje dat voorspeld wordt door andere modellen. Dit is een zeer prettige bijkomstigheid, omdat de snelheidsverdeling dus in principe gebruikt kan worden om te bepalen of een nieuw gevonden deeltje daadwerkelijk het Higgsdeeltje uit het Standaardmodel is of iets anders. Deze mogelijkheid was nog niet eerder bekend en kan de analyse van de LHC data omtrent het Higgsdeeltje aanzienlijk vereenvoudigen.

Dankwoord

Allereerst wil ik mijn begeleider Daniël Boer bedanken voor de mogelijkheid om, na een geslaagd masteronderzoek onder zijn begeleiding, door te gaan met een promotieonderzoek. Bedankt ook voor je enthousiasme, betrokkenheid, nauwkeurigheid, je positieve insteek en je goede ideeën, want niets is zo belangrijk in de wetenschap als een goed idee. Je positieve houding is een grote steun geweest. Wanneer ik soms het idee had dat resultaten tegenvielen of niet interessant waren, wist jij me altijd weer te overtuigen dat het wel degelijk van belang was wat we deden en kon ik weer met frisse moed aan de slag. Ik stel het ook zeer op prijs dat je me meenam naar conferenties in de VS, waar je me liet kennismaken met de collegaonderzoekers in het veld. Ook waardeer ik al het correctiewerk dat je verricht hebt voor mijn manuscript zeer, zelfs na vele iteraties blijf jij scherp en mis je geen enkele fout. Als laatste wil ik je bedanken voor het aanbevelen van mij bij collegaonderzoekers en daarmee het scheppen van de mogelijkheid om door te gaan in de wetenschap.

Mijn promotor Piet Mulders wil ik ook bedanken voor de mogelijkheid tot het doen van promotieonderzoek. Bedankt ook voor jouw ‘DIS notes’, die voor mij het standaardwerk op het gebied van de TMD-factorisatie vormen, als ook voor het altijd bereid zijn vragen hierover te beantwoorden. Daarnaast ben ik ook erg blij met de prettig samenwerking bij het geven van het vak quantummechanica, waarvoor ik werkcollege-assistent was. Als laatste wil ik ook jou bedanken voor het schrijven van aanbevelingsbrieven.

De derde persoon die zich bezig heeft gehouden met de voortgang van het promotieonderzoek en ook wel de C3-persoon genoemd wordt is Stan Bentvelsen. Jou wil ik bedanken voor je onafhankelijke ‘bird-eye view’ op ons onderzoek, je concrete tips en vooral ook je enthousiasme. Marja Herronen wil ik bedanken voor al haar hulp bij het regelen van alle praktische zaken omtrent het doen van een promotieonderzoek.

Then I would like to thank all the people I collaborated with in the past years: Aram Kotzinian, Cristian Pisano, Marc Schlegel, and Werner Vogelsang. In particular I would also like to thank Werner Vogelsang for giving me the opportunity to continue doing what I like in Tübingen and also for his understanding on how difficult such a decision is. His flexibility and understanding really made me accept the offer, thanks for this. I am also very much indebted to Eric Laenen for allowing me to be a regular guest at the Nikhef institute for the coming years.

I am also very grateful that Rob Timmermans, Robert Fleischer, Mauro Anselmino, and Werner Vogelsang were willing to be part of the reading committee, as I know that that must be very time consuming. Thank you for that.

The past four years have not only been hard work, but also fun. I do not want to elaborate too much on this, but I do want you to know that I am really happy with the pleasurable working environment provided by: Ana Julia Mizher, Ben Bakker, Bert Schellekens, Damien George, Erik Wessels, Gerco Onderwater, Giuseppe d’Ambrosi, Giuseppe Dibitto, Irene Niessen, Ivano

Lodato, Jacob Noordmans, Jan Kuipers, Jan Weenink, Jan-Willem van Holten, Jordy de Vries, Jorn Boomsma, Jory Sonneveld, Jos Vermaseren, Keri Vos, Krijn de Vries, Lisa Hartgring, Lotje Wansbeek, Maarten Buffing, Marco Volponi, Marieke Postma, Mathieu Blom, Mert Aybat, Olena Romanets, Reinier de Adelhart Toorop, Rob Kneijens, Rob Timmermans, Robbert Rietkerk, Robert Fleischer, Sander Mooij, Shreyas Raghunathan, Sophie Schlessler, Thijs Stegeman, Thijs van den Broek, Thomas van Dijk, Tiago Nunes, Valentin Reys and Yiannis Malamos.

In het bijzonder wil ik Lisa en Jordy bedanken, niet alleen omdat zij paranimf willen zijn, maar ook omdat het echt goede vrienden zijn geworden.

Als laatste wil ik Hannah bedanken voor haar steun in periodes dat ik er misschien wat minder zin in had, als ook voor het zorgen voor afleiding in de periodes dat ik er misschien wat *teveel* zin in had. Ik ben je ook heel dankbaar voor je begrip dat ik naar Duitsland ga om door te gaan in de wetenschap en natuurlijk gewoon voor het zijn van een lieve vriendin.

Bibliography

- [1] <http://www.cas.org/news/media-releases/60-millionth-substance>
- [2] D. Boer and P. J. Mulders, Nucl. Phys. B **569**, 505 (2000) [hep-ph/9906223].
- [3] A. V. Belitsky, X. Ji and F. Yuan, Nucl. Phys. B **656**, 165 (2003) [hep-ph/0208038].
- [4] D. Boer, P. J. Mulders and F. Pijlman, Nucl. Phys. B **667**, 201 (2003) [hep-ph/0303034].
- [5] M. G. A. Buffing and P. J. Mulders, JHEP **1107**, 065 (2011) [arXiv:1105.4804 [hep-ph]].
- [6] J. C. Collins, Acta Phys. Polon. B **34**, 3103 (2003) [hep-ph/0304122].
- [7] J. C. Collins, T. C. Rogers and A. M. Stasto, Phys. Rev. D **77**, 085009 (2008) [arXiv:0708.2833 [hep-ph]].
- [8] J. C. Collins and D. E. Soper, Nucl. Phys. B **194**, 445 (1982).
- [9] J. Collins, PoS LC **2008**, 028 (2008) [arXiv:0808.2665 [hep-ph]].
- [10] X. -d. Ji, J. -p. Ma and F. Yuan, Phys. Rev. D **71**, 034005 (2005) [hep-ph/0404183].
- [11] X. -d. Ji, J. -P. Ma and F. Yuan, Phys. Lett. B **597**, 299 (2004) [hep-ph/0405085].
- [12] J. C. Collins and A. Metz, Phys. Rev. Lett. **93**, 252001 (2004) [hep-ph/0408249].
- [13] J. C. Collins, D. E. Soper and G. F. Sterman, Nucl. Phys. B **250**, 199 (1985).
- [14] B. U. Musch, P. Hagler, J. W. Negele and A. Schafer, Phys. Rev. D **83**, 094507 (2011) [arXiv:1011.1213 [hep-lat]].
- [15] B. U. Musch, P. Hagler, M. Engelhardt, J. W. Negele and A. Schafer, Phys. Rev. D **85**, 094510 (2012) [arXiv:1111.4249 [hep-lat]].
- [16] M. G. A. Buffing, A. Mukherjee and P. J. Mulders, arXiv:1207.3221 [hep-ph].
- [17] R. Brock *et al.* [CTEQ Collaboration], Rev. Mod. Phys. **67**, 157 (1995).
- [18] V. N. Gribov and L. N. Lipatov, Sov. J. Nucl. Phys. **15**, 438 (1972) [Yad. Fiz. **15**, 781 (1972)].
- [19] G. Altarelli and G. Parisi, Nucl. Phys. B **126**, 298 (1977).
- [20] J. Collins, Int. J. Mod. Phys. Conf. Ser. **4**, 85 (2011) [arXiv:1107.4123 [hep-ph]].

-
- [21] J. Collins, “Foundations of perturbative QCD,” (Cambridge monographs on particle physics, nuclear physics and cosmology. 32)
- [22] S. M. Aybat and T. C. Rogers, Phys. Rev. D **83**, 114042 (2011) [arXiv:1101.5057 [hep-ph]].
- [23] S. M. Aybat, J. C. Collins, J. -W. Qiu and T. C. Rogers, Phys. Rev. D **85**, 034043 (2012) [arXiv:1110.6428 [hep-ph]].
- [24] P. J. Mulders and J. Rodrigues, Phys. Rev. D **63**, 094021 (2001) [hep-ph/0009343].
- [25] S. Meissner, A. Metz and K. Goeke, Phys. Rev. D **76**, 034002 (2007) [hep-ph/0703176 [HEP-PH]].
- [26] D. W. Sivers, Phys. Rev. D **41**, 83 (1990).
- [27] A. Airapetian *et al.* [HERMES Collaboration], Phys. Rev. Lett. **94**, 012002 (2005). [arXiv:hep-ex/0408013].
- [28] A. Airapetian *et al.* [HERMES Collaboration], Phys. Rev. Lett. **103**, 152002 (2009). [arXiv:0906.3918 [hep-ex]].
- [29] M. G. Alekseev *et al.* [COMPASS Collaboration], Phys. Lett. B **692**, 240 (2010). [arXiv:1005.5609 [hep-ex]].
- [30] Z. B. Kang and J. W. Qiu, Phys. Rev. Lett. **103**, 172001 (2009). [arXiv:0903.3629 [hep-ph]].
- [31] A. Metz and J. Zhou, Phys. Lett. B **700**, 11 (2011) [arXiv:1006.3097 [hep-ph]].
- [32] R. D. Tangerman and P. J. Mulders, Phys. Rev. D **51**, 3357 (1995). [arXiv:hep-ph/9403227].
- [33] B. Parsamyan, J. Phys. Conf. Ser. **295**, 012046 (2011) [arXiv:1012.0155 [hep-ex]].
- [34] J. Huang *et al.* [Jefferson Lab Hall A Collaboration], Phys. Rev. Lett. **108**, 052001 (2012) [arXiv:1108.0489 [nucl-ex]].
- [35] G. Bunce, N. Saito, J. Soffer and W. Vogelsang, Ann. Rev. Nucl. Part. Sci. **50**, 525 (2000). [arXiv:hep-ph/0007218].
- [36] C. Bourrely and J. Soffer, Nucl. Phys. B **423**, 329 (1994). [arXiv:hep-ph/9405250].
- [37] D. Boer, Phys. Rev. D **60**, 014012 (1999). [arXiv:hep-ph/9902255].
- [38] D. Boer, Phys. Rev. D **62**, 094029 (2000). [arXiv:hep-ph/0004217].
- [39] D. Boer, W. J. den Dunnen and A. Kotzinian, Phys. Rev. D **83**, 114032 (2011) [arXiv:1103.0908 [hep-ph]].
- [40] W. J. den Dunnen, D. Boer and A. Kotzinian, arXiv:1106.6164 [hep-ph].
- [41] H. Kawamura, J. Kodaira and K. Tanaka, Nucl. Phys. B **777**, 203 (2007). [arXiv:hep-ph/0703079].

- [42] H. L. Lai *et al.* [CTEQ Collaboration], *Eur. Phys. J. C* **12**, 375 (2000) [hep-ph/9903282].
- [43] P. Schweitzer, T. Teckentrup and A. Metz, *Phys. Rev. D* **81**, 094019 (2010). [arXiv:1003.2190 [hep-ph]].
- [44] M. Anselmino, M. Boglione, U. D'Alesio, A. Kotzinian, F. Murgia and A. Prokudin, *Phys. Rev. D* **71**, 074006 (2005) [arXiv:hep-ph/0501196].
- [45] M. Anselmino *et al.*, *Eur. Phys. J. A* **39**, 89 (2009). [arXiv:0805.2677 [hep-ph]].
- [46] H. Avakian, A. V. Efremov, P. Schweitzer and F. Yuan, *Phys. Rev. D* **81**, 074035 (2010). [arXiv:1001.5467 [hep-ph]].
- [47] R. Jakob, P. J. Mulders and J. Rodrigues, *Nucl. Phys. A* **626**, 937 (1997). [arXiv:hep-ph/9704335].
- [48] A. M. Kotzinian and P. J. Mulders, *Phys. Rev. D* **54**, 1229 (1996). [arXiv:hep-ph/9511420].
- [49] S. Wandzura and F. Wilczek, *Phys. Lett. B* **72**, 195 (1977).
- [50] R. D. Tangerman and P. J. Mulders, arXiv:hep-ph/9408305.
- [51] D. de Florian, R. Sassot, M. Stratmann and W. Vogelsang, *Phys. Rev. Lett.* **101**, 072001 (2008). [arXiv:0804.0422 [hep-ph]].
- [52] A. Accardi, A. Bacchetta, W. Melnitchouk and M. Schlegel, *JHEP* **0911**, 093 (2009). [arXiv:0907.2942 [hep-ph]].
- [53] B. Pasquini, S. Cazzaniga and S. Boffi, *Phys. Rev. D* **78**, 034025 (2008). [arXiv:0806.2298 [hep-ph]].
- [54] J. Zhu and B. -Q. Ma, *Phys. Lett. B* **696**, 246 (2011) [arXiv:1104.4564 [hep-ph]].
- [55] B. Parsamyan [COMPASS Collaboration], *Eur. Phys. J. ST* **162**, 89 (2008). [arXiv:0709.3440 [hep-ex]].
- [56] A. Kotzinian, B. Parsamyan and A. Prokudin, *Phys. Rev. D* **73**, 114017 (2006). [arXiv:hep-ph/0603194].
- [57] Ph. Hägler, B. U. Musch, J. W. Negele and A. Schäfer, *Europhys. Lett.* **88**, 61001 (2009). [arXiv:0908.1283 [hep-lat]].
- [58] J. C. Collins and D. E. Soper, *Phys. Rev. D* **16**, 2219 (1977).
- [59] M. Anselmino *et al.*, *Phys. Rev. D* **75**, 054032 (2007). [arXiv:hep-ph/0701006].
- [60] M. Anselmino *et al.*, *Nucl. Phys. B (Proc. Suppl.)* **191**, 98 (2009). [arXiv:0812.4366 [hep-ph]].
- [61] O. Martin and A. Schäfer, *Z. Phys. A* **358**, 429 (1997). [arXiv:hep-ph/9607470].
- [62] O. Martin, A. Schäfer, M. Stratmann and W. Vogelsang, *Phys. Rev. D* **57**, 3084 (1998). [arXiv:hep-ph/9710300].

-
- [63] V. L. Rykov, arXiv:hep-ex/9908050.
- [64] D. Boer and W. J. den Dunnen, Phys. Rev. Lett. **105**, 071801 (2010). [arXiv:1005.2956 [hep-ph]].
- [65] P. M. Nadolsky and C. P. Yuan, Nucl. Phys. B **666**, 31 (2003). [arXiv:hep-ph/0304002].
- [66] K. Nakamura *et al.* [Particle Data Group Collaboration], J. Phys. G **37**, 075021 (2010).
- [67] J. P. Ralston, D. E. Soper, Nucl. Phys. **B152**, 109 (1979).
- [68] R. N. Mohapatra and J. C. Pati, Phys. Rev. D **11**, 566 (1975).
- [69] G. Senjanovic and R. N. Mohapatra, Phys. Rev. D **12**, 1502 (1975).
- [70] G. Senjanovic, Nucl. Phys. B **153**, 334 (1979).
- [71] R. N. Mohapatra and G. Senjanovic, Phys. Rev. D **23**, 165 (1981).
- [72] N. Arkani-Hamed, A. G. Cohen, E. Katz and A. E. Nelson, JHEP **0207**, 034 (2002) [hep-ph/0206021].
- [73] M. Bando, J. Sato and T. Takahashi, Phys. Rev. D **52**, 3076 (1995) [hep-ph/9411201].
- [74] J. Sato, Prog. Theor. Phys. **96**, 597 (1996) [hep-ph/9602212].
- [75] R. N. Mohapatra and J. C. Pati, Phys. Rev. D **11**, 2558 (1975).
- [76] R. N. Mohapatra and D. P. Sidhu, Phys. Rev. D **17**, 1876 (1978).
- [77] Y. -L. Wu and Y. -F. Zhou, Sci. China G **51**, 1808 (2008) [arXiv:0709.0042 [hep-ph]].
- [78] W. -L. Guo, L. -M. Wang, Y. -L. Wu, Y. -F. Zhou and C. Zhuang, Phys. Rev. D **79**, 055015 (2009) [arXiv:0811.2556 [hep-ph]].
- [79] W. -L. Guo, Y. -L. Wu and Y. -F. Zhou, Phys. Rev. D **82**, 095004 (2010) [arXiv:1008.4479 [hep-ph]].
- [80] N. G. Deshpande, J. F. Gunion, B. Kayser and F. I. Olness, Phys. Rev. D **44**, 837 (1991).
- [81] P. Ball, J. M. Frere and J. Matias, Nucl. Phys. B **572**, 3 (2000) [hep-ph/9910211].
- [82] P. Ball and R. Fleischer, Phys. Lett. B **475**, 111 (2000) [hep-ph/9912319].
- [83] G. Barenboim, M. Gorbahn, U. Nierste and M. Raidal, Phys. Rev. D **65**, 095003 (2002) [hep-ph/0107121].
- [84] A. Maiezza, M. Nemevsek, F. Nesti and G. Senjanovic, Phys. Rev. D **82**, 055022 (2010) [arXiv:1005.5160 [hep-ph]].
- [85] G. Aad *et al.* [ATLAS Collaboration], Phys. Lett. B **705**, 28 (2011) [arXiv:1108.1316 [hep-ex]].
- [86] [CMS Collaboration], CMS-PAS-EXO-11-024.

- [87] S. Chatrchyan *et al.* [CMS Collaboration], Phys. Lett. B **704**, 123 (2011) [arXiv:1107.4771 [hep-ex]].
- [88] G. Beall, M. Bander and A. Soni, Phys. Rev. Lett. **48**, 848 (1982).
- [89] A. Hillairet *et al.* [TWIST Collaboration], arXiv:1112.3606 [hep-ex].
- [90] K. Ackerstaff *et al.* [OPAL Collaboration], Eur. Phys. J. C **8**, 3 (1999) [hep-ex/9808016].
- [91] H. Abramowicz, F. Dydak, J. G. H. de Groot, J. Knobloch, J. May, P. Palazzi, F. Ranjard and W. D. Schlatter *et al.*, Z. Phys. C **12**, 225 (1982).
- [92] S. R. Mishra, W. C. Leung, C. Arroyo, K. T. Bachmann, R. E. Blair, C. Foudas, B. J. King and W. C. Lefmann *et al.*, Phys. Rev. Lett. **68**, 3499 (1992).
- [93] G. Onengut *et al.* [CHORUS Collaboration], Phys. Lett. B **632**, 65 (2006).
- [94] N. Severijns, M. Beck and O. Naviliat-Cuncic, Rev. Mod. Phys. **78**, 991 (2006) [nucl-ex/0605029].
- [95] T. Yamazaki *et al.* [RBC + UKQCD Collaboration], Phys. Rev. Lett. **100**, 171602 (2008) [arXiv:0801.4016 [hep-lat]].
- [96] J. C. Hardy and I. S. Towner, Phys. Rev. C **79**, 055502 (2009) [arXiv:0812.1202 [nucl-ex]].
- [97] B. Sciascia [FlaviaNet Kaon Working Group Collaboration], arXiv:1101.5024 [hep-ph].
- [98] M. Antonelli, D. M. Asner, D. A. Bauer, T. G. Becher, M. Beneke, A. J. Bevan, M. Blanke and C. Bloise *et al.*, Phys. Rept. **494**, 197 (2010) [arXiv:0907.5386 [hep-ph]].
- [99] A. J. Buras, K. Gemmler and G. Isidori, Nucl. Phys. B **843**, 107 (2011) [arXiv:1007.1993 [hep-ph]].
- [100] W. J. Marciano and A. Sirlin, Phys. Rev. Lett. **71**, 3629 (1993).
- [101] E. Follana *et al.* [HPQCD and UKQCD Collaborations], Phys. Rev. Lett. **100**, 062002 (2008) [arXiv:0706.1726 [hep-lat]].
- [102] J. Beringer *et al.* [Particle Data Group Collaboration], Phys. Rev. D **86**, 010001 (2012).
- [103] M. Antonelli, V. Cirigliano, G. Isidori, F. Mescia, M. Moulson, H. Neufeld, E. Passemar and M. Palutan *et al.*, Eur. Phys. J. C **69**, 399 (2010) [arXiv:1005.2323 [hep-ph]].
- [104] V. Cirigliano and I. Rosell, JHEP **0710**, 005 (2007) [arXiv:0707.4464 [hep-ph]].
- [105] Y. Zhang, H. An, X. Ji and R. N. Mohapatra, Nucl. Phys. B **802**, 247 (2008) [arXiv:0712.4218 [hep-ph]].
- [106] O. Martin, A. Schafer, M. Stratmann and W. Vogelsang, Phys. Rev. D **60**, 117502 (1999) [hep-ph/9902250].
- [107] B. Surrow, J. Phys. Conf. Ser. **230**, 012036 (2010) [arXiv:1004.4884 [hep-ex]].

- [108] G. Aad *et al.* [ATLAS Collaboration], [arXiv:1207.7214 [hep-ex]].
- [109] S. Chatrchyan *et al.* [CMS Collaboration], Phys. Lett. B [arXiv:1207.7235 [hep-ex]].
- [110] L. D. Landau, Dokl. Akad. Nauk. USSR **60**, 207 (1948).
- [111] C. -N. Yang, Phys. Rev. **77**, 242 (1950).
- [112] J. Ellis and D. S. Hwang, arXiv:1202.6660 [hep-ph].
- [113] S. Y. Choi, D. J. Miller, Z. M. M. Muhlleitner and P. M. Zerwas, Phys. Lett. B **553**, 61 (2003) [hep-ph/0210077].
- [114] Y. Gao, A. V. Gritsan, Z. Guo, K. Melnikov, M. Schulze and N. V. Tran, Phys. Rev. D **81**, 075022 (2010) [arXiv:1001.3396 [hep-ph]].
- [115] A. Djouadi, Phys. Rept. **457**, 1 (2008) [hep-ph/0503172].
- [116] T. Plehn, D. L. Rainwater and D. Zeppenfeld, Phys. Rev. Lett. **88**, 051801 (2002); [hep-ph/0105325].
- [117] F. Campanario, M. Kubocz and D. Zeppenfeld, Phys. Rev. D **84**, 095025 (2011) [arXiv:1011.3819 [hep-ph]].
- [118] S. Berge and W. Bernreuther, Phys. Lett. B **671**, 470 (2009); [arXiv:0812.1910 [hep-ph]].
- [119] S. Berge, W. Bernreuther, B. Niepelt and H. Spiesberger, Phys. Rev. D **84**, 116003 (2011) [arXiv:1108.0670 [hep-ph]].
- [120] C. Balazs and C. P. Yuan, Phys. Lett. B **478**, 192 (2000) [hep-ph/0001103].
- [121] E. L. Berger and J. -w. Qiu, Phys. Rev. D **67**, 034026 (2003) [hep-ph/0210135].
- [122] E. L. Berger and J. -w. Qiu, Phys. Rev. Lett. **91**, 222003 (2003) [hep-ph/0304267].
- [123] A. Kulesza, G. F. Sterman and W. Vogelsang, Phys. Rev. D **69**, 014012 (2004) [hep-ph/0309264].
- [124] G. Bozzi, S. Catani, D. de Florian and M. Grazzini, Phys. Lett. B **564**, 65 (2003); [hep-ph/0302104].
- [125] G. Bozzi, S. Catani, D. de Florian and M. Grazzini, Nucl. Phys. B **737**, 73 (2006); [hep-ph/0508068].
- [126] G. Bozzi, S. Catani, D. de Florian and M. Grazzini, Nucl. Phys. B **791**, 1 (2008) [arXiv:0705.3887 [hep-ph]].
- [127] S. Catani and M. Grazzini, Nucl. Phys. B **845**, 297 (2011) [arXiv:1011.3918 [hep-ph]].

-
- [128] D. de Florian, G. Ferrera, M. Grazzini and D. Tommasini, JHEP **1111**, 064 (2011) [arXiv:1109.2109 [hep-ph]].
- [129] D. de Florian, G. Ferrera, M. Grazzini and D. Tommasini, JHEP **1206**, 132 (2012) [arXiv:1203.6321 [hep-ph]].
- [130] D. Boer, W. J. den Dunnen, C. Pisano, M. Schlegel and W. Vogelsang, Phys. Rev. Lett. **108**, 032002 (2012) [arXiv:1109.1444 [hep-ph]].
- [131] W. J. den Dunnen, D. Boer, C. Pisano, M. Schlegel and W. Vogelsang, arXiv:1205.6931 [hep-ph].
- [132] A. Metz and J. Zhou, Phys. Rev. D **84**, 051503 (2011); [arXiv:1105.1991 [hep-ph]].
- [133] F. Dominguez, J. -W. Qiu, B. -W. Xiao and F. Yuan, Phys. Rev. D **85**, 045003 (2012) [arXiv:1109.6293 [hep-ph]].
- [134] J. W. Qiu, M. Schlegel and W. Vogelsang, Phys. Rev. Lett. **107**, 062001 (2011) [arXiv:1103.3861 [hep-ph]].
- [135] B. Coleppa, K. Kumar and H. E. Logan, arXiv:1208.2692 [hep-ph].
- [136] D. Boer and C. Pisano, arXiv:1208.3642 [hep-ph].
- [137] R. Mertig, M. Bohm and A. Denner, Comput. Phys. Commun. **64**, 345 (1991).
- [138] T. Hahn and M. Perez-Victoria, Comput. Phys. Commun. **118**, 153 (1999) [hep-ph/9807565].
- [139] W. J. Marciano, C. Zhang and S. Willenbrock, Phys. Rev. D **85**, 013002 (2012) [arXiv:1109.5304 [hep-ph]].